Electrochemistry and Galvanic Deposition of Group 10 & 11 Transition Metals Using Deep Eutectic Solvents

Thesis submitted for the degree of
Doctor of Philosophy
at the University of Leicester

by

Gregory Charles Hereward Forrest
Department of Chemistry

September 2014

“Science is, on the whole, an informal activity, a life of shirt sleeves and coffee served in beakers.” – George Porter

(I) Abstract

The galvanic deposition of metals has wide ranging applications in many industries. One example is the printed circuit board industry, where galvanic coatings are used as both a catalyst for the activation of the surface of a substrate and protective coating to prevent the oxidation of the surface.

Deep Eutectic Solvents (DESs) have received growing interest in the area of metal processing, due to the unique solvation properties and ability to dissolve metal salts, without the need for addition of acids or bases. The DESs have been widely applied in electrochemical processes, where electrochemistry can be performed without the need for addition of an electrolyte.

In this work, the speciation of the group 10 and 11 metals has been characterised using UV – Vis spectroscopy. The electrochemistry of the group 10 and 11 elements has been characterised using cyclic and linear sweep voltammetry and related to the speciation of the metal centres. Further characterisation of the electrochemistry was performed using an electrochemical quartz crystal microbalance, allowing for the rate and current efficiency of the electrochemical reaction to be measured.

Galvanically deposited coating of group 10 and 11 metals, were produced on a standardised copper substrate. The morphology of the coatings was characterised by atomic force (AFM) and scanning electron microscopy (SEM) and the composition by energy dispersive X – ray (EDX) and X – ray photoelectron spectroscopy (XPS).

The mechanism by which the galvanic coatings are formed was probed. The reaction mechanism was predicted from the formal electrode potential of the metal redox couples. The predicted mechanisms were experimentally investigated using quartz crystal microbalance experiments. The quartz crystal microbalance also allowed for the determination of the rate of the galvanic reactions.

(II) Acknowledgements

I would like to thank Prof. Karl Ryder for providing me with an interesting and challenging research project. The time spent working as part of the Leicester Materials and Interfaces group has provided me with invaluable experience, as well as the opportunity to learn and grow as a chemist. I would also like to thank Karl for the advice and support provided throughout the project

I would like to thank the Leicester Materials and Interfaces group as a whole, for support and helping me achieve my goals in this project.

My thanks also go to the entire Department of Chemistry, where I have now spent 8 years of my life. I have enjoyed my time as part of an inclusive department, the members of which, will go out of their way for a person in need of help.

I would also like to thank my family and friends, with special mention to the Dream Team (Andrew Fallows, Stuart Phillips and Luka Wright), Nino Iakobachvili and especially Jessica Loraine. They have provided support, advice and abuse in equal measure, as well as massive amounts of entertainment throughout my time at Leicester.

(III) Contents

(IV) Abbreviations

Abs.	Absorption
AFM	Atomic force microscopy
ChCl	Choline chloride
Ca.	*Circa*
cps	Counts Per Second
CV	Cyclic voltammetry
DCM	Dichloromethane
DES	Deep Eutectic Solvent
(DES)	Solvated in Deep Eutectic Solvent
DI	Deionised
E	Potential
E^o	Standard electrode potential
EDX	Electron Depressive X-ray spectroscopy
EG	Ethylene Glycol
EMF	ElectroMotive Force
EQCM	Electrochemical Quartz Crystal Microbalance
EXAFS	Extended X – ray Absorption Fine Structure spectroscopy
I.e.	*Id est*
IL	Ionic liquid
(IL)	Solvated in Ionic liquid
LMCT	Ligand to Metal Charge Transfer
phen	1,10-phenanthroline
QCM	Quartz Crystal Microbalance
RoSH	Restriction of the use of Certain Hazardous Substances
SEM	Scanning electron microscopy
UV – Vis	Ultraviolet – Visible spectroscopy
XPS	X-ray photoelectron spectroscopy

(V) List of Figures

(VI) List of Tables

Chapter 1: Introduction

1.1 Deep Eutectic Solvents

1.1.1 Theory

When two compounds are combined in a binary liquid system, the system can be described as ideal or non-ideal. In an ideal system, the activity of a compound is proportional to the mole fraction of the compound.[1] This means that the molecular interactions between two molecules of the different compounds are similar to the molecular interactions between two molecules of the same compound. The effect on the freezing point of a solution is a linear relationship between the freezing point of the pure solutions and the mole fraction of the components.

When two compounds are combined in a non-ideal binary liquid system, the molecular interactions are stronger or weaker between similar compounds than between the two different compounds. The affect is a depression of the freezing point of both parts of the system, *Figure 1.1*.[2] In *Figure 1.1* a binary phase diagram is shown, at the eutectic point, a single freezing point is observed; here both components freeze at the same time, freezing as the pure components. If the mole fraction of B is greater than that of the eutectic point, when cooling the liquid the temperature reaches the curve to the right of the eutectic point, compound B starts to precipitate and the liquid becomes richer in compound A. As the precipitation of B continues and the mole fraction of B in the liquid becomes less, the temperature of the liquid reduces along the curve until the eutectic point is reached. When the eutectic point is reached, both components freeze at the same temperature. The converse is true when the mole fraction of B is less than that of B at the eutectic point.[2]

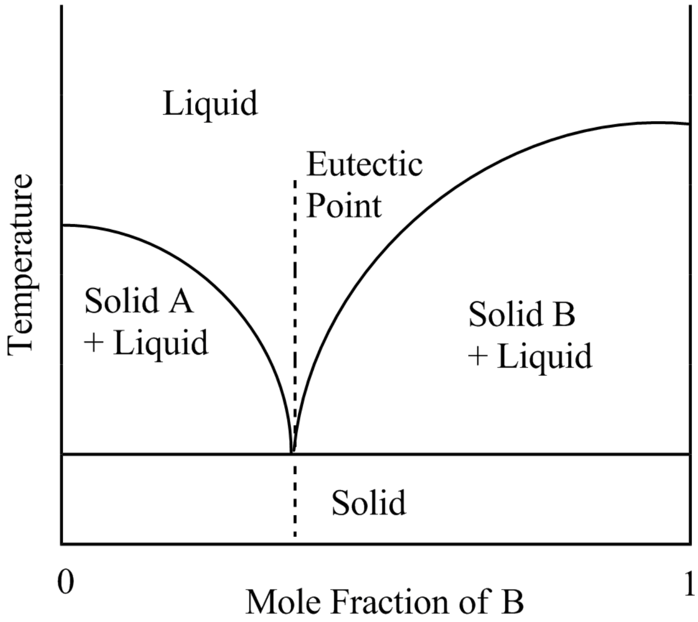

Figure 1.1: Eutectic phase diagram for a two phase system (A and B)

Deep Eutectic Solvents (DESs) were patented in 2000[3] and first reported in academic literature in 2001 by Abbott *et. at*.[4] Where two DESs were produced by mixing Lewis acidic metal salts, with quaternary ammonium halides. The DESs where produced and the freezing point of the melt as a function of molar ratio of the components were studied. The lowest melting point was found to be at a 2:1 ratio of metal salt ($SnCl_2$ or $ZnCl_2$) to ammonium salt (choline chloride (ChCl)). This is the first example of what has come to be known as a type 1 DES. There is prior precedent for production of Zn salt based melts using a pyridinium salt,[5] however the melting point as a function of molar fraction has not been examined and organic solvent was used to reduce the viscosity of the melt.

There are four types of DES presented in academic literature, Types I, II and III can be defined by the general formula $R_1R_2R_3R_4N^+ [X \cdot Y]^-$, where X is an anionic halide anion and Y is a neutral species capable of complexing the halide ion.[6] The most commonly used cation is the choline cation, $(C_2H_5O)(Me)_3N^+$.

Type I: $Y = MCl_x$, M = Zn,[4,7] Sn,[4,7] Fe,[7] Al,[8] Ga[9]

Type II: $Y = MCl_x \cdot ZH_2O$, M = Cr[10]

Type III: Y = $CONH_2$,[11] COOH,[12] OH[13]

Type I and II DESs rely on the Lewis acidity of metal salts, to associate an anion from the ammonium salt to a metal centre.[4,7] In the case of type II DESs, water molecules can be displaced by the anion to produce a DESs.

Type IV eutectics were patented in 2007[14] and do not use quaternary ammonium salts in the eutectic. Instead metal salts are mixed with complexing agents, producing a DES formed from two neutral species.[6,15] For example $ZnCl_2$ can be mixed with a variety of complexing agents (acetamide, urea, ethylene glycol or hexanediol) to form DES with a lower freezing point than that of the equivalent type I DES.[4,6] Type IV DESs exploit neutral Lewis base donors, which coordinate with the Lewis acidic metals and dissociate an anion, which intern can coordinate to Lewis acidic metal centres.[6]

Type III DESs differ because they do not really on Lewis acid – base interactions or metal salts. Instead type III DESs, employ hydrogen bond donors (HBDs) to associate with the anion of an ammonium salt, producing an anionic complex.[11]

The range of hydrogen bond donors used to produce type III Deep Eutectic Solvents in published literature is vast, including but not limited to urea, acetamide and oxalic acid. The full range of hydrogen bond donors been reviewed else where.[9,16,17] It is necessary to note a couple of important examples of type III Eutectics. These are Ethaline 200, which is produced from a combination of ethylene glycol and choline chloride in a 2 : 1 ratio respectively[13] and Reline 200, which is produed from a combination of urea and choline chloride in the same ratio.[11]

DESs are formed in an endothermic process, by mixing the two components with mild heating, equation **(1.1)**. As equation **(1.1)** demonstrates, the reaction for the formation of DESs based on ChCl, produces large non – symmetrical cations (choline$^+$) and large complex anions.

$$(C_2H_4OH)(Me)_3N^+ Cl^- + zY \rightarrow Ch^+ + [zY \cdot Cl]^- \quad \textbf{(1.1)}$$

It is suggested that Deep Eutectic solvents offer an alternative, green media in which chemistry can be performed. Choline chloride is a biodegradable and non – toxic chemical,[17,18] which is in contrast to traditional ionic liquids where the imidazolium ions have been found to be toxic.[19] The use of heavy metal salts in the production of type I, II and IV eutectics, will obviously increase the toxicity of these liquids, however as the application of these liquids is the processing of these metals, the toxicity issue is unavoidable. As the hydrogen bond donors used to produce type III eutectics varies, the toxicity of the liquid will vary. However, for the most common liquids, where urea, ethylene glycol and glycerol are used as the hydrogen bond donors, the complexing agents are non – toxic.

1.1.2 Metal Processing

Deep Eutectic Solvents have been used in a wide range of applications such as electrochemistry, materials chemistry, catalysis and bio – diesel treatment.[18,17] As discussed above, oxidised metal species can be readily dissolved in Deep Eutectic Solvents. As DESs are ionic media, electrochemistry can be performed in these solutions without the need for supporting electrolyte. These properties make DESs an appropriate solvent for the electrochemical processing of metals.

The first published application of Deep Eutectic Solvents by Abbott *et. al.*, was the use of Ethaline as a media for the electropolishing of stainless steel.[13] The paper discusses the linear sweep voltammetry of Ethaline *versus* a commercial electropolishing solution, performed using a stainless steel working electrode. It was shown that whilst the linear sweep voltammetry of the commercial electropolishing solution showed passivation of the working electrode, the electropolishing performed in Ethaline did not show passivation in the voltammetry.

The paper also discussed the electropolishing of larger samples, so that morphology of the electropolished sample could be observed. The SEM images show that there is significant smoothing of the surface of the electropolished compared to the original sample.

Finally the paper discusses the use of inductively coupled plasma atomic emission spectroscopy to determine the concentration of metal ions dissolved in the electrolyte. When the concentration ratios of the metals dissolved in Ethaline were determined, the concentrations were compared to the concentrations of the metals in the alloy. It was found that the concentration of metal ions dissolved in the electrolyte were similar to that of the stainless steel alloy. This indicates that de – alloying of the steel does not occure. This is important, as de-alloying could affect the mechanical and chemical properties of the alloy.

This work has been expanded by Abbott *et. al.*[20] with a paper on the electropolishing of various grades of stainless steel. This work again uses linear sweep voltammetry to characterise the oxidation of the stainless steel. It was found that if the surface oxide of the stainless steel was removed, by *in situ* polishing of the surface of the electrode, the oxidation onset potential is shifted significantly negative for all substrates.

The morphology of bulk substrates was characterised using scanning electron and atomic force microscopy. Whilst the composition of elements present in the sample was analysed using energy dispersive X – ray and X – ray photoelectron spectroscopy. It was found that there was little difference in the elemental composition at the surface or in the bulk sample, indicating that de – alloying does not occur as shown in the previous paper.

The use of Deep Eutectic solvents as a media for electropolishing has not only been used for the electropolishing of stainless steels. It has also been used for the electropolishing of aerospace superalloys, in research carried out by Abbott *et. al.*[21]

Whilst there is little published on the electropolishing of metals using Deep Eutectic Solvents, the literature precedent for the electrochemical deposition of metals from these media is much greater. The first paper to demonstrate the use of Ethaline as a media for the deposition of metals was published by Abbott *et. al.*[22] The paper describes the electrolytic deposition of tin – zinc systems. The electrochemistry of $SnCl_2$ and $ZnCl_2$ metal salts were investigated in both Reline and Ethlane using cyclic voltammetry. The metal salts dissolved in Ethaline giving a much more defined electrochemical response compared to Reline. It was discussed that the poor solubility of the metal salts in Reline could be responsible for the poor electrochemical response.

The paper also attempted to relate the electrochemical response to the speciation of the metal centres when dissolved in the Deep Eutectic Solvents. The paper used fast atom bombardment – mass spectrometry to characterise the metal species present in solution. In the mass spectra for both Reline and Ethaline the $[SnCl_3]^-$ complex was observed, it should be noted that this does agree with more recent literature.[23] The same is true of the zinc ion speciation, where the $[ZnCl_3]^-$ complex was observed in both the Reline and Ethaline spectra, along with the singularly anionic zinc chloride dimer and trimer in Ethaline. This demonstrates that whilst mass spectrometry can be used observe metal complexes in Deep Eutectic Solvents, the technique requires supporting data to obtain the true speciation of the metal complexes, such as extended X – ray absorption fine structure (EXAFS).

In the paper SEM was used to examine the morphology of the electrodeposited tin – zinc coatings. It was found that depending on the Deep Eutectic Solvent used, the morphology of the coating deposited was altered. Using EDX the composition of the deposits were analysed and found to be mostly zinc, with the amount of tin present dependent on the electrolyte it was deposited from.

Since the paper was published there has been a large amount of interest in the use of these electrolytes are media for electrolytic deposition. These applications include the electrolytic deposition of single elements such as copper,[24] silver,[25] and nickel.[26] As well as attempts to produce binary systems, such as an copper – indium,[27] cobalt – nickel[28] and copper – gallium.[29]

1.1.3 Characterisation of Metal Salt Speciation and Electrochemistry

When metal salts are dissolved in a solvent, it is common for the local environment around the metal centre to undergo solvolysis, whether this is association of further ligands or dissociation and exchange of ligands that were originally part of the metal salt with the solvent. When dissolved in aqueous solution the Cu^{2+} ion will undergo solvolysis to form the $[Cu(H_2O)_6]^{2+}$ complex.[30] However if an aqueous solution has an abundance of chloride ions present, instead of forming the hexaaqua complex, the copper centre will associate two chloride ions forming the $[CuCl_4]^{2-}$ complex.[16] It should be noted, that the change in speciation of the copper centre directly affects the electrochemical processes which the metal centre will undergo, i.*e*. it is well known that it is thermodynamically favourable for the $[Cu(H_2O)_6]^{2+}$ complex to undergo a two electron reduction from Cu (II) → Cu (0). However, it has been shown that when in a high chloride aqueous environment, the $[CuCl_4]^{2-}$ complex can undergo the single electron reduction of Cu (II) → Cu (I).[16]

It has been realised that the speciation of metal salts when dissolved in Deep Eutectic Solvents is an important area of study. The determination of the speciation of metal salts has mainly been performed by EXAFS,[16,23,25,31] as well as mass spectrometry, NMR, UV – Vis, vibrational and neutron spectroscopy.[32,33] It was found that when a metal salt was dissolved in a Deep Eutectic Solvent, that the metal salt undergoes solvolysis to form an ionic complex. The complexes formed in Ethaline, usually take the form of an anionic multi chloro complex, *i.e.* $[AgCl_2]^-$ or $[CuCl_4]^{2-}$,[23] however it was found that after solvolysis nickel salts formed a triethylene glycol complex, $[Ni(C_2H_6O_2)_3]^{2+}$.[23]

The speciation of a number of metal salts dissolved in Ethaline has been analysed by the Leicester Materials group.[23] The speciation of metal (II) chloride salts was characterised and the speciation of Mn, Fe, Co, Cu, Zn, Pd, Sn and Pt were all found to be the tetrachloro complexes. The speciation of metal (I) chloride salts was characterised and the speciation of Cu, Ag and Au were found to be the dichloro complexes, however it was also found that the Cu and Ag solutions also contained some of the trichloro complexes.

The paper by our group also showed that when non chloride salts of silver and copper are dissolved in Ethaline, the metal centres will undergo solvolysis, where the original ligand will undergo dissociation and chloride ligands will be associated. It has also been discussed by Abbott *et. al.*[34] that the use of various silver salts does not affect the electrochemistry of the silver ion when dissolved in Ethaline.[34]

It has been noticed that solution of nickel complexes can undergo thermochromic behaviour when dissolved in ionic liquid[35] and Ethaline.[36] In a paper by Chen *et. al.*[33] it was suggested that the thermochromic behaviour was due to the conversion of octahedral nickel complexes present at lower temperature to the $[NiCl_4]^{2-}$ complex at higher temperatures.

A paper by Gu *et. al.*,[36] the thermochromic behaviour for nickel salts dissolved in Ethaline, has been characterised. In the paper it is shown that the nickel solution undergoes a number of changes in colour due to heating, however the UV – Vis spectra displayed only have a range of 30 – 75 ^{o}C due to experimental limitations. It should be noted that whilst the peaks representing the $[NiCl_4]^{2-}$ complex agree with published literature,[35] the octahedral complex that was assigned $[Ni(H_2O)]^{2+}$, does not agree with the literature published by our group.[23]

The change in nickel speciation of the nickel complex in Ethaline was not electrochemically characterised in the paper by Gu *et. al.* However, the electrochemistry of a 0.1 M solution of $NiCl_2.6H_2O$ dissolved in Ethaline was characterised at varying temperature Ali *et. al.*[26]. The cyclic voltammetry of a nickel ion solution of concentration 0.1 M and at a temperature of 30 ^{o}C, displays both a reduction and oxidation wave for the deposition and stripping of nickel from the electrode surface. It is shown that an increase in temperature does have an effect on the electrochemistry of the solution, but this change in electrochemical response is not linked to the speciation of the nickel ion.

The discussion of the speciation of nickel ions in the paper by Ali *et. al.*,[26] does not agree with either our group[23] or Gu *et. al.*[36] The paper presents results obtained from fast atom bombardment mass spectrometry, suggesting that the solution contains solely anionic chloride species. Due to the choice of technique, it is suggested that the speciation results presented by ourselves and Gu are more likely to be representative of the solution.

It was discussed above that the use of metal salts other than chloride as a source metal ions, showing displacement of the non chloride ligand when dissolved in Ethaline. However, it has been shown that the use of molar equivalents of strongly binding ligands can displace chloride ligands associated with metal centres. The exchange of ligands has been shown in the paper by our group.[23] The paper discussed that the speciation of the nickel metal centre, when dissolved in Ethaline, was the nickel (II) triethylene glycol complex.

There is an earlier paper published by the Leicester Material group, the paper is published by Abbott *et. al*.[31] Importantly the paper discusses how to determine electrode potentials from cyclic voltammagrams in Deep Eutectic Solvents, which will be discussed fully in **Chapter 2**. The paper also includes 17 formal electrode potentials determined for a range of redox couples in Ethlaine, these include the Fe (III)/(II), Cu (I)/(0), Cu (II)/(I), Zn (II)/(0), Pd(II)/(0), Ag (I)/(0), Sn (II)/(0) and Au (I)/(0) redox couples, *Figure 1.2*. *Figure 1.2* displays a straight line where $E^{o}{}'_{(aq)} = E^{o}{}'_{(Ethaline)}$ and each redox couples is plotted by its value in Ethaline and aqueous conditions, differences in concentration and temperature were corrected for using the Nernst equations. It should be noted that the formal electrode potentials of the redox couples for Mn, Co, Ni and Pt are not determined.

Another important part of the electrochemical characterisation of metal redox couples is the determination of the rate of reaction. The rate of electrochemical reaction can be determined by uses of electrochemical techniques, by measuring the resulting current from applied potential and calculating using Faraday's constant and the electrode area. It should be noted however, that for the rate of reaction to be calculated this way, all of the current passed must be due to the redox chemistry of the species under examination, hence the reaction must be 100% efficient.

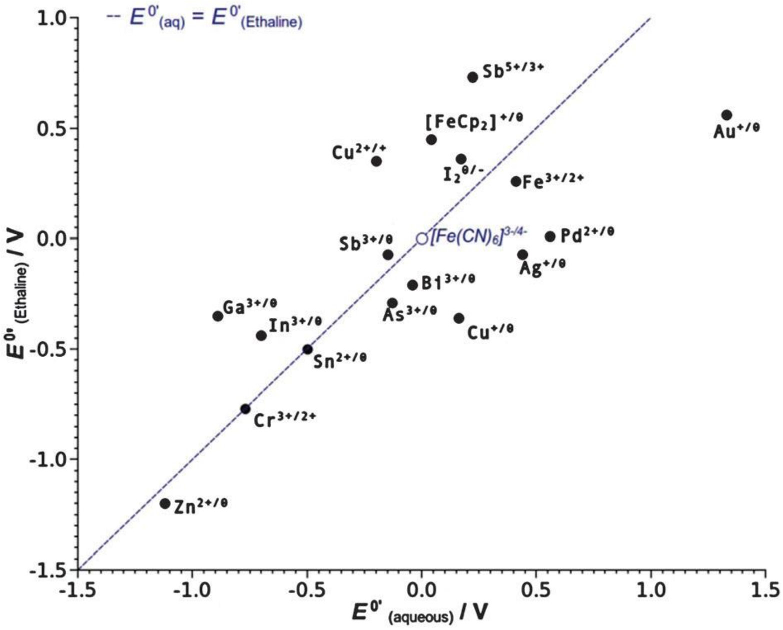

Figure 1.2: Plot of formal redox potential, E^{o}', data in Ethaline for 17 couples versus the corresponding aqueous redox potential.[31]

The electrochemical plating of metals from aqueous solutions often involves the use of acidic solutions,[37,38] this means there is an abundance of H^+ ions present in the plating solutions. The hydrogen ions can undergo reduction to form H_2, meaning that when performing electrochemistry on these solutions, some of the current passed could be due to side reactions. Hence, it is not possible to calculate the rate of reaction from the current passed in the reaction. However, it is possible to calculate the rate of reaction using a combined electrochemical and gravimetric method.

An electrochemical quartz crystal microbalance (EQCM) can be used to perform electrochemical experiments, while simultaneously measuring the change in mass on the surface of the electrode.[39] This allows for the calculation of the rate of reaction for processes where mass is either gained or lost on the surface of an electrode, provided oxides or inclusions are not present . The process of calculating the rate of reaction will be examined in **Chapter 2**. Determination of the rate of electrochemical reaction in a

Deep Eutectic Solvent using an EQCM, has been shown in the literature by Abbott *et. al*.[24] The paper calculated the rate of deposition of copper using the change in mass *versus* time data giving a rate constant of 14.5 g cm^{-2} s^{-1}, this can be easily converted to a rate constant in mol cm^{-2} s^{-1} by dividing by the relative molecular mass of copper.

Finally the paper by Abbott *et. al*. discusses the use of an EQCM to calculate the current efficiency of the deposition of copper. As discussed above, when performing an electrochemical reaction, some of the current passed can be due to side reactions and not the species under analysis. Using an EQCM, a comparison between the theoretically possible mass – charge ratio and the experimentally determined mass – charge ratio, was used to calculate the current efficiency of an electrolytic deposition of copper from the surface of the electrode.

It should be noted that whilst analysis of the rate and current efficiency of the deposition reaction has been performed for copper in Ethaline,[24] this type of analysis has not been performed for any of the other metal redox couples discussed above.

1.2 Galvanic Deposition of Metals

1.2.1 Theory

The galvanic or corrosive deposition of metals is a well established process and is of interest in both industrial and academic settings.[40] The driving force for the deposition of metals *via* a galvanic reaction, is based on the difference in electrode potentials of relevant redox couples. In aqueous solution, the standard electrode potentials of a wide variety of redox couples is well established.[40,41] This is known as the electrochemical series, where metals with more positive standard electrode potential are more noble than those with a less positive standard electrode potential. This means that a solution containing ions of a more noble metal will react with a less noble metal substrate.

The driving force of these reactions, under standard conditions, can be calculated using the equation **(1.2)**.

$$\Delta \mathrm{G}^{\mathrm{o}} = -\,\mathrm{nFE}^{\mathrm{o}}_{\mathrm{e.m.f.}} \quad (\mathbf{1.2})$$

Where ΔG^{o} is the change in the standard Gibbs free energy, n is the number of electrons being transferred in the reaction, F is Faraday's constant and $\mathrm{E}^{\mathrm{o}}_{\mathrm{e.m.f.}}$ is the electromotive force calculated from the standard electrode potentials. The electromotive force can be calculated using equation **(1.3)**.

$$\mathrm{E}^{\mathrm{o}}_{\mathrm{e.m.f}} = \mathrm{E}^{\mathrm{o}}_{\mathrm{Ox}} - \mathrm{E}^{\mathrm{o}}_{\mathrm{Red}} \quad (\mathbf{1.3})$$

Where $\mathrm{E}^{\mathrm{o}}_{\mathrm{Ox}}$ is the standard electrode potential of the oxidised species and $\mathrm{E}^{\mathrm{o}}_{\mathrm{Red}}$ is the standard electrode potential of the reduced species.

It is important to note, that most reactions are not performed under standard conditions and hence the electrode potentials of the reduced and oxidised species will deviate from the standard electrode potentials. It is possible to calculate the change in electrode potentials using the Nernst equation **(1.4)**. Where E is the electrode potential, E^{o} is the standard electrode potential, R is the gas constant, T is the temperature of the reaction, [Ox] is the concentration of the oxidised species and [Red] is the concentration of the reduced species.[42]

$$\mathrm{E} = \mathrm{E}^{\mathrm{o}} + \frac{\mathrm{RT}}{\mathrm{nF}} \ln\left(\frac{[\mathrm{Ox}]}{[\mathrm{Red}]}\right) \quad (\mathbf{1.4})$$

1.2.2 Application

The galvanic deposition of metals has applications in a number of areas, where the use of electrolytic coatings is not feasible. For example surface protection a tarnishable substrate, such as the printed circuit board industry. A noble metal is galvanically deposited on the surface of sample, to prevent the formation of oxides that would be detrimental to the application of the substrate.

A good example of the application of galvanic deposits for surface protection is the printed circuit board industry, where both the galvanic deposition of silver and gold is used to protect the copper tracks of a PCB. The coatings prevent the formation of copper oxides, which are known to cause the production of brittle solder joints.[43]

The galvanic deposition of silver is performed directly on the surface of the copper of the printed circuit board.[44,45] The galvanic deposition of silver on a copper substrate has been performed from aqueous media, normally using silver nitrate as the source of the silver ions present in the plating solution.[46,47]

Further, the galvanic deposition of silver on to a copper substrate used to produce hydrophobic surfaces.[47,48] C. D. Gu *et. al*.[47] have presented a paper discussing the silver deposition on to a cold rolled copper foil from an aqueous solution of 0.01 or 0.001 M $AgNO_3$. By varying the composition and deposition time of the silver, different morphologies of silver deposit can be produced. The silver deposits mimics hydrophobic structures formed in nature, these deposits have a “coral like” structure with a high surface area. J. Yao *et. al*.[48] have presented a silver deposit on a etched copper plate using a aqueous solution of 0.03 M $[Ag(NH_3)_2]OH$. The galvanic process produced a “flower like” deposit with a highly ordered crystalline deposit.

The galvanic deposition of gold is performed on to an electroless coating of nickel.[49] Copper and gold are known to form a solid state solution and hence the copper will be able to mix with the gold and undergo diffusion to the surface of the sample, where it can form copper oxides. The electroless nickel is employed as a barrier layer between the copper and gold to prevent this diffusion. The galvanic deposition of gold on to electroless nickel is performed from acidic and/or cyanide based solutions solution. The galvanic deposition of gold on to electroless nickel substrate from an acid solution can lead to a defect called black pad, which causes brittle solder joints.[49]

Galvanic coatings have been employed is the production of catalytic surfaces. The galvanic deposition of palladium on to a copper substrate has been employed as a surface catalyst, which is used to initiate the electroless deposition of nickel *via* hypophosphite reduction.[50]

Another application for the galvanic deposition of Pd, has been for the production of an electrocatalysits for the electrochemical activation of carbon – halogen bonds.[51] Palladium – copper nanoparticales were produced by electrochemical deposition of copper nanoparticales on to a glassy carbon electrode, followed by galvanic deposition of palladium. Palladium was deposited from an aqueous of 0.5 mM $PdSO_4$ and 0.1 M K_2SO_4, where the cell potential of the reaction between copper metal and palladium ions was found to be 0.609 V. By varying the deposition time of the palladium the morphology and composition of the nanoparticales can be altered.

Galvanic deposition of gold on to a copper substrate has been used to produce copper – gold alloy nanostructures. L. Tamašauskaitė-Tamašiūnaitė *et. al.*[52] presented electrolessly deposited copper, on to a titamium substrate. Which was then immersed in to a $[AuCl_4]^-$ solution to produce copper – gold nanostructures. These nanostructures were employed as a heterogeneous catalyst for the oxidation of borohydride.[52] N. Zhang *et. al.*[53] produced copper – gold nanoparticales by a galvanic reaction of a colloidal suspension of copper nanoparticales with a 0.05 M solution of $[AuCl_4]^-$. These nanoparticales were use as catalysits in the reduction of *p*-nitrophenol and epoxidation of styrene

The galvanic reaction of platinum with copper has been exploited to produce platinum nanotubes, by plating platinum around a sacrificial copper nanowire.[54,55] Y. Yan *et. al.*[54] have presented the production of platinum coated copper nanowires by galvanic reaction. Copper nanowire were produced by reduction of $(CuNO_3)_2$ with hydrazine. The isolated nanowires were coated with platinum by reaction with $[PtCl_6]^{2-}$. These nanotubes were investigated for catalytic activity for the hydrogen oxidation reaction, which has applications in fuel cells.[54] N. V. Myung *et. al*.[55] synthesized 1D platinum nanostructures using sacrificial coppoer nano wires. Copper nanowires were produced by the template – directed electrode position method. The isolated copper nanowires were used coated with platinum using an aqueous solutions of 0.01 – 0.1 M $[PtCl_6]^{2-}$. Depending on the concentration of the platinum solution the morphology and composition was shown to change. As the concentration of $[PtCl_6]^{2-}$ increaded the average external diameter of the platinum nanowires decreased.

The use of Deep Eutectic Solvents as an alternative media for the production of galvanic coatings can be used to overcome the need for acidic solutions or the use of hazardous chemicals.

1.2.3 Galvanic Reactions in Deep Eutectic Solvents

There is existing precedent in the literature for the galvanic deposition of silver from Deep Eutectic Solvents.[34,56] Research by Gu *et. al*. used silver chloride, dissolved in Ethaline, to galvanically deposit silver on to a copper substrate in an attempt to produce a super hydrophobic material. Morphology of the silver deposit was altered by varying the concentration of silver ions and the temperature of a silver chloride solution.[56] The resulting deposits where characterised using scanning electron microscopy (SEM), energy dispersive X-ray spectroscopy (EDX), powder X-ray diffraction (XRD) and measurement of the water contact angle

Research by Abbott *et. al*. has investigated the galvanic deposition of silver on to a copper substrate for use as a protective coating.[34] The paper investigated the deposition of silver from an Ethaline solution, using a variety of silver salts as the silver ion source

The work also discussed the implication of the values of the copper and silver redox couples, where it is possible to calculate the reaction that will occur when a copper substrate is immersed in a silver ion solution. But did not calculate the values of the change in Gibbs free energy associated with the reactions. The paper discussed the use of the QCM to perform analysis of the stoichiometry of the galvanic reaction, so that the theoretical reaction proposed from analysis of the electrode potentials can be proved.

Whilst the paper did report the surface morphology of the silver deposits, the elemental composition at the surface of the coating was not investigated. Also at the time of publishing, work investigating the speciation of the metal salts dissolved in Ethaline had not been performed. So whilst the redox couples involved have been identified, the overall reaction has not been proposed.

Another paper by Ali *et. al*. published in 2014, shows that nickel can be both galvanically and electrolyticly deposited from Ethaline.[26] The paper investigates the voltammetry of the nickel ion in the Ethaline solution at varying temperatures, however it is important to note the concentration of nickel ions used. The paper uses a concentration of 0.1 M nickel ions, whereas this work uses 0.01 M to characterise the voltammetry. This will directly affect the concentration of electroactive species present in solution and hence the electrochemical response. They do not discuss the electrode potential of copper and the driving force for the reaction is not established and the change in Gibbs free energy for the reaction is not calculated. Also whilst there is some discussion on speciation of the nickel ion when dissolved in Ethaline, the discussion is not conclusive and does not take into account newly published literature, as discussed above.[23] Hence the overall reaction of the nickel ions with the copper substrate has not been proposed or experimentally scrutinised.

The paper characterised the deposits using SEM and XRD to characterise the deposits. However, as the paper covers more than the galvanic deposition of nickel, the morphology of the galvanic deposit is not extensively discussed. The composition of the sample is studied using XRD to establish which elements are present, however XRD does not provide quantitative data for the composition of the surface of the sample, due to the large interaction volume of the technique.

The galvanic deposition of silver and nickel have been shown from Deep Eutectic Solvent have been discussed above. At the time of writing, the author of this work is unaware of any papers investigating the galvanic deposition of gold, palladium or platinum from Deep Eutectic Solvents.

A paper published by Abbott *et. al*.[57] discussed the use of the galvanic reaction in sedimentation of lead from Deep Eutectic Solvent. A Deep Eutectic Solvent composed of choline chloride, urea and ethylene glycol in a molar ratio of 1 : 0.5 : 1.5 respectively was produced. This liquid has been shown to perform selective extraction of zinc and lead salts from electrical arc furnace dust, without the extraction of other salts such as aluminium, copper, iron and silicon that are present in the arc furnace dust.[58] Addition of zinc metal powder, to the solvent containing extracted zinc and lead salts, leads to the precipitation of Pb metal via a galvanic reaction. It was shown that up to 97% of the Pb could be recovered from the solution, as long as the concentration of Zn ions does not become so large that the electrode potential is shifted more positive than the Pb electrode potential. However, it is possible to electrowin the Zn from solution, hence it is possible to regenerate and reuse the Deep Eutectic Solvent for further extraction of furnace dust.

1.3 Project Aims

This project aims to expand on the existing literature concerning characterisation of the speciation and electrochemistry of group 10 and 11 metals in Ethaline. The specific aims are:

- Characterisation of the speciation of group 10 and 11 metal salts solution using UV – Vis spectroscopy.
- Investigate the change in speciation of nickel ions leading to the thermochromic effect observed in nickel salt, Ethaline solutions.
- Determine the formal electrode potentials of nickel and platinum in Ethaline.
- Characterise the rate and current efficiency of the electrochemical reaction of the group 10 and 11 elements.
- Produce galvanic deposited coatings of group 10 and 11 metals on a copper substrate.
- Characterise the stoichiometry and rate of the galvanic reaction between group 10 and 11 metals with a copper substrate.
- Investigate the morphology and composition of the galvanically deposited coatings of group 10 and 11 metals.

The literature precedent for the galvanic deposition of the group 10 and 11 metals on to a copper substrate is limited to the galvanic deposition of silver[34] and nickel.[26] However as discussed above, there are various areas such as the composition of the silver coating or the rate of the galvanic reaction of nickel with copper that have not been investigated. It should also be noted that an investigation in to the galvanic coating of gold, palladium or platinum on a copper substrate, have not been investigated. These coatings and reactions kinetics are of academic interest and may turn out to be industrially relevant when developing a process involving these reactions.

To understand the galvanic reaction fully, it is necessary to characterise the electrochemistry of redox couples associated with the galvanic reactions. As discussed above, it is important to relate the electrochemical response of the metal ions to the speciation of the metal ions in solution. Hence the speciation of the metal chloride salts dissolved in Ethaline will be analysis using UV – Vis spectroscopy.

The electrochemistry of the metal chloride solutions will be analysed using various electrochemical techniques performed using a macro electrode, as well as an electrochemical quartz crystal microbalance. From data obtained from the EQCM it will be possible to calculate the rate and current efficiency of the electrochemical reaction.

The galvanic reactions will be investigated using QCM to determine the stoichiometry and rate of the galvanic reaction. Using a standard electrolytic deposited copper substrate, the morphology of the galvanically deposits group 10 and 11 metal coatings will be investigated using atomic force microscopy and scanning electron microscopy. The composition of the galvanically deposited coatings will be investigated using energy dispersive X – ray and X – ray photoelectron spectroscopy.

1.4 References

1. P. Atkins and J. de Paula, *Atkins' Physical Chemistry*, Oxford University Press, Oxford, 8th edn., 2006.
2. P. Atkins and J. de Paula, *Atkins' Physical Chemistry*, Oxford University Press, Oxford, 8th edn., 2006.
3. A. P. Abbott and D. L. Davies, *WO. 2000056700*, 2000.
4. A. P. Abbott, G. Capper, D. L. Davies, H. L. Munro, R. K. Rasheed, and V. Tambyrajah, *Chem. Comm.*, 2001, 2010 – 2011.
5. N. Koura, T. Endo, and Y. Idemoto, *J. Non-Cryst Solids*, 1996, **205**, 650 – 655.

6. A. P. Abbott, J. C. Barron, K. S. Ryder, and D. Wilson, *Chem. Eur. J.*, 2007, **13**, 6495 – 6501.

7. A. P. Abbott, G. Capper, D. L. Davies, and R. Rasheed, *Inorg. Chem.*, 2004, **43**, 3447 – 3452.

8. A. P. Abbott, F. Qiu, H. M. A. Abood, R. M. Ali, and K. S. Ryder, *Phys. Chem. Chem Phys.*, 2010, **12**, 1862 – 1872.

9. W.-G. Xu, X.-M. Lu, Q. Zhang, J.-S. Gui, and J.-Z. Yang, *Chinese J. Chem.*, 2006, **24**, 331 – 335.

10. A. P. Abbott, G. Capper, D. L. Davies, and R. K. Rasheed, *Chem. Eur. J.*, 2004, **10**, 3769 – 3774.

11. A. P. Abbott, G. Capper, D. L. Davies, R. K. Rasheed, and V. Tambyrajah, *Chem. Comm.*, 2003, 70 – 71.

12. A. P. Abbott, D. Boothby, G. Capper, D. L. Davies, and R. K. Rasheed, *J. Am. Chem. Soc.*, 2004, **126**, 9142 – 9147.

13. A. P. Abbott, G. Capper, B. G. Swain, and D. A. Wheeler, *T. I. Met. Finish.*, 2005, **83**, 51 – 53.

14. A. P. Abbott, *WO 2007003956*, 2007.

15. H. M. A. Abood, A. P. Abbott, A. D. Ballantyne, and K. S. Ryder, *Chem. Comm.*, 2011, **47**, 3523 – 2525.

16. J. Hartley, Ph.D. Thesis, University of Leicester, 2013.

17. B. Tang and K. H. Row, *Monatshefte für Chemie - Chem. Mon.*, 2013, **144**, 1427–1454.

18. Q. Zhang, K. De Oliveira Vigier, S. Royer, and F. Jérôme, *Chem. Soc. Rev.*, 2012, DOI: 10.10.

19. *1-butyl -3-methylinidazolium chloride,* MSDS No. 94128, Sigma Aldirch, Gillingham, Dorset.

20. A. P. Abbott, G. Capper, K. J. McKenzie, A. Glidle, and K. S. Ryder, *Phys. Chem. Chem. Phys.*, 2006, **8**, 4214 – 4221.

21. A. P. Abbott, N. Dsouza, P. Withey, and K. S. Ryder, *Trans. I. Met. Finish.*, 2012, **90**, 9 – 14.

22. A. P. Abbott, G. Capper, K. J. McKenzie, and K. S. Ryder, *J. Electroanal. Chem.*, 2007, **599**, 288 – 294.

23. J. M. Hartley, C.-M. Ip, G. C. H. Forrest, K. Singh, S. J. Gurman, K. S. Ryder, A. P. Abbott, and G. Frisch, *Inorg. Chem.*, 2014, **53**, 6280 – 6288.

24. A. P. Abbott, K. El Ttaib, G. Frisch, K. J. McKenzie, and K. S. Ryder, *Phys. Chem. Chem. Phys.*, 2009, **11**, 4269 – 4277.

25. A. P. Abbott, K. El Ttaib, G. Frisch, K. S. Ryder, and D. Weston, *Phys. Chem. Chem Phys.*, 2012, **14**, 2443 – 2449.

26. M. R. Ali, M. Z. Rahman, and S. S. Saha, *Indian J. Chem. Techn.*, 2014, **21**, 127 – 133.

27. J. C. Malaquias, M. Steichen, M. Thomassey, and P. J. Dale, *Electrochim. Acta.*, 2013, **103**, 15 – 22.

28. Y. H. You, C. D. Gu, X. L. Wang, and J. P. Tu, *Surf. Coatings Technol.*, 2012, **206**, 3632 – 3638.

29. M. Steichen, M. Thomassey, S. Siebentritt, and P. J. Dale, *Phys. Chem. Chem. Phys.*, 2011, **13**, 4292 – 4302.

30. C. E. Housecroft and A. G. Shapre, in *Inorganic chemistry,* Pearson Education Limited, Harlow, 2008, 3 rd edn., ch. 22, pp. 734 - 736.

31. A. P. Abbott, G. Frisch, S. J. Gurman, A. R. Hillman, J. Hartley, F. Holyoak, and K. S. Ryder, *Chem. Commun. (Camb).*, 2011, **47**, 10031 – 10033.

32. C. Hardacre, *Annu. Rev. Mater. Res.*, 2005, **35**, 29 – 49.

33. J. Estager, J. D. Holbrey, M. Swadźba – Kwaśny, *Chem. Soc. Rev.*, 2014, **43**, 847 – 886.

34. A. P. Abbott, S. Nandhra, S. Postlethwaite, E. L. Smith, and K. S. Ryder, *Phys. Chem. Chem Phys.*, 2007, **9**, 3735 – 3743.

35. X. Wei, L. Yu, D. Wang, X. Jin, and G. Z. Chen, *Green Chem.*, 2008, **10**, 296 – 305.

36. C.D. Gu and J.-P. Tu, *RSC Adv.*, 2011, **1**, 1220 – 1227.

37. W. Canning plc., in *The Canning Handbook*, E. & F. N. Spon Ltd., London, 21 st ed., 1970, Ch. 16, pp. 488.

38. W. Canning plc., in *The Canning Handbook*, E. & F. N. Spon Ltd., London, 21 st ed., 1970, Ch. 13, pp. 375.

39. A. R. Hillman, *J. Solid State Electrochem.*, 2011, **15**, 1647 – 1660.

40. M. Stratmann and G. S. Frankel, in *Encyclopedia of Electrochemistry*, ed. A. J. Bard and M. Stratmann, Wiley-VCH GmbH & Co. KGaA, Weinheim, 2003, vol. 4, ch. 1, pp. 3 - 24.

41. P. Atkins and J. de Paula, in *Atkins' Physical Chemistry*, Oxford University Press, Oxford, 8th edn., 2006, ch. 7, pp. 222 - 224.

42. P. Atkins and J. de Paula, in *Atkins' Physical Chemistry*, Oxford, 8th edn., 2006, ch. 7, pp. 218 - 220.

43. J. Mittal, Y. W. Lin, and K. L. Lin, *Appl. Surf. Sci.*, 2010, **256**, 3531 – 3540.

44. M. Arra, D. Shangguan, D. Xie, J. Sundelin, T. Lepistö, and E. Ristolainen, 2004, **33**, 977 – 990.

45. W. Wang, A. Choubey, M. H. Azarian, and M. Pecht, *J. Electron. Mater.*, 2009, **38**, 815 – 827.

46. A. Safaee, D. Sarkar, and M. Farzaneh, *Appl. Surf. Sci*, 2008, **254**, 2493 – 2498.

47. C. Gu, H. Ren, J. Tu, and T.-Y. Zhang, *Langmuir*, 2009, **25**, 12299 – 12307.

48. Z. Cao, D. Xiao, L. Kang, Z. Wang, S. Zhang, Y. Ma, H. Fu and J. Yao, *Chem. Comm.* 2008, 2692 – 2694.

49. Y. S. Won, S. S. Park, J. Lee, J.-Y. Kim, and S.-J. Lee, *Appl. Surf. Sci.*, 2010, **257**, 56 – 61.

50. R. C. Agarwala and V. Agarwala, *Sadhana*, 2003, **28**, 475 – 493.

51. C. Durante, V. Perazzolo, A. A. Isse, M. Favaro, G. Granozzi and A. Gennaro, *ChemElectrochem.*, 2014, **1**, 1370 – 1381.

52. L. Tamašauskaitė-Tamašiūnaitė, A. Balčiūnaitė, A. Zabielaitė, I. Stankevičienė, V. Kepenienė, A. Selskis, R. Juškėnas, and E. Norkus, *J. Electroanal. Chem.*, 2013, **700**, 1 – 7.

53. D. Zhao, X. Xiong, C. L. Qu and N. Zhang, *J. Phys. Chem. C*, 2014, **118**, 19007 – 19016.

54. S. M. Alia, B. S. Pivovar, and Y. Yan, *J. Am. Chem. Soc.*, 2013, **135**, 13473 – 13478.

55. D.-Y. Park, H. S. Jung, Y. Rheem, C. M. Hangarter, Y.-I. Lee, J. M. Ko, Y.-H. Choa, and N. V. Myung, *Electrochim. Acta*, 2010, **55**, 4212 – 4216.

56. C. D. Gu, X. J. Xu, and J. P. Tu, *J. Phy. Chem. C*, 2010, **114**, 13614 – 13619.

57. A. P. Abbott, J. Collins, I. Dalrymple, R. Harris, R. Mistry, F. Qiu, J. Scheirer and W. Wise, *Aust. J. Chem.*, 2009, **62**, 341 – 347.

58. A. P. Abbott, G. Capper, D. L. Davies and P. Shikotra, *Trans. Inst. Min. Metall. C*, 2006, **115**, 15 – 18.

Chapter 2: Experimental

2.1 General Experimental Procedure

Unless otherwise stated all experimental procedures were carried out under ambient conditions. All chemicals were obtained from Sigma Aldrich, Alfa Aesar or Acros, were used as received and had a purity of at least 99%. Anopol Cleaner C was obtained from Anopol. Kwiky-Mask was obtained from GreenTree-Sherconn. Copper hull cell test panels were obtained from Schloetter Plating Technology. Iridium oxide coated titanium electrodes were obtained from DeNora.

All voltammetry experiments were performed using a FRA2 µAutolab type III potentiostat, run using GPES software. Precious metal coated quartz crystals were obtained from the International Crystal Manufacturing Company. The crystals were AT cut quartz crystals with piezoelectric active electrode area of 0.205 cm^2. Polished Au coated quartz crystals had 100 Å of Cr, as a binding layer, and 1000 Å of Au, as the electrode surface. Polished Pt coated quartz crystals had 100 Å of Ti, as a binding layer, and 1000 Å of Pt, as the electrode surface. Etched Au coated quartz crystals, had 1000 Å of Au as the electrode surface. Impedance spectra were recorded every *ca*. 3 – 4 s, using a Hewlett Packard HP8751A network analyser. Electrochemical Quartz crystal microbalance (EQCM) experiments were performed using a µAutolab type III potentiostat, run using GPES software. The potentiostat was connected to the network analyser *via* Solartron Schlumberger 7060 system voltmeters, to record the voltammetric data. Alternatively EQCM was performed using a Gamry Instruments eQCM 10 M was used to record reduced impedance spectra, every ca. 0.2 s, and a Gamry Instruments Reference 600 Potentiostat/ Galvanostat/ ZRA. Ultraviolet – Visible (UV-Vis) spectroscopy was performed using a Perkin Elmer, *Lambda* 850, with a heated cuvette holder manufactured by the workshop in the Department of Chemistry at the University of Leicester. Spectroscopy was performed using Hellma Analytics, synthetic quartz glass cuvettes, path length 1 cm. Atomic force microscopy (AFM) was performed using a Digital Instruments Nanoscope IV, Dimension 3100 instrument run by Nanoscope 6.12 software. AFM images were obtained in resonance mode using a Veeco cantilever (model: RTESP, part MPP-11100-10). Scanning electron microscopy (SEM) and energy dispersive X-ray spectroscopy (EDX) was performed using two machines; a Philips XL30 ESEM, or a FEI Sirion 200 FEG SEM. X-ray photoelectron spectroscopy (XPS) was performed on two instruments; a Scienta ESCA 300 photoelectron spectrometer, or a Thermo Scientific K – Alpha .

2.2 Synthesis of the Deep Eutectic Solvent Ethaline 200

Ethaline 200 was produced by stirring choline chloride (279 g, 2 mol) and ethylene glycol (248 g, 4 mol) at 50 ^{o}C, until a viscous, clear, colourless and homogenous solution was formed.[1]

2.3 Voltammetry

2.3.1 Cyclic Voltammetry of Group 10 & 11 Metal Salt

Cyclic voltammetry (CV) in Ethaline 200 was performed using a three electrode cell consisting of: 2 mm (diameter) Pt disc working electrode, Pt foil flag counter electrode, and Ag wire *pseudo* reference electrode. Prior to each experiment the working electrode was polished using 0.05 μm alumina and rinsed using water and ethanol. CV was performed at a scan rate of 10 mVs^{-1} and a step potential of 0.45 mV.

The CV of Ethaline 200 (10 mL) was performed , at varying temperature of 30 – 130 ^{o}C with 20 ^{o}C increments, was performed between 1 V and – 1 V.

The CV of metal salts dissolved in Ethaline 200 (10 mL), at room temperature was performed as shown in *Table 2.1*. The potential windows were chosen to start in a region where no electrochemical activity occurs, scan across all the reduction potentials present in the electrochemical window of Ethaline and return across the oxidation potential to the start potential.

Table 2.1: Conditions for cyclic voltammetry experiments at room temperature.

Metal Salt	Weight / mg	Conc. / mM	Moles / mmol	Potential window / V
CuCl	10	10	0.1	0.2 to – 0.6
AgCl	28	20	0.2	0.5 to – 0.5
AuCl	46	20	0.2	1.0 to – 0.5
$PdCl_2$	35	20	0.2	1.0 to – 1.0

The CVs of metal salt solutions, dissolved in Ethaline 200 (10 mL), at varying temperature of 30 – 130 ^{o}C with 20 ^{o}C increments, was performed as shown in *Table 2.2*. Varying temperature was required to obtain a well defined electrochemical response. Potential windows were chosen to start in a region where no electrochemical activity occurs, scan across the reduction potential and return across the oxidation potential to the start potential.

Table 2.2: Conditions for cyclic voltammetry experiments at variable temperature.

Metal Salt	Weight / mg	Conc. / mM	Moles / mmol	Potential window / V
$CuCl_2$	13	10	0.1	1 to – 1.0
$NiCl_2$	12	10	0.1	1 to – 1.0
$PtCl_2$	27	10	0.1	0.8 to – 0.8

The CV of mixed metal salt solutions, dissolved in Ethaline 200 (20 mL), was performed as shown in *Table 2.3*. The potential windows were chosen to start in a region where no electrochemical activity occurs, scan across all reduction potentials present in the electrochemical window of Ethaline and return across the oxidation potential to the start potential.

Table 2.3: Conditions for mixed metal cyclic voltammetry experiments.

Metal Salt	Weight / mg	Conc. / mM	Moles / mmol	Potential window / V	Temp. / ^{o}C
$CuCl_2$ and AgCl	27 and 29	10	0.2	0.9 to – 0.8	30
$CuCl_2$ and AuCl	27 and 47	10	0.2	0.9 to – 0.8	30
$CuCl_2$ and $NiCl_2$	27 and 26	10	0.2	0.9 to – 0.8	130
$CuCl_2$ and $PdCl_2$	27 and 36	10	0.2	0.9 to – 0.8	30
$CuCl_2$ and $PtCl_2$	27 and 53	10	0.2	0.8 to – 0.8	130

2.3.2 Linear Sweep Voltammetry of Deposited Nickel

Nickel was deposited on the surface of a working electrode from an aqueous solution. This allows for LSV to be performed on nickel in Ethaline at temperatures lower than required for nickel deposition from Ethaline.

Chronoamperometry was performed in water using a three electrode cell; 2 mm (diameter) Pt disc working electrode, Pt flag counter electrode and Ag/AgCl wire *pseudo* reference electrode. Prior to each experiment the working electrode was polished using 0.05 μm alumina and rinsed using water and ethanol and conditioned at: 0.3 V, at 70 ^{o}C, for 30 s in aqueous nickel solution.

Nickel was deposited via chronoamperometry, performed at – 0.7 V, at 70 ^{o}C, for 10 s, using an aqueous nickel solution (10 mL) from the Canning HandBook containing: $NiSO_4.6H_2O$ (300 g, 1.14 mol, 1.14 M), NaCl (30 g, 0.51 mol, 0.51 M), $B(OH)_3$ (40 g, 0.65 mol, 0.65 M), water (1000 mL).[2] These conditions were determined from the voltammetry of the aqueous nickel solution. The deposit was washed with water and ethanol, and dried using nitrogen gas.

Linear sweep voltammetry (LSV), in Ethaline 200 solutions, was performed using a three electrode cell; 2 mm (diameter) Pt disc working electrode, Pt flag counter electrode and Ag wire *pseudo* reference electrode. Prior to each experiment the working electrode was electrolytically plated with Ni, using the above method. LSV was performed at a scan rate of 10 mVs^{-1} and a step potential of 0.45 mV.

The LSV of Ni, platted from the aqueous nickel solution on to a working electrode, in Ethaline 200 (10 mL), at varying temperature of 30 – 130 ^{o}C with 20 ^{o}C increments, was performed between 0 V and 1 V.

2.4 Electrochemical Quartz Crystal Microbalance

2.4.1 Cyclic Voltammetry of Group 10 & 11 Metal Salts

The EQCM of metal salts was performed to determine the rate and current efficiency of the reduction and oxidation of the group 10 and 11 metals.

An EQCM was used to perform cyclic voltammetry in Ethaline 200. The cyclic voltammetry was performed using a three electrode cell,[3] Pt QCM crystal working electrode, Pt mesh flag counter electrode, and Ag wire *pseudo* reference electrode. Prior to each experiment, the working electrode was washed with DI water and ethanol. CV was performed at scan rate of 10 mVs^{1} and a step potential of 1 mV.

The CV / EQCM of Ethaline 200 (20 mL) was performed, at varying temperature of 30 – 130 ^{o}C with 20 ^{o}C increments, was performed between 0.8 V and – 0.8 V.

The CV / EQCM of metal salts dissolved in Ethaline 200 (10 mL), at 30 ^{o}C was performed as shown in *Table 2.4*. The experiment for $PtCl_2$ was performed in Ethaline (20 mL) at 130 ^{o}C, *Table 2.4*. Potential windows were chosen as shown appropriate from the experiments outlined in section *2.3.1*.

Table 2.4: Conditions for the CV / EQCM experiments.					
Metal Salt	Weight / mg	Conc. / mM	Moles / mmol	Potential window / V	Temp. / ^{o}C
CuCl	10	10	0.1	0.0 to – 0.7	30
AgCl	14	10	0.2	0.35 to – 0.35	30
AuCl	46	20	0.2	1.0 to 0.3	30
$PdCl_2$	17	10	0.1	0.9 to – 0.8	30
$PtCl_2$	53	20	0.2	0.8 to – 0.8	130

The CV / EQCM of metal salt solutions, dissolved in Ethaline 200 (20 mL), at varying temperature of 30 – 130 ^{o}C with 20 ^{o}C increments, was performed as outlined in T*able 2.5*. Potential windows were chosen as shown appropriate from the experiments outlined in section *2.3.1*.

Table 2.5: Conditions for the CV / EQCM experiments at variable temperature.				
Metal Salt	Weight / mg	Conc. / mM	Moles / mmol	Potential window / V
$CuCl_2$	26	10	0.2	0.8 to – 0.8
$NiCl_2$	25	10	0.2	0.9 to – 0.8

The CV / EQCM of mixed metal salt solutions, dissolved in Ethaline 200 (20 mL), was performed as outlined in *Table 2.6*. Potential windows were chosen as shown appropriate from the experiments outlined in section *2.3.1*.

Table 2.6: Conditions for mixed metal CV / EQCM experiments.					
Metal Salt	Weight / mg	Conc. / mM	Moles / mmol	Potential window / V	Temp. / ^{o}C
$CuCl_2$ and AgCl	27 and 29	10	0.2	0.9 to – 0.8	30
$CuCl_2$ and AuCl	27 and 47	10	0.2	0.9 to – 0.8	30
$CuCl_2$ and $NiCl_2$	27 and 26	10	0.2	0.9 to – 0.8	130
$CuCl_2$ and $PdCl_2$	27 and 36	10	0.2	0.9 to – 0.8	30
$CuCl_2$ and $PtCl_2$	27 and 53	10	0.2	0.8 to – 0.8	130

2.4.2 Linear Sweep Voltammetry of Deposited Nickel

Nickel was deposited on the surface of a working electrode from an aqueous solution. This was transferred to an Ethaline solution, meaning the rate and current efficiency of the nickel oxidised in Ethaline at temperatures lower than required for nickel deposition from Ethaline.

Chronoamperometry was performed in water using a three electrode call; Pt QCM crystal working electrode, Pt flag counter electrode and Ag/AgCl wire *pseudo* reference electrode. Prior to each experiment, the working electrode was rinsed using water and ethanol and conditioned at: 0.3 V, at 70 ^{o}C, for 30 s in aqueous nickel solution.

Nickel was deposited via chronoamperometry, performed at – 0.7 V, at 70 ^{o}C, for 60 s, using an aqueous nickel solution (10 mL) containing: $NiSO_4.6H_2O$ (300 g, 1.14 mol, 1.14 M), NaCl (30 g, 0.51 mol, 0.51 M), $B(OH)_3$ (40 g, 0.65 mol, 0.65 M), water (1000 mL).[2] The deposit was washed with water and ethanol, and dried using nitrogen gas.

The LSV of Ni in Ethaline 200 (20 mL), at varying temperature of 30 – 130 ^{o}C with 20 ^{o}C increments, was performed between 0 V and 0.8 V.

2.5 Ultraviolet – Visible Spectroscopy

UV – Vis spectroscopy was performed at a frequency step of 0.5 nm, between 800 – 200 nm. Before spectra were recorded the instrument was set up and calibrated. The conditions for the UV – Vis experiments are outlined in *Table 2.7*. The varying temperature experiments were performed from 30 – 130 ^{o}C with 20 ^{o}C increments.

Table 2.7: Conditions for UV – Vis experiments.

Metal Salt	Weight / mg	Conc. / mM	Moles / mmol	Vol. / mL	Temp. / ^oC
$CuCl_2$	13	10	0.1	10	Variable
CuCl	2	1	0.02	20	30
AgCl	3	1	0.02	20	30
AuCl	4	1	0.02	20	30
$NiCl_2$	13	10	0.1	10	Variable
$PdCl_2$	4	1	0.02	20	30
$PtCl_2$	6	1	0.02	20	30 and 130

2.6 Galvanic Coatings on a Copper Substrate

2.6.1 Preparation of Copper Substrate

A Cu Hull cell test piece was cut to size (dimensions: 0.370 dm x 0.076 dm, surface area: 0.056 dm^2). The pieces were degreased by immersion in Anopol Cleaner C for 300 s and washed twice by immersion in deionised (DI) water for 60 s. The washed pieces were etched for 60 s by immersion in an ammonium persulfate solution (10 mL) containing: ammonium persulfate (200 g, 0.876 mol, 0.876 M), H_2SO_4 (50 g, 0.51 mol, 0.51 M) in water (1 L). The etched pieces were washed twice by immersion in DI water for 60 s. Copper was electrolytically plated at 2 A dm^{-2} for 720 s, using an iridium oxide coated titanium anode and an acid copper solution (50 mL) containing: $CuSO_4.2H_2O$ (150 g, 0.60 mol, 0.60 M), H_2SO_4 (50 g, 0.51 mol, 0.51 M), ethanol (50 g, 1.1 mol, 1.1 M), water (1L).[4] Rinsed using DI water, methanol and dichloromethane respectively for 1 min and dried using compressed air. The procedure produced a uniform non-reflective copper coating.

Kwiky-Mask was applied to the top half of the copper substrate and left to dry for 30 min.

As a final preparation step, the copper substrate was etched by immersion in an ammonium persulfate solution (10 mL), for 60 s. Thereafter, it was rinsed in DI water then methanol for 60 s each and dried using compressed air.

2.6.2 Galvanic Coatings on a Copper Substrate

The prepared copper substrates were immersed in metal chloride solutions (10 mL), *Table 2.8*. The resulting coating was rinsed in DI water then methanol for 60 s each, dried using compressed air and the Kwiky-Mask was peeled away. The procedure produces uniform coatings that were characterised by AFM, SEM, EDX and XPS.

Table 2.8: Conditions for the galvanic deposition of the group 10 & 11 elements.

Metal Salt	Weight / mg	Conc. / mM	Moles / mmol	Time / s	Temp. / ^{o}C
AgCl	143	100	1	120	50
AuCl	232	100	1	600	50
$NiCl_2$	129	100	1	600	130
$PdCl_2$	177	100	1	120	50
$PtCl_2$	26	10	0.1	600	130

2.6.3 Preparation for Quartz Crystal Microbalance Measurements

The resonance frequency of an etched gold QCM crystal was recorded.

The QCM was electrolyticly plated using a three electrode cell consisting of: Au QCM crystal working electrode, Pt mesh counter electrode, Ag/AgCl wire *pseudo* reference electrode. Copper was plated at 2 A dm^{-2} for 60 s, 120 s or 180 s, using an aqueous acid copper solution (25 mL).[4] The coated crystal was then rinsed using DI water, methanol and dichloromethane respectively for 1 min and dried using compressed air. The resonance frequency of the copper plated QCM was recorded.

2.6.4 Stoichiometry Experiments using a Quartz Crystal Microbalance

After plating, the copper coated QCMs were immersed in metal chloride solution (10 mL), *Table 2.9*. The experiment was allowed to proceed until completion, judged to be when there was no longer a change in frequency of the QCM. The resulting coatings were washed using DI water then methanol then DCM for 60 s and dried using compressed air. The resonance frequency of the metal plated QCMs was recorded. The procedure was repeated for each time scale described in section *2.6.3*.

Table 2.9: Conditions for the QCM experiments measuring the galvanic deposition of the group 10 & 11 elements.

Metal Salt	Weight / mg	Conc. / mM	Moles / mmol	Time / s	Temp. / ^{o}C
AgCl	143	100	1	120	50
AuCl	232	100	1	600	50
$NiCl_2$	129	100	1	600	130
$PdCl_2$	177	100	1	120	50
$PtCl_2$	26	10	0.1	600	130

2.8 Techniques

2.8.1 Voltammetry

Cyclic voltammetry and linear sweep voltammetry are both types of linear potential sweep techniques, where the potential is swept at a constant rate between two potential vertices and the resulting change in current is measured with respect to the of change in potential. The change in voltage is controlled using a three electrode cell.

Voltammetry allows the study of redox behaviour of species in solution *e.g.* $\mathrm{Cu^{2+}_{(l)} + e^- \rightarrow Cu^{+}_{(l)}}$, as well as the deposition and stripping of molecules on the surface of the working electrode *e.g.* $\mathrm{Cu^{+}_{(l)} + e^- \rightarrow Cu^{0}_{(s)}}$, *Figure 2.1*.

The electrode potentials are calculated by taking the average of the onset reduction and oxidation potentials. *Figure 2.1* demonstrates calculation of the electrode potential (E), where the red lines represent the determination of the onset reduction potentials and the blue lines represent the determination of the onset oxidation potentials. Once the onset potentials of a given redox couple has been determined, the electrode potential is calculated by taking an average of the two points.[5] By using the Nernst equation, it is possible to caluclate the formal electrode potential. The formal electrode potential is where all conditions are the same as standard conditions except the referance electrode is not a standard hydrogen electrode.

This method of electrode potential determination was used as most of the redox couples under analysis were either quasi-reversible or irreversible redox couples, *i.e.* the electrochemical deposition and stripping of metals on the surface of an electrode. These processes are susceptible to kinetic and chemical environment influences, hence the error in the potentials caused by these effect is mitigated by employing the above method. Also, dissolution and deposition of metals on to an electrode surface require a phase change. This means depending on the amount of metal deposited on the surface of the electrode the voltage of the peak current will change.

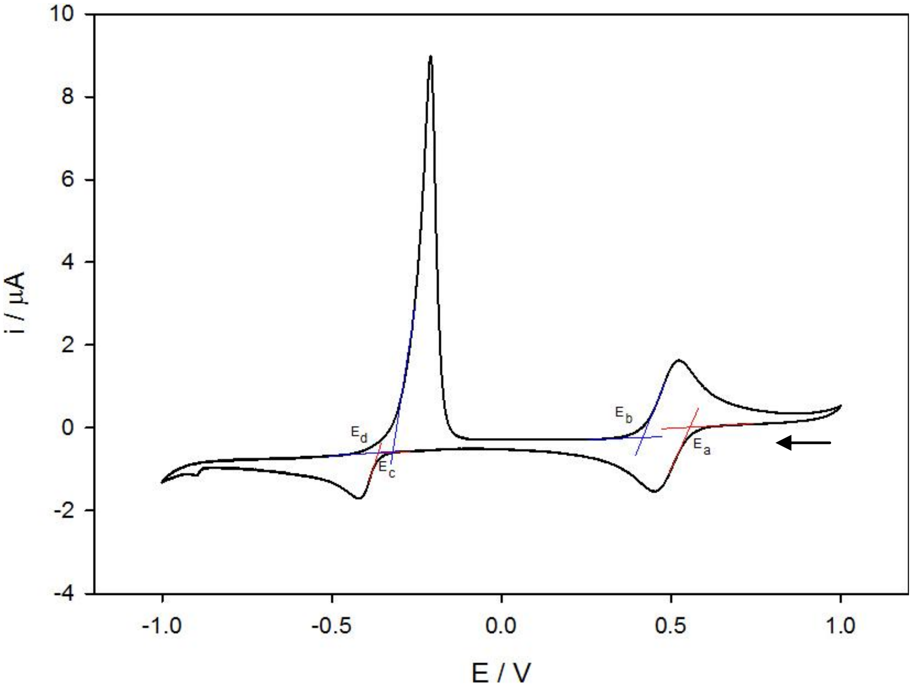

Figure 2.1: Cyclic voltammetry of 10 mM $CuCl_2$ *dissolved in Ethaline 200. Pt working electrode, 3.14 x* 10^{-2} cm^2*. Pt flag counter electrode. Ag wire reference electrode.* E_a *and* E_b *represent the onset reduction and oxidation potentials of the Cu (II)/(I) respectively.* E_c *and* E_d *represent the onset reduction and oxidation potentials of the Cu (I)/(0) respectively.*

Reversible redox couples, such as the Cu (II)/(I) couple in *Figure 2.1*, are represented by a well defined response in the measured current, where both the anodic and cathodic currents pass a similar charge and there is a small separation in the peak potentials.[6] The profile of the current response in a reversible system is defined by the sum of Butler – Volmer kinetics and diffusion of ions from the bulk solution in to the electrical double layer.[7]

Butler – Volmer kinetics are be used to describe rate of the electrochemical reactions with respect to potential, were both the cathodic and anodic reactions are occuring. Where the rate of reaction is an exponential function with respect to potential applied to the cell less the formal electrode potential, equations **(2.1a)** and **(2.1b)**. Where k_c and k_a are the rate constants for reduction and oxidation of the species under investigation respectively, E_f^o is the formal electrode potential of the redox couple under investigation, α and β are the transfer coefficients and k^o is the standard electrochemical rate constant.[8]

$$k_c = k^o \exp\left[\frac{-\alpha F\,(E - E_f^o)}{RT}\right] \quad (\mathbf{2.1a})$$

$$k_a = k^o \exp\left[\frac{\beta F\,(E - E_f^o)}{RT}\right] \quad (\mathbf{2.1b})$$

In terms of current in a cyclic voltammogram, where a constant scan rate is applied, as the voltage increases linearly with respect to time, the rate of reaction and hence the current will increase exponentially with respect to time. Up until the electrical double layer is depleted of an excess of species that can undergo electrochemical reaction and diffusion of species from the bulk of the solution in to the double layer is required for reaction to occur.[7]

Diffusion occurs when ions from a high concentration of the bulk solution, diffuse to the interfacial region where there is a low concentration of ions. This to try and establish an equilibrium, where the entire solution is of the same concentration. The concentration of electroactive species in the environment adjacent to the electrical double layer, will be depleted species. The thickness of this depleted layer, commonly known as the diffusion layer, increases with time and hence the concentration of electroactive species that can diffuse to the electrode is decreased, which leads to a decrease in the current of the cell. The decrease in current with respect to time is the reciprocal of the square route of time, represented by the Cottrell equation **(2.2)**. Where n is the number of electrons passed in the reaction at the electrode, A is the area of the electrode, D is the diffusion coefficient, c^* is the concentration of electroactive species and t is time.[9]

$$\mathrm{I} = \frac{\mathrm{nFA}\sqrt{\mathrm{D}}\mathrm{c}^*}{\sqrt{\pi \mathrm{t}}} \quad (\mathbf{2.2})$$

The Cu (I)/(0) redox couple, represented above, displays quasi-reversible behaviour for the deposition and dissolution of copper from the surface of an electrode.

The wave form of the deposition of the copper on the surface of the electrode is similar to that of the reversible couple. Where the initial rate of deposition and hence the current, is controlled by the potential of the cell compared to the formal electrode potential and the second stage of deposition is controlled by the diffusion of Cu (I) ions into the electrical double layer.

However, for the dissolution of metal from the surface of the electrode, the current associated with dissolution is completely controlled by the potential of the cell. As the species being oxidised is immobilised on the surface of the electrode, it is not required that the electroactive species undergoes diffusion to the electrode. This means that the current on the surface of the electrode will increase exponentially until all of the deposited metal has been removed from the surface, where upon the current will sharply drop. This affect can also be cause by passivation where a salt film completely covers the surface of the electrode, preventing the further electrochemical reaction of the underlying species. However, if this film undergoes dissolution a secondary current peak will be observed.

Finally, the third type of electrochemical behaviour is irreversible behaviour. This is characterised by a large potential difference in the peak separation for corresponding oxidative and reductive processes. The effect of which means that a large over potential, greater than the formal electrode potential, is required for either process to occur, at the formal electrode potential there is no electrochemical activity. This is unlike in the reversible system, where at the formal electrode potential, the forward and backward reactions are occurring at the same rate.[6]

An example of reversible electrochemical process is the $[Fe(CN)_6]^{3-}/[Fe(CN)_6]^{4-}$ redox couple and an example of an irriversible system is the $[Co(NH_3)_6]^{3+}/[Co(NH_3)_6]^{2+}$.

2.8.2 Quartz Crystal Microbalance

A quartz crystal microbalance is made of a wafer of quartz, where upon each side of the wafer metal electrodes have been sputter coated. With electrodes either side of the quartz wafer, it is possible to produce an alternating potential across the wafer. When a potential is applied to quartz crystal, the crystal undergoes a mechanical deformation. If an alternating voltage is applied to a crystal wafer, it is possible to make the microbalance oscillate at a specific frequency with respect to the mass on the surface of the crystal.[9] As the mass on the surface of the microbalance changes, the frequency at which the microbalance vibrates will also change, i.*e.* as the mass on the surface increases, the frequency at which the crystal oscillates will be reduced. It is possible to calculate the mass deposited on the surface of the crystal using the Sauerbrey equation **(2.3)**.[10,11]

$$\frac{\Delta f}{\Delta m} = \frac{-2 f_o^2}{A\sqrt{\rho_q\ \mu_q}} \quad (\mathbf{2.3})$$

where Δf represents the change in frequency of the crystal, Δm is the change in mass on the surface of the crystal, f_o is the resonant frequency of the crystal, A is the piezoelectric active area, ρ_q is the density of quartz and μ is the shear modulus of quartz. Hence, the change in mass is proportional to the change in frequency as all of the values on the right hand side of equation **(2.3)** are constants. It should be noted that the above equation applies to rigid, thin films, where the film must be significantly thinner than the thickness of the quartz crystal.

When immersed in a viscous liquid, such as a Deep Eutectic Solvent, energy can be transferred from the microbalance to the liquid. This causes a decrease in the resonance frequency of the crystal, as well as broadening of the peak.[12]

As precious metals are used to produce the electrodes that drive the QCM, it is also possible to use one of these electrodes as an electrode to perform electrochemistry, this is called an electrochemical quartz crystal microbalance EQCM. Hence it is possible to simultaneously measure the change in mass on the surface, the current passed in the solution and the time of the reaction.

From the data gathered from an EQCM experiment, it is possible to calculate the rate of electrochemical deposition of metal films, as long as the pure metal is the only thing being deposited. If the change in mass for the electrochemical deposition is a linear trend with respect to time, it is possible to covert the change in mass with respect to time to a change in moles with respect to time using equation **(2.4)**. Where RMM represents relative molecular mass, m represents mass, mol represents moles and t represents time.

$$\frac{\Delta \mathrm{m}}{\Delta \mathrm{t}} = \frac{\Delta \mathrm{mol}}{\Delta \mathrm{t}} \text{ x RMM} \qquad (\mathbf{2.4})$$

The value of the change in moles with respect to time is then easily converted a rate of deposition by dividing by the surface area of the electrode. Equation **(2.5)**, where A is the area of the electrode.

$$\text{Rate of Deposition} = \frac{\Delta \text{mol}}{\Delta \text{t x A}} \quad \mathbf{(2.5)}$$

It is also possible to calculate the current efficiency for the deposition of metals, by recording the change in charge with respect to change in mass. By plotting this data, if there is a linear trend, the gradient of the plot will be a value called the mass – charge ratio. If the plot is not linear, the mass – charge ration is not constant. Once the value of the mass – charge ratio is established, it can be compared to the theoretical mass – charge ratio, to establish the current efficiency of an electrolytic deposition.

It is possible to calculate a theoretical mass – charge ratio using Faraday's Law, equation **(2.6a)**. Once the theoretical mass – charge ratio is established the current efficiency is calculated using equation **(2.6b)**.

$$\text{Theo}\frac{\delta \text{m}}{\delta \text{Q}} = \frac{\text{RMM}}{\text{nF}} \quad \mathbf{(2.6a)}$$

$$\text{Current Efficiency} = \frac{\text{Exp}\frac{\delta \text{m}}{\delta \text{Q}}}{\text{Theo}\ \frac{\delta \text{m}}{\delta \text{Q}}} \text{ x } 100 \quad \mathbf{(2.6b)}$$

The mass – charge ratio has some limitations, discussed in a paper by Hillman.[13] It is discussed that absorbed species or electrolyte, trapped in electrochemically deposited film, can lead to mass on the surface of the QCM that can convolute the results of mass – charge ratio analysis. Also, it is discussed that if the deposited layer is acoustically thick or "soft" that the change in frequency of the QCM will also be affected.

A further application of the mass – charge ratio is to calculate the ratio of metals that are electrolyticly deposited in a binary system, *i.e.* a copper and silver system, equation **(2.7)**.[14] The results of these experiments can be used to analyse how a binary system may alloy or de – alloy or form a co - deposit.

$$\chi_{\mathrm{Cu}} = \frac{(\mathrm{RMM}_{\mathrm{Ag}} - \frac{\delta \mathrm{m}}{\delta \mathrm{Q}}\mathrm{F})}{(\frac{\delta \mathrm{m}}{\delta \mathrm{Q}}\mathrm{F} - \mathrm{RMM}_{\mathrm{Cu}} + \mathrm{RMM}_{\mathrm{Ag}})} \quad \mathbf{(2.7)}$$

It should be noted however, that the above equation **(2.7)**, assumes that the current efficiency of the deposition is 100%. As discussed above the current efficiency for the deposition of both in a binary system can be calculated. As an attempt to quantify to the ratio of deposited metals, taking in to account the current efficiency, equation **(2.8)** was derived, **Appendix 1**.

$$\chi_{\mathrm{Cu}} = \frac{(\mathrm{RMM}_{\mathrm{Ag}} - \frac{\delta \mathrm{m}}{\delta \mathrm{Q}}\mathrm{Fb})}{(\frac{\delta \mathrm{m}}{\delta \mathrm{Q}}2\mathrm{Fa} - \frac{\delta \mathrm{m}}{\delta \mathrm{Q}}\mathrm{Fb} - \mathrm{RMM}_{\mathrm{Cu}} + \mathrm{RMM}_{\mathrm{Ag}})} \quad \mathbf{(2.8)}$$

Where a is the reciprocal of the current efficiency for the deposition of copper and b is the reciprocal of the current efficiency for the deposition of silver.

It is also possible to use a QCM experiment to calculate the stoichiometry of galvanic processes and support predicted reaction made for the reactions, from the electrode potentials of the individual metals.[15]

By taking the initial frequency of QCM crystal in air, then electrolytically depositing copper on the surface of the QCM, washing and drying the crystal and then taking the frequency of the copper coated crystal. It is possible to calculate the mass of copper deposited from the change in frequency between the two dry crystals. Hence, it is possible to calculate the number of moles of copper deposited on the surface of the crystal.

The copper coated crystal can then be immersed in to a noble metal ion solution so that a galvanic reaction will take place. The reaction should be allowed to proceed to completion, where there is no longer a change in frequency of the QCM. At completion, in theory, all of the electrolytically deposited copper should have been oxidised and undergone dissolution, leaving the surface of the QCM coated in just the noble metal. Once the QCM has been washed and dried, the frequency can be taken of the dry crystal. By comparing the frequency of the noble metal coated crystal to the frequency of the crystal before copper deposition, it is possible to calculate the mass of noble metal deposited on the surface of the crystal and hence the number of moles of noble metal deposited.

By comparing the number of moles of copper deposited on the surface of the crystal to the number of moles of noble metal deposited, it is possible to make a comparison between the two and comment on the stoichiometry of the reaction between copper and a noble metal. The results of this experiment should support productions made from voltammetry data.

If the deposited metal forms a complete layer on the surface of the electrode, it is possible the reaction will cease to proceed before all of the copper is oxidised from the surface of the electrode, which can lead to errors in the results of the experiment. Any copper remaining on the surface of the electrode, will lead to a low mass compared to the theoretical mass for a 100% yield, because the copper ways less than the metal deposited.

It is also possible to calculate the rate of reaction between noble metal ions and a copper substrate on the surface of a QCM crystal. By tracking the change in frequency on the surface of a QCM crystal with respect to time, it is possible to convert the change in frequency to the change in mass using the Sauerbrey equation and hence produce a plot of change in mass *versus* time. If the deposition of the noble metal produces a linear change in mass with respect to time, the gradient of the plot can be taken and used to calculate the rate of reaction. For the example of silver ions reacting with a copper substrate, it is possible to convert the change in mass with respect to time to the change in moles with respect to time using equation **(2.9)**, where **n** is the number of moles involved in the reaction.

$$\delta \mathrm{m} = \mathrm{nRMM}_{\mathrm{Ag}} - \mathrm{nRMM}_{\mathrm{Cu}} \quad (\mathbf{2.9})$$

Hence, once the change in moles with respect to time is known, the rate of the reaction can be calculated using the above equation **(2.5)**. This experiment was repeated for three different amounts of copper deposited on the surface of QCM to ensure consistency.

2.8.3 UV – Vis Spectroscopy

UV – Vis spectroscopy is a well established technique for the analysis of metal ion solutions.[16] Transition metals absorb light in the visible region of the electromagnetic spectrum, which causes the excitation of electrons from filled to unfilled d orbitals.[16,17] Light being absorbed in the visible region of the electromagnetic spectrum, will lead to the solutions of transition metal complexes being coloured. This was evident in group 10 metal salt solutions, where group 10 metal salts, with an oxidation state of 2+ will have a d^n configuration of d^8, hence the promotion of d orbital electrons is possible.

It should be noted that group 11 metal salts, in a +1 oxidation state will have a d^n configuration of d^{10}. Hence the solutions of the group 11 salts are not expected to be coloured, as the d orbitals are full and it is not possible to excite electrons between d orbitals. However, it is possible for these complexes to absorb ultra violet or visible light. The absorbed light causes charge transfer to occur, where an electron from a donating species, usually a ligand, is transferred to an accepting species, usually a metal centre. This type of charge transfer reaction is called ligand to metal charge transfer (LMCT).[16,17] LMCT transitions usually occurs in the UV region of the spectrum, however it can occur visible region leading to coloured solutions, such as the $[MnO_4]^-$ ion.

The molar extinction coefficient can be calculated using the Beer – Lambert law, equation **(2.10)**. Where A represents the absorption, ε is the molar absorptivity, c is the concentration of the species under investigation in solution and l is the path length.

$$A = \varepsilon cl \quad (\mathbf{2.10})$$

Using the Beer – Lambert law, it is possible to calculate the molar absorptivity from the measured absorption if both the concentration of the species under analysis and the path length is known. When dealing with d – d transition of transition metal complexes the molar absorptivity can be an indication of the metal centre's coordination geometry, *Table 2.1*.[17] Hence in the case of metal salts dissolved in Ethaline, it should be possible to theorise the speciation of metal centres investigated.

Table 2.10: Magnitude of molar absorptivity for various d – d electron transitions.[16]

Transition type	ε_{max} / $dm^3\ mol^{-1}\ cm^{-1}$
Spin forbidden	<1
Laporte forbidden	20 – 100
Laporte allowed	*ca.* 250
Symmetry allowed	1000 – 50000

2.8.4 Atomic Force Microscopy

Atomic force microscopy (AFM) is a form of scanning probe microscopy, where a probe is rastered across the surface in a predetermined XY dimension pattern and the height of the surface is measured in the Z dimension.[18]

AFM uses a cantilever with a very sharp tip, ideally with a single atom at the point of the tip, as a stylus. When the tip is scanned across the surface of a sample, changes in height of the surface causes the tip to rise and fall bending the cantilever. A laser beam reflected off the back of the cantilever and when the cantilever bends the laser is deflected. The angle of the laser beams reflection is recorded by a segmented photodiode. The data produced from the AFM is then deconvoluted by the Nanoscope software.

The AFM uses piezoelectric motors to control the position of the tip, and keep the tip at a constant position in relation to the surface of the sample. A change in height of the surface of the sample will be registered by the control unit and the data will be feed back to the piezoelectric motors and the height of the tip adjusted accordingly.

In tapping mode, an oscillating cantilever is used so that at the bottom oscillation the tip of the stylus comes in to contact with the surface of the sample. Tapping mode has advantages over the standard contact mode of AFM, as in contact mode constant contact with the surface can lead to dulling of the styles, or if there are large sudden changes in the morphology of the sample, the tip can be easily broken.[18]

The surface roughness of a sample can be calculated using AFM. This is performed by comparing the surface area of a sample measured by the AFM, to a the area of a completely flat sample, i.e. if the lateral distance scanned is 5 μm x 5 μm in the X and Y dimensions then a completely flat sample would have a surface area of 25 μm^2. This give a value called the image surface area difference, which is expressed as a percentage.

2.8.5 Scanning Electron Microscopy

Like AFM, scanning electron microscopy (SEM) scans a predetermined raster pattern across the surface in the XY dimensions. SEM uses a beam of electrons, typically *ca*. 2 – 10 nm in diameter, that impinge on the surface of a sample. When the electron beam impacts the surface a number of interactions occur and back scattered electrons (BSEs), secondary electrons (SEs) and X-rays are produced. The region of the sample affected by the electron beam is called the interaction volume and is shaped like a falling droplet of water. The size of the interaction volume is determined by the acceleration voltage of the electron beam and material under scrutiny. For an electron beam with an accelerating voltage of 20 keV, the depth of penetration is 1.5 μm or more.[19]

BSEs are electrons that have undergone an elastic interaction with the sample and can penetrate deep in to the sample, *ca*. half the interaction volume. BSEs can undergo a number of elastic interactions before leaving the surface of the sample, meaning the area producing BSEs is much larger than the incident beam. This means that BSEs give poor resolution of the surface morphology. However, BSEs do give good contrast between different elements, this is because heavier elements have more chance of back scattering an electron than lighter elements. Hence heavier elements will produce more electron counts at the detector and appear lighter in shade in BSE images.

SEs are produced when an electron undergoes an inelastic interaction with an electron in the conduction band, at the surface of the sample. The inelastic interaction produces an electron with low energy, which means that only electron near the surface of the sample have enough energy to escape the surface. Hence secondary electrons are produce only in a depth, of up to 500 Å of the interaction volume. The area producing SE is approximately the same as the area of the beam. This means the resolution of an image produced from SEs in much higher than that produced by BSEs

2.8.6 Energy Dispersive X-ray Spectroscopy

EDX is often used in conjunction with SEM, as characteristic X-rays are also produced when an electron beam is impinged on a surface. X-rays produced by an electron beam originate from the entire interaction volume, meaning it is difficult to detect trace elements on the surface of a sample. As the bulk of the sample, gives a large signal that will swamp the small signal from the trace elements.[19]

X-rays are produced when a core electron of an atom is ejected by a collision with a primary electron from the electron beam in a SEM. The electron is ejected from the atom, leaving a vacant, low energy site for an electron in a high energy orbital to fill. As the electron drops to the lower energy level, an X-ray is produced to disperse the excess energy the electron had in the higher energy level. The X-ray produced has a characteristic energy that depends on the element that is relaxing and the orbitals that the electron is relaxing from and to.[20]

2.8.7 X-Ray Photoelectron Spectroscopy

XPS uses X-rays of a specific energy to excite the electrons in an atom of a sample. In the case of this work monochromatic Al Kα X-Ray radiation was used, 1486.6 eV. When an X-ray impinges on the surface of a sample it can excite electrons from various obitals of an atom to the continuum, these electrons are called a photoelectron. These photoelectrons have poor ability to travel through samples and are often reincorporated into other ionised atoms. Hence photoelectrons only escape from the top *ca.* 10 nm of a sample, even though X-rays can penetrate deep in to the sample and produce photoelectrons. This means that XPS is an excellent technique for examining trace elements present at the surface of a sample, without the signals getting swamped by the signals from the bulk sample.

The spectrometer records the kinetic energy of the emitted photoelectrons and the number of photoelectrons emitted. By recording the kinetic energy of a photoelectron it is possible to calculate the binding energy of the electron in an atom, using equation **(2.11)**. Where E_b represents the binding energy, E_k is the kinetic energy of the liberated photoelectron and w is the work function of the spectrometer. Once the binding energy is calculated it is possible to produce a spectrum of electron counts vs. binding energy.

$$E_b = hv - E_k - w \quad (\mathbf{2.11})$$

Each element has specific binding energies for electrons in different electron shells. Hence, due to the unique set of binding energies measured for each element, it is simple to determine which elements are present at the surface of a sample depending on the peaks produced in a full spectrum, from 1325 – 0 eV. It is also possible to determine the atomic percentages of each element on the surface, this is performed by integrating the area under peaks.

XPS can also take high resolution spectra of defined regions. The high resolution spectra can be used to observe narrow binding energy regions and observe the presence of surface oxides or impurities. When an element is oxidised it loses electrons, this means that the attraction of the remained electrons to the nucleus is stronger. Hence there is an increase in binding energy for the remaining electrons. The inverse effect is seen when an element is reduced. When an element gains an electron, the attraction of all the electrons to the nucleus is reduced. Hence there is a reduction in the binding energy for all the remaining electrons. The high resolution spectra allows the ability to fit the data, meaning it possible to determine which oxides are present and in what quantities.

2.9 References

1. A. P. Abbott, G. Capper, B. G. Swain, and D. A. Wheeler, *T. I. Met. Finish.*, 2005, **83**, 51 – 53.
2. W. Canning plc., in *The Canning Handbook*, E. & F. N. Spon Ltd., London, 21 st ed., 1970, Ch. 13, pp. 375.
3. C. Zaleski, Ph.D Thesis, University of Leicester, 2015.
4. W. Canning plc., in *The Canning Handbook*, E. & F. N. Spon Ltd., London, 21 st ed., 1970, Ch. 16, pp. 488.

5. A. P. Abbott, G. Frisch, S. J. Gurman, A. R. Hillman, J. Hartley, F. Holyoak, and K. S. Ryder, *Chem. Commun. (Camb).*, 2011, **47**, 10031 – 10033.
6. R. G. Compton and C. E. Banks, in *Understanding Voltammetry*, Imperial Collage Press, London, 2nd edn., 2011, ch. 4, pp. 111 – 126.
7. R. G. Compton and C. E. Banks, in *Understanding Voltammetry*, Imperial Collage Press, London, 2nd edn., 2011, ch. 3, pp. 97 – 100.
8. R. G. Compton and C. E. Banks, in *Understanding Voltammetry*, Imperial Collage Press, London, 2nd edn., 2011, ch. 2, pp. 40 – 45.
9. R. G. Compton and C. E. Banks, in *Understanding Voltammetry*, Imperial Collage Press, London, 2nd edn., 2011, ch. 3, pp. 88 – 96.
10. F. J. Holler, D. A. Skoog, and S. R. Crouch, in *Principles of Instrumental Analysis*, Brooks/Cole, Belmont, 6th edn., 2007, ch. 1C, pp. 9 – 10.
11. A. R. Hillman, *J. Solid State Electrochem.*, 2011, **15**, 1647 – 1660.
12. E. Ahmed, Ph.D Thesis, University of Leicester, 2015.
13. A. R. Hillman, *J. Solid State Electrochem.*, 2011, **15**, 1647 – 1660.
14. A. Alhaji, Ph.D Thesis, University of Leicester, 2011.
15. A. P. Abbott, S. Nandhra, S. Postlethwaite, E. L. Smith, and K. S. Ryder, *Phys. Chem. Chem Phys.*, 2007, **9**, 3735 – 3743.
16. F. J. Holler, D. A. Skoog, and S. R. Crouch, in *Principles of Instrumental Analysis*, Brooks/Cole, Belmont, 6th edn., 2007, ch. 14B, pp. 370 – 374.
17. D. F. Shriver, P. W. Atkins, and C. H. Langford, in *Inorganic Chemistry,* Oxfrod University Press, Oxford, 2nd edn, 1994 , ch. 14, pp. 589 – 602.
18. F. J. Holler, D. A. Skoog, and S. R. Crouch, in *Principles of Instrumental Analysis,* Brooks/Cole, Belmont, 6th edn., 2007, ch. 21G, pp. 613 – 619.

19. F. J. Holler, D. A. Skoog, and S. R. Crouch, in *Principles of Instrumental Analysis*, Brooks/Cole, Belmont, 6th edn., 2007, ch. 21F, pp. 608 – 613.

20. F. J. Holler, D. A. Skoog, and S. R. Crouch, in *Principles of Instrumental Analysis*, Brooks/Cole, Belmont, 6th edn., 2007, ch. 1C, pp. 9 – 10.

Chapter 3: Characterisation of Group 11 Chlorides Salts in Ethaline 200

3.1 Introduction

3.2 Copper Chlorides in Ethaline 200

3.2.1 $CuCl_2$ in Ethaline 200

3.2.2 CuCl in Ethaline 200

3.3 Silver (I) Chloride in Ethaline 200

3.4 Gold (I) Chloride in Ethaline 200

3.5 Conclusions

3.6 References

3.1 Introduction

This chapter expands on the existing literature, for the characterisation of both the speciation and electrochemistry, of group 11 metal salts when dissolved in Ethaline 200.

The speciation of group 11 metal salts dissolved in Ethaline 200 has previously been characterised using EXAFS.[1,2,3] This chapter aims to expand on the previous literature by analysis of the UV – Visible spectra of the group 11 metal salts dissolved in Ethaline 200. Producing supporting results for published litrature.[3]

The electrochemistry of group 11 metal salts dissolved in Ethaline has been studied previously.[1,2,4] This chapter aims to expand on the existing knowledge by discussing the results of the EQCM experiments and establishing the rate and current efficiency of reactions.

Finally, it is important to know how the presence of copper ions, present in solution with other metal salts, affects the electrochemical behaviour of both species. This is important to ascertain, as when galvanic plating of copper substrates, copper ions will be introduced in to the electrolyte. Hence, the results of the CV and EQCM experiments have been discussed.

The goals to be achieved in this chapter are:

- Determination of the speciation of group 10 and 11 metals salts, when dissolved in Ethaline 200.
- Determination of the electrode potentials of the group 11 metal salts.
- Determination of the rate and current efficiency of the electrochemical reactions.
- Analysis of mixed metal systems.

3.2 Copper Chlorides in Ethaline

3.2.2 $CuCl_2$ in Ethaline 200

The UV – Vis spectrum of $CuCl_2$ dissolved in Ethaline 200 is displayed in *Figure 3.1*. The spectrum displays λ_{max} at 291 nm (ε = 3950 dm mol^{-1} cm^{-1}) as well as two more peaks at 405 (ε = 2850 dm mol^{-1} cm^{-1}) and 238 nm (ε = 3000 dm mol^{-1} cm^{-1}). The peaks at 291 and 405 nm correspond well with established literature for a tetrahedral $[CuCl_4]^{2-}$ complex[5,6], with variation in peak position due to the unique solvation environment.[5-7]

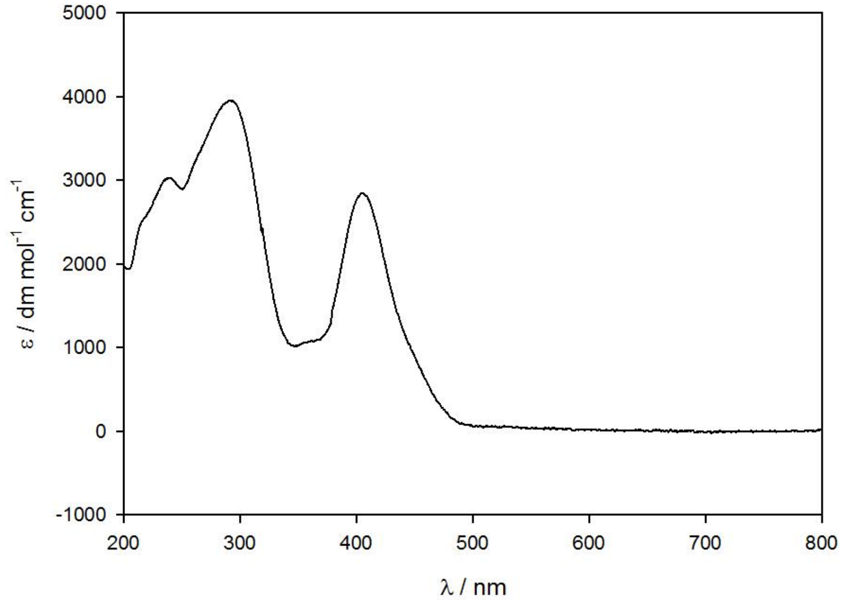

Figure 3.1: The UV -Vis spectra of 1 mM $CuCl_2$ dissolved in Ethaline 200.

The absorption of light in the blue region of the visible spectrum, gives the solution the bright yellow colour indicative of $[CuCl_4]^{2-}$ complexes. The absorption of blue light is due to the d – d orbital promotion. Where electrons are promoted from the *e* to the t_2 set of orbital in the tetrahedral crystal field splitting pattern.

Further work has been performed by R. Van Deun *et. al.*[6] and J. Hartley *et. al.*,[1,2] comparing the UV – Vis and EXAFS spectrum of $CuCl_2$ dissolved in Ethaline 200. This work has demonstrated similar UV – Vis data to the above and uses EXAFS to deduce the speciation of the Copper centre, confirming the $[CuCl_4]^{2-}$ speciation.

The CV of $CuCl_2$ dissolved in Ethaline 200, *Figure 3.2*, displays two distinct redox couples. The first redox couple appears at 0.475 V (Ag wire *pseudo* reference electrode) and represents the Cu (II)/(I) reversible redox couple. The second redox couple appears at *ca*. – 0.325 V (Ag wire *pseudo* reference electrode) and represents the Cu(I)/(0) *quasi* – revisable redox couple. Where Cu (I) ions are reduced on the surface of an electrode and Cu(0) in the form of copper metal is deposited.

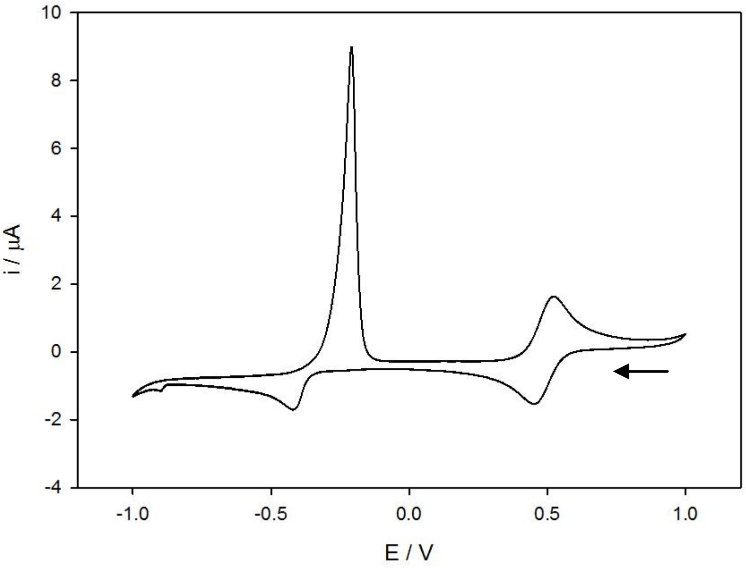

Figure 3.2: CV of 10 mM $CuCl_2$ *dissolved in Ethaline 200. Pt working electrode, 3.14 x* 10^{-2} cm^2*. Pt flag counter electrode. Ag wire reference electrode. Scan rate 10 mV* s^{-1}.

This is evidence that the Cu (I) species formed is stable in the Ethaline 200 solution, possibly due to the high chloride concentration of Ethaline. However it is important to note there is literature president for the disproportionation of the species Cu (I) in the similar system of Reline 200.[8] It should be noted that a high concentration of chloride ions in an aqueous solution will also stabilise the Cu (I) ion.[2,9]

This is in contrast to the aqueous electrochemistry of copper, where it is well established that the Cu (I) ion is unstable and will disproportionate to form Cu (II) and Cu (0).[10] This is due the electrode potential values of the Cu (II)/(I), (I)/(0) and (II)/(0) species, where the standard electrode potentials are E^0 = 0.16, 0.52 and 0.34 respectively. Which means it is thermodynamically favourable for Cu (I) to undergo disproportionation. As Cu (I) disproportionates, it follows that for aqueous systems the reduction of Cu(II) proceeds via the reaction represented in equation **(3.1)**.

$$\mathrm{Cu}^{2+} + 2\mathrm{e}^{-} \rightarrow \mathrm{Cu} \quad (\mathbf{3.1})$$

However before we can start writing the equations for the copper reactions in Ethaline 200, it is important to know the Cu(I) species formed upon the reduction of Cu(II). This will be discussed further in section *3.1.2 CuCl in Ethaline 200*.

Further information can be obtained about the electrochemistry of copper, by performing the CV using an EQCM. *Figure 3.3* shows the results from the EQCM, with the CV plotted with a change in moles *versus* potential plot.

For the cathodic sweep, starting at 0.8 V and sweeping to – 0.8 V. Before the Cu(II)/(I) redox couple, from *ca*. 0.8 to 0.4 V, no change in mass is observed. After the Cu(II)/(I) redox couple, from *ca*. 0.4 to – 0.4 V, there is a constant negative current representing reduction of copper and a small but steady increase in the mass. It is unclear what is causing this feture, but it may be explained by two possible processes. Diffusion of Cu(II) ions in to the diffusion layer, or thickening of the diffusion layer with an increasing voltage. After the Cu(I)/(0) redox couple, *ca*. – 0.4 to – 0.8 there is a large steady increase in mass, which is attributed to copper being deposited on the surface of the working electrode. As the change in mass on the surface of the electrode displays a linear response, it is possible to determine the rate of deposition of copper from the gradient of the change in moles *versus* potential plot, by dividing the gradient of the deposition by the scan rate and surface area of the electrode. The rate of deposition is determined to be 7.85 x 10^{-10} mol s^{-1} cm^{-2}. This value for the rate of reaction agrees well with previously published literature by Ryder *et. al.*[11]

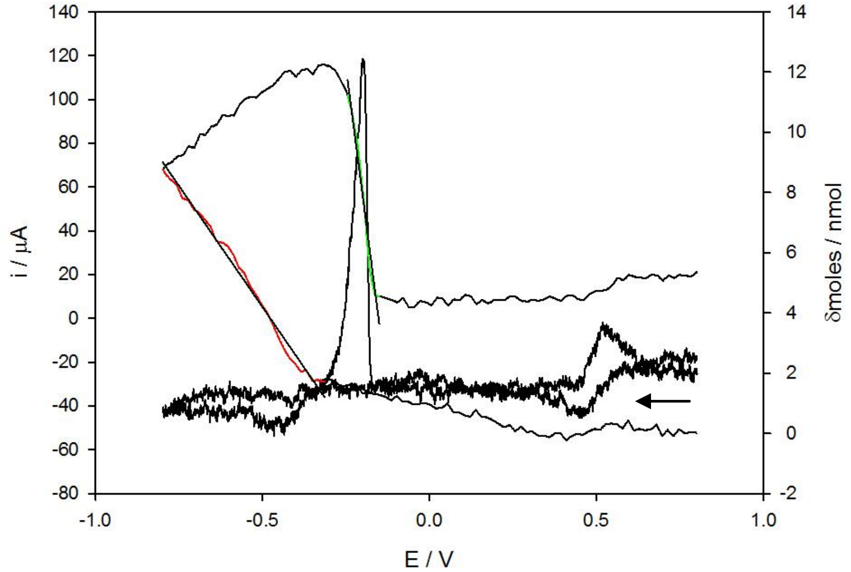

Figure 3.3: Using an EQCM to produce CV data of 10 mM $CuCl_2$ dissolved in Ethaline 200. Red: deposition of copper, gradient – 1.61 x 10^{-8} mol V^{-1} Green: stripping of copper, gradient – 9.10 x 10^{-8} mol V^{-1}. Pt working electrode, 0.205 cm^2. Pt gauze counter electrode. Ag wire reference electrode. Scan rate 10 mV s^{-1}.

For the reverse, anodic sweep, from – 0.8 V positive to 0.8 V. At the beginning of this sweep copper is still being deposited on the working electrode from *ca.* – 0.8 to – 0.3 V. Where at *ca.* – 0.3 to – 0.2 V the copper is oxidised and stripped from the surface of the electrode, which is represented by a characteristic positive peak in current as well as a large drop in mass on the surface of the working electrode. From *ca.* – 0.2 to 0.5 V the mass on the surface of the electrode does not appear to change, with a small gain in mass from *ca.* 0.5 to 0.8 V. It is important to note that the mass on the electrode does not return to zero. This is potentially due to copper alloying with the platinum of the working electrode, which prevents some of the deposited copper being removed.

Again it is possible to determine the rate of stripping, from the moles *versus* E plot. The rate of stripping is determined as 4.44 x 10^{-9} mol s^{-1} cm^{-2}. The rates of reaction for all metal salts discussed in this chapter are given *Table 3.1*. It should be noted that all rates of reaction where recorded at 10 mV s^{-1}, as change in scan rate will affect the rate of reaction. This is due to the potential reaching a greater over potential faster at a faster scan rate and hence a higher rate of reaction due to Butler – Volmer kinetics, will be reached faster.

Table 3.1: Comparison of the rates of reaction of group 11 metal salts dissolved in Ethaline at a scan rate of 10 mV s^{-1}.

Metal salt	Rate of Deposition / x 10^{-10} mol s^{-1} cm^{-2}	Rate of Dissolution / x 10^{-10} mol s^{-1} cm^{-2}
$CuCl_2$	7.85	44.4
CuCl	11.3	48.5
AgCl	9.12	53.7
AuCl	24.1	68.8

Further analysis of the EQCM data, can be performed using the mass – charge ratio, to determine the current efficiency for the deposition of copper. The expected mass charge ratio for a Cu (II) system, with 100% current efficiency is calculated by, equation **(3.2),** as discussed in **Chapter 2**.

$$\frac{\delta m}{\delta Q} = \frac{63.55}{2F} = 3.29 \times 10^{-4} \text{ g C}^{-1} \quad \textbf{(3.2)}$$

It is important to note, that for the reverse process, when copper is undergoing dissolution from the electrode, instead of a two electron process, a one electron process is expected. This means the mass – charge ratio, for the 100% current efficiency, for stripping of copper, is calculated by.

$$\frac{\delta m}{\delta Q} = \frac{63.55}{F} = 6.59 \times 10^{-4} \text{ g C}^{-1} \quad \textbf{(3.3)}$$

It is then possible from the EQCM data displayed in *Figure 3.3*, to produce a δm *versus* δQ plot for the deposition and stripping of copper, *Figure 3.4*, from which the experimental mass – charge ratio can be calculated.

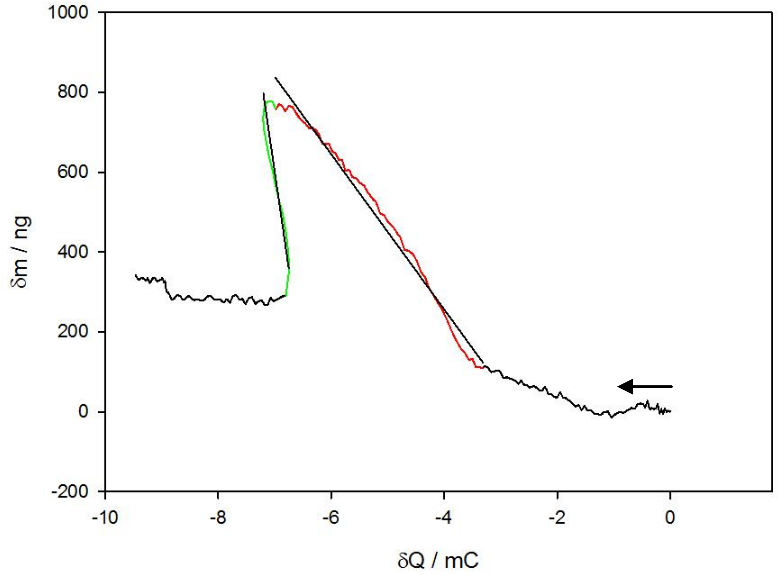

Figure 3.4: Plot of mass versus charge for CV of 10 mM $CuCl_2$ dissolved in Ethaline 200. Red; deposition of copper, gradient – 1.94 x 10^{-4} g C^{-1}. Green; stripping of copper, gradient – 9.73 x 10^{-4} g C^{-1}.

For the deposition of copper, the experimental mass – charge ratio has a calculated value of 1.94 x 10^{-4} g C^{-1}, which suggests a current efficiency of 59%. For the stripping of copper the experimental mass – charge ratio has a value of 9.73 x 10^{-4} g C^{-1}, this value is much higher than the expected ratio and suggests a process that is more than 100% efficient. The result can be accounted for by a loss of unoxidised copper from the surface of the electrode, where copper is being removed without being oxidised and hence no current is passed, which increases the mass charge ratio. Hence, it is not possible to calculate the current efficiency for delamination under these experimental conditions, to do so would require a slow dissolution process, where detachment of unoxidised pieces of copper does not occur.

The unoxidised copper is possibly due to a high concentration of copper ions in the double layer preventing any more copper undergoing dissolution by oxidation. The high concentration of copper in the double layer increases the oxidation potential according to the Nernst equation and hence preventing further oxidation. Or a dissolution mechanism where the surface of the copper is undercut leading to the formation of flakes, which can detach when all the copper connecting the flake to the electrode is dissolved. This effect has been shown by Rayment *et. al.*[12]

3.2.2 CuCl in Ethaline 200

The speciation of CuCl dissolved in Ethaline 200 has previously been studied using EXAFS.[2] However, as shown by Hartley *et. al.*,[2,3] when resolving EXAFS data, the average coordination of the bulk solution is obtained, *i.e.* the number of chloride ions found coordinating to the copper centre when CuCl is dissolved in Ethaline is 2.4 ± 0.3. The UV -Vis spectra of $[CuCl_2]^-$ however is expected to show only a small absorption, with a molar extinction coefficient of less than 1000 dm mol^{-1} cm^{-1}.[13,14] Where as $[CuCl_3]^{2-}$ has a much larger molar extinction coefficient, close to 3000 dm mol^{-1} cm^{-1} at 280 nm,[13,14] which would mask any response from $[CuCl_2]^-$ in the region.

The UV – Vis spectra of CuCl dissolved in Ethaline 200, *Figure 3.5,* displays a λ_{max} at 279 nm which suggests that $[CuCl_3]^{2-}$ is present in solution. It is important to note there are peaks at 237 and 404 nm, which indicates the presence of a small amount of $[CuCl_4]^{2-}$. Most likely this is due to its presence in the CuCl reagent or oxidation with O_2 in solution, but also could be due to disproportionation as discussed above.[8]

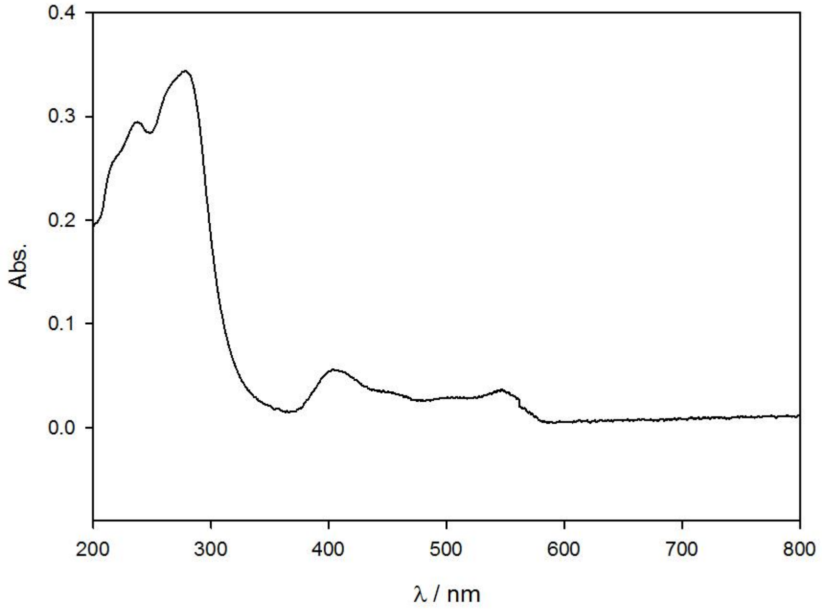

Figure 3.5: The UV – Vis spectra of 1 mM CuCl in Ethaline 200.

Now that the species of both Cu (II) and Cu (I) ions in solution, has been ascertained, it is possible to determine the reaction occurring at the working electrode. It is expected that for the electrochemical reduction of $[CuCl_4]^{2-}$, that $[CuCl_4]^{3-}$ will be formed and quickly lose a labile Cl^- ligand to form $[CuCl_3]^{2-}$, which in turn can lose a Cl^- ligand to form $[CuCl_2]^-$, equation **(3.4)**. Where an equilibrium exists between the copper dichloride and trichloride complex.

$$2[\mathrm{CuCl_4}]^{2-} + 2e^- \rightarrow [\mathrm{CuCl_3}]^{2-} + [\mathrm{CuCl_2}]^- + 3\mathrm{Cl}^- \quad (\mathbf{3.4})$$

The CV of CuCl dissolved in Ethaline 200, *Figure 3.6*, has only been scanned across the Cu(I)/(0) redox couple, in an effort to prevent any back ground current for the Cu(II)/(I) redox couple.

The CV displays a single redox couple at -0.28 V (*v.s.* an Ag wire *pseudo* reference electrode) This value is significantly more positive than the value of the corresponding redox couple in the Cu(II) CV. This is attributed to a referencing issue with the in the solely Cu (I) system. Where repeat measurements with the Cu(II) system appears to give a stable redox potential of – 0.325 V, whilst the Cu(I) appears to vary by up to 60 mV. This uncertainty will be propagated when it comes to calculating the change in Gibbs free energy for the reactions in chapters 4 and 6.

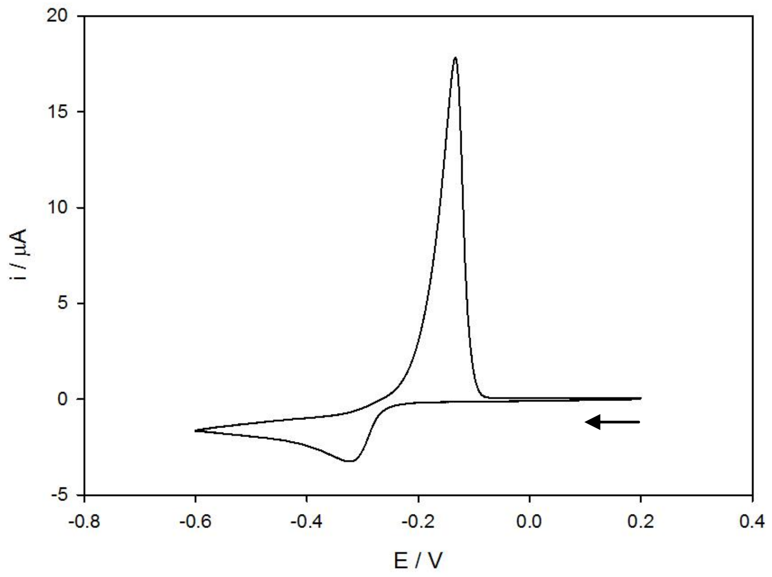

Figure 3.6: CV of 20 mM CuCl dissolved in Ethaline 200. Pt working electrode, 3.14 x 10^{-2} cm^{2}. Pt flag counter electrode, Ag wire reference electrode. Scan rate 10 mV s^{-1}.

EQCM has been used to perform CV and gain further information on the Cu(I)/(0) redox process. Allowing analysis of the current efficiency for the Cu(I)/(0) redox couple without a current contribution from the Cu(II)/(I) redox couple. *Figure 3.7* shows the results of the EQCM, with the CV plotted with a δmoles *versus* E plot.

For the cathodic sweep, sweeping from 0 V down to – 0.7 V. Before the Cu(I)/(0) redox couple, from *ca*. 0 to – 0.3 V, there is no current being passed, implying that the amount of Cu(II) present in solution is negligible. Also there is only a small increase in mass, analogues to that which was seen in *Figure 3.3*, which can be attributed to the same cause as above. After the Cu(I)/(0) redox couple, *ca*. 0.3 to – 0.7 V, there is a steady increase in mass on the surface of the crystal, as well as a negative current in the CV, which is representative of a reduction and deposition of copper on to the surface of the crystal.

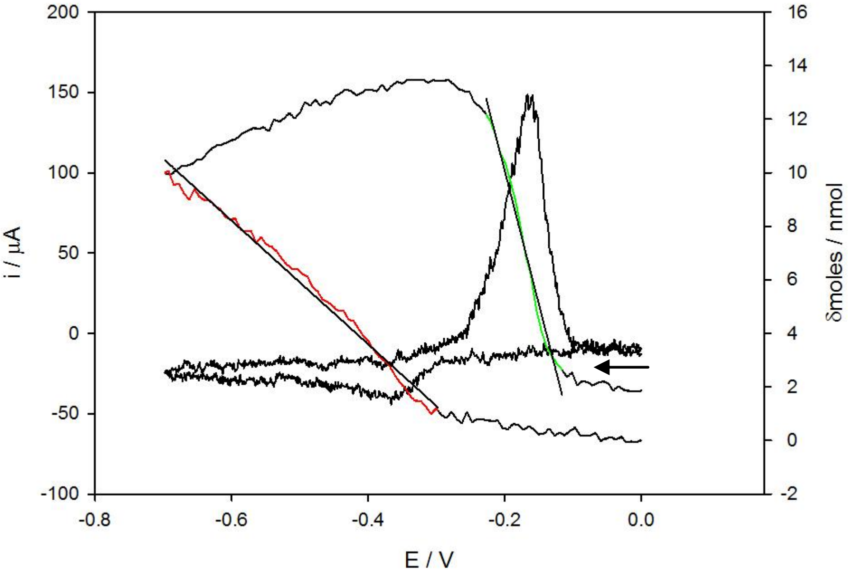

Figure 3.7: Using an EQCM to produce CV data of 10 mM CuCl dissolved in Ethaline 200. Red: deposition of copper, gradient – 2.31 x 10^{-8} mol V^{-1} Green: stripping of copper, gradient – 9.95 x 10^{-8} mol V^{-1}. Pt working electrode, 0.205 cm^2. Pt gauze counter electrode. Ag wire reference electrode. Scan rate 10 mV s^{-1}.

It is possible to calculate the rate of deposition from the δmoles *versus* E plot, which is determined to be 1.13 x 10^{-9} mol s^{-1} cm^{-2}. The difference in rate of reaction, between the $CuCl_2$ and CuCl systems, can be accounted for by the size of the Cu(II) and Cu(I) species diffusing towards the electrode. This an effect of mass transport being slower for the $[CuCl_4]^{2-}$ ion than it is for the $[CuCl_2]^-$ ion, as the $[CuCl_4]^{2-}$ ion is bigger than the $[CuCl_2]^-$ ion

For the anodic, reverse sweep, sweeping form – 0.7 V back to 0 V. At the beginning of this sweep, copper is still being deposited, from *ca*. – 0.7 to –0.3 V. From *ca*. – 0.3 to – 0.1V, there is a large loss in mass on the surface of the electrode, which is represented by a positive current in the CV and represents oxidation and stripping of copper at the surface of the electrode. Again it is important to note that the mass does not return to zero, due to possible alloying of copper with the working electrode. The rate of dissolution for this process was found to be 4.85 x 10^{-9} mol s^{-1} cm^{-2}, similar to the rate of dissolution in the Cu(II) system.

Further analysis of the EQCM results can be performed to ascertain the current efficiency of copper deposition and stripping in a solely Cu(I) solution. This is performed by calculating the mass – charge ratio. In this case of a Cu(I) reduction or oxidation, we can use the theoretical mass – charge calculated in **(3.2)** for 100% current efficiency.

From the EQCM data it is possible to produce a δm *versus* δQ plot, *Figure 3.8,* from which it is possible to calculate the experimental mass – charge ratio. By comparing the experimental mass – charge ratio, with theoretical mass – charge ratio, it is possible to determine the current efficiency for the deposition and stripping of copper in a solely Cu(I)/(0) system. For the deposition, the experimental mass – charge ratio is 4.13 x 10^{-4} g C^{-1}, allowing the current efficiency to be calculated as 63%. Whereas for the stripping, the experimentally calculated mass – charge ratio is, again, above the theoretical calculated mass – charge ratio, with a value of 6.78 x 10^{-4} g C^{-1}. This is accounted for by loss detached copper metal from the surface, copper being removed from the surface without undergoing oxidation. The reason this could occur have been discussed above in section **3.1** above.

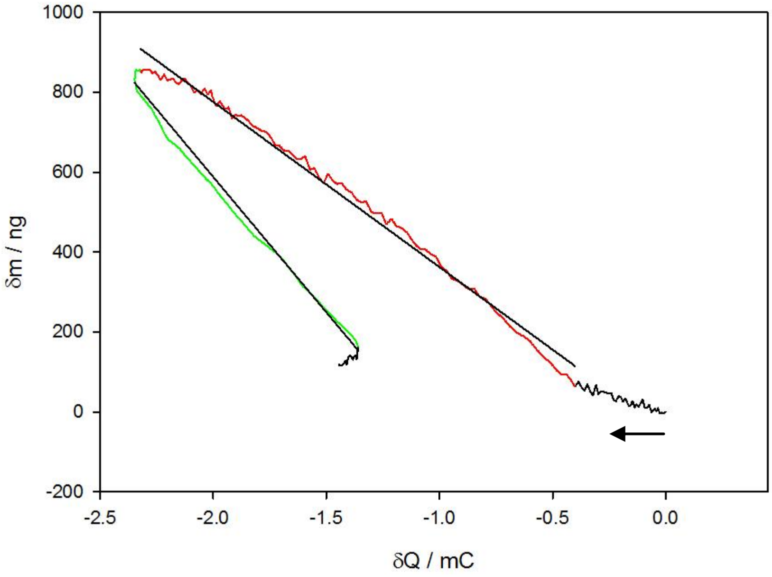

Figure 3.8: Plot of mass versus charge for CV of 10 mM CuCl dissolved in Ethaline 200. Red; deposition of copper, gradient – 4.13 x 10^{-4} *g* C^{-1}*. Green; stripping of copper, gradient – 6.78 x* 10^{-4} *g* C^{-1}*.*

3.3 Silver (I) Chloride in Ethaline 200

Pervious work on the speciation of AgCl dissolved in Ethaline 200 has been performed, using EXAFS and the species present has been determined to be a $[AgCl_2]^-$ complex.[2,3] However, as discussed previously the limitations of EXAFS mean that only the average coordination number is given. The coordination number established by Hartley *et. al.*[2] by EXAFS for AgCl dissolved in Ethaline is 2.5. Hence it follows that there is possibly $[AgCl_3]^{2-}$ is also present in solution.

The UV – Vis of AgCl dissolved in Ethaline 200, *Figure 3.9*, shows one peak in the spectrum, λ_{mas} at 237 nm (ε = 4400 dm mol^{-1} cm^{-1}), this peak is possibly masking a second peak at *ca*. 325 nm (ε = 1000 dm mol^{-1} cm^{-1}). Which indicates that, possibly, there are two species are present in solution.

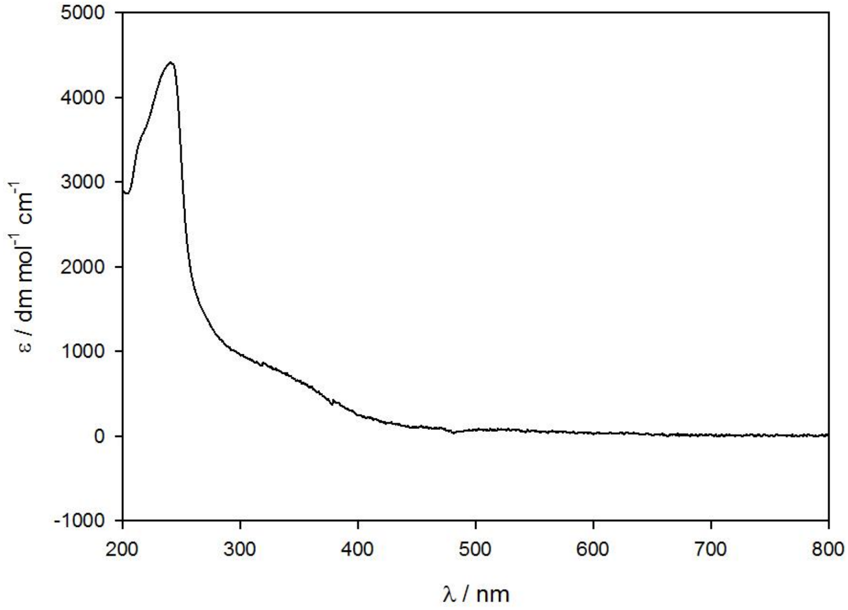

Figure 3.9: The UV – Vis spectra of 1 mM AgCl in Ethaline 200.

The CV of AgCl dissolved in Ethaline 200, *Figure 3.10*, displays a single *quasi* – reversible redox couple for Ag(I)/(0). The redox couple has an electrode potential of *ca*. -0.075 V (Ag wire *pseudo* reference electrode). It should be noted that only one redox couple is present in the CV, suggesting that only one electrochemically active silver species is present in solution. However, it is possible that the difference between the redox potentials of $[AgCl_2]^-$ and $[AgCl_2]^{2-}$ is negligible. As the experiment is examining the Ag (I)/(0) redox couple, using a Ag (I)/(0) reference system, it would be expected that the electrode potential would be zero. However as the reaction represented in equation **(3.5)** is *quasi* – reversible , there will be an error in determination of the electrode potential.

$$[\mathrm{AgCl_2}]^-_{(\mathrm{DES})} + \mathrm{e}^- \rightarrow \mathrm{Ag_{(s)}} + 2\mathrm{Cl}^- \quad (\mathbf{3.5})$$

It is important to note that AgCl is not soluble in Ethaline 200 and has to undergo solvolysis before dissolution can occur, as implied by the data obtained from UV – Vis. The extra chloride ligand will stabilise the silver complex, making it harder to reduce. If the reference electrode is undergoing a reaction to form AgCl instead of

$[AgCl_2]^-$ then the loss of an extra chloride ligand will cause a discrepancy between the electrode potential of silver at the working electrode and the reference electrode.

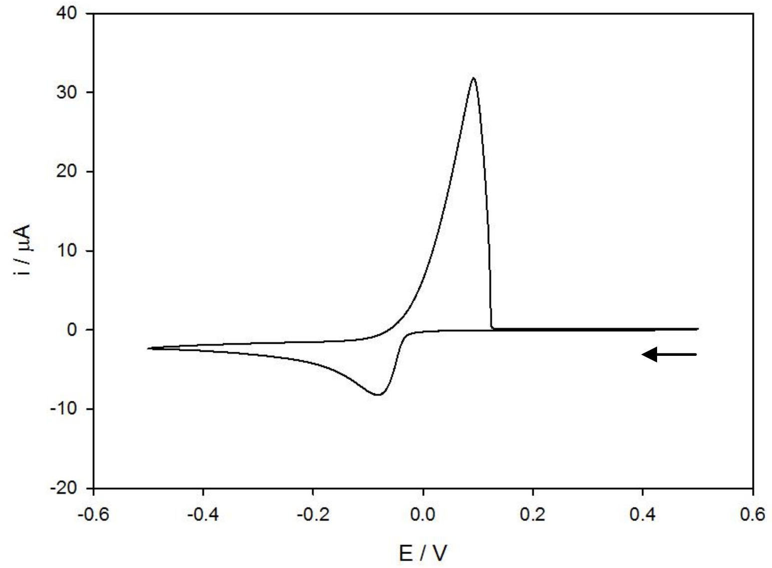

Figure 3.10: CV of 20 mM AgCl dissolved in Ethaline 200. Pt working electrode, 3.14 x 10^{-2} *cm*^{2}*. Pt flag counter electrode. Ag wire reference electrode. Scan rate 10 mV s*$^{-1}$*.*

To further analyse the Ag (I)/(0) redox couple, EQCM was used to perform CV. *Figure 3.11* shows the δmoles *versus* E plot overlaid with the CV for the AgCl dissolved in Ethaline 200 system.

For the cathodic sweep, sweeping negative from 0.35 V down to – 0.35 V. Before the redox couple at *ca*. 0 V, the scan from *ca*. 0.35 to 0 V, there is no significant change in mass and there is no flow of current.

After the silver redox couple at *ca*. 0 V, for the potentials between *ca*. 0 to – 0.130 V, there is a steady increase in mass where silver is being deposited, in potential controlled regime. This is represented by a linear increase in the change in moles of silver and in the CV, a negative current that increases exponentially to *ca*. – 0.048 V. The rate of deposition in the potential controlled regime is determined to be 1.76 x 10^{-9} mol s^{-1} cm^{-2}.

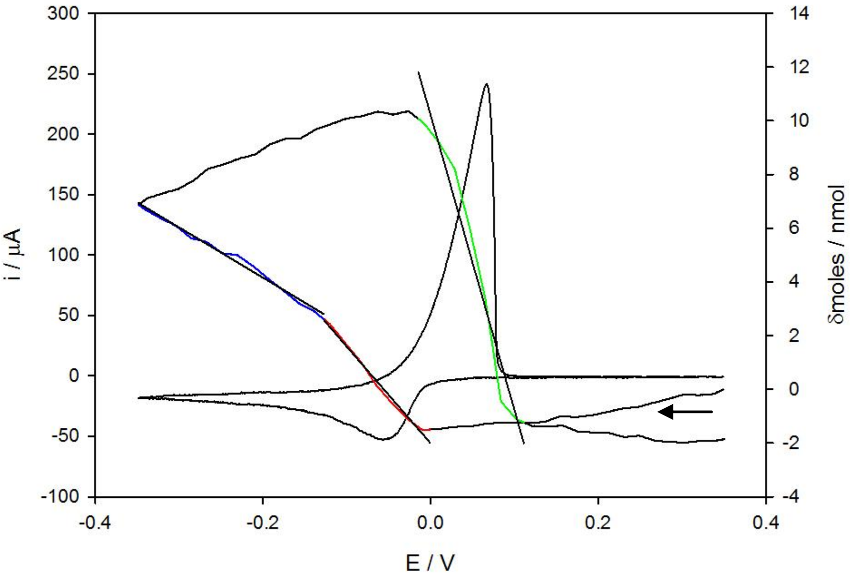

Figure 3.11: Using an EQCM to produce CV data of 10 mM AgCl dissolved in Ethaline 200. Red: deposition of silver, gradient – 3.60 x 10^{-8} mol V^{-1}. Blue: deposition of silver, gradient – 1.87 x 10^{-8} mol V^{-1}. Green: stripping of silver, gradient – 1.10 x 10^{-7} mol V^{-1}. Pt working electrode, 0.205 cm^2. Pt gauze counter electrode. Ag wire reference electrode. Scan rate 10 mV s^{-1}.

At *ca* – 0.130 V the deposition appears to slow and the rate of deposition becomes 9.12 x 10^{-10} mol s^{-1} cm^{-2}, this is due to the CV moving from a potential controlled regime to a diffusion controlled regime. Meaning silver ions must diffuse from the bulk solution in to the electrical double layer to be deposited. In the change in moles plot, this effect is shown by a shallower gradient. In the CV this is represented by an 1 / $t^{1/2}$ decrease in current from the peak at *ca.* – 0.048 V to – 0.35 V.

For the anodic sweep, sweeping positive from – 0.35 V back to 0.35 V. At the beginning of this sweep, from *ca.* – 0.35 to 0 V, the potential is still in the deposition regime for silver. This is representing by a steady increase in mass, as well as the negative current in the CV. At *ca*. 0 to 0.1 V oxidation of silver takes place, stripping the metal from the surface of the electrode. The stripping process is represented by a positive peak in current and a large loss in mass. Unlike with the copper system however, the mass lost in the stripping process is equivalent to the mass gained in the deposition process. The rate of stripping can also be determined form the δmoles *versus* E plot and is found to be 5.37 x 10^{-9} mol s^{-1} cm^{-2}.

As the electrochemistries of both the copper and silver systems are recorded at the same scan rate, the results may be compared. The rate of silver deposition and stripping is faster than that of copper. The fast kinetics of silver deposition and dissolution is an effect that is well documented in aqueous systems.[15] It is important to note that this is for the reduction of Ag^+ ion rather than a $[AgCl_2]^-$. The electrochemistry of $[AgCl_2]^-$ has also previously been studied in water with a high chloride content, where AgCl can be dissolved in a high chloride aqueous enviroment.[2] The results of which are analogues to that reported above.

Further analysis of the deposition and stripping of silver can be performed by analysis of the mass – charge ratio, to determine the current efficiency of these processes. For 100 % current efficiency the theoretical mass – charge ratio is calculated using equation **(3.6)**.

$$\frac{\delta \mathrm{m}}{\delta \mathrm{Q}} = \frac{107.87}{\mathrm{F}} = 1.12 \times 10^{-3}\ \mathrm{g\,C^{-1}} \qquad \mathbf{(3.6)}$$

From the EQCM a δm *versus* δQ plot, *Figure 3.12*, it is possible to produce an experimental mass – charge ratio. For the deposition, the experimental mass – charge ratio is 9.25 x 10^{-4} g C^{-1}, which is equivalent to a current efficiency of 83%. For the stripping, unlike the copper system, the mass – charge ratio of the silver system does not exceed the maximum possible value. The experimental mass – charge ratio for the stripping of silver is 7.60 x 10^{-4} g C^{-1}, which corresponds to a current efficiency of 68%.

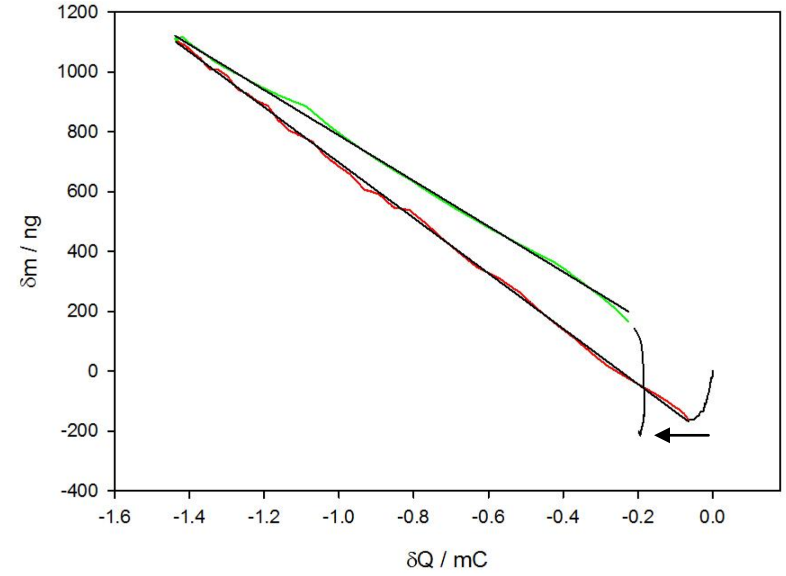

Figure 3.12: Plot of mass versus charge for CV of 10 mM AgCl dissolved in Ethaline 200. Red; deposition of silver, gradient – 9.25 x 10^{-4} g C^{-1}. Green; stripping of silver, gradient – 7.60 x 10^{-4} g C^{-1}.

The mass – charge ratio for the dissolution of the silver system is less than that of the deposition. There are two possible reasons for the higher value. First that there are side reactions occurring increasing the current passed, or second that chloride ions are coordinating to silver ions on the surface of the elecrtrode, increasing the mass on the surface and decreasing the mass – charge ratio associated with the dissolution.

Making a solution containing both copper and silver salts it is possible to analyse the effect one has on the other with regard to the electrochemistry. *Figure 3.13* displays the CV of a mixed Cu(II) and Ag(I) salt solution. The CV displays three redox processes at 0.475, -0.125 and -0.400 V (Ag wire *pseudo* reference electrode) and represent the Cu(II)/(I), Ag(I)/(0) and Cu(I)/(0) redox couples respectively.

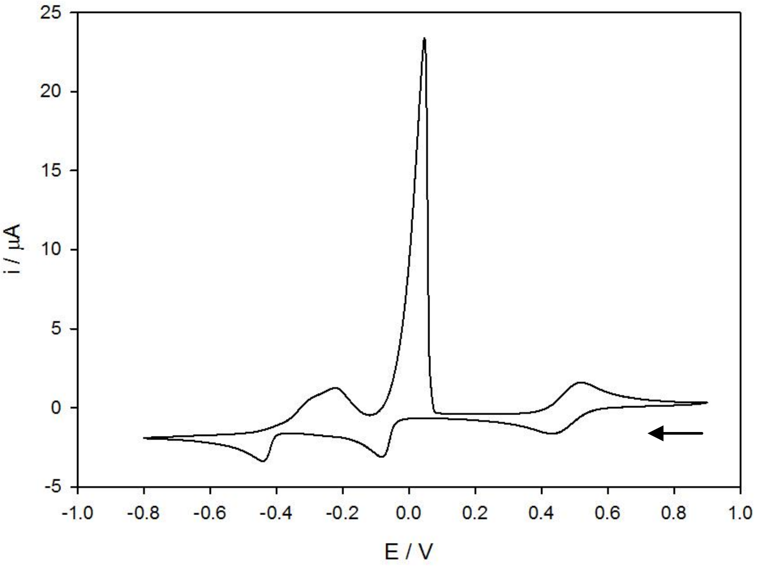

Figure 3.13: CV of 10 mM AgCl and $CuCl_2$ dissolved in Ethaline 200. Pt working electrode, 3.14 x 10^{-2} cm^2. Pt flag counter electrode. Ag wire reference electrode. Scan rate 10 mV s^{-1}.

Interestingly, the shape of the oxidation peak for the Cu(I)/(0) dissolution is not what would be customarily expected for the stripping of metal from the surface of an electrode. It is proposed that this effect is due silver somehow inhibiting the removal of copper from the surface of the electrode. It is proposed that deposition of silver occurs on top of the copper, meaning the copper cannot be undergo oxidation and dissolution until the silver on top of the copper is removed. Silver can be deposited on top of copper as the silver electrode potential is more positive than the copper electrode potential and hence will be scanned after the copper couple.

To do further analysis the mixed system the CV was performed using an EQCM, to determine what ratio the components are deposited in. It is easier in this instance to analyse the mass – charge ratio, *Figure 3.14*, before seeing what effect the mixed system has on the potential and the rate of reaction in the electrochemistry.

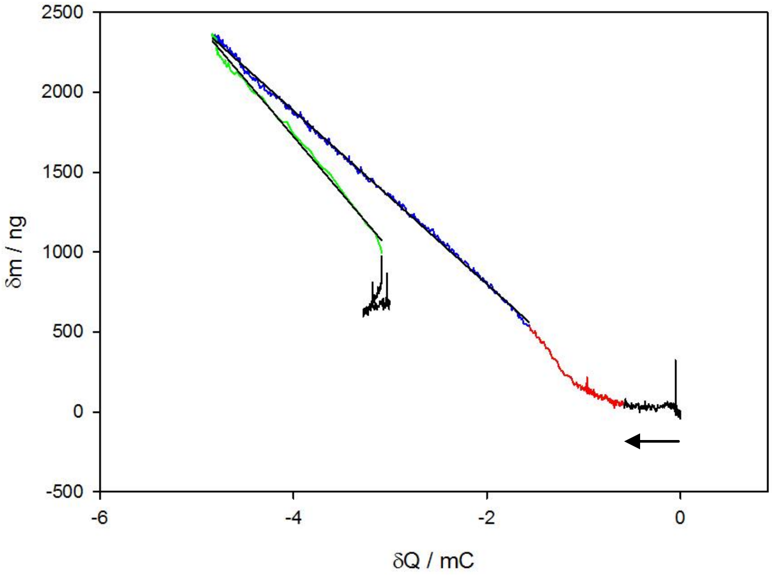

Figure 3.14: Plot of mass versus charge for CV of 10 mM AgCl & $CuCl_2$ dissolved in Ethaline 200. Red; deposition of metals, gradient – 5.43 x 10^{-4} g C^{-1}. Green; stripping of metals, gradient – 7.13 x 10^{-4} g C^{-1}.

In *Figure 3.14*, the black regions represent where current is passed is due to the Cu (II)/(I) redox couple, hence current is passed without gain or loss in mass. The red regime represents where, first the deposition of silver has started and second where the deposition of copper has started. When the gradient of the mass – charge ratio has stabilised, it displays a linear response, implying that the deposition of both metals occurs at the same time. The same is evident in the dissolution regime of the experiment, where both metals are being stripped at the same time, with possibly a small amount of copper removed to begin with. This observation agrees with CV, lending support to the theory, that not all of the copper is removed with the initial oxidation current. However, it does not fully support the theory that a silver coating is deposited on top of the copper, preventing removal of copper from the surface.

Analysis of the mass – charge ratio also allows for determination of the composition of the film being deposited. Determination of the composition of the film was performed by using equation **(3.7)**.[16]

$$\chi_{\mathrm{Cu}} = \frac{(\mathrm{RMM}_{\mathrm{Ag}} - \frac{\delta\mathrm{m}}{\delta\mathrm{Q}}\mathrm{Fb})}{(\frac{\delta\mathrm{m}}{\delta\mathrm{Q}}2\mathrm{Fa} - \frac{\delta\mathrm{m}}{\delta\mathrm{Q}}\mathrm{Fb} - \mathrm{RMM}_{\mathrm{Cu}} + \mathrm{RMM}_{\mathrm{Ag}})} = 0.28 \quad (\mathbf{3.7})$$

The above equation calculates the composition of the deposit using the mass – charge ratio from the combined experiment, as well as the current efficiency calculated from the individual metal salt experiments. Where **a**, is the current efficiency of the copper deposition and **b**, is the current efficiency of the silver deposition. The result of which gives the atomic percentage of copper in the deposit as 28 % and the atomic percentage of silver as 72%.

Interestingly the mass – charge ratio for the dissolution of the coating is greater than that for the deposition. This implies that there is a greater mole fraction of silver in the coating being removed than that of the one being deposited. As it has not been possible to calculate the current efficiency for the dissolution of copper, due to loss of unoxidised particulate matter, it is not possible to calculate the mole fraction of the metals undergoing dissolution.

A reasonable explanation for this result is that some copper has in fact been removed from the surface of the working electrode before the main dissolution process occurs, due to the Cu (0)/(I) redox couple being more negative than the Ag (0)/(I) redox couple, as discussed above. This result implies that a co-deposit has been formed where silver has been deposited on top of copper sites preventing the oxidation of copper from the surface.

This result is supported by the CV plotted with δm *versus* E, *Figure 3.15*. For the cathodic sweep, sweeping from 0.9 negative down to – 0.8 V, from *ca*. 0.9 to – 0.1 V there is only a small increase in mass that was seen previously for the Cu (II)/(I) redox couple. From *ca*. – 0.1 to – 0.8 V there is a large steady increase in mass, this is assigned to the deposition of silver and subsequently silver and copper on the surface of the electrode.

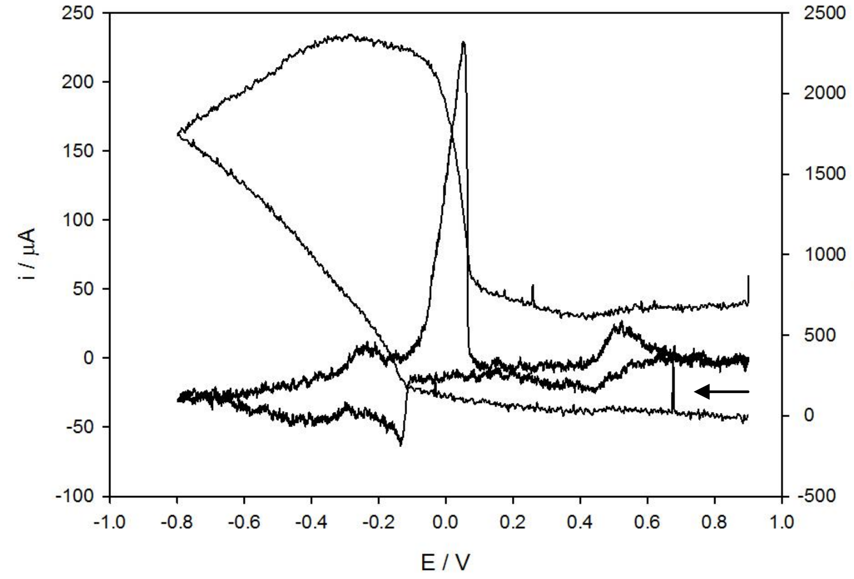

Figure 3.15: Using an EQCM to produce CV data of 10 mM AgCl & $CuCl_2$ dissolved in Ethaline 200. Pt working electrode, 0.205 cm^2. Pt gauze counter electrode. Ag wire reference electrode. Scan rate 10 mV s^{-1}.

For the anodic sweep, sweeping from – 0.8 V positive up to 0.9 V, initially the potential is at a value where deposition is still occurring, where deposition continues from *ca*.– 0.8 to – 0.3 V. After *ca*. – 0.3 up until 0.05 V there is a small drop in mass on the surface of the electrode, which can be attributed to loss of copper It is important to note at this point, that the potential is still in a regime where silver can be deposited. Hence it is theorised that silver being deposited, accounts for the unusual shape of the CV, preventing copper being oxidised fully from the surface. As well as the discrepancy in the mass – charge ratio, with the bulk dissolution being more silver rich than the deposition.

3.4 Gold (I) Chloride in Ethaline 200

When dissolved in Ethaline 200, AuCl forms a yellow solution. The implication of this that an $[AuCl_3]^{2-}$ complex is formed, as well as the expected $[AuCl_2]^-$, which is colourless.[17] This is supported by EXAFS data revealing the speciation to be $[AuCl_2]^-$.[2] The electronic spectrum for AuCl dissolved in Ethaline 200, *Figure 3.16*, displays a number of peaks, with the λ_{max} at 214 nm (ε = 2600 mol^{-1} dm^3 cm^{-1}) and two more at 239 nm (ε = 2200 mol^{-1} dm^3 cm^{-1}) and 300 nm (ε = 1900 mol^{-1} dm^3 cm^{-1}). It is important to note that the onset of the peak at 300 nm, occurs in the violet region of the spectrum, hence giving the solution a yellow colour. The peak at 239 nm is indicative of the $[AuCl_2]^-$ complex and as expected is outside of the visible region.[18] Whilst the peak 300 nm has been assigned to the $[AuCl_3]^{2-}$ species.[19]

The disproportion of $[AuCl_2]^-$ is a known process in aqueous solution, however in high chloride aqueous solution the $[AuCl_2]^-$ complex is known to be stabilised.[17] Hence it is expected that in an Ethaline 200 solution the $[AuCl_2]^-$ should be stable in solution. The $[AuCl_3]^-$ ion is known to be stable in solution.[17]

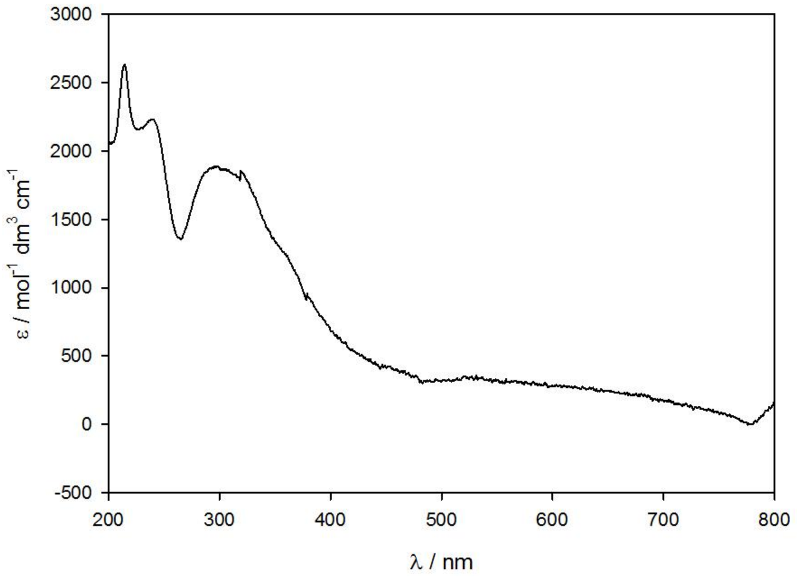

Figure 3.16: The electronic spectra of 1 mM AuCl dissolved in Ethaline 200.

The CV of AuCl dissolved in Ethaline 200, *Figure 3.17*, displays a single redox couple at 0.575 V(Ag wire *pseudo* reference electrode), representing the Au(I)/(0) redox couple. The presence of two gold species does not seem to be discernible in the CV.

There is also a positive, irreversible, current between 0.7 and 1 V, which represents the brake down of Ethaline 200. The fact that this peak is irreversible, means it is unlikely to represent the oxidation of Au(I) → Au(III), where the Au(I)/(III) redox couple would be expected to be reversible. Whilst it is not possible to electrochemically observe the oxidation Au(I) to obtain an Au(III) species in solution, it is expected that Au(III) species would be stable in solution, especially considering the high chloride concentration of Ethaline 200.

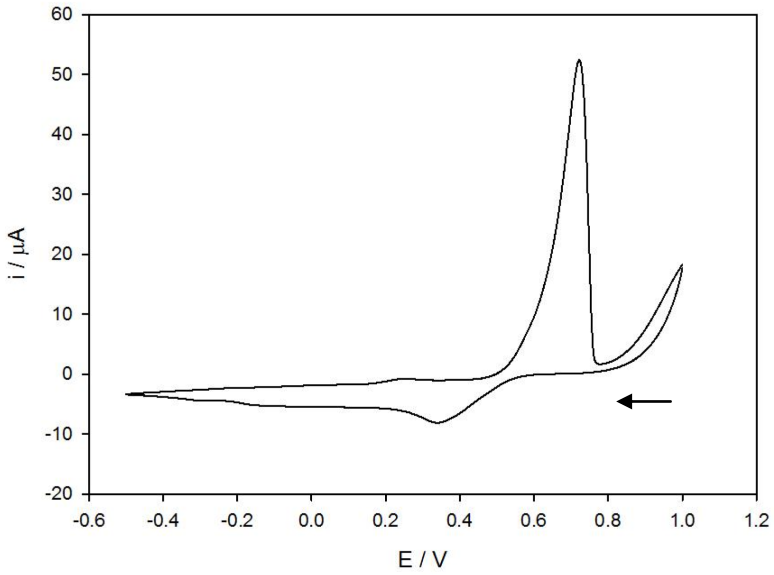

Figure 3.17: CV of 20 mM AuCl dissolved in Ethaline 200. Pt working electrode, 3.14 x 10^{-2} cm^2. Pt flag counter electrode. Ag wire reference electrode. Scan rate 10 mV s^{-1}.

Further information about the Au(I)/(0) redox couple can be obtained from performing the CV of AuCl dissolved in Ethaline 200, using EQCM. *Figure 3.18* displays the CV plotted with the δmoles *versus* E, for the AuCl dissolved in Ethaline 200 system.

For the cathodic sweep, sweeping from 1 V negative down to 0.3 V. Before the redox couple for *ca.* 1 to 0.5 V there is no change in mass on the surface of the electrode, suggesting that any oxidation is likely to be due to breakdown of the liquids at the electrode surface. After the redox couple, from *ca.* 0.5 to 0.3 V deposition is occurring, represented by a negative current in the CV, as well as a large steady increase in mass on the surface of the crystal. The rate of deposition can be determined form the moles *versus* E plot and is found to be 2.41 x 10^{-9} mol s^{-1} cm^{-2}

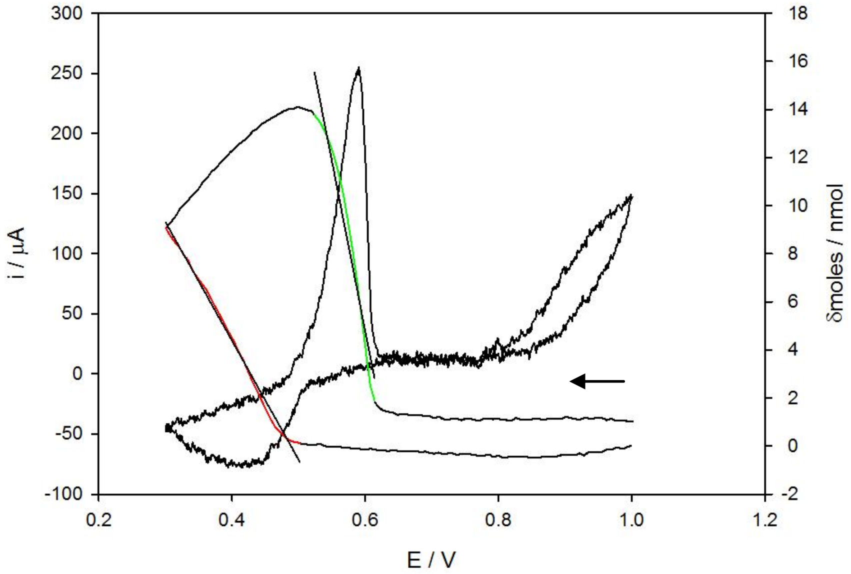

Figure 3.18: Using an EQCM to produce CV data of 10 mM AuCl dissolved in Ethaline 200. Red: deposition of gold, gradient – 4.95 x 10^{-8} *mol* V^{-1} *Green: stripping of gold, gradient – 1.41 x* 10^{-7} *mol* V^{-1}*. Pt working electrode, 0.205* cm^2*. Pt gauze counter electrode. Ag wire reference electrode. Scan rate 10 mV* s^{-1}*.*

For the anodic sweep, sweeping from 0.3 V positive up to 1 V. The sweep starts at a potential where deposition is occurring and continues until *ca*. 0.5 V, this is represented by a negative current and a large steady increase in mass. At *ca*. 0.5 to 0.6 V, the gold is oxidised and stripped from the surface of the crystal, this is represented by a large spike of positive current and a large decrease in mass on the surface of the electrode. The rate of dissolution can be determined from the δmoles v*ersus* E plot and is determined to be 6.88 x 10^{-9} mol s^{-1} cm^{-2}, it should be noted that the rate of dissolution will be affected by the scan rate of the CV. Again as with the copper system, the mass on the surface of the electrode does not return to zero. This is explained by gold alloying with the platinum surface of the electrode, preventing all of the gold being removed.

Further analysis can be performed on with the data gathered from the EQCM, by performing mass – charge ratio analysis of the data collected during the CV, allowing for determination of the current efficiency of the deposition and dissolution processes, 100% current efficiency is calculated using equation **(3.8)**.

$$\frac{\delta \mathrm{m}}{\delta \mathrm{Q}} = \frac{196.97}{\mathrm{F}} = 2.04 \times 10^{-3}\ \mathrm{g\ C^{-1}} \qquad (\mathbf{3.8})$$

From the experimental data, *Figure 3.19*, it is possible to determine an experimental value for the mass – charge ratio. Once this is established it is possible to determine the current efficiency for this process.

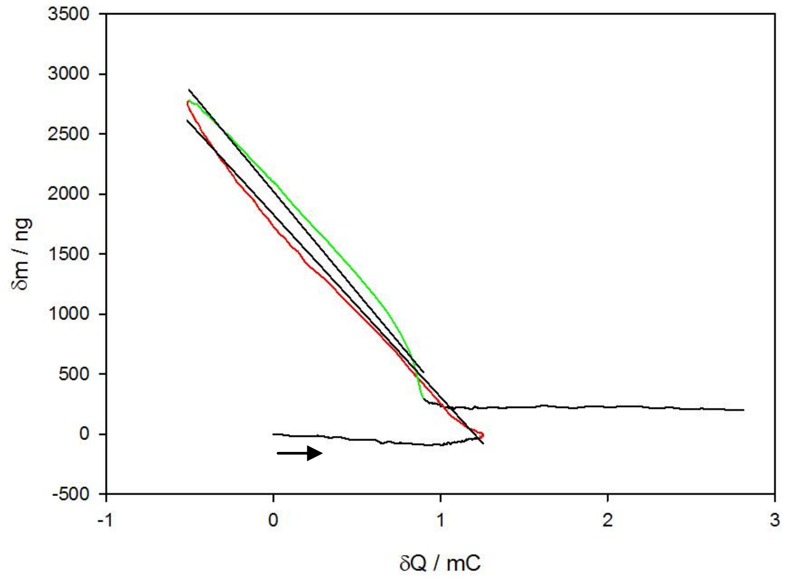

Figure 3.19: Plot of mass versus charge for CV of 10 mM AuCl dissolved in Ethaline 200. Red; deposition of gold, gradient – 1.52 x 10^{-3} g C^{-1}. Green; stripping of gold, gradient – 1.68 x 10^{-3} g C^{-1}.

For the deposition the experimental mass – charge ratio has been calculated to be 1.52 x 10^{-3} g C^{-1}, this suggests that the current efficiency for the deposition of gold is 74 %. Whilst for the dissolution of gold, the experimental mass – charge ratio was found to be 1.68 x 10^{-3}, which represents a current efficiency of 82%.

In *Figure 3.19* there is a large change in current without a change in mass. This is displayed in black between *ca*. 0 to 1.2 mC and *ca*. 1 to 2.9 mC. The current that is passed is attributed to the oxidation and breakdown of Ethaline.

In this system, it should be noticed that unlike the copper, but similar to the silver system, loss of unoxidised gold particles from the surface of the working electrode does not occur. Instead all the gold removed is done so by oxidation and dissolution. Again the rate of dissolution for gold is greater than that of copper, when performed by CV at 10 mV s^{-1}.

By making a solution containing both gold and copper salts, it is possible to study the effect each would have on the others electrochemistry. *Figure 3.20* displays the CV for a mixed solution of AuCl and $CuCl_2$.

Interestingly there appears to be a number of processes occurring. Unlike the silver and copper system where all three redox couples were present and distinct in the CV, the gold and copper system displays significantly altered behaviour. The Au (I)/(0) and the Cu (II)/(I) redox couple are overlapping but can be separated, the electrode potentials are 0.507 V and 0.424 V respectively. There are two reduction waves at – 0.375 and – 0.525 V which could be attributed to the reduction of Cu (I) → (0). Interestingly the expected oxidation peak for Cu (0) → (I) and the dissolution of copper from the surface of the electrode appears as a very broad peak. It should be noted that the current at this point is still negative, due to the reduction of gold.

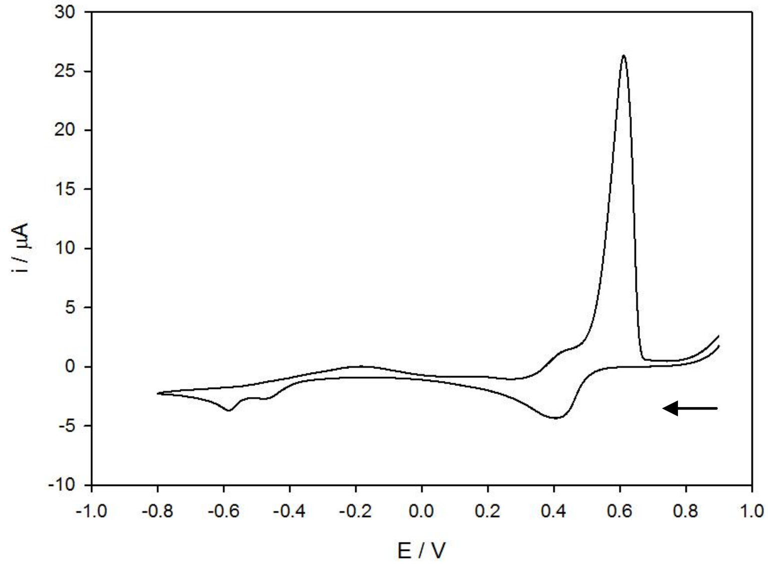

Figure 3.20: CV of 10 mM AuCl and $CuCl_2$ dissolved in Ethaline 200. Pt working electrode, 3.14 x 10^{-2} cm^2. Pt flag counter electrode. Ag wire reference electrode. Scan rate 10 mV s^{-1}.

To further analyse the behaviour of this system the EQCM was used to perform CV. In this case, again, it is instructive to analyse the mass – charge ratio, *Figure 3.21*, before looking at the δmass *versus* E with the CV overlaid, *Figure 3.22*. The data for the mass – charge ratio was obtained from the CV presented in *Figure 3.22*.

The mass – charge ratio demonstrates a number of different deposition regimes, and singular dissolution regime. However, it is possible that dissolution of copper is occurring whilst deposition of gold is occurring, as seen in the CV.

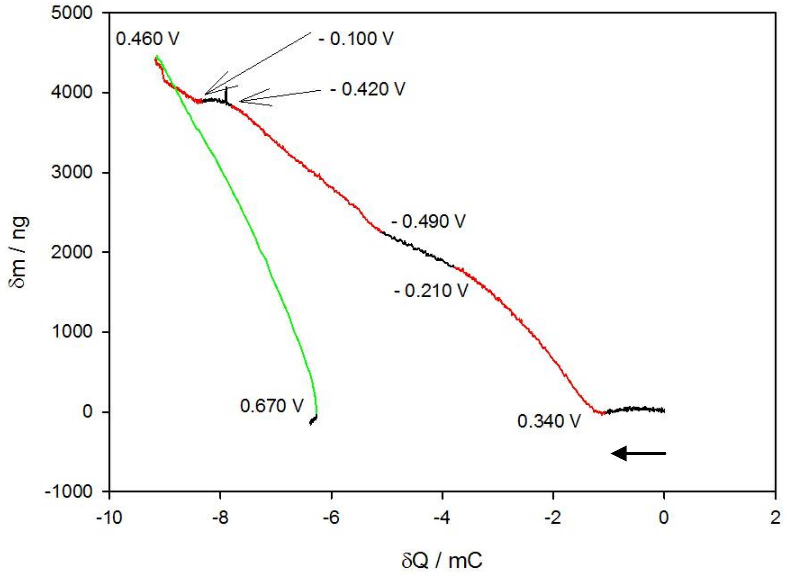

Figure 3.21: Plot of mass versus charge for CV of 10 mM AuCl & $CuCl_2$ dissolved in Ethaline 200.

For the initial deposition, from *ca.* 0.34 to – 0.21 V, the mass charge ratio is determined to be 7.38 x 10^{-4} g C^{-1}. This value is half that determined for the mass charge – ratio for the deposition of gold. Implying that two electrons are being transferred instead of one, which is accounted for by the Cu(II) → (I) reduction occurring at the same time as the Au(I) → (0) reduction.

The second stage of deposition, between *ca.* – 0.210 to – 0.490 V, displays a mass – charge ratio of 3.32 x 10^{-4} g C^{-1}. At this voltage, gold will still be being reduced and deposited on the surface of the electrode, however the amount of gold that can be deposited is controlled by the mass transport of $[AuCl_2]^-$ ions to the surface. Whereas $[CuCl_2]^-$ will be present in the electrical double layer in a high concentration, due to the reduction of Cu (II) → Cu (I). Hence the deposition of copper will be under potential control and not under diffusion control. So the amount of copper being deposited in this regime is expected to be greater than the amount of gold deposited. This can be calculated using equation **(3.9)**.

$$\chi_{\mathrm{Cu}} = \frac{(\mathrm{RMM_{Au}} - \frac{\delta m}{\delta Q}\mathrm{Fb})}{(\frac{\delta m}{\delta Q}2\mathrm{Fa} - \frac{\delta m}{\delta Q}\mathrm{Fb} - \mathrm{RMM_{Cu}} + \mathrm{RMM_{Au}})} = 0.54 \quad (\mathbf{3.9})$$

The atomic percentage of copper that has been deposited in this regime is shown to be 54 % and hence the atomic percentage of gold is 46%. This is in line with the above discussion and once the amount of Cu (I) ions in the electrical double layer have been reduced, the deposition of copper will come under mass transport control. Meaning that once under mass transport the amount of copper in the deposit is expected to be less.

The third deposition regime, between *ca.* – 0.490 to – 0.798 V and – 0.798 to – 0.420 V, is where both copper and gold are being deposited under mass transport controlled condition, the mass – charge ratio is 5.87 x 10^{-4} g C^{-1}. Substituting this mass – charge ratio in to **(3.9)**, it is shown that the atomic percentage of copper being deposited in this regime is 30 % and hence the atomic percentage of gold is 70%. This is as expected as the deposition of gold is both kinetically faster and more current efficient.

The fourth regime, between *ca.* – 0.42 to – 0.1 V, is scanning over a potential where copper is expected to undergo dissolution, whilst the deposition of gold is still under mass transport control. It is not possible to apply equation **(3.9)** to a regime where both deposition and dissolution is occurring. However it is expected that the rate of deposition of gold will be hindered, due to a large concentration of copper ions present is the double layer, slowing the diffusion of gold ions in to the double layer.

The fifth regime, between *ca.* – 0.1 to 0.46 V, it is expected that gold will continue to be deposited and copper will be reduced from Cu(II) → (I) under mass transport control. The mass – charge ratio for this regime is 6.42 x 10^{-4} g C^{-1}, akin to but slightly lower than the initial regime. This demonstrates the deposition of gold with approximately half the mass – charge ratio of that in the solely gold system. The discrepancy explained by possible copper dissolution from the surface of the working electrode.

Finally, the dissolution of gold from the surface of the electrode occurs. The mass – charge ratio for the dissolution is 1.45 x 10^{-3} g C^{-1}. This is less than solely gold dissolution which, above, was found to be 1.68 x 10^{-3} g C^{-1}. So it is expected that whilst most of the copper has been removed from the surface of the electrode, that some is still present in the deposit, due to alloying of copper and gold as deposition of both elements is occuring. As the current efficiency for the dissolution of copper cannot be calculated, it is not possible to calculate a molar ratio of metals in the dissolution.

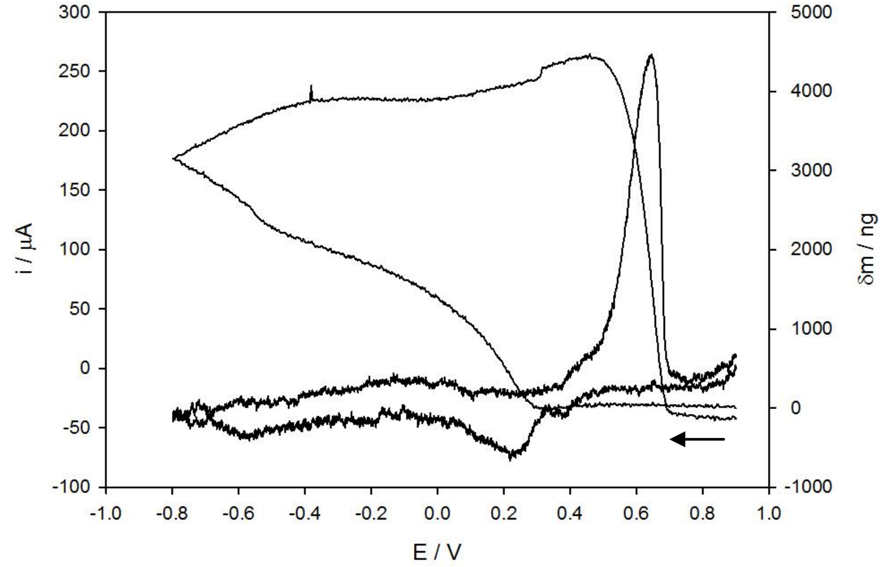

Figure 3.22: Using an EQCM to produce CV data of 10 mM AuCl & $CuCl_2$ dissolved in Ethaline 200. Pt working electrode, 0.205 cm^2. Pt gauze counter electrode. Ag wire reference electrode. Scan rate 10 mV s^{-1}.

The results discerned from the mass – charge ratio plot are supported by the CV plotted with the δm *versus* E plot. In the cathodic sweep, negative from 0.9 V down to – 0.8 V. Form *ca*. 0.9 to 0.34 V there is no change in mass and the corresponding current is also close to zero. There is a small peak in the current at *ca*. 0.4 V which corresponds to the Cu (II)/(I) redox couple. From *ca*. 0.34 to – 0.21 V there is a large increase in mass and a negative current in the CV, representing reduction and deposition of gold on the surface on the electrode. The profile of the change in mass is a curve, can be accounted for by the deposition of gold that is coming under mass transport control. At *ca*. – 0.21 V there is a change in the profile of the δm *versus* E, the profile becomes a straight line, this is where copper in being deposited under potential control and gold is under mass transport control. At *ca*. – 0.49 V copper comes under mass transport control, represented by a small curve in the δm *versus* E profile. Finally both gold and copper are under mass transport control, which is represented by a straight line in the δm *versus* E profile.

In the anodic sweep, from – 0.8 V positive to 0.9 V, the sweep starts in the deposition regime where both copper and gold are under mass transport control. At *ca*. – 0.42 V the copper starts to undergo dissolution whilst gold continues to be deposited under mass transport control, which is represented by almost no change in mass in the δm *versus* E profile. Once most of, but not all, the copper has been removed, at *ca*. – 0.1 V the mass in the δm *versus* E profile starts to increase again. This is representative of the deposition of gold that is still occurring at this potential. Finally at *ca.* 0.46 V there is a large decrease in mass, as well as a large positive spike in current. This represents the dissolution of gold from the surface, it is important to note that some copper will be involved in this dissolution. Interestingly in this case, unlike in the copper and silver mixed system, the mass at the end of the cycle returns to a similar value as the start of the cycle. This can be attributed one of two reasons, to the copper and gold forming an alloy together, preventing the copper interacting with the platinum of the working electrode. The alternative is that gold is deposited before the copper, preventing the copper being deposited directly on to the platinum of the working electrode.

3.5 Conclusions

In this chapter, the electrochemistry of group 11 elements has been investigated. With use of UV – Vis spectroscopy and previously performed work, it has been possible, not to only assign the oxidation states the redox couples represent, but also the molecular species involved.

The electrochemical experiments have yielded a number of important properties of these reactions. The rate of deposition and dissolution of metals has been compared and it has been found that whilst both silver and gold have a faster dissolution process, they do not lose mass from the surface of the electrode without oxidation, unlike copper.

Mixed metal systems have also been analysed, to see what effect copper ions present in solution will have on the deposition of silver and gold. The deposition and dissolution for both these systems has been characterised and the mole fraction of the deposits determined. The results for the gold system are explained with classic electrochemical behaviour and show the possibility of an alloy for copper and gold on the surface of the crystal. The results for the silver system imply a co – deposit is formed on the surface of the crystal, unlike the gold system however, it is difficult to separate the electrochemistry of the different metals. This is due to the two redox couples, for the deposition of the metals, being close in potential and the scan rate being fast enough to scan over both without one of the redox couples dominating the electrochemical behaviour. If the scan rate was slowed then separation of the electrochemical behaviour could be observed.

With regards to the aims of this chapter, the speciation of the metal centres in solution has been established. The electrode potentials for the deposition of the group 11 metals have been characterised. The rate of the electrochemical reactions has been characterised, with respect to gain and loss of mass on the surface of a QCM crystal. The current efficiency of the deposition reactions has been calculated, however due to loss of unoxidised material, the current efficiency of the dissolution process could not be calculated.

The use of slower rates of electrochemical reaction, governed by the scan rate of the CV or by choosing a judicious potential to perform chronoamperometry, would allow for characterisation of current efficiency of the dissolution of copper.

3.6 References

1. A. P. Abbott, G. Frisch, S. J. Gurman, A. R. Hillman, J. Hartley, F. Holyoak, and K. S. Ryder, *Chem. Commun. (Camb).*, 2011, **47**, 10031 – 10033.
2. J. Hartley, Ph.D. Thesis, University of Leicester, 2013.
3. J. M. Hartley, C.-M. Ip, G. C. H. Forrest, K. Singh, S. J. Gurman, K. S. Ryder, A. P. Abbott, and G. Frisch, *Inorg. Chem.*, 2014, **53**, 6280 – 6288.
4. A. P. Abbott, S. Nandhra, S. Postlethwaite, E. L. Smith, and K. S. Ryder, *Phys. Chem. Chem Phys.*, 2007, **9**, 3735 – 3743.
5. M. A. Khan, J. Meullemeestre, M. J. Schwing, and F. Vierling, *Polyhedron*, 1983, **2**, 459 – 463.
6. P. De Vreese, N. R. Brooks, K. Van Hecke, L. Van Meervelt, E. Matthijs, K. Binnemans, and R. Van Deun, *Inorg. Chem.*, 2012, **51**, 4972 – 4981.
7. G. Li, D. M. Camaioni, J. E. Amonette, Z. C. Zhang, T. J. Johnson, and J. L. Fulton, *J. Phys. Chem. B*, 2010, **114**, 12614 – 12622.

8. A. Popescu, V. Constantin, A. Cojocaru, and M. Olteanu, *Rev. Chim.*, 2011, 206 – 211.

9. M. B. Davies, R. J. Mortimer, and T. R. Vine, *Inorganica. Chim. Acta.*, 1988, **146**, 59 – 63.

10. D. F. Shriver, P. W. Atkins, and L. C. H., in *Inorganic chemistry*, Oxford University Press,, Oxford, 2nd edn., 1996, ch. 7, pp. 295 - 297, 1996, pp. 295 – 297.

11. A. P. Abbott, K. El Ttaib, G. Frisch, K. J. McKenzie, and K. S. Ryder, *Phys. Chem. Chem. Phys.*, 2009, **11**, 4269 – 4277.

12. T. Rayment, presented in part at the University of Birmingham, Midland Electrochemistry Group Meeting, Birmingham, 2012.

13. B. E. Etschmann, J. R. Black, P. V. Grundler, S. Borg, D. Brewe, D. C. McPhail, L. Spiccia, and J. Brugger, *RSC Adv.*, 2011, **1**, 1554 – 1566.

14. J. Brugger, B. Etschmann, W. Liu, D. Testemale, J. L. Hazemann, H. Emerich, W. van Beek, and O. Proux, *Geochim. Cosmochim. Ac.*, 2007, **71**, 4920 – 4941.

15. L. M. C. Pinto, E. Spohr, P. Quaino, E. Santos, and W. Schmickler, *Angew. Chem. Int. Ed. Engl.*, 2013, **52**, 7883 – 7885.

16. K. S. Ryder, Personal Communication.

17. R. J. Puddephatt, in *Comprehensive Coordination Chemistry, The Synthesis, Reactions, Properties & Applications of Coordination Compounds*, eds. G. Wilkinson, R. D. Gillard, and J. A. McCleverty, Pergamon Press, Oxford, 1987, vol. 5 Late Transition Elements, ch. 55, pp. 871.

18. L. Aldous, D. S. Silvester, C. Villagr?n, W. R. Pitner, R. G. Compton, M. Cristina Lagunas, and C. Hardacre, *New J. Chem.*, 2006, **30**, 1576 – 1583.

19. T. M. Salama, T. Shido, R. Ohnishi, and M. Ichikawa, *J. Phys. Chem.*, 1996, **100**, 3688 – 3694.

Chapter 4: Galvanic Deposition of Group 11 Elements from Ethaline 200

4.1 Introduction

In this chapter, the results of the galvanic deposition are discussed. The electrochemistry of the group 11 salts, established in **Chapter 3**, has been used to discuss how galvanic reactions proceed.

The use of the galvanic reaction to produce metal coatings of a substrate established.[1] The use of precious metals coatings can be found in a wide range of industrial applications. This includes the printed circuit board industry, where the galvanic silver and electroless nickel immersion gold (ENIG) processes were used for the protection of copper solder pads.[2,3] The ENIG process uses the galvanic palladium reaction to activate the surface of the copper substrate for the electroless deposition of nickel. Also, the ENIG process uses galvanic reaction of gold with electroless nickel to produce a coating that does not react with air. The galcanic reation of gold with copper has also been using to produce a copper – gold alloy catalyst for the oxidation of borohydride.[4]

The Gibbs free energy of the reaction between group 11 metal ions and a Cu (0) substrate, under standard conditions, have been calculated from the electrode potentials determined in **Chapter 3**. From the results of the Gibbs free energy calculations, it was possible to predict the stoichiometry of the galvanic reactions. The stoichiometry predictions have been compared to the results of the QCM experiment, to verify the results. The rate of reaction between group 11 metal ions and a copper substrate will also be discussed using the results from the QCM data.

Finally, the results of the precious metal deposition on a standard copper substrate were discussed.. The morphology of the deposits were characterised by AFM and SEM and the compositions were characterised using EDX and XPS.

The aims of this chapter were:

- Discussion of the Gibbs free energy of the galvanic reaction between group 11 metals and a copper substrate.
- Discussion of the predicted and experimentally determined stoichiometry of the galvanic reactions.
- Discussion of galvanically deposited group 11 metal coatings on to a copper substrate. Including morphology and composition.

4.2 Galvanic Deposition of Silver on a Copper Substrate

Using the electrode potentials calculated in **Chapter 3** it is possible to calculate the change in Gibbs free energy, for the reaction of Ag (I) ions with a Cu (0) substrate, under standard conditions. From the calculated value for the Gibbs free energy, it is possible to predict whether a spontaneous galvanic reaction will occur. The Gibbs free energy is calculated using equation **(4.1)**.

$$\Delta \mathrm{G} = -\mathrm{nFE} \quad (\mathbf{4.1})$$

Where E is the electromotive force, which for the work in this chapter can be calculated using equation **(4.2)** and n is the number of electrons being transferred. For the reaction between Ag (I) ions and a Cu (0) substrate, n = 1.

$$\mathrm{E} = \mathrm{E}_{\mathrm{Ox}} - \mathrm{E}_{\mathrm{red}} \quad (\mathbf{4.2})$$

Where E_{ox} is the electrode potential of oxidised species, in this case silver, and E_{red} is the electrode potential of the reduced species, in this case copper. Formally the electromotive force is defined by taking the most positive electrode potential from the least positive electrode potential, for any system.

Using the electrode potentials determined **Chapter 3**, – 0.075 V and – 0.325 ± 0.06 V for silver and copper respectively, it is possible to determine the value of the Gibbs free energy.

To calculate the Gibbs free energy, the formal electrode potential of the Cu (I)/(0) and Ag (I)/(0) redox couples, referenced against a Ag wire *pseudo* reference electrode, was calculated using the Nernst equation and the electrode potential determined form the cyclic voltammetry. The formal electrode potentials were found to be – 0.205 ± 0.06 V and 0.024 V respectively. Using the formal electrode potentials, it is possible to calculate the Gibbs free energy of the reaction, under standard conditions, $\Delta G = -\ 22.2 \pm 5.8 \text{ x } 10^3 \text{ J mol}^{-1}$. Hence is it thermodynamically favourable for the Ag (I) ions with undergo a spontaneous galvanic reaction with a Cu (0) substrate. The result of the reaction will be Ag (I) ions being reduced and deposited on to the surface of a copper substrate and Cu (0) atoms being oxidised and undergoing dissolution.

It should be noted that the formal electrode potential for the Cu (II)/(I) redox couple is at 0.595 V. Hence, once the copper has been oxidised to the Cu (I) species, it is not expected to undergo further oxidation to the Cu (II) species, as the Ag (I)/(0) redox couple is more negative than the Cu (II)/(I), hence the value of the electromotive force will be negative and hence the Gibbs free energy will be positive. It should be noted that if any Cu (II) ions were present in the solution, the Cu (II) would react with the Ag (0) and form Cu (I) and Ag (I).

From the above discussion, it is possible to theorise about the reaction occurring at the surface of a copper substrate and write a balanced equation for the reaction, **(4.3)**. It is proposed that the $[AgCl_2]^-$ species reacts with the copper substrate to produce, reduced silver metal, whilst the copper is oxidised to the Cu (I) species $[CuCl_2]^-$.

$$[\mathrm{AgCl_2}]^-_{(\mathrm{DES})} + \mathrm{Cu}^0_{(\mathrm{s})} \rightarrow \mathrm{Ag}^0_{(\mathrm{s})} + [\mathrm{CuCl_2}]^-_{(\mathrm{DES})} \qquad (\mathbf{4.3})$$

To investigate the reaction between Ag (I) ions and Cu (0) atoms, as well as test the hypothesis that the reaction proceed by equation **(4.3)**, a QCM experiment was performed. The amount of copper deposited on the surface of a crystal was compaired with the amount of silver deposited after the galvanic reaction had proceeded to completion. Completion was judged to be when there ceased to be a change in frequency of the QCM.

Copper was electrochemically deposited on the surface of a QCM crystal, at 2 A cm^{-2} for varying lengths of time. By varying the time of copper deposition, it is possible to see what effect a larger amount of copper will have on the galvanic process.

The copper coated QCM crystal was immersed in a Ag (I) ion solution and the reaction was allowed to proceed to completion. Completion being when there is no longer a change in mass on the surface of the electrode. At this point all the copper should have undergone oxidation and dissolution, leaving only a layer of the reduced silver deposited on the electrode.

It should be noted that all the copper may not have been oxidised and undergone dissolution from the surface of the electrode, prevented in doing so by the silver deposited on top of the copper, acting as a barrier between the copper and the solution. The incomplete oxidation of copper would skew the results of the results of the experiment, as copper atoms weigh less than silver atoms the mass calculated on the surface of the electrode will be low and hence so will the calculation of the number of moles. This should be investigated by EDX analysis to look for residual copper.

By taking the resonance frequency of the QCM before any deposition, after copper deposition and after silver deposition, *Figure 4.1*, it is possible to calculate the mass of copper and silver deposited during the experiment, using the Sauerbrey equation. Hence, it possible to calculate the number of moles of copper and silver taking part in the reaction, meaning the stoichiometry of the reaction can be established.[2] These results are summarised in *Table 4.1*. It should be noted that if impurities are present in deposit, such as trapped DES or metal oxides, then the results of the reaction will be skewed.

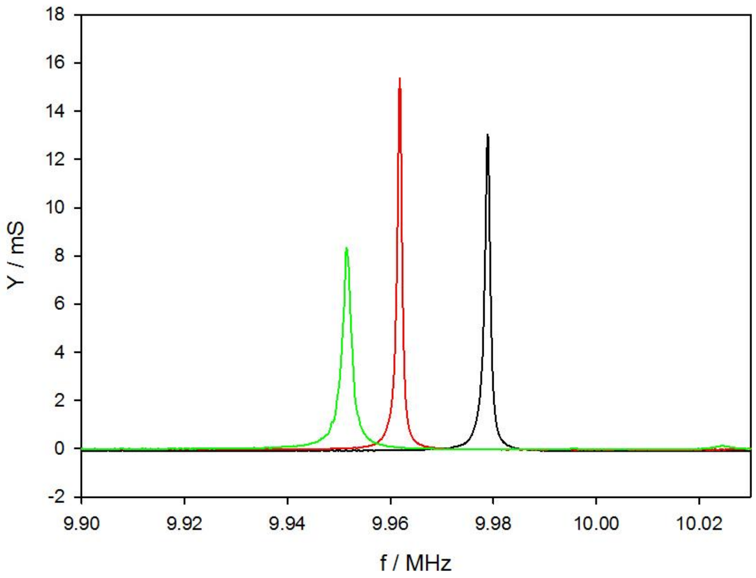

Figure 4.1: Admittance data showing the frequency of change of a QCM during the silver stoichiometry experiment. Black: Uncoated QCM. Red: Copper coated QCM. Green: Silver coated QCM.

Table 4.1: Comparison of the number of moles of copper and silver deposited on the surface of a QCM crystal.

Cu deposition time / s	Moles of Cu deposited / x 10^{-7} mol	Moles of Ag deposited / x 10^{-7} mol	Yield / %
60	1.20	1.12	93
120	2.43	2.29	94
180	3.80	2.83	74

In *Table 4.1*, the reactions proceed with 93, 94 and 74% yield. The loss in mass of the sliver deposit is accounted for by loss of unoxidised copper particulate, as seen in the electrochemical characterisation in **Chapter 3**. It is also possible that not all the copper has undergone dissolution, be prevented in doing so by a coating of silver. As copper weighs less than silver, the mass deposited on the crystal at the end of the experiment will be less than expected, hence lowering the yield of the experment. It is proposed that the reaction occurring after 180 s of copper deposition, has a much lower yield due to a larger percentage of copper disintegration or a silver coating preventing the oxidation of copper from the surface of the electrode.

Figure 4.2 shows the change in mass of a copper coated QCM, from when the QCM was immersed in a 0.1 M solution of AgCl dissolved in Ethaline. The change in mass displays a linear response until 162 s, where the reaction appears to have finished. The end of the reaction is represented by the change in mass ceasing to rise. After the end of the reaction, the mass on the surface of the crystal seems to be falling slightly. This is possibly due to loss of silver from the surface of the electrode. By tracking the change in mass for the reaction it is possible to determine the rate of reaction.

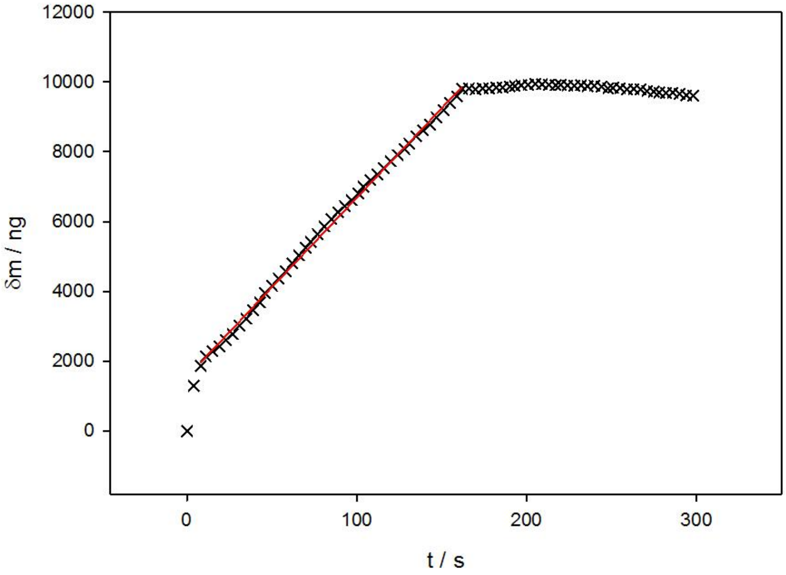

Figure 4.2: Change in mass versus time plot, for the galvanic deposition of silver on a copper substrate. Gradient of change in mass plot 5.13 x 10^{-8} *g* s^{-1}. Pt working electrode, 0.205 cm^2.

Using the gradient of the change in mass *versus* time plot, it is possible to calculate the rate of reaction. The change in mass can be converted to a change in moles using equation **(4.4)**.

$$\delta \mathrm{m} = \delta \mathrm{mol} \times \left(\mathrm{RMM_{Ag}} - \mathrm{RMM_{Cu}}\right) \quad \mathbf{(4.4)}$$

Once the change in moles has been calculated, it is possible to calculate the rate of reaction from the gradient of the trend and the area of the working electrode. The rate of reaction was calculated to be 5.65 x 10^{-9} mol s^{-1} cm^{-2}.

To investigate the morphology and composition of deposits, a copper substrate was prepared by electrolytically plating a copper Hull cell test peace. Once the standard substrate had been prepared, it was immersed in a 0.1 M AgCl dissolved in Ethaline. Once plating was complete, the morphology was analysed using AFM and SEM.

A 3D representation of the surface has been measured using AFM, *Figure 4.3*. The micrograph displays similar bulk morphology to that of the underlying copper substrate (see **Appendix 2**), on top of which a fine granular structure has been deposited. The size of the grains ranges from *ca*. 200 – 600 nm in diameter.

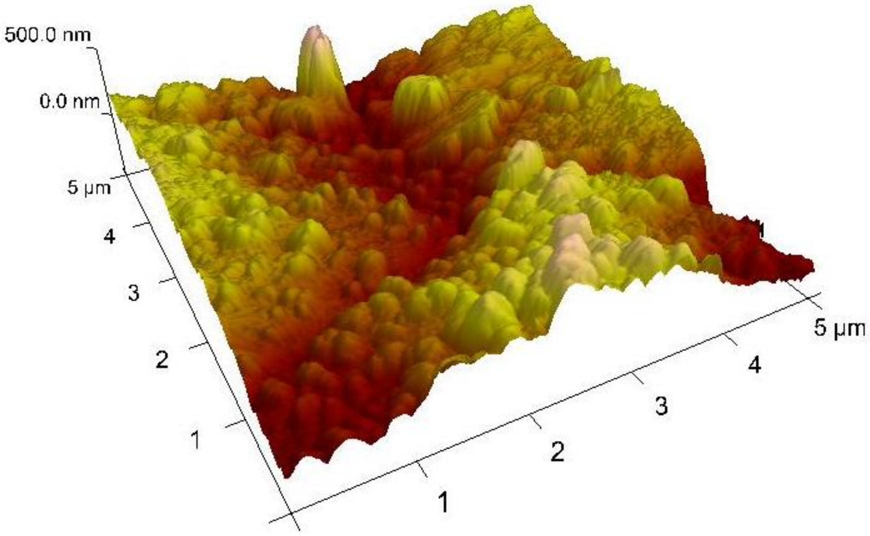

Figure 4.3: Atomic force micrograph of a galvanic silver coating of a copper substrate.

Using AFM, it is possible to calculate the surface area of the deposit and hence the roughness of the surface. The average surface area of the silver deposit has been calculated from five 25 µm^2 sections. The surface area was found to be 33.8 ± 2.7 µm^2, which is a difference in surface area of 35 ± 10%. This is a marked increase when compared to the average surface area and difference in surface area of the copper substrate, which has an average surface area of 28.2 ± 0.8 μm^2, which is a difference in surface area of 12 ± 3%, *Table 4.2*.

Table 4.2: Surface areas and difference of surface area of galvanicly produced coatings and electrolytic copper substrate.

Sample	Surface area / μm^2	Difference of surface area / %
Electrolytic copper	28.2 ± 0.8	12 ± 3
Galvanic silver	33.8 ± 2.7	35 ± 10
Galvanic gold	29.5 ± 2.3	18 ± 9

The secondary electron, SEM image of the galvanic silver coating is displayed in *Figure 4.4*. The bulk of deposit appears as a uniform surface, akin to the underlying copper substrate. With, as seen in the AFM image, appears to be a fine granular structure on the surface of the deposit.

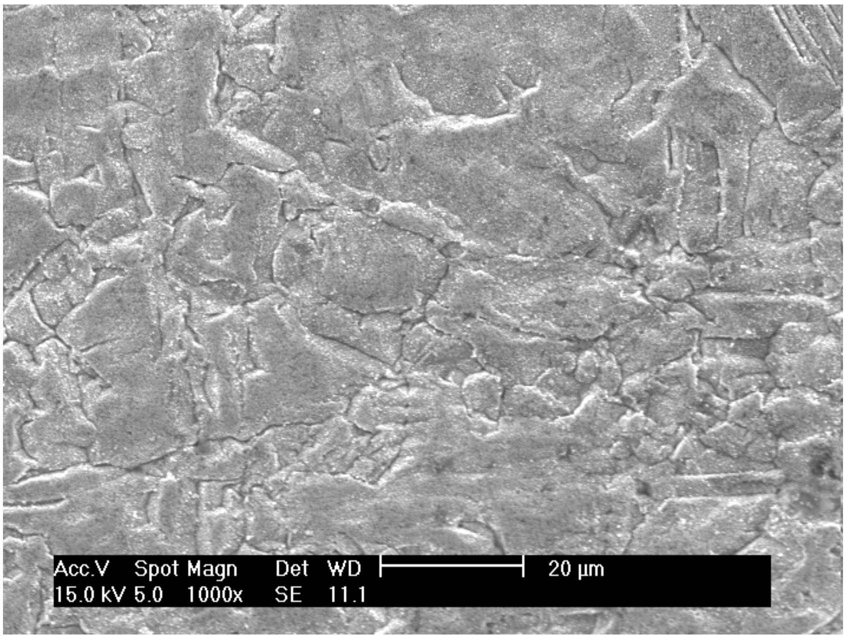

Figure 4.4: Secondary electron SEM image of a galvanic silver coating of a copper substrate.

There also appears to be pores and cracks in the surface of the silver. These pores allow for the underlying copper to undergo dissolution from the surface. Hence, copper can undergo oxidation and silver can be reduced and deposited on the surface of the substrate.

The cracks and pores, circled in red, on the surface are more evident when the coating is viewed using back scattered electron, SEM image, *Figure 4.5*. From SEM the pores appear to be on a sub micron scale and when analysed by AFM, the pores appear to be *ca*. 200 nm in diameter.

It should be noticed, in the back scattered electron image, that the majority of the surface appears to be of the same elemental composition. As shown by the even shading of the back scattered electron image, the composition of the surface was analysed using EDX and XPS. There is a darker shaded area in the bottom right hand corner of the deposit, indicating that is area could be of a different composition.

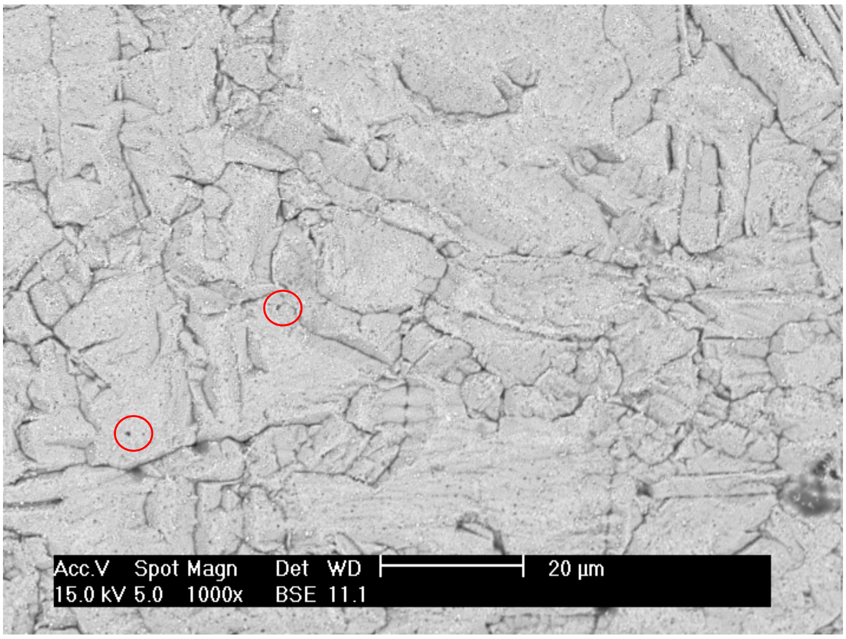

Figure 4.5: Back scattered electron SEM image of galvanic silver coating of a copper substrate.

To characterise the elements present in the sample, EDX analysis was performed, *Figure 4.6*. The spectrum acquired from EDX analysis shows copper, silver and carbon in the spectrum, with atomic percentages of 27 %, 42 % and 31 % respectively. There is no oxygen present in the spectrum, suggesting limited presence of copper or silver oxide in the sample.

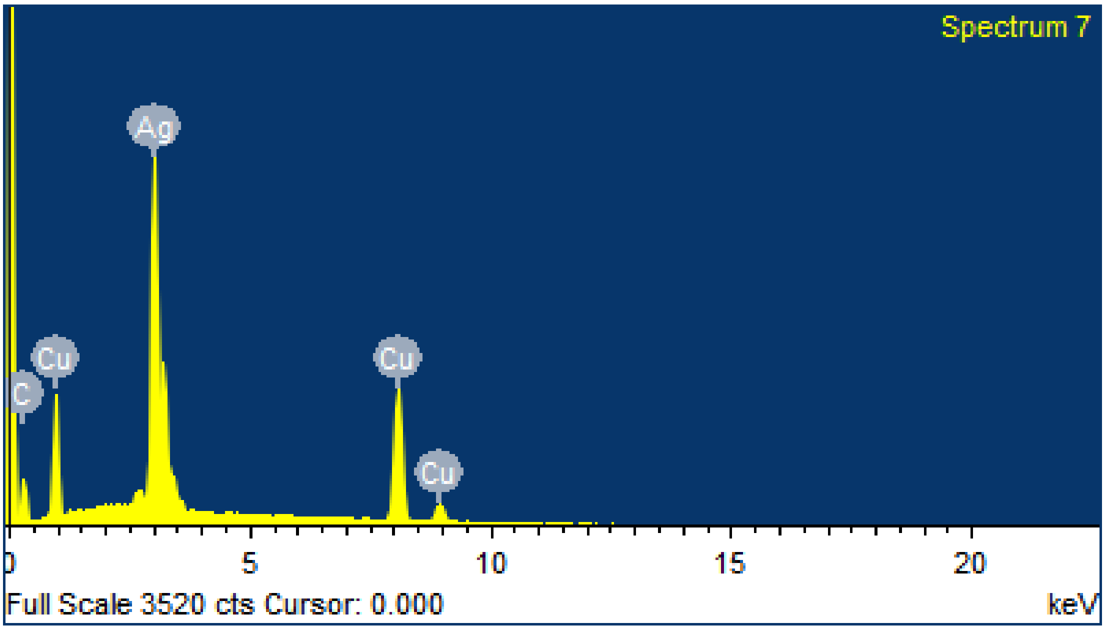

Figure 4.6: EDX spectrum of a galvanic silver coating of a copper substrate.

As discussed in **Chapter 2** the primary electron beam of an SEM has a large interaction volume with the sample, greater than the thickness of the coating. Hence, XPS was used to analyse the composition of just the surface. *Figure 4.7* displays the full XPS spectrum, with the expected silver spectral lines superimposed on the spectrum. It should be noted that there are other peaks present in the spectrum, not just the peaks for silver.

Unlike with the EDX analysis above, in the full XPS spectrum, there does not appear to be any peaks that would be associated with copper, in the spectrum. However there does appear to be peaks associated with oxygen, nitrogen and carbon at 532 eV, 399 eV and 285 eV respectively. Due to the proportion of contaminants remaining on the surface, it is purposed that residual Ethaline remains on the surface of the sample, despite cleaning.

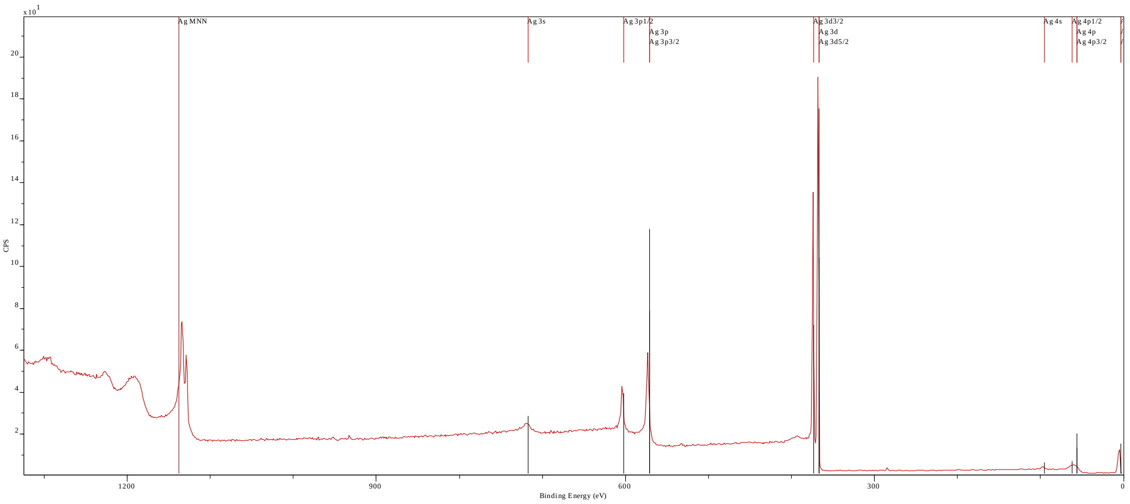

Figure 4.7: XPS spectrum of galvanic of a silver coating of a copper substrate.

Further XPS analysis has been performed where the high resolution spectra of Ag, Cu, C, O, N and Cl have been analysed, *Figure 4.8*, and using these spectra the composition of elements at the surface of the sample has been established, *Table 4.3*. The expected atomic ratios for residual Ethaline are C 9 : N 1 : O 5 : Cl 1, which is similar to the results obtained from the high resolution spectra. The Ethaline could be trapped by in the pores or cracks in the surface of the sample, due to capillary forces.[6]

Table 4.3: Elemental composition of a silver coating of a copper substrate.

Element	Orbital Scanned	Atomic Percentage / %
Ag	3d	82
Cu	2p	1
C	1s	11
O	1s	4
N	1s	1
Cl	2p	1

The high resolution spectra for Ag, displays two sets of doublets. The appearance of a second set of peaks suggests that the Ag surface has undergone oxidation as the binding energy of the peaks has been shifted.

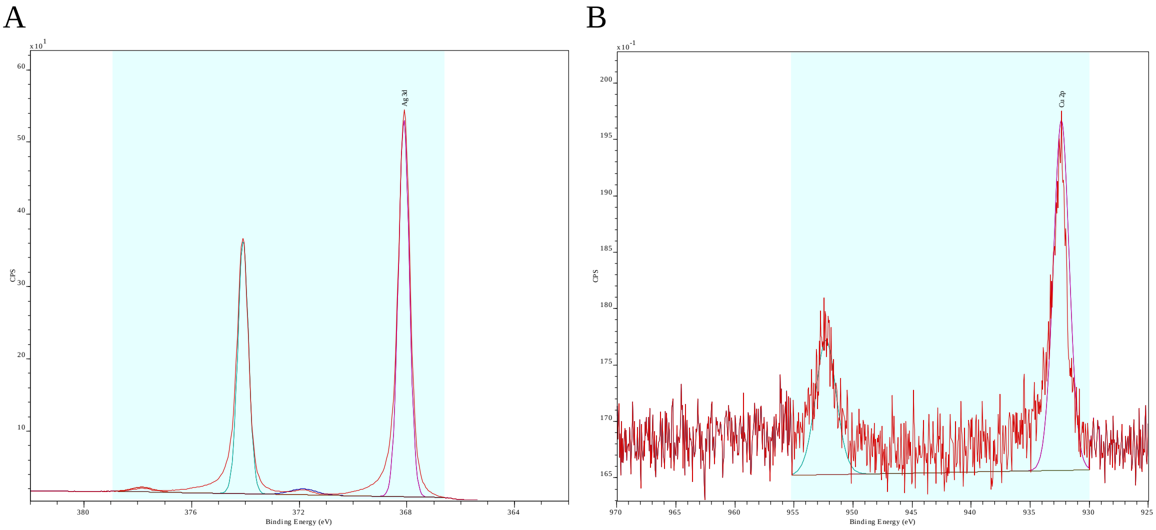

Figure 4.8: High resolution XPS data of A: Ag and B: Cu, of a galvanic silver coating of a copper substrate.

Both sets of doublets display a peak separation of 6 eV. This separation is consistent with the peak separation in the Scofield element library in the CasaXPS software,[5] indicating that the second set of doublets is indeed due to Ag being in a different chemical environment. The area of both sets of peaks, also display the expected 2 : 3 area ratio for the 3d 3/2 and 3d 5/2 electron transitions. The surface of the coating contains an 82 % atomic percentage of silver, of which 4 % is the silver oxide and 96 % is pure silver.

The surface only contains *ca*. 1 % copper, which does not appear to be oxidised as there are not observable shifted doublets in the spectrum. The doublet repressing the 2p 1/2 and 2p 3/2 electron transitions, appears with the appropriate peak separation and the characteristic 1 : 2 area ratio respectively.

The lack of copper on the surface of the sample indicates that silver is forms a distinct layer on top of the copper, preventing copper from diffusing through the silver, to the surface of the sample. This is an unsurprising result when considering the electrochemistry presented in **Chapter 3.2**. The EQCM showed that copper and silver display separate electrochemistry, when both are combined in the same system, indicating that an alloy is not formed on the surface of the galvanic deposit sample. This supposition is supported by the binary phase diagram of copper and silver, as produced by Subramanian *et. al.*,[7] which shows that copper and silver do not form alloys at 50 °C.

4.3 Galvanic Deposition of Gold on a Copper Substrate

Unlike in the above system with the deposition of silver, the Au (I)/(0) redox couple has a more positive value than the Cu (II)/(I) redox couple. This means that, in theory, that Cu could undergo a (0) → (II) oxidation, depositing two moles of gold for every one mole of copper that undergoes dissolution. It should also be noted that the Au (I)/(0) redox couple is more positive than the Ag (I)/(0) and hence it would be expected that a solution of AuCl dissolved in Ethaline will undergo a reaction with Ag (0) substrate.

From the above discussion, it is possible to suggest a number of different oxidation pathways of Cu (0) and Cu (I), by which the reaction could proceed, as shown in equations **(4.5a)**, (**4.5b)**, **(4.5c)**.

$$[\mathrm{AuCl_2}]^-_{(\mathrm{DES})} + \mathrm{Cu}^0_{(\mathrm{s})} \rightarrow \mathrm{Au}^0_{(\mathrm{s})} + [\mathrm{CuCl_2}]^-_{(\mathrm{DES})} \quad (\mathbf{4.5a})$$

$$2[\mathrm{AuCl_2}]^-_{(\mathrm{DES})} + \mathrm{Cu}^0_{(\mathrm{s})} \rightarrow \mathrm{Au}^0_{(\mathrm{s})} + [\mathrm{CuCl_4}]^{2-}_{(\mathrm{DES})} \quad (\mathbf{4.5b})$$

$$[\mathrm{AuCl_2}]^-_{(\mathrm{DES})} + [\mathrm{CuCl_2}]^-_{(\mathrm{DES})} \rightarrow \mathrm{Au}^0_{(\mathrm{s})} + [\mathrm{CuCl_4}]^{2-}_{(\mathrm{DES})} \quad (\mathbf{4.5c})$$

There are three separate oxidation pathways of copper, by which gold may be reduced and deposited on the surface of the copper substrate. To examine the mechanism by which the reaction proceeds, a QCM experiment was performed to investigate the stoichiometry of the reaction. Where varying amounts of copper were deposited on the surface of a QCM crystal and then immersed in a Au (I) ion solution until all the copper has been oxidised from the surface. The number of moles of copper and gold deposited were compared and the stoichiometry of the reaction was assigned.[2]

The results of the stoichiometry experiment are summarised is *Table 4.4*. The number of moles of gold deposited are less than a 1 : 1 stoichiometry for copper and gold respectively. For reactions that proceed via equations **(4.5b)** or **(4.5c)**, the expected stoichiometry would be 1 : 2 for Cu and Au respectively. As the ratio of the metals is closer to 1 : 1 thank 1 : 2 it is posited that the reactions proceed with a 1 : 1 stoichiometry and hence proceeds following equation **(4.5a)**.

Table 4.4: Comparison of the number of moles of copper and silver deposited on the surface of a QCM crystal.

Cu deposition time / s	Moles of Cu deposited / x 10^{-7} mol	Moles of Au deposited / x 10^{-7} mol	Yield / %
60	1.11	0.42	37
120	2.23	0.99	44
180	3.58	2.94	82

Using the electrode potentials obtained in **Chapter 3**, the Gibbs free energy for the reaction of Au (I) ions, with a Cu (0) substrate, in an Ethaline 200 medium, can be calculated. Using the Nernst equation it is possible to calculate the formal electrode potential of gold, 0.675 V. Using the formal electrode potentials of copper and gold the EMF of the system under standard conditions can be calculated. The value of the EMF is E = 0.88 ± 0.06 V. Then using equation **(4.1)** value of the change in Gibbs free energy, under standard condition, can be calculated to be $\Delta G = -84.9 \pm 5.8 \times 10^3$ J mol^{-1}. Hence it is expected that Au (I) ions with spontaneously react with a Cu (0) substrate.

For the reaction of Au (I) ions and Cu (I), the EMF is E = 0.07 V and the change in Gibbs free energy is $\Delta G = -6.4 \times 10^{-3}$ J mol^{-1}. Whilst there will still be a thermodynamic driving force for the reaction between Au(I) and Cu (I) ions, it is thermodynamically favourable for the Au (I) ion to react with the Cu (0) substrate.

The stoichiometry experiments proceeds with 37 %, 44 % and 82 % yields, the loss in yield is attributed to the delamination of copper from the surface of the QCM crystal, as shown in the EQCM CV experiments. It is also possible, like with the silver system, not all of the copper has undergone oxidation because gold has formed complete layer at the surface, preventing the copper coming in to contact with the solution and undergoing oxidation. As copper weighs less than gold and the value of mass on the surface of the electrode would be less than expected if the reaction had reach completion. It is also possible that the copper has formed an alloy with the deposited gold on the surface of the electrode, producing a thermodynamically stable coating that is resistant to the oxidation by Au (I) ions, hence reaching an end point of the reaction where not all of the copper has been removed from the surface of the electrode.

Figure 4.9 shows the change in mass of a copper coated QCM crystal when immersed in a 0.1 M solution of AuCl dissolved in Ethaline. The change in mass shows a curve at the start of the experiment, that levels off in to a straight line. The reaction proceeds for *ca*. 332 s, where the change in mass stops rising and hold a constant value, this indicated that the reaction has proceeded to completion. By tracking the change in mass with respect to time, it is possible to calculate the rate of reaction, this should be performed when the change in mass is linear. The gradient of the change in mass with respect to time is represented by a red trend line between *ca*. 224 – 332 s, where the gradient is constant.

The rate of reaction can be calculated by knowing the area of the surface of the electrode and by converting the change in mass the change in moles using equation **(4.6)**, the rate of reaction was calculated to be 3.76 x 10^{-9} mol s^{-1} cm^{-2}.

$$\delta\mathrm{m} = \delta\mathrm{mol}\ \mathrm{x}\ (\mathrm{RMM_{Au}} - \ \mathrm{RMM_{Cu}}) \quad \mathbf{(4.6)}$$

There is an unusual anomaly in the change in mass trace, between *ca*. 189 – 224 s where there appears to be a loss in mass from the surface of the electrode, which could be due to three different reasons. First is an effect of the loss of unoxidised copper particulate from the surface of the electrode, where a large amount of copper has left the surface of the electrode, leading to a loss in mass great enough to be visible in the change in mass plot. Second that a large concentration of insoluble species is formed on the surface of the electrode, if these species undergo a solvolysis and dissolution, this could lead to a large loss of mass from the surface of the electrode. Or third the concentration of Cu (I) ions in the double layer becomes so large and the concentration of Au (I) ions becomes so depleted that the reverse reaction can occur.

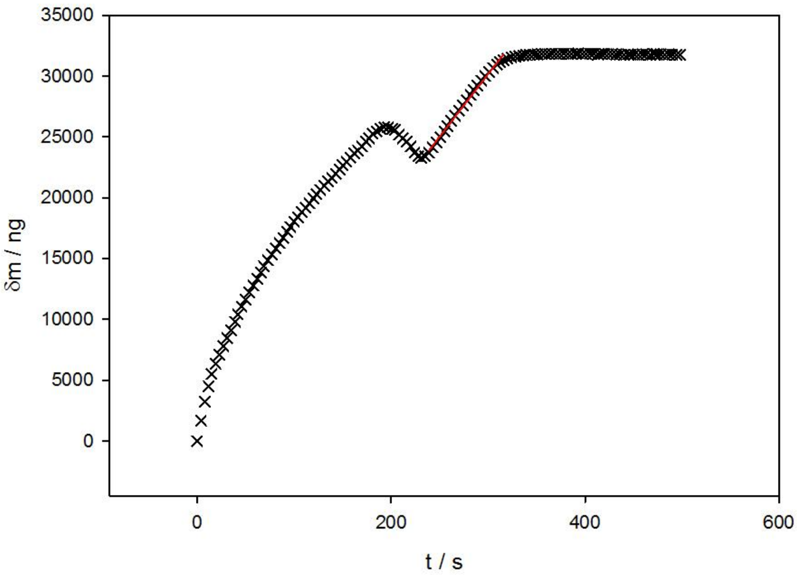

Figure 4.9: Change in mass versus time plot, for the galvanic deposition of gold on a copper substrate. Gradient of change in mass plot 1.029 x 10^{-7} *g* s^{-1}*. Pt working electrode, 0.205* cm^2*.*

It is possible to calculate the concentration of Cu (I) and Au (I) ions required in the electrical double layer to cause the reaction represented in equation **(4.1a)** to be performed. The EMF of the reverse reaction under ideal conditions is E = – 0.88 ± 0.06 V, this potential must be overcome before the reverse reaction can occur. To calculate the concentration of Cu (I) ions require in the double layer to cause reverse reaction the Nernst equation for the reverse reaction is employed, **(4.7)**.[8,9]

$$E_{cell} = E + \frac{RT}{nF}\ln(\frac{a_{Cu^+}}{a_{Au^+}}) \quad (\mathbf{4.7})$$

Where the reduced species of the copper and gold are in the metal state and hence have an activity of unity. The activity of the Cu (I) and Au (I) ions are calculated using equation **(4.8)**.[8]

$$a_{Au} = \gamma_{Au} \times C_{Au} \approx C_{Au} = [Au^+] \quad (\mathbf{4.8})$$

It is assumed for dilute solutions, that the activity coefficient is approximately one, $\gamma = 1$, and hence the activity is equal to the concentration of a species in solution.

To calculate the concentration of Cu (I) and Au (I) present in the double layer, it is assumed that the overall concentration of metal ions in the double layer is always 0.1 M, (**4.9)**. As the stoichiometry of the reaction is a 1 : 1 ratio and as the initial concentration of Au (I) ions is 0.1 M, it is assumed that as an Au ion is reduced in the double layer it is replaced with a Cu ion.

$$[Au^+] + [Cu^+] = 0.1\ M \quad (\mathbf{4.9})$$

To calculate the concentrations of Cu (I) and Au (I) ions required for the reverse reaction to occur, the point at which no reaction is occurring should be calculated. Hence, when the Gibbs free energy is zero, $\Delta G = 0\ J\ mol^{-1}$. Where the Gibbs free energy is calculated by multiplying the Nernst equation for the reverse reaction by – nF, **(4.10)**.

$$\Delta G_{cell} = -\,nFE - RT\ln\left(\frac{a_{Cu^+}}{a_{Au^+}}\right) \quad (\mathbf{4.10})$$

Then using the assumption in equation **(4.9)**, that the concentration of metal ions in the electrical double layer is always 0.1 M, it is possible to create a theoretical straight line graph for varying concentrations of the Cu (I) and Au (I) ions. By plotting ΔG_{cell} against $\ln\frac{[Cu^+]}{[Au^+]}$, where the units of ΔG_{cell} are $J\ mol^{-1}$, *Figure 4.10.*

This plot generates a line where the Y axis intercept is C = – nFE and the gradient of the line is m = – RT. From the equation of the straight line, it is possible to calculate the value of X where the change in the cell Gibbs free energy is zero, equation **(4.11)**. Hence, two equations can now be obtained for the calculation of the concentrations of Cu (I) and Au (I), equation **(4.9)** and **(4.11)**.

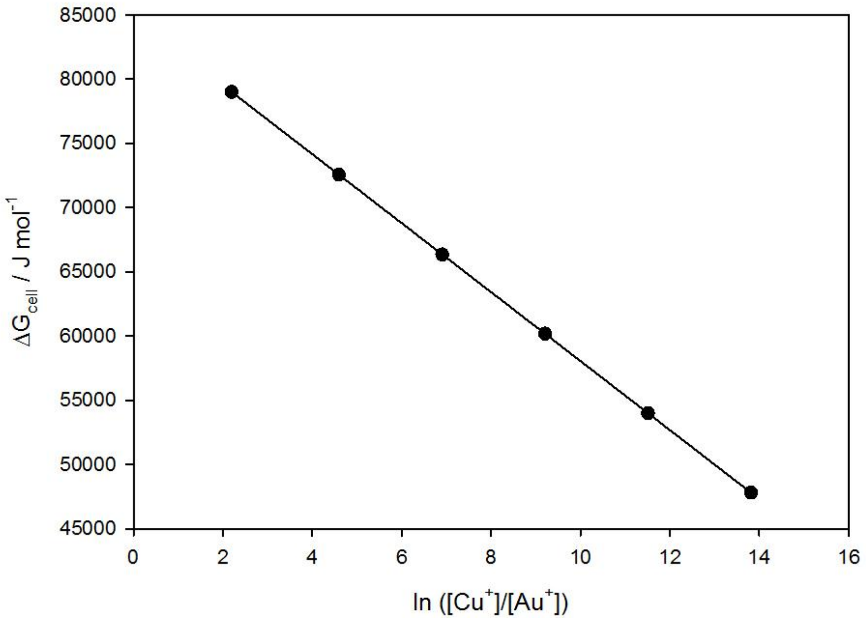

Figure 4.10: Straight line plot generated using theoretical concentrations of Cu(I) and Au (I) in the electrical double layer.

$$\text{For } Y = 0, X = \frac{-C}{M} = \frac{nFE}{-RT} = \ln\left(\frac{[Cu^+]}{[Au^+]}\right) \quad (\mathbf{4.11})$$

This means the simultaneous equations can be solved, hence the concentration of Cu (I) ions is *ca*. 0.10 M and the concentration of Au (I) ions is 1.86 x 10^{-14} M. This demonstrates that the concentration of Au (I) ions has to reach an improbably small value for the reverse reaction to occur. So it is proposed that the reverse galvanic reaction does not occur.

Hence, it is proposed that the loss of mass, in change in mass profile of the galvanic reaction is caused by loss of copper particulate from the surface of the crystal and not due to the reverse reaction.

To investigate the morphology and composition of the gold deposit, a standard electrolyticly plated copper substrate was prepared. The standard substrate was immersed in a 0.1 M AuCl dissolved in Ethaline. Once plating was complete, the morphology was analysed using AFM and SEM.

Figure 4.11 displays a 3D representation of the galvanic gold deposit on a standard copper substrate. As with the silver deposit previously, the bulk morphology of the sample is the same as the underlying copper substrate, with a fine granular structure on the surface of the substrate. However, the grains in the gold sample appear to be finer, with grain size in the range of *ca*. 140 – 290 nm in diameter. There also appears to be larger grains deposited on the surface, which have a diameter of *ca*. 550 – 650 μm.

Using the surface area of the calculated from the 3D plot, it is possible to calculate the roughness of the gold coated sample. The surface area of the sample was found to be 29.5 ± 2.3 μm^2, which is a change in surface area of 18 ± 9 %. When compared to the previous results of copper and silver, the surface is smoother than the silver deposit and rougher than the copper deposit.

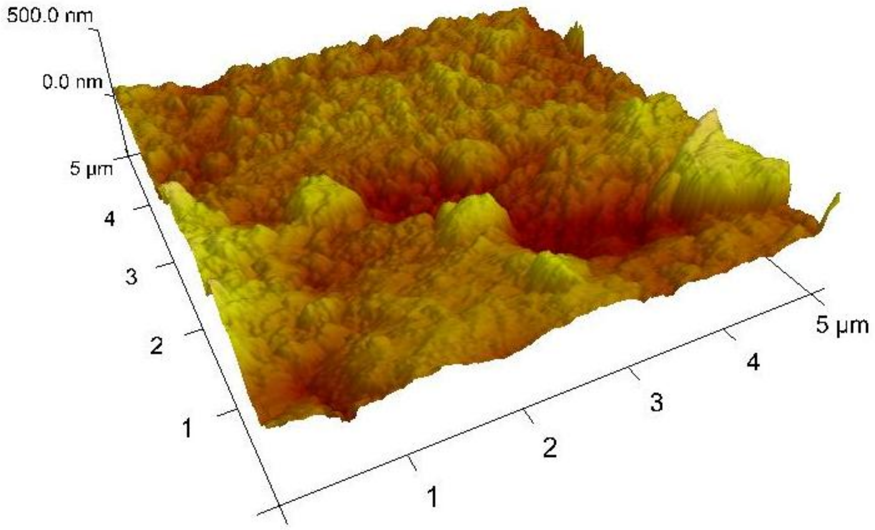

Figure 4.11: Atomic force micrograph of a galvanic gold coating of a copper substrate.

The smaller grain size means that gold can be packed more efficiently on the surface of the copper, than the silver deposit, meaning the surface is less rough. Also with the denser nucleation, it means that the gold grains will likey grow less before aggregating with a neighbouring nucleation site, hence the height of individual grains will be less than in the case of silver

The secondary electron, SEM image of the galvanic gold coating, *Figure 4.12*, displays the fine granular structure and the larger grains, which were found in the AFM micrograph. The morphology of the gold coating, as with the silver case, has been largely influenced by the underlying copper substrate. However, in the case of gold, the coating appears to be smoother than the silver coating.

Unlike the silver deposit, the gold deposit does not appear to have cracks in the coating. There are still pores evident in the gold coating, circled in red, meaning that the reaction can still proceed. By gold being reduced and deposited on the surface of the sample and copper being oxidised and diffusing out in to the solution via these pores.

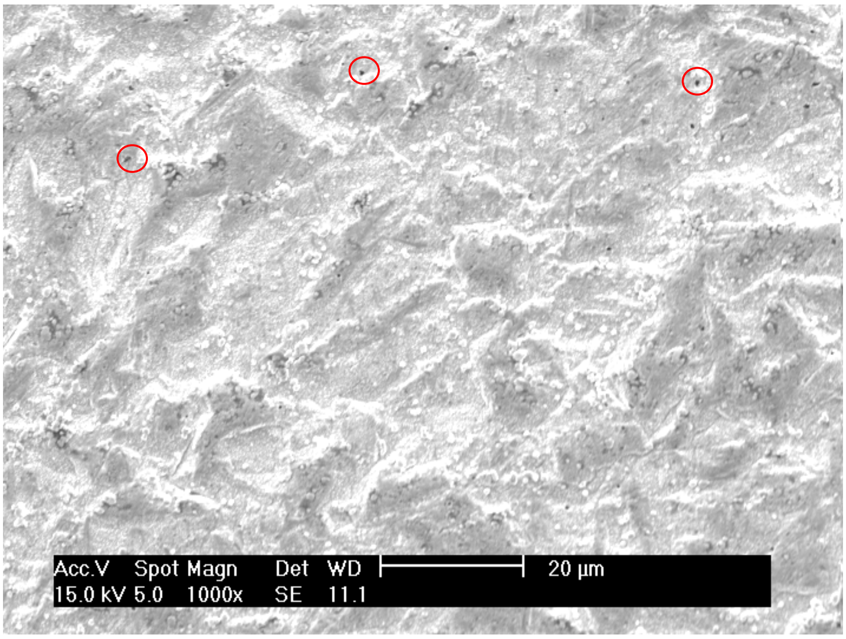

Figure 4.12: Secondary electron SEM image of a galvanic gold coating of a copper substrate.

The back scattered electron, SEM image, *Figure 4.13*, gives better definition when examining the pores in the surface. Again the pores appear to be of a diameter, on the sub micro meter scale. When analysing the pores by AFM, it appears that the pores are *ca*. 150 nm in diameter.

It should be noted that the bulk of the back scattered electron image, appears to be of the same shade. This indicates that bulk of the surface of a similar elemental composition. It should be noted that around the larger nodes on the surface, the shade of the image is darker. This caused by the back scattered electrons, interacting with the raised nodes, preventing the electrons from escaping the surface, making the area darker.

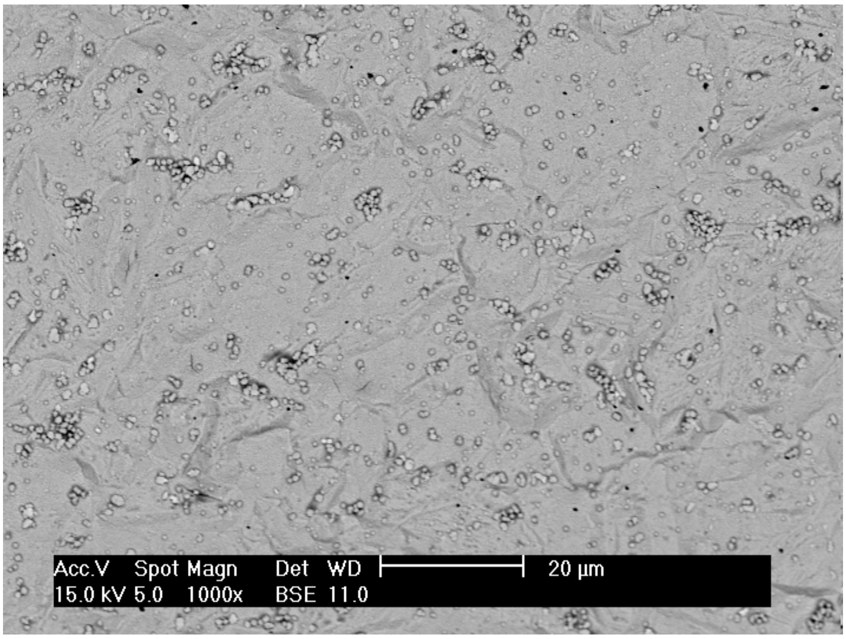

Figure 4.13: Back scattered electron SEM image of a galvanic gold coating of a copper substrate.

EDX was used to characterise the elements present in the sample, *Figure 4.14*. In the sample the elements found were carbon, oxygen, chlorine, copper and gold, with atomic percentages of 18 %, 7 %, 4 %, 30 % and 42 % respectively. Unlike the silver sample, the coating contains a number of impurities. These trace elements could be from residual Ethaline on the surface, where the Ethaline has failed to be washed off fully. It is possible that pores on the surface have trapped some of the liquid on the surface.

Interestingly the proportion of copper to gold in this sample is higher than the proportion of copper to silver in the previous sample. This could be an indication that either the gold coating is thinner, or more copper has been incorporated in to the coating, which will be investigated using XPS.

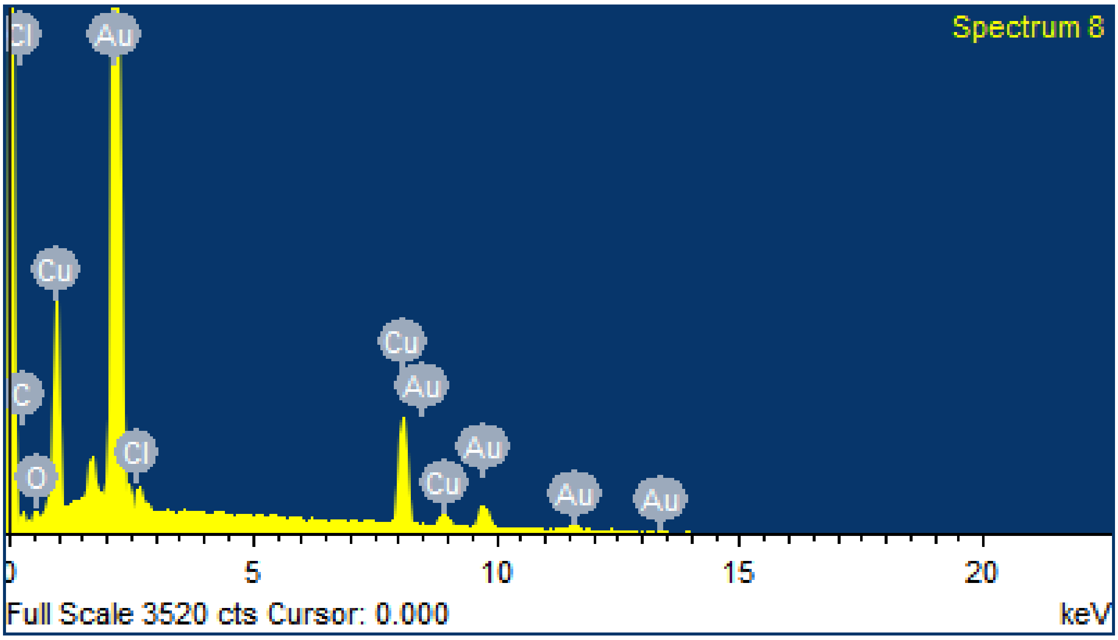

Figure 4.14: EDX spectrum of a galvanic gold coating of a copper substrate.

The XPS of the gold coating, *Figure 4.15*, produces a spectrum that displays the expected peaks for gold. There are significant peaks representing copper present in the spectrum, with the copper 2p doublet at 952 eV and 932 eV. It is expected that the concentration of copper in the sample is going to be significantly higher than it was in the silver sample, as shown by EDX analysis. Also present are peaks representing carbon, oxygen and chlorine at 285 eV, 530 eV and 198 eV respectively. As these elements were present in the EDX spectra, it is expected they will be present in the XPS spectra.

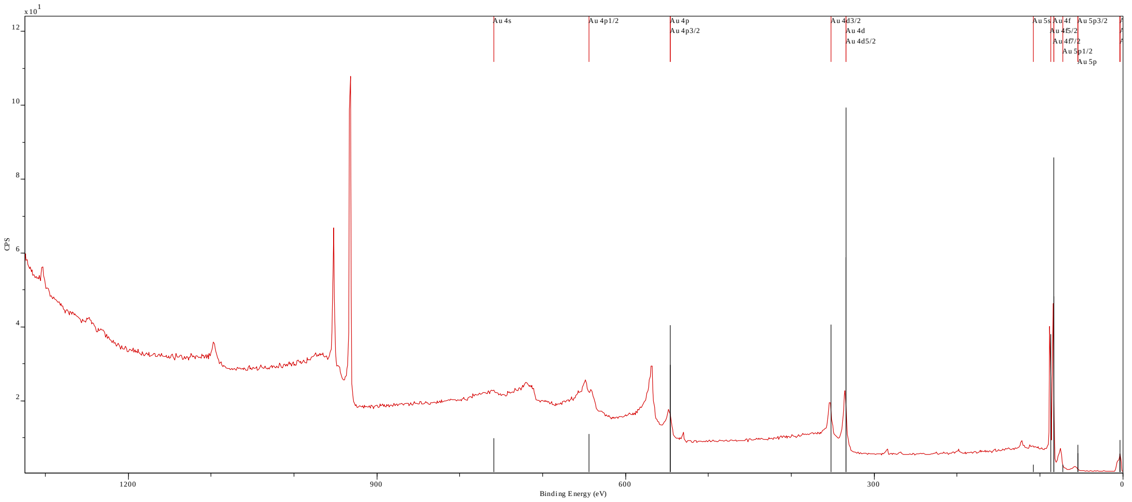

Figure 4.15: XPS spectrum of a galvanic gold coating of a copper substrate.

The high resolution XPS spectra of C, O, N, Cl, Cu and Au was taken to quantify the atomic concentration of species on the surface of the sample, *Table 4.5*. Like with the sliver system there is residual Ethaline trapped on the surface of the sample, the atomic ratio of the residual elements is similar to that of Ethaline.[6] The atomic percentage of gold in the sample is surprisingly lower than the atomic percentage of copper. It appears that the gold has mixed with copper on the surface of the sample, forming an alloy. The proposed alloy contains atomic percentages of 35 % gold and 65 % copper. The formation of an alloy is unsurprising when the copper – gold binary phase diagram is considered. The phase diagram shows that gold and copper can form an alloy with atomic percentages of nearly any composition.[10]

Table 4.5: Elemental composition of a gold coating of a copper substrate.

Element	Orbital Scanned	Atomic Percentage / %
Au	4f	25
Cu	2p	46
C	1s	14
O	1s	9
N	1s	1
Cl	2p	5

Figure 4.16 shows the high resolution spectra for the copper 2p and gold 4f electron transitions. The gold 4f spectra shows the 4f 5/2 and 4f 7/2 electron transitions

with the expected 3 : 4 ratio respectively. There only appears to be a single doublet in the spectrum, indicating that the gold has not undergone oxidation.

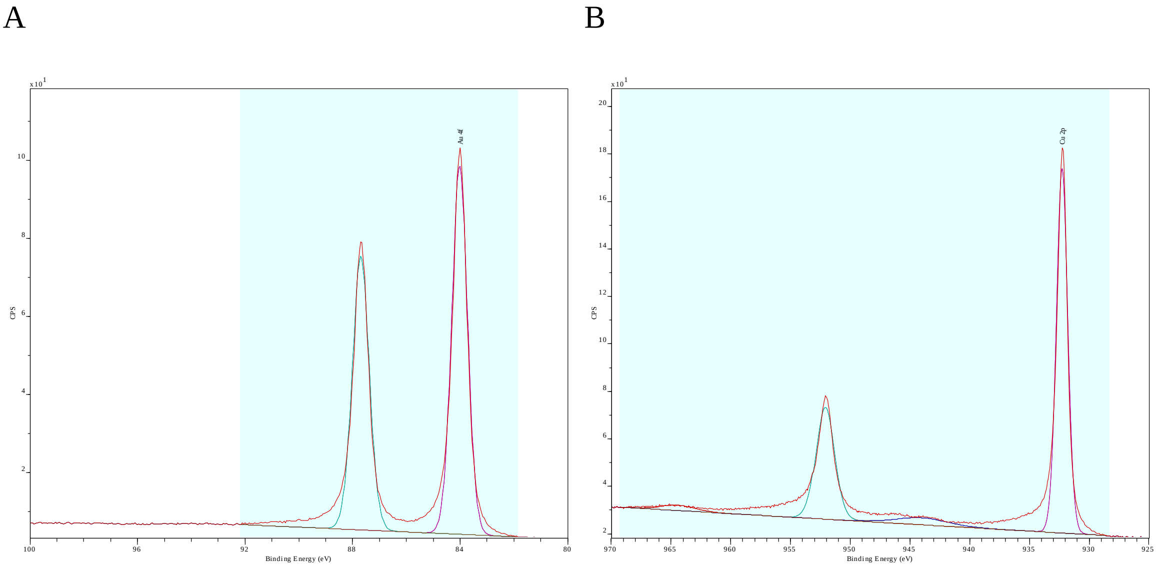

Figure 4.16: High resolution XPS data of A: Au and B: Cu, of a galvanic gold coating of a copper substrate.

The high resolution copper spectrum displays the expected 2p doublet for copper metal, as well as two smaller peaks that represent the oxidised Cu (II) species.[11] The electron transitions for the bulk copper, 2p 1/2 and 2p 3/2 electron transitions, display the expected 1 : 2 ratio for the area of the peak, with a peak separation of 20 eV. The other, smaller peaks in the spectrum display the expected 1 : 2 ratio for the peak area, as well as having a peak separation of 20 eV. This shows that these peaks do represent copper 2p electron transitions, where the copper is in a Cu (II) oxidation state,[11] with the increase in electron binding energy caused by the oxidation state of the copper atoms. The copper oxide represents 7 % of the copper concentration in the sample. Unlike with the silver sample, where there was no evidence of copper oxidation.

As XPS has shown there is both copper and gold at the surface of sample, it is proposed that the coating has formed an alloy. This allows copper to come in to contact with the atmosphere. Copper being in contact with the atmosphere has oxidised some of the copper in the sample. So unlike with the silver system, gold does not act like a barrier layer for the protection of a copper substrate.

4.4 Conclusions

For the industrial applications of this work see **Appendix 3**.

Measurement of the thickness of the sample was attempted by AFM, however due to the roughness of the standard copper deposit, results were unobtainable. It would be possible to perform the galvanic reaction on a flat copper substrate to create a step that would be measurable by AFM. It would also be possible to measure the thickness of the coating using X-ray fluorescence techniques.

Further XPS work could also be performed. Depth profiling of the gold deposit would reveal how copper came to be included in the coating. Where, if an increasing concentration of copper was found as the coating was etched away, then the copper present in the sample is due to diffusion of copper from the substrate in to the coating. If the converse was true and there was a higher concentration of copper near the surface of the sample than closer to the substrate, then the copper in the sample is being galvanically redeposit with the from solution with the gold.

Further experiments could be performed on the gold deposit. As copper – gold has been previously shown to act as a catalyst for the oxidation of borohydride,[4] the coating produced from the galvanic deposition of gold could be tested for similar reactivity.

In this chapter, the galvanic deposition of group 11 elements on to a copper substrate has been characterised. Using QCM experiments, the stoichiometry of the galvanic reactions has been discerned and found to be in a 1 : 1 stoichiometry. *i.e.* the reduction of silver and gold ions proceeds via the Cu (0) → (I) oxidation. Whilst the change in Gibbs free energy for the individual reactions has been calculated under ideal conditions. The results of which support the stoichiometry calculated from the QCM experiments.

Calculations have also be made to determine the concentration of Cu (I) ions required in the double layer to cause the reverse reactions to occur. It was found that the concentration of Au (I) ions was unfeasibly small, and the loss in mass in the change in mass trace was due to delamination.

It has also been possible to calculate the rate of the galvanic reactions by tracing the change in mass with respect to time using QCM experiments. It was found that the silver galvanic reaction proceeded faster than the gold galvanic reaction.

Gold and silver have also been deposited on a standard electrolytic copper substrate and the morphology of the deposit characterised using AFM and SEM. It was found that both coatings contained pores, which allow for the dissolution of copper from the underlying substrate. However, the silver sample also contained cracks, which were not present in the gold sample.

Finally, the elemental composition of the samples was analysed by EDX and XPS. It was found that the silver coating did not contain much copper and what copper that was present at the surface was not oxidised. Thus silver acts as a good barrier layer between the atmosphere and the copper substrate and could be used in an application where prevention of copper oxidation is important.[12] The gold coating contained a large atomic percentage of copper. It is proposed that the copper and gold have formed an alloy, allowing for copper to come into contact with the atmosphere. As the copper has been exposed to the atmosphere, it has undergone oxidation. Gold coatings are very good barrier layers for protecting substrates from oxidation, however this process does not produce a good barrier.

4.5 References

1. P. Atkins and J. de Paula, in *Atkins' Physical Chemistry*, Oxford University Press, Oxford, 8th edn., 2006, ch. 7, pp. 222 - 224.
2. A. P. Abbott, S. Nandhra, S. Postlethwaite, E. L. Smith, and K. S. Ryder, *Phys. Chem. Chem Phys.*, 2007, **9**, 3735 – 3743.
3. Y. S. Won, S. S. Park, J. Lee, J.-Y. Kim, and S.-J. Lee, *Appl. Surf. Sci.*, 2010, **257**, 56 – 61.
4. L. Tamašauskaitė-Tamašiūnaitė, A. Balčiūnaitė, A. Zabielaitė, I. Stankevičienė, V. Kepenienė, A. Selskis, R. Juškėnas, and E. Norkus, *J. ELECTROANAL. CHEM.*, 2013, 700, 1 – 7.
5. *CasaXPS 2.3.15*, 2009, Casa Softwere Ltd.
6. K. El ttaib, Ph.D Thesis, University of Leicester, 2010.
7. P. R. Subramanian and J. H. Perepezko, *J. Phase Equlib.*, 1993, **14**, 62 – 75.
8. A. P. Abbott, G. Frisch, S. J. Gurman, A. R. Hillman, J. Hartley, F. Holyoak, and K. S. Ryder, *Chem. Commun. (Camb).*, 2011, **47**, 10031 – 10033.
9. M. Stratmann and G. S. Frankel, in *Encyclopedia of Electrochemistry*, ed. A. J. Bard and M. Stratmann, Wiley-VCH GmbH & Co. KGaA, Weinheim, 2003, vol. 4, ch. 1, pp. 14 - 15.
10. H. Okamoto, D. J. Chakrabari, D. E. Laughlin, and T. B. Massalskl, *J. Phase Equlib.*, 1987, **8**, 454 – 474.
11. I. Platzman, R. Brener, H. Haick, and R. Tannenbaum, *J. Phy. Chem. C*, 2008, **112**, 1101 – 1108.
12. W. Wang, A. Choubey, M. H. Azarian, and M. Pecht, *J.Electron. Mater.*, 2009, **38**, 815 – 827.

Chapter 5: Characterisation of Group 10 Chlorides Salts in Ethaline 200

5.1 Introduction

In this chapter both the electrochemistry and speciation of group 10 metal salts dissolved in Ethaline is discussed.

One of the aims of this chapter is to link the study in to speciation of nickel ions using EXAFS[1,2] to the UV – Vis spectroscopy and X – ray crystallography data obtained. Further this chapter seeks to expand on the speciation work by characterising the thermochromic behaviour of a solution of nickel chloride dissolved in Ethaline.[3,4] The UV – Vis spectra of the other group 10 metal chloride dissolved in Ethaline was also investigated.

Whilst the electrochemistry of palladium has previously been established, this work aims to expand current knowledge using EQCM to determine the rate and current efficiency of the electrochemical reaction.

The electrochemistry and formal electrode potential of have not previously been established of the Ni (II) ion when dissolved in Ethaline.[5] This is because the nickel complex formed at room temperature is electrochemically stable in the electrochemical window of Ethaline. It was observed that solution of a nickel(II) salt and Ethaline undergoes thermochromisum, this indicated a change in speciation of the metal centre when the solution is heated. This change in speciation was characterised using UV – Vis spectroscopy and will be discussed in this chapter. Electrochemistry was performed at various temperatures to see how the change in speciation affected the electrochemical reactivity of the Ni (II) ion. A further investigation using EQCM was performed to establish the rate and current efficiency of the electrochemical reaction and will be discussed in this chapter.

The electrochemistry of platinum has not been previously established due to the slow kinetics of reaction at lower temperature and high value of the oxidation onset potential, which is close to the end of the electrochemical window. The electrochemistry of a Pt (II) solution was investigated using cyclic voltammetry using a macroelectrode and to further investigate the electrochemistry was performed using EQCM to establish the rate and current efficiency of the reaction.

It is also important, for the application of group 10 metals in a galvanic reaction, to know how the electrochemistry of the group 10 metals is affected by the presence of copper ions. Hence, the electrochemistry of the mixed group 10 and copper metal salts has been investigated and EQCM performed.

The specific aims of this chapter are:

- Characterisation of the group 10 metal salt species when dissolved in Ethaline.
- Investigate the change in nickel speciation in Ethaline with respect to temperature.
- Measure the electrode potentials of the group 10 metal salts in Ethlaine
- Determine the rate and current efficiency of the electrochemical reactions.

5.2 Nickel (II) Chloride in Ethaline 200

Previous work performed in this group[1] has shown that at room temperature the speciation of nickel (II) chloride, when dissolved in Ethaline 200, is actually triethylene glycol nickel (II) dichloride with the two chlorides ions acting as counter ions, $[Ni(C_2H_6O_2)]Cl_2$, *Figure 5.1*.

Figure 5.1 displays the Fourier transform of the EXAFS data obtained for $NiCl_2{\cdot}6H_2O$ dissolved in three different Deep Eutectic Solvents. EXAFS data are generated by excitation of core shell electrons using X – rays. These photoelectrons interact with neighbouring atoms and are backscattered, these backscattered electrons form interference patterns the primary photoelectrons. The Fourier transform of the interference pattern produces a real space radial distribution function for the atoms surrounding a metal centre. In other words a peak in the radial distribution function represents a back scattering atom at the measured distance.

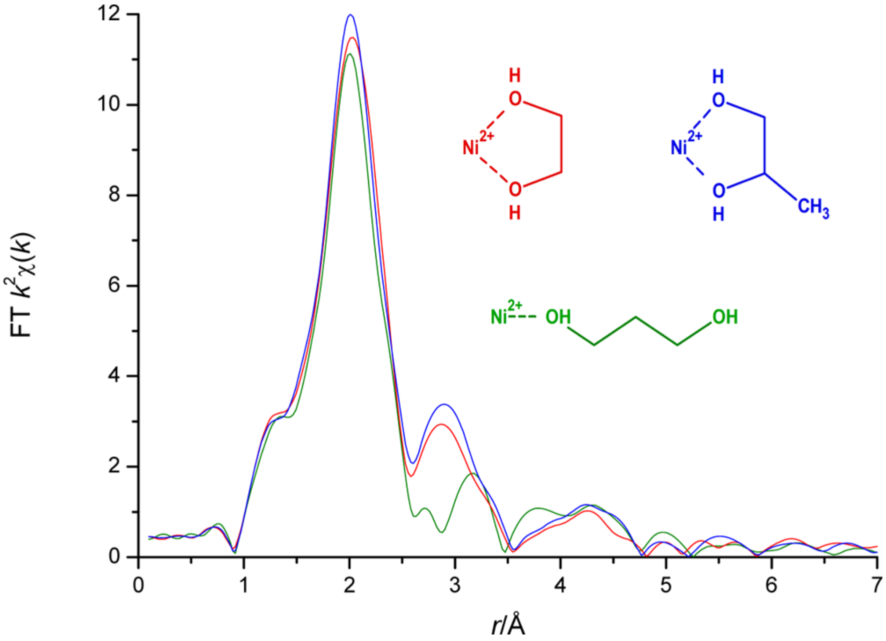

Figure 5.1: Fourier transform of the EXAFS data for 100 mM solutions of 6NiCl$_2$·H$_2$O dissolved in deep eutectic solvent. Red: Ethaline. Blue: 1,2 – Propaline. Green: 1,3 – Propaline (1 : 2, choline chloride : propylenediol).[1,2]

Figure 5.1 shows the radial distribution of atoms surrounding a Ni (II) centre in three different DESs. The data for all of the DESs shows that there are six oxygen atoms at a distance of 2.08 Å from the metal centre. For Ethaline and 1,2 – Propaline a second coordination sphere is observed of six carbon atoms at a distance of 2.89 Å, this effect is not shown in the 1,3 – Propaline system. It is proposed that in the Ethaline and 1,2 – Propaline systems, the ethylene and propylene glycol act as chelating ligands. Whereas in the 1,3 – Propaline system, the bite angle (the angle formed at the metal centre, between the two binding sites of a bidentate, chelating ligand) of the 1,3 – propanediol is too large and hence the ligands coordinates as a mono dentate ligand.

These are unexpected results as nearly every other metal centre investigated was shown to have chloride ligands coordinating to the metal centre.[1]

To further investigate the coordination of ethylene glycol as a ligand, a crystal structure was obtained of $[Ni(phen)_2(C_2H_6O_2)]Cl_2$, *Figure 5.2,* the addition of phenanthroline was used to replace glycol ligands and encourage crystallisation. The use of X – ray structure is to mitigate the uncertainty with EXAFS, which involves multiple fitting parameters, which are determined from solid structure data.

Figure 5.2 shows that there are two chlorine atoms included in the crystal structure, these represent counter ions, balancing the dicationic charge on the nickel complex. As the charge on the complex is balanced by counter ions, this implies that the ethylene glycol ligand is still protonated and is hence acting as a neutral ligand forming a dative bond with the metal centre.

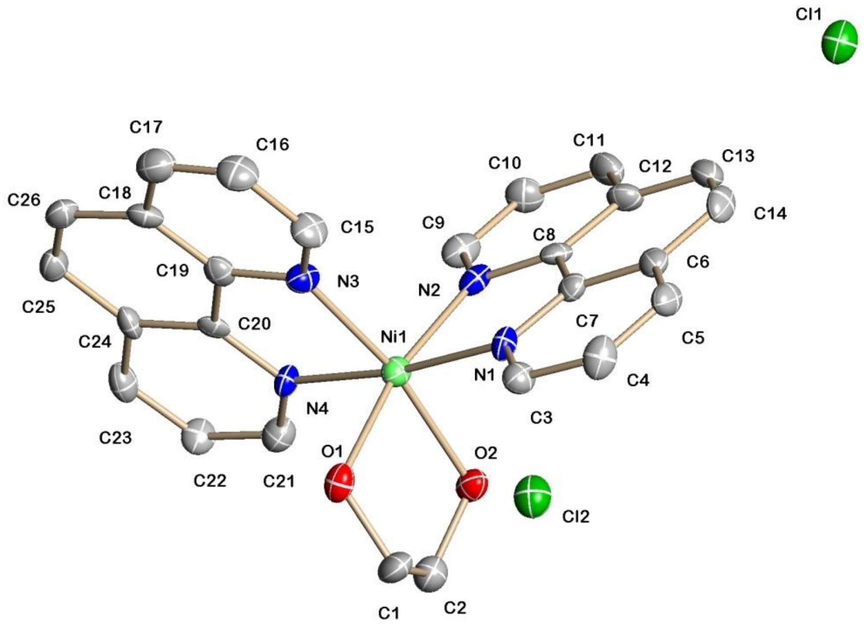

Figure 5.2: Crystal structure of $[Ni(phen)_2(C_2H_6O_2)]2Cl$ *with hydrogen atoms and solvent molecules omitted. Displacement ellipsoids represent 50% probability.*

An interesting comparison can be drawn between the crystal structure and the EXAFS data. This is that the bond length between the metal centre and the oxygen donor atom in the crystal structure was found to be 2.08 Å. This is similar to the Ni – O bond length established in the EXAFS. It should be noted that X – ray structure determination provides data for a molecule in the solid state and hence it may not represent the metal speciation in solution. However, as the X – ray crystal structure agrees well with the EXAFS, it is suggested that the speciation of the Ni (II) metal centre in Ethaline will be $[Ni(C_2H_6O_2)_3]^{2+}$.

It was noticed that when a solution of $NiCl_2$ dissolved in Ethaline 200 was heated, the solution would display thermochromic behaviour. At room temperature the colour of the solution was a pale green colour, whereas at *ca*. 70 ^{o}C the solution turns a more intense emerald green and at *ca*. 130 ^{o}C the solution turns and intense turquoise colour. This implies there is at least two, if not three different metal species present as a solution of $NiCl_2$ in Ethaline 200 is heated. This effect has been noticed previously, in both deep eutectic solvents by Gu *et. al.*[4] and in imidazolium ionic liquids by Chen *et. al.*[3]

To analyse what effect the change in temperature has on the speciation of the nickel in solution, UV – Vis spectroscopy was performed over a range of temperatures, between 30 – 130 ^{o}C, at 20 ^{o}C increments, *Figure 5.3*.

At 30 ^{o}C the UV – Vis spectra displays λ_{max} at 237 nm (ε = 36 dm mol^{-1} cm^{-1}), with two shoulders at 278 nm and 218 nm, a second peak at 422 nm (ε = 13 dm mol^{-1} cm^{-1}) and a third peak at 764 nm (ε = 9 dm mol^{-1} cm^{-1}). The peaks at 422 and 764 nm relate to absorptions in the violet and red regions of the visible spectrum respectively and are responsible for the pale green colour of the nickel solution at 30 ^{o}C. The molar extinction coefficients displayed, are indicative of an octahedral complex that has spin allowed, symmetry disallowed electronic transitions.[6]

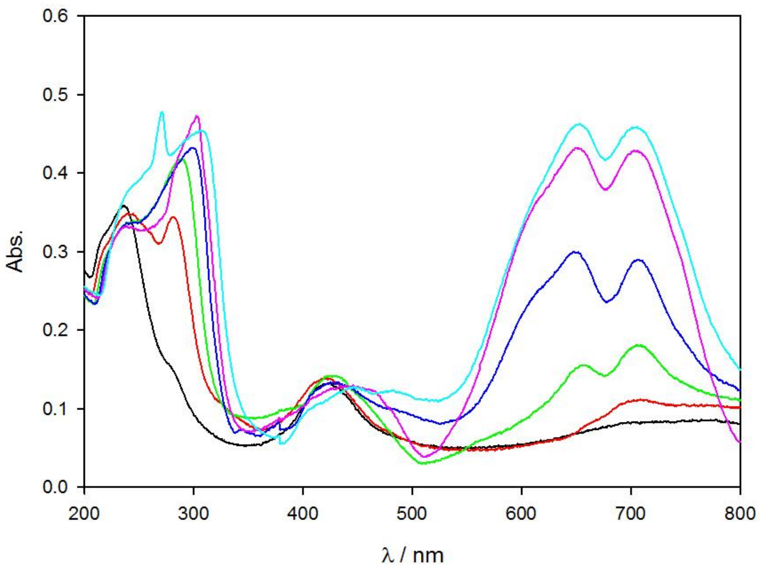

Figure 5.3: The electronic spectra of 10 mM $NiCl_2$ dissolved in Ethaline 200 at varying temperature. Black: 30 °C, red: 50 °C, green: 70 °C, blue: 90 °C, pink: 110 °C, turquoise: 130 °C.

When the solution is heated from 30 °C to 50 °C, there is noticeable change in the UV – Vis spectra. The shoulder at 279 nm appears to have formed in a separate peak at 280 nm and a more defined peak is formed at 709 nm. While the peaks at 238 and 421 nm are still present in the spectrum. It is suggested that the peak which have developed are representative of the $[NiCl_4]^{2-}$ complex.[7] This indicates that, even at room temperature, a small amount of $[NiCl_4]^{2-}$ is present in solution and when heated $[Ni(C_2H_6O_2)_3]^{2+}$ undergoes a ligand exchange to from the $[NiCl_4]^{2-}$ complex. This reaction will be reversible and hence a stable equilibrium will be set up between the concentrations of the two complexes.

Heating the solution to 70 °C, shows a further, pronounced change in the UV –Vis spectrum. The peaks at 239 and 426 nm are still present in the spectrum and the absorption of these peaks has not significantly changed. The peak at 289 nm has undergone a red shift and the absorption has significantly increased. Importantly the absorption in the red region has greatly increased, as well as forming two distinct peaks at 654 and 705 nm. These two peaks are indicative of the $[NiCl_4]^{2-}$ complex.[7]

As the solution is further heated from 70 °C up to 130 °C, the two peaks at 654 and 705 nm increase in absorption. The peak at 289 nm, continues to grow in absorption and undergo red shift to an eventual value of 306 nm. The peak at 426 nm also undergoes red shift and decreases in absorption. The large increase in absorption in the red region of the spectrum, as well as the smaller violet absorption, accounts for the turquoise colour of the solution at 130 °C.

Using the literature value for the molar extinction coefficient of $[NiCl_4]^{2-}$ (λ = 645 nm, ε = 170 dm mol^{-1} cm^{-1}),[7] it is possible to determine the concentration of the different species at varying temperatures, *Table 5.1*.

Table 5.1: Concentration of nickel species with respect to temperature

Temp. / °C	Abs. (λ = 654 nm)	Conc. of $[NiCl_4]^{2-}$ / mM	Conc. of $[Ni(C_2H_6O_2)]^{2+}$ / mM
70	0.16	0.9	9.0
90	0.3	1.7	8.2
110	0.43	2.5	7.4
130	0.46	2.7	7.2

It is important to note there does not appear to be an isosbestic point in the UV – Vis spectrum. This implies that the change in speciation is not a simple switch between the two species. Instead there is at least one other species present as an intermediate between the two.

This change is speciation is expected to have a direct effect of the electrochemistry. This was investigated using cyclic voltammetry and linear sweep voltammetry as well as the EQCM. The cyclic voltammetry of a 10 mM $NiCl_2$ dissolved in Ethaline 200 was also performed at 20 °C increments, between 30 – 130 °C, *Figure 5.4* (for clarity only the CVs at 30, 70 and 130 °C are displayed). It is clear from the CV that the speciation of nickel centre has a marked effect of the electrochemistry, however it is proposed that this is not the only contributing factor.

At 30 °C, the CV shows no electrochemistry that can be attributed to nickel, the negative current in the CV corresponds to the end of the electrochemical window. It is proposed that the $[Ni(C_2H_6O_2)_3]^{2+}$ species is very thermodynamically stable because glycol is acting as a chelating ligand. This prevents any nickel being electrochemically deposited on the surface of the electrode.

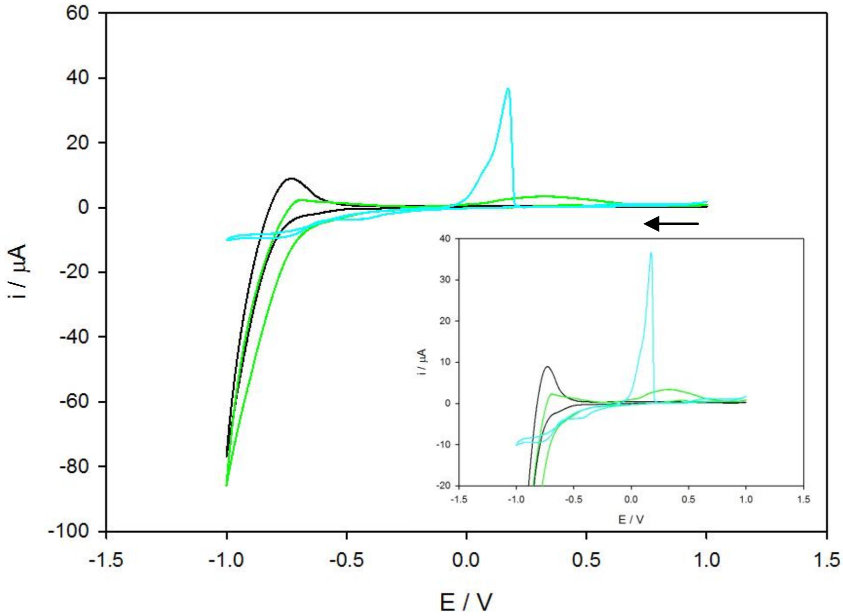

Figure 5.4: CV of 10 mM $NiCl_2$ *dissolved in Ethaline 200 at varying temperatures. Black: 30 °C, green: 70 °C, turquoise: 130 °C. . Pt working electrode, 3.14 x* 10^{-2} cm^2*. Pt flag counter electrode. Ag wire reference electrode. Scan rate 10 mV* s^{-1}*. Insert: magnified CV.*

At 70 °C, there is 0.9 mM of $[NiCl_4]^{2-}$ present in solution established from UV – Vis, the CV starts to show a small negative current that could be attributed to the deposition nickel, however most of what is observed is the breakdown of the liquid. The positive current in the CV is part of the Ethaline 200 breakdown process and is not attributed to the oxidation of nickel. There is a very broad positive current that starts at *ca*. 0 V, corresponding to the oxidation of nickel. This implies that a small amount of nickel can be deposited at this low temperature, indicating there is an electrochemically active species present in the solution. It is proposed that it is the $[NiCl_4]^{2-}$ species that is undergoing electrochemical reaction. However, due to the low concentration of $[NiCl_4]^{2-}$ and high viscosity of Ethaline 200, the reaction is slow leading to reaction that is difficult to observe.

At 130 °C, the CV exhibits well defined redox behaviour. Which means the electrode potential can be calculated and is revealed to be – 0.124 V (Ag wire *pseudo* reference electrode) at 130 °C. Using the Nernst equation, it is possible to correct for temperature and concentration to calculate the electrode potential of $[NiCl_4]^{2-}$ under standard conditions. This is found to have a value of – 0.021 V with respect to an Ag wire *psudo* reference electrode. Or to put this in to perspective of existing literature,[5] – 0.096 V with respect to a $[Fe(CN)_6]^{3-/4-}$ internal reference.

It must be considered, that at 70 °C $[NiCl_4]^{2-}$ should undergo an observable electrochemical reaction like that observed at 130 °C. However it is proposed that at 130 °C the higher concentration of $[NiCl_4]^{2-}$ and lower viscosity of the Ethaline 200 increases the rate of reaction.

To test the hypothesis, that at the lower temperatures tested, the lack of electrochemical response that can be attributed to nickel not being deposited, rather than the inability of the nickel to oxidise and it to undergo dissolution. Linear sweep voltammetry of nickel deposited on the surface of a platinum working electrode was performed. The nickel was deposited from an aqueous Watts nickel solution, washed dried and the transferred to an Ethaline solution.

Figure 5.3 shows that nickel can be stripped from the surface of an electrode at a variety of temperatures, ranging from 30 – 130 °C. Proving that at the lower temperatures studied, it is the case that nickel is prevented from depositing. It is suggested this is the case because the $[Ni(C_2H_6O_2)_3]^{2+}$ species is thermodynamically stable in solution and hence has a reduction potential outside of the electrochemical window. However, it is also possible that the reduction potential for the $[Ni(C_2H_6O_2)_3]^{2+}$ species is inside the electrochemical window and the dissociation of the ethylene glycol ligand from the nickel centre is so slow that the deposition process is outside of the time frame of the experiment.

There is an interesting effect observed in *Figure 5.5*, where the peak and onset potentials, for the oxidation of nickel, shift negative with the increase in temperature. It is proposed that the increase in temperature reduces the overpotential required for the oxidation and dissolution of nickel as there is more energy already in the system.

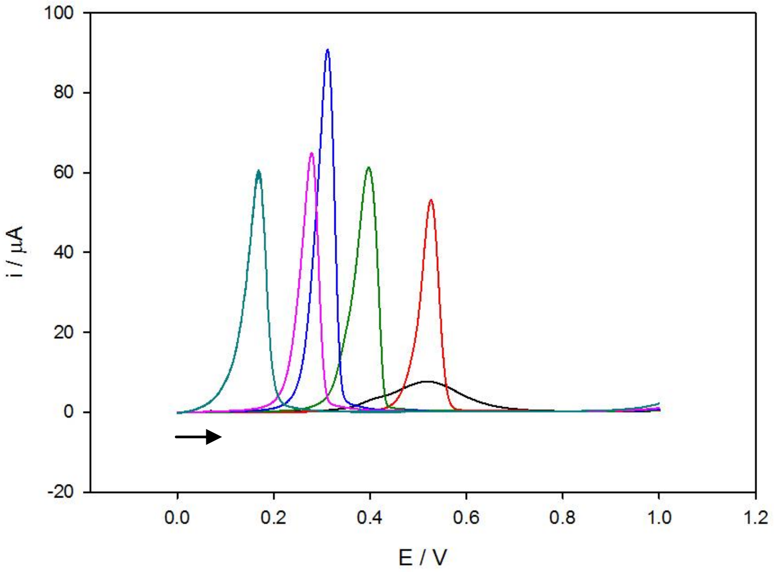

Figure 5.5: Linear sweep voltammetry of nickel deposited on a platinum working electrode. Black: 30 ^oC, red: 50 ^oC, green: 70 ^oC, blue: 90 ^oC, pink: 110 ^oC, turquoise: 130 ^oC. Pt working electrode, 3.14 x 10^{-2} cm^2. Pt flag counter electrode. Ag wire reference electrode. Scan rate 10 mV s^{-1}

To further investigate the reactivity of nickel, the electrochemistry was performed using the EQCM. *Figure 5.6* shows the results for the EQCM, with the CV plotted with the δmoles *versus* E plot at 130 °C. Interestingly, in the CV performed on the platinum QCM crystal, a new redox couple has appeared at – 50 mV. This couple is slightly more positive then the main redox couple (– 75 mV), shown on the 2mm working electrode.

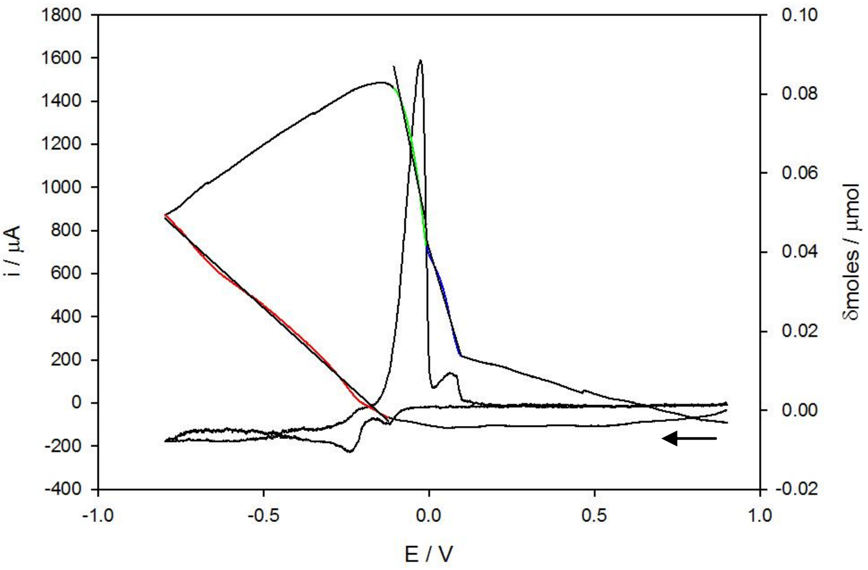

Figure 5.6: Using an EQCM to produce CV data of 10 mM $NiCl_2$ dissolved in Ethaline 200. Red: deposition of nickel, gradient – 7.59 x 10^{-8} mol V^{-1}. Green: dissolution of nickel, gradient – 4.08 x 10^{-7} mol V^{-1}. Blue: dissolution of nickel, gradient – 2.80 x 10^{-7}. Pt working electrode, 0.205 cm^2. Pt gauze counter electrode. Ag wire reference electrode. Scan rate 10 mV s^{-1}.

The source of this new redox couple is unclear, with at least two possible sources. As the QCM crystal is oscillating, this could induce a nucleation of nickel on the surface of the electrode. This means there could be two different phases of nickel deposited on the surface, with different electrode potentials. To check if multiple phases of nickel deposited thin film X-ray diffraction could be performed. Another source of the new couple, could be due to the size of the QCM electrode compared to the working electrode used to perform the standard voltammetry. The final source is that, due to the large amount of nickel being oxidised, the abundance of the stronger binding ligand is depleted close to the surface of the electrode. It is then more likely the oxidised nickel will from a second nickel species. It would be difficult to check the species formed when the nickel is undergoing dissolution, as the speciation of the nickel could change between the electrolysis and transferring it to any kind of spectrometer. However, from the results of the LSV discussed below, it is suspected that the second redox couple is an artifat of the deposition process not the dissolution process.

For the cathodic sweep, starting at 0.9 V and sweeping negative to – 0.8 V, before the Ni redox couples, between *ca*. 0.9 to – 0.1 V, there is no current passed and no change in the number of moles on the surface of the QCM crystal. At *ca*. – 0.1 V to – 0.8 V nickel is deposited on the surface of the electrode, which is represented by a negative current in the CV as well as a large change in moles. From the change in moles plot the rate of deposition is determined to be 3.70×10^{-9} mol s^{-1} cm^{-2}.

For the anodic sweep, sweeping from – 0.8 V positive to 0.9 V, the sweep starts in the deposition regime for nickel, which is deposited from *ca*. – 0.8 to – 0.1 V. At *ca*. – 0.1 V the nickel metal deposited on the surface of the electrode is oxidised and undergoes dissolution. Interestingly the dissolution process appears to proceed in a two stage process. Between *ca*. – 0.1 to 0 V the main dissolution process takes place, this is represented by a large loss of nickel deposited on the surface of the QCM crystal and a large, positive spike in current. The rate of dissolution in this first stripping regime is 1.99×10^{-8} mol s^{-1} cm^{-2}. Between *ca*. 0 to 1 V the secondary dissolution process occurs, it is still unclear what the cause of this process is. The rate of this second dissolution process is 1.37×10^{-8} mol s^{-1} cm^{-2}. After the second dissolution process, from *ca*. 0.1 to

0.9 V, the mass on the surface of the QCM crystal returns to the starting mass with no current being passed from the electrode. It is suggested that this process is caused by the rapid oxidation of the nickel but the slow diffusion of the resulting complexes away from the surface of the electrode.

Further analysis can be performed by analysing the mass – charge ratio, to determine the current efficiency of the deposition and dissolution of nickel from the surface of the electrode. The theoretical mass – charge ratio can be calculated for the Ni (II)/(0) redox couple where nickel metal is deposited on the surface of the electrode. The theoretical mass – charge ratio is calculated by equation **(5.1)**.

$$\frac{\delta\mathrm{m}}{\delta\mathrm{Q}} = \frac{58.69}{2\mathrm{F}} = 3.04 \times 10^{-4}\,\mathrm{g\,C^{-1}} \quad (\mathbf{5.1})$$

From the data used to produce *Figure 5.4*, it is possible to calculate the experimental mass – charge ratio, *Figure 5.7*.

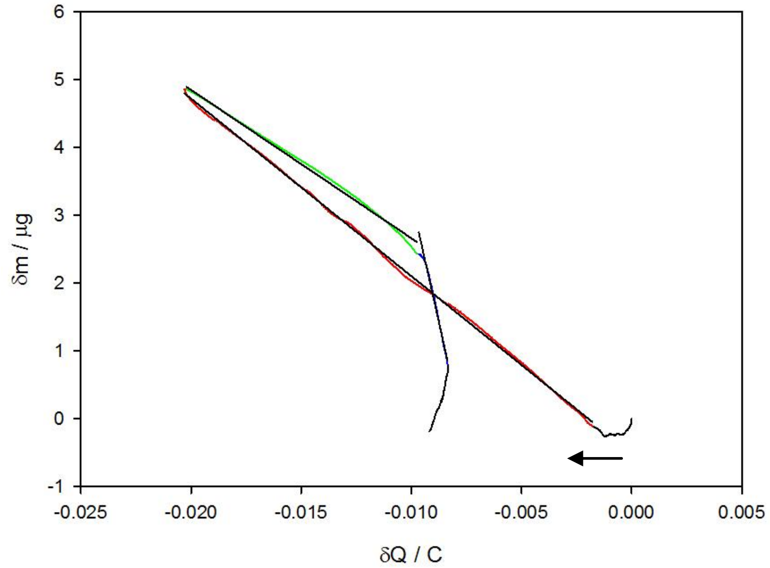

Figure 5.7: Plot of mass versus charge for CV of 10 mM $NiCl_2$ dissolved in Ethaline 200. Red; deposition of nickel, gradient – 3.62 x 10^{-4} g C^{-1}. Green; stripping of nickel, gradient 2.19 x 10^{-4} g C^{-1}. Blue; stripping of nickel, gradient – 1.45 x 10^{-3} g C^{-1}.

Analysis of the mass – charge ratio can determine the current efficiency of the deposition and stripping processes. The experimental mass – charge ratio for the deposition of nickel was found to be 3.62 x 10^{-4} g C^{-1}. This value is higher than the expected mass – charge ratio for the deposition of nickel, this is possibly due to chloride being trapped on the surface of the electrode.

For the first dissolution process the mass – charge ratio is 2.19 x 10^{-4} g C^{-1}, this suggest a current efficiency of 72 %. For the second dissolution process the mass – charge ratio is 1.45 x 10^{-3} g C^{-1}, which is significantly larger than expected. This suggests that loss of metal particulate from the surface occurs, a process where mass is lost from the surface of the QCM crystal without charge being passed.

It is suggested, loss of unoxidised nickel from the surface occurs via an undercutting mechanism, where pits grow under the surface of the nickel and form flakes that fall away from the surface. This effect is in line with what has been shown by Rayment *et. al.*,[8] it is important to note that when comparing these systems, that Rayment *et. al.* used a water based electrolyte, not a deep eutectic solvent.

The linear sweep voltammetry experiments were repeated using the EQCM, *Figure 5.8*, this experiment was performed to investigate the dissolution from the surface of the electrode. The experiment will also demonstrate, if the new redox couple present in the CV is an effect of the deposition or dissolution process.

Figure 5.8, once again shows the negative shift of the onset and peak oxidation potential with an increase in temperature. There also only appear to be one peak present for the oxidation of the nickel. As the nickel in the LSV experiments has been deposited from Watts nickel not Ethaline, it is suggested that the second redox couple in the CV performed using EQCM, is an artefact of the deposition of nickel from Ethaline.

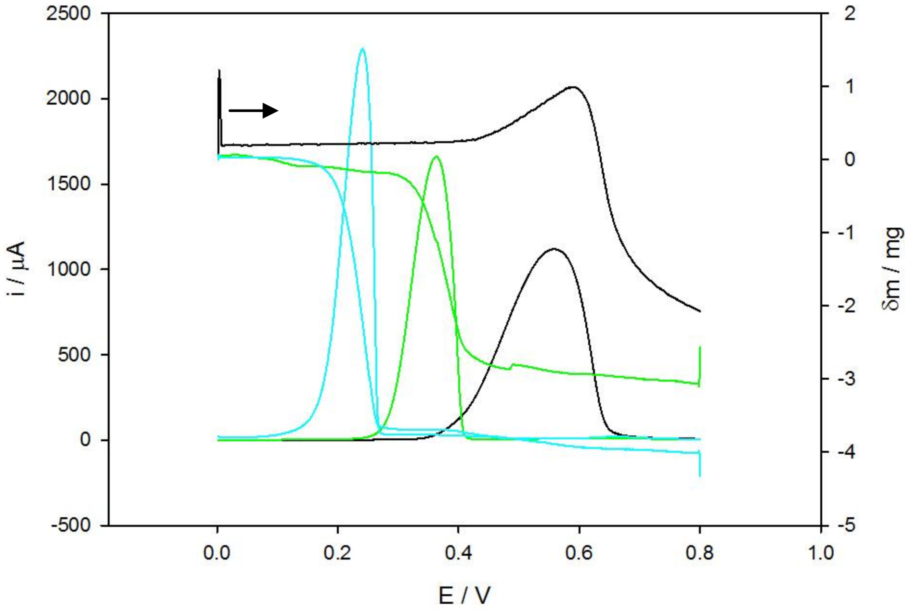

Figure 5.8: Using an EQCM to produce lsV data of nickel deposited on a platinum working electode. Black: 30 ^{o}C. Green: 70 ^{o}C. Turquoise: 130 ^{o}C. Pt working electode, 0.205 cm^{2}. Pt gauze counter electrode. Ag wire reference electrode. Scan rate 10 mV s^{-1}.

Figure 5.8 displays another interesting effect, observed when the nickel is stripped at 30 ^{o}C. Where upon oxidation of the metal, there is an increase in mass on the surface of the electrode. This increase in mass is attributed to ligands coordinating to metal centres on the surface of the electrode, as the nickel is oxidised, before it undergoes dissolution and leaves the surface. This effect is only partially observed at 50 ^{o}C and at 70 ^{o}C the effect is not observed in the change in mass plot. It is proposed that this effect is caused by slow dissolution of the nickel species from the surface at low temperatures. The slow dissolution is caused by the high viscosity of Ethaline 200, meaning it is slow for both the transport of nickel complexes away from the surface of the electrode and transport of chloride ions to the surface of the electrode. The slow transport of chloride means that the generation of soluble nickel species is slow, hence chloride is absorbed on to the surface of the electrode forming nickel complexes that do not undergo dissolution.

The gain in mass on the surface of the electrode will also affect the results from the mass – charge ratio analysis, *Figure 5.9*. As the deposit on the surface is gaining mass due to the absorption of ligands, the mass charge ratio for the dissolution of nickel will be skewed with a lower value than would be expected. This effect is clearly demonstrated in the mass – charge ratio plots for nickel dissolution at 30 and 70 ^oC, by both a lower than expected mass – charge ratio (the mass – charge ratio established in *Figure 5.7*), 2.23 x 10^{-4} g C^{-1} and 6.68 x 10^{-5} g C^{-1} respectively. Additionally the profile of the mass – charge ratio, once most of the charge is passed, there continues to be a loss in mass from the surface of the electrode, producing a curve in the profile.

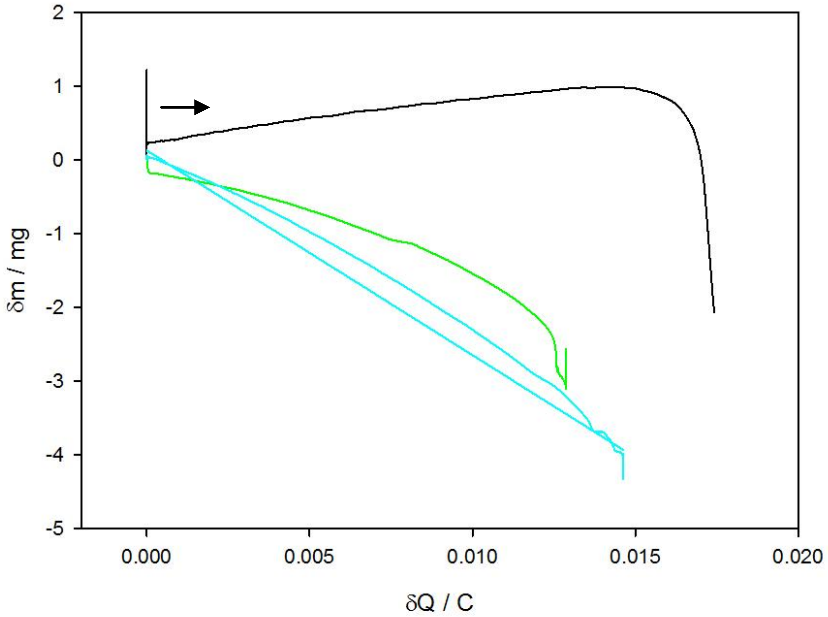

Figure 5.9:Plot of mass versus charge for LSV of nickel deposited on a Pt QCM crystal working electrode, 0.205 cm^2. Black: 30 ^oC. Green: 70 ^oC. Turquoise: 130 ^oC, gradient – 2.78 x 10^{-4} g C^{-1}.

As the mass – charge ratios, especially at low temperatures, are curved, it is not possible to analyse the current efficiency for the dissolution of nickel from the surface.

Even at 130 ^{o}C, where the dissolution of the nickel is fastest, the mass – charge ratio is still slightly curved, indicating that chloride absorption ligands have been coordinated, adding mass on the surface of the electrode. However, if a linear plot is fitted to the data, a mass – charge ratio of 2.78 x 10^{-4} g C^{-1} is calculated. This corresponds with the mass charge ratio obtained from CV.

It is interesting, that for the dissolution of nickel at 30 ^{o}C, there is actually an increase in mass whilst the nickel on the surface is being oxidised. This effect is caused by an excess of nickel complexes with limited solubility formed on the surface of the electrode, meaning that the weight of chloride is added to the surface of the QCM electrode.

To determine the effect dissolved copper species has on the electrochemistry of nickel, a solution, containing both nickel and copper salts, was produced. *Figure 5.10* displays the CV of a mixed $NiCl_2$ and $CuCl_2$ system at 130 ^{o}C. The CV displays two distinct redox couples at 0.575 and -0.250 V, which represent the Cu (II)/(I) and the Ni (II)/(0) and Cu (I)/(0) redox couples respectively, where the Ni (II)/(0) and Cu (I)/(0) redox couples come at a similar potential. The Cu (II)/(I) redox couple has shifted positive when compared to the results in **Chapter 3**, however when compared to the Cu (II)/(I) redox couple, in a solely Cu system at 130 ^{o}C, the electrode potential is analogous.

The redox couple displayed at - 0.25 V (Ag wire *pseudo* reference electrode), for the Ni (II)/(0) and Cu (I)/(0) redox couples, has an electrode potential that is approximately half way between the electrode potentials for the individual redox couples, – 0.125 and – 0.4 V respectively. It is tempting to think that the redox couple represents deposition of both metals at the same time, however this may not be the case and EQCM measurements were made to analysis the deposition process.

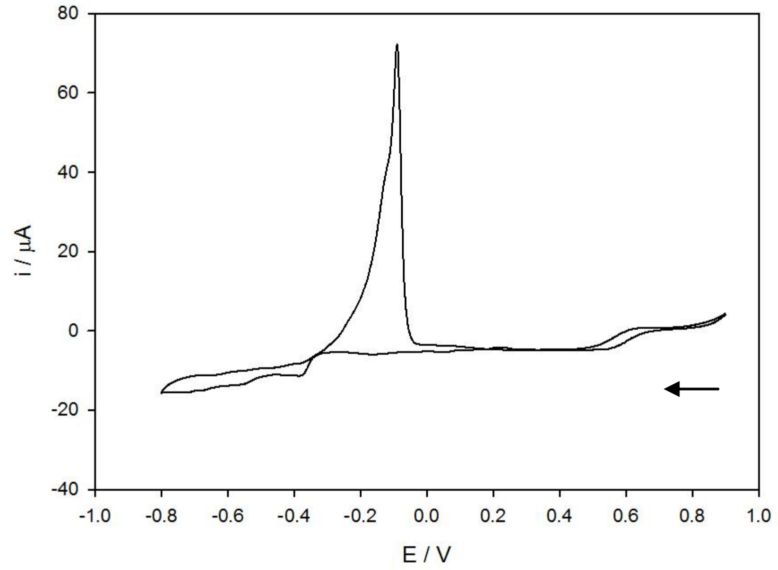

Figure 5.10: CV of 10 mM $NiCl_2$ *&* $CuCl_2$ *dissolved in Ethaline 200. Pt working electrode, 3.14 x* 10^{-2} cm^2*. Pt gauze counter electrode. Ag wire reference electrode. Scan rate 10 mV* s^{-1}*.*

To further analysis the mixed system, the CV was run using the EQCM. From the results obtained, it will be possible to determine the ratio of metals deposited and comment made on the possibility of alloy or co – deposit deposition.

By analysing the mass – charge ratio, *Figure 5.11*, it is possible to determine the ratio of metals deposited and comment of the possible morphology of the deposit. In *Figure 5.8*, there is an initial change in current that is associated with the Cu (II) → (I) reduction. For the deposition regime, the mass – charge ratio displays a linear trend, which implies that both metals are being deposited at the same time and an alloy could be forming on the surface of the electrode.

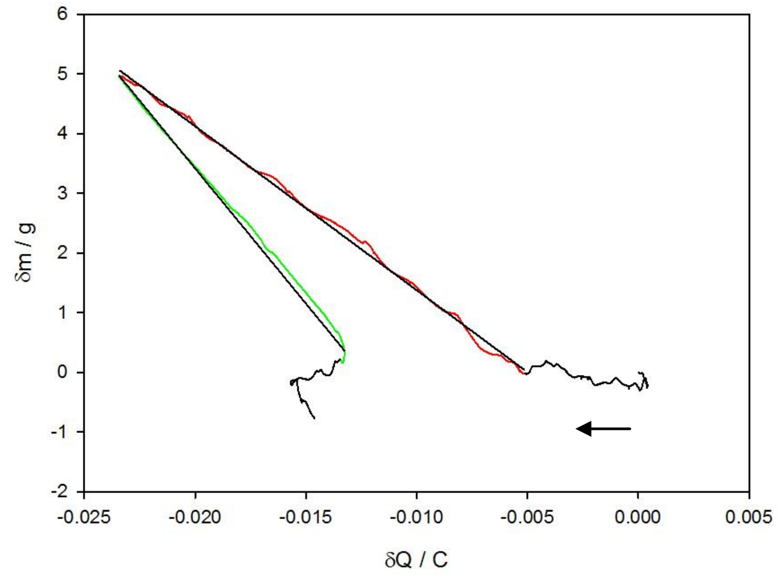

Figure 5.11: Plot of mass versus charge for CV of 10 mM $NiCl_2$ *&* $CuCl_2$ *dissolved in Ethaline 200. Red; deposition of metals, gradient 2.75 x* 10^{-4} *g* C^{-1}*. Green; stripping of metals, gradient 4.53 x* 10^{-4} *g* C^{-1}*. Pt working electrode, 0.205* cm^2*.*

As shown in **Chapter 3** the ratio of nickel to copper can be calculated using the mass – charge ratio and the current efficiency for each individual process. As shown above, the mass – charge ratio for the deposition of nickel is greater than the theoretical mass – charge ratio, hence for the purposes of calculation **(5.2)** the current efficiency of nickel will be assumed to be 100 %. It is important to note that the current efficiency calculated for the deposition of copper in **Chapter 3** cannot be used, as this was calculated for the deposition of copper at 30 ^{o}C. For the deposition of copper at 130 ^{o}C, the mass – charge ratio displays a similar trend to nickel, where the experimental value is greater than the theoretically calculated value. It is proposed that the deposition of metals at higher temperatures produces coatings that trap DES on the surface of the electrode, leading to an increase in mass and hence a higher than theoretically possible value for the mass – charge ratio. Hence, for the purposes of calculation **(5.3)**, the current efficiency used for copper will be assumed to be 100 %. Unfortunately, the mass

– charge ratio for the deposition in the mixed system, is smaller than both theoretical mass – charge ratios for copper and nickel. Hence equation **(5.2)** will not give a valid result for the mole fraction of copper.

$$\chi_{\mathrm{Cu}} = \frac{(\frac{\delta \mathrm{m}}{\delta \mathrm{Q}} 2\mathrm{F} - \mathrm{RMM}_{\mathrm{Ni}})}{(\mathrm{RMM}_{\mathrm{Cu}} - \mathrm{RMM}_{\mathrm{Ni}})} = -1.99 \times 10^{-3} \quad (\mathbf{5.2})$$

It is suggested that the deposits of copper and nickel at 130 ^{o}C are porous and trap some of the solution near the surface of the crystal. This would account for the high mass charge ratios.

Again it is not possible to calculate the mole fractions for the dissolution of the metals from the surface of the electrode. This is due to the fact that both the copper and nickel metals disintegrate from the surface and hence it is not possible to calculate the current efficiency for either process. It is important to note that the mass – charge ratio for the dissolution is linear. This implies that the dissolution of both metals is occurring at the same time. This implies that the deposit is forming an alloy.

Analysis of the CV when compared to the change in mass is also instructive when trying to decide if an alloy or co – deposit is fromed for the deposition of nickel and copper, *Figure 5.12*. It is interesting to note there is only one redox couple present in the CV for deposition and dissolution process. This is interesting because for the second, small, redox couple associated with the deposition of nickel is not present in this experiment.

For the cathodic sweep, negative from 0.9 V down to – 0.8 V. From *ca.* 0.9 to – 0.25 V, there is a small increases in mass, which is seen in the previous systems containing the Cu (II)/(I) redox couple. From *ca.* – 0.25 to – 0.8 V there is a large, linear increase in mass and negative current in the CV indicating the deposition of both metals on to the surface of the electrode.

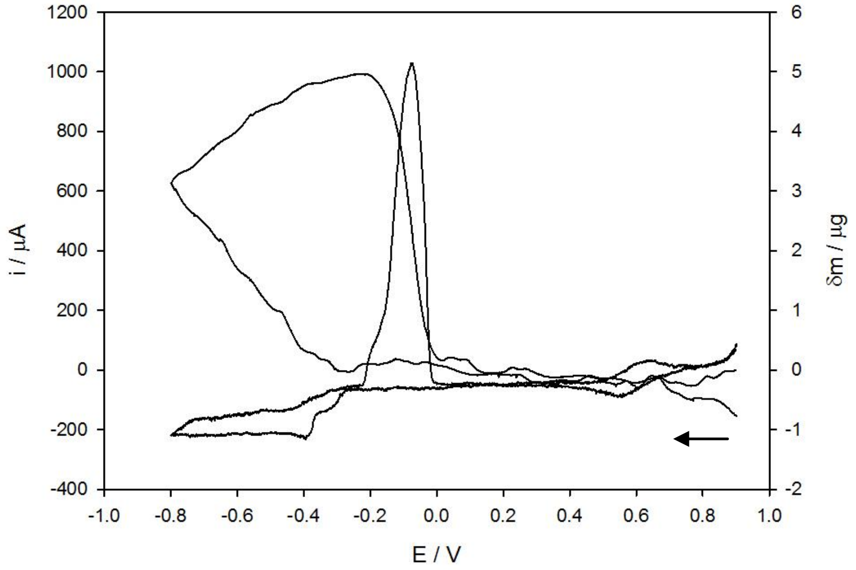

Figure 5.12: Using an EQCM to produce CV data of 10 mM $NiCl_2$ & $CuCl_2$ dissolved in Ethaline 200. Pt working electrode, 0.205 cm^2. Pt gauze counter electrode. Ag wire reference electrode. Scan rate 10 mV s^{-1}

For the anodic sweep, positive from – 0.8 V up to 0.9 V. The sweep starts in the deposition regime for both metals and there is a negative current from *ca*. – 0.9 to – 0.25 V, indicating deposition is continuing. However, looking at the change in mass plot, there appears to be a change in the gradient of the change in mass plot at *ca*. – 0.4 V. There is also a change in the profile CV at this point. This indicates that the copper has either started to dissolve or stopped depositing. If copper is being dissolved at this point, it points to the main bulk deposit being an alloy, which would be analogous to results previously seen in **Chapter 3**. From *ca*. – 0.2 to 0 V, the bulk dissolution takes place, represented by a large loss in mass and a large positive spike in current. From *ca*. 0 to 0.9 V the mass returns to zero, showing that all metal has been removed from the surface of the electrode.

5.3 Palladium (II) Chloride in Ethaline 200

Previous work on palladium (II) chloride has been performed using EXAFS, the speciation of $PdCl_2$ dissolved in Ethaline 200 was determined to be $[PdCl_4]^{2-}$.[2] Unlike nickel there does not appear a mixed speciation, probably due to the bite angle of the ethylene glycol being too small and hence not binding to the metal centre. Being a palladium (II) species, with d^8 configuration and 16 electrons in the outer electron shell, it is expected that the palladium centre will form a square planar configuration. The palladium (II) tetrachloride species has been well documented in both aqueous[9,10] and organic solutions[11]. It has been noted that in solutions containing high chloride content, higher chloride palladium complexes, *e.g.* $[PdCl_5]^{3-}$, are accesable.[11,12] Also in aqueous solutions, conversion of palladium (II) tetrachloride complexes has been documented, where the palladium (II) tetrachloride complex can convert between $[PdCl_4]^{2-}$ to $[Pd(H_2O)_4]^{2+}$ via the expected range in intermediate complexes.[10]

When dissolved in Ethaline 200 the $[PdCl_4]^{2-}$ complex forms a red / orange solution. This is caused by the absorption of visible light between *ca.* 400 – 550 nm, *Figure 5.13.* The UV – Vis spectra displays the λ_{max} at 247 nm ($\varepsilon = 250\ dm^3\ mol^{-1}\ cm^{-1}$) with a shoulder at 275 nm ($\varepsilon = 193\ dm^3\ mol^{-1}\ cm^{-1}$), there are two more peaks at 332 and 400 nm ($\varepsilon = 94\ dm^3\ mol^{-1}\ cm^{-1}$, $\varepsilon = 77\ dm^3\ mol^{-1}\ cm^{-1}$ respectively). These peaks and extinction coefficients are similar to that of $[PdCl_4]^{2-}$ in other media.[10,11,12] It should be noted that the peaks are blue shifted, when compared to organic and aqueous media.

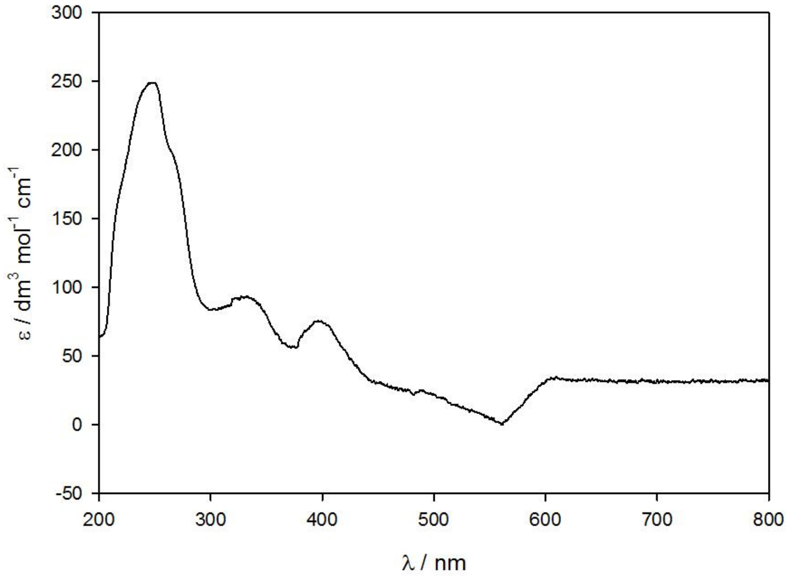

Figure 5.13: The electronic spectra of 1 mM $PdCl_2$ dissolved in Ethaline 200.

As palladium (II) chloride form the $[PdCl_4]^{2-}$ species when dissolved in Ethaline 200, it means, that unlike nickel, heating is not required to generate a electrochemically active species and hence the CV can be performed at 30 ^{o}C, *Figure 5.14*.

The CV of $PdCl_2$ dissolved in Ethaline 200, *Figure 5.14*, displays an irreversible redox couple associated with the Pd (II)/(0) redox couple. The peaks that represent this couple are at *ca*. – 0.43 V for the reduction and 0.66 V with a shoulder at 0.47 V for the oxidation, with the electrode potential for the process calculated to be 0.01 V (Ag wire *pseudo* reference electrode). It is proposed that the shoulder represents that there are two phases of palladium deposited on the surface, and the oxidation of one phase of palladium creates the shoulder and the other creates the peak. It is possible that the two phases of palladium are caused by the kinetics of the deposition processes. As the kinetics of deposition are slower in the mass transport controlled region of the deposition than in the potential controlled region, it is possible a separate crystal phase could be deposited in each region.

There also appears to be a much smaller redox process occurring, which appears as a peak at 0.05 V for the oxidation and a shoulder to the end of the electrochemical window at – 0.88 V for the reduction process, with the electrode potential for this process calculated to be – 0.43 V(Ag wire *pseudo* reference electrode), it is unclear what this process represents.

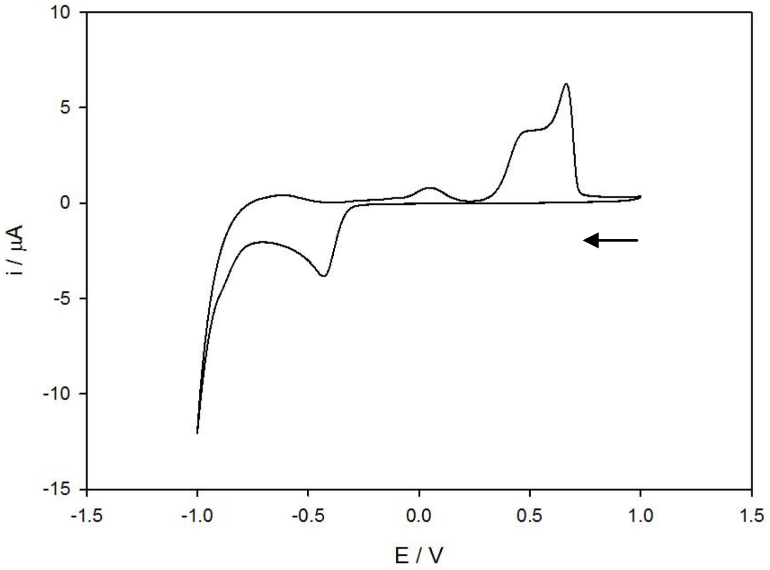

Figure 5.14: CV of 20 mM $PdCl_2$ dissolved in Ethaline 200. Pt working electrode, 3.14 x 10^{-2} cm^2. Pt flag counter electrode. Ag wire reference electrode. Scan rate 10 mV s^{-1}

To obtain further information about the electrochemistry of the Pd (II)/(0) redox couple, the EQCM has been used to perform CV, *Figure 5.15*. It is important to note, that in the CV performed using the EQCM, the range of the electrochemical window is smaller than in *Figure 5.14*. As the window sweeps to a smaller negative value, the reduction for the unidentified redox couple does not occur, hence on the reverse sweep, the oxidation peak also does not occur. This shows that the smaller redox process, with the electrode potential of – 0.43 V, is due to an initially oxidised species that is in solution and not a reduced species.

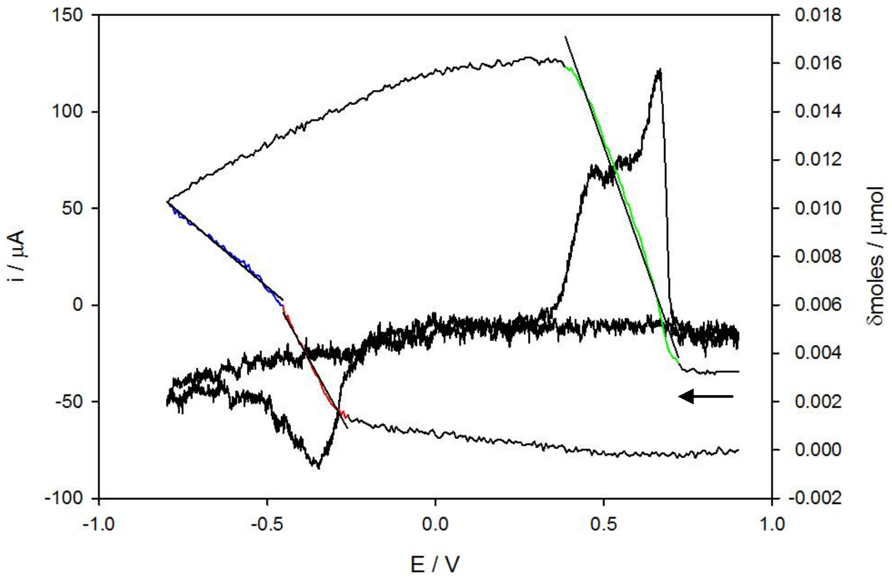

Figure 5.15: Using an EQCM to produce CV data of 10 mM $PdCl_2$ dissolved in Ethaline 200. Red: deposition of palladium, gradient: – 3.95 x 10^{-8} mol V^{-1}. Blue: deposition of palladium, gradient: – 2.50 x 10^{-8} mol V^{-1}. Green: stripping of palladium, gradient: – 1.18 x 10^{-7} mol V^{-1}. Pt working electrode, 0.205 cm^2. Pt gauze counter electrode. Ag wire reference electrode. Scan rate 10 mV s^{-1}

For the cathodic sweep, starting at 0.9 V and sweeping negative down to – 0.8 V. At *ca*. – 0.25 V reduction begins to occur, this is represented by a negative current and an increase in mass, and hence the number of moles of palladium, on the surface of the QCM crystal. It appears that the deposition of palladium occurs in two stages. The first stage, which occurs between *ca*. – 0.25 to – 0.45 V, is where the palladium deposition is controlled by the applied potential and is deposited at a rate of 1.93 x 10^{-9} mol s^{-1} cm^{-2}. The second stage of deposition, which occurs between – 0.45 to – 0.8 V, is where the deposition is controlled by the diffusion of $[PdCl_4]^{2-}$ ions from the bulk solution in to the depleted double layer and the rate of deposition is 1.22 x 10^{-9} mol s^{-1} cm^{-2}.

For the anodic sweep, starting at – 0.8 V and sweeping positive up to 0.9 V. The sweep starts at a potential where palladium is being deposited and deposition continues until *ca*. 0.35 V. It should be noted that the mass continues to rise between *ca*. – 0.25 and 0.35 V, which is positive of the onset reduction potential. It is proposed that ligands could be being coordinated to the palladium centres, as shown by nickel above, increasing the mass on the surface of the electrode.

Oxidation and dissolution occurs between *ca*. 0.35 to 0.75 V. The rate of dissolution for the stripping of palladium is 5.76 x 10^{-9} mol s^{-1} cm^{-2}. It should be noted that the rate of dissolution is constant for the entire oxidation process and does not seem to be affected by the two oxidation processes in the CV. It is proposed that the two different deposition regimes of palladium, results in two different morphologies of palladium deposit, which are responsible for the shoulder in the CV. The change in moles plot shows that the when the dissolution occurs, not all of the palladium in removed from the surface. This is possibly due to the electrodeposited palladium alloying with platinum electrode surface, preventing the palladium being removed from the surface.

To further analyse the deposition of palladium, the mass – charge ratio can be determined and used to calculate the current efficiency. The theoretical mass charge ratio is calculated in **(5.3)**.

$$\frac{\delta \mathrm{m}}{\delta \mathrm{Q}} = \frac{106.42}{2\mathrm{F}} = 5.51 \times 10^{-4}\,\mathrm{g}\,\mathrm{C}^{-1} \quad (\mathbf{5.3})$$

Figure 5.16 displays the plot of the experimentally determined mass – charge ratio. For the initial deposition, where the reduction of palladium is under potential control, the mass – charge ratio is 3.65 x 10^{-4} g C^{-1}, which corresponds to a current efficiency of 66 %. For the second stage of deposition, where the deposition of palladium is controlled by the diffusion of palladium ions in solution, the mass – charge ratio is 2.61 x 10^{-4} g C^{-1}, which corresponds to a current efficiency of 47 %. It was discussed above that the rate of deposition could be affecting the morphology of the deposit. Another possibility is that the lower current efficiency of the mass transport controlled regime could also lead to a change in deposit morphology and hence there would be two deposit morphologies on the surface of the electrode. Two different morphologies would lead to two oxidation waves in the anodic sweep.

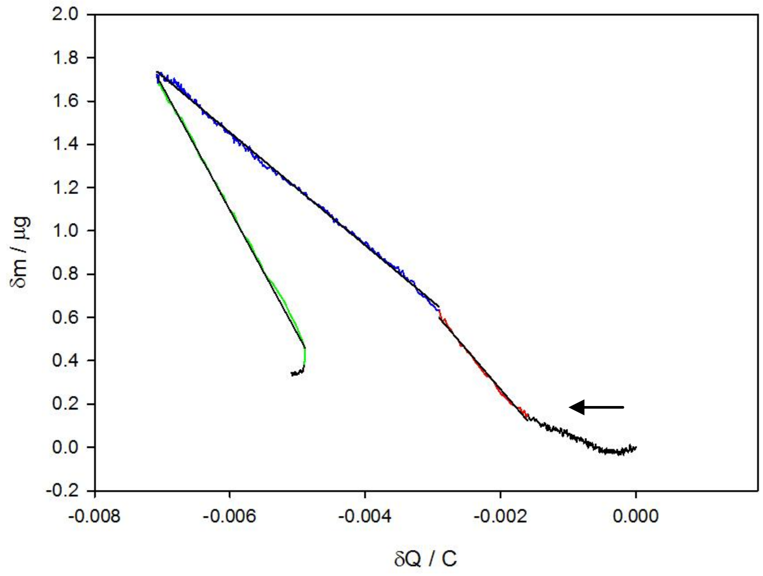

Figure 5.16: Plot of mass versus charge for CV of 10 mM $PdCl_2$ dissolved in Ethaline 200. Red; deposition of palladium, gradient – 3.65 x 10^{-4} g C^{-1}. Blue; deposition of palladium, gradient 2.61 x 10^{-4} g C^{-1}. Green; stripping of palladium, gradient – 5.73 x 10^{-4} g C^{-1}. Pt working electrode, 0.205 cm^2.

It should be noted that the mass – charge ratio for the dissolution of palladium is constant, even though the CV has a shoulder in the oxidation process. The mass – charge ratio for the dissolution process is 5.73 x 10^{-4} g C^{-1}, this value is greater than the theoretically calculated mass – charge ratio, equation **(5.3)**. A mass – charge ratio that is greater than the theoretical value, for the dissolution of a metal, indicates that unoxidised palladium is loosed from the surface of the electrode. This is in line with the results obtained for both the nickel and copper systems.

To investigate the effect copper has on the electrochemistry of palladium, a solution containing both palladium and copper salts was produced. *Figure 5.17* displays the CV of the mixed $CuCl_2$ and $PdCl_2$ system. The CV displays what appears to be two redox couples. One for the Cu (II)/(I) redox couple with an electrode potential of 0.48 V(Ag wire *pseudo* reference electrode). The other for both the Pd (II)/(0) and Cu (I)/(0) redox couples with an electrode potential of – 0.04 V(Ag wire *pseudo* reference electrode). This suggests that both copper and palladium undergo deposition and dissolution at the same time, forming either an alloy or co – deposit.

It is worth noting that at *ca*. – 0.23 V on the reverse sweep, the current is positive. Suggesting that an oxidative process is occurring, this could well be attributed to the dissolution of copper.

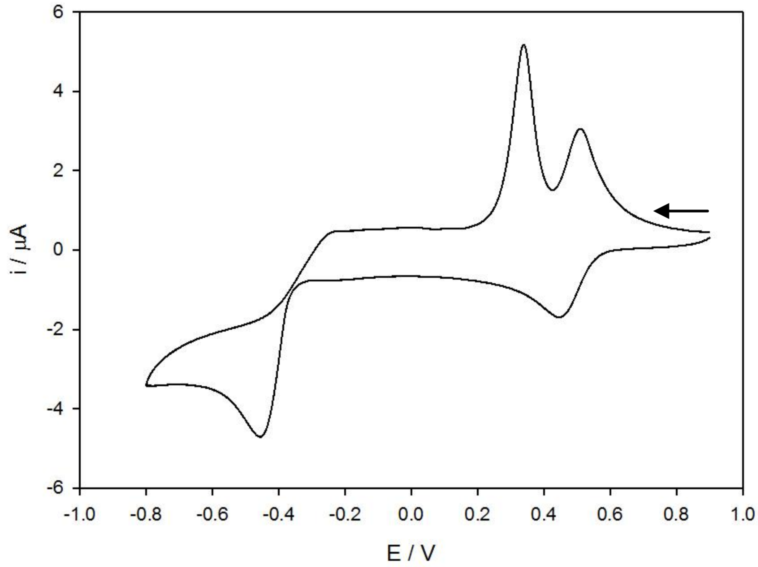

Figure 5.17: CV of 10 mM $PdCl_2$ & $CuCl_2$ dissolved in Ethaline 200. Pt working electrode, 3.14×10^{-2} cm^2. Pt flag counter electrode. Ag wire reference electrode. Scan rate 10 mV s^{-1}

To try and further investigate the electrochemistry of the mixed system, EQCM has been employed to perform CV, *Figure 5.18*, from which mass – charge ratio analysis can be performed.

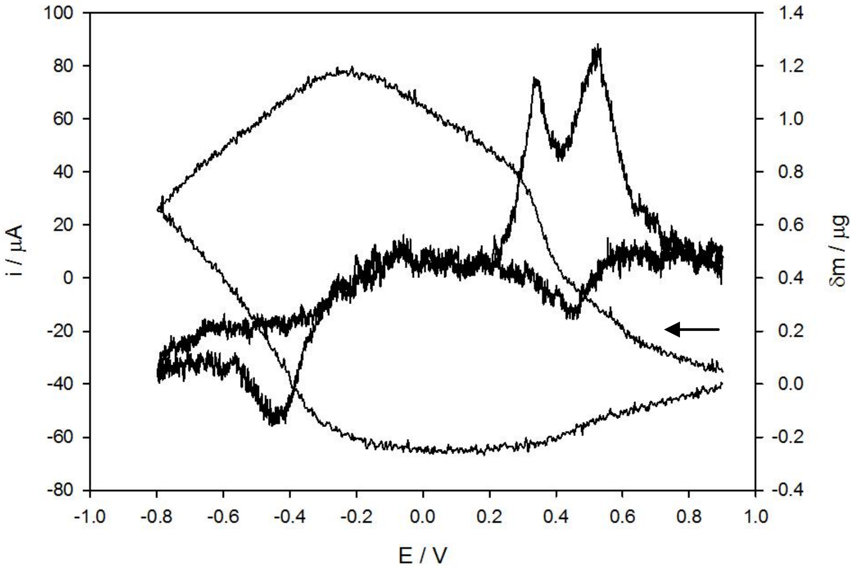

Figure 5.18: EQCM performing CV of 10 mM $PdCl_2$ & $CuCl_2$ dissolved in Ethaline 200. Pt working electrode, 0.205 cm^2. Pt gauze counter electrode. Ag wire reference electrode. Scan rate 10 $mV\ s^{-1}$

It should be noted, that the CV presented in *Figure 5.18*, displays the second scan of the CV experiment, this is in line with all other voltammetry experments. This means that at the beginning of the scan, 0.9 V. Mass is being lost, as metal deposited in the previous scan is undergoing dissolution. This dissolution occurs between *ca*. 0.9 to 0.3 V. The current associated with dissolution is masked in the CV by the reduction of Cu (II) → (I). It is also possible that a galvanic reaction may be occurring between deposited Pd (0) and Cu (II), this would lead to a loss in mass on the surface of the electrode negative of the onset oxidation potential, however this does not appear to be occurring.

Following the dissolution of metal and the Cu (II)/(I) redox couple, a stable mass and current is displayed, between *ca*. 0.3 to – 0.2 V. After – 0.2 V the deposition of both metals occurs, represented by a large, uniform increase in mass and a negative current in the CV.

For the reverse, anodic sweep, from – 0.8 V positive up to 0.9 V. The sweep start at a voltage where deposition of both metals is occurring, from *ca*. – 0.9 to – 0.2 V. At *ca*. – 0.2 V, the profile of the change in mass plot shows that mass has started to be lost from the surface of the electrode. Although unclear in the CV produced using the EQCM, *Figure 5.17* displays a positive current at – 0.2 V. This is attributed to the dissolution of copper from the surface, which is represented by a constant loss in mass between *ca*. – 0.2 to 0.3 V.

At *ca*. 0.3 V there is a change in the profile of the change in mass plot, this is represents the start of the dissolution of palladium. It is proposed, during this second stage of dissolution, that it is both palladium and copper undergoing dissolution.

At *ca*. 0.4 V there is another change in profile of the change in mass plot, this is attributed to the Cu (II)/(I) redox couple. Whilst the Cu(II)/(I) redox couple will not directly affect the loss of mass from the surface of the electrode. As some of the current passed will be associated with the Cu(II)/(I) redox and hence will slow the dissolution of the metals form the surface.

The final stage of dissolution occurs at *ca*. 0.62 V, when the Cu(II)/(I) has reached diffusion control. The rate of mass lost here is the slowest in *Figure 5.18*. It is proposed that the rate of dissolution is slow due to alloying of copper and palladium with the platinum QCM electrode.

To gain a further insight into the electrochemistry, the mass charge ratio of the CV was analysed, *Figure 5.19*.

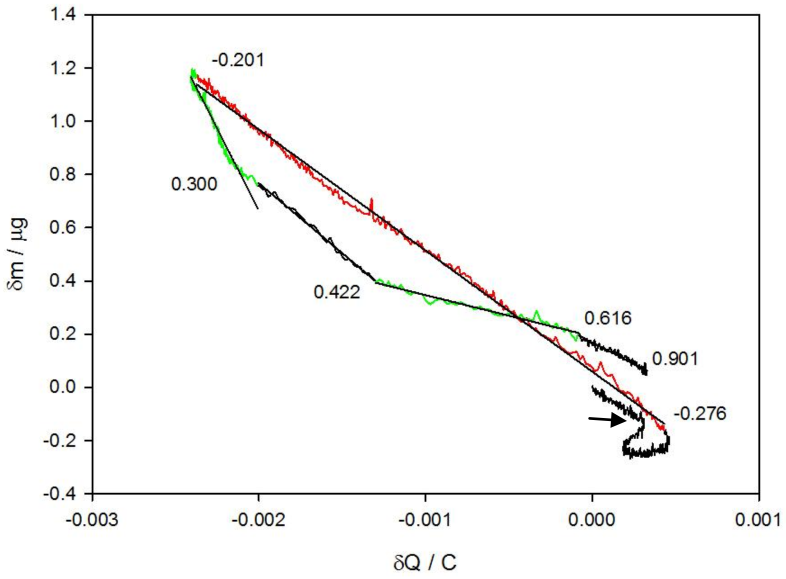

Figure 5.19: Plot of mass versus charge for CV of 10 mM $PdCl_2$ & $CuCl_2$ dissolved in Ethaline 200.

As stated above, because the mass – charge data displayed is taken from the second cycle of the experiment, dissolution is still occurring as metal is present on the surface from the previous scan. The deposition of both metals appears to be initiated at the same potential of – 0.276 V. The mass – charge ratio displays a linear response for the entire deposition until the potential returns to – 0.201 V. The mass charge ratio for the deposition is 4.55 x 10^{-4} g C^{-1}. Interestingly the mass – charge ratio value for the mixed system is greater than both that of the individual palladium and copper systems. This implies that the current efficiency could be being improved for both metals in the mixed system. It does however mean that we apply the same analysis that has been performed for the other binary metal systems, an erroneous result will be returned, equation **(5.4a)**.

$$\chi_{Cu} = \frac{(RMM_{Pd} - \frac{\delta m}{\delta Q}2Fb)}{(\frac{\delta m}{\delta Q}2Fa - \frac{\delta m}{\delta Q}2Fb - RMM_{Cu} + RMM_{Pd})} = -16.4 \quad \mathbf{(5.4a)}$$

The implication of the above discussion, is that the presence of both copper and palladium, increases the current efficiency for the deposition of both metals. Unfortunately, however, this does mean current efficiency of the individual metals can't be used to calculate the mole fractions of each of those metals in the deposit. If we assume both individual metals are deposited at 100 % current efficiency, then a valid answer is obtained, as shown in **(5.4b)**. The mole fraction of copper deposited is 0.43 and the mole fraction of palladium 0.57.

$$\chi_{\mathrm{Cu}} = \frac{(\frac{\delta \mathrm{m}}{\delta \mathrm{Q}} 2\mathrm{F} - \mathrm{RMM}_{\mathrm{Pd}})}{(\mathrm{RMM}_{\mathrm{Cu}} - \mathrm{RMM}_{\mathrm{Pd}})} = 0.43 \quad (\mathbf{5.4b})$$

For the first stage of dissolution, form – 0.201 to 0.300 V, which from the CV has been assigned to copper dissolution. The mass – charge ratio is 1.23 x 10^{-3} g C^{-1}. This value is greater than both the experimental and theoretical values for the mass – charge ratio of copper. It is proposed that loss of unoxidised metal from the surface is occurring. However, instead of the loss of just copper particulate, both metals are disintegrate, accounting for the higher mass – charge ratio.

The second stage of dissolution, between 0.300 and 0.422 V, the mass – charge ratio is found to be 5.26 x 10^{-4} g C^{-1}. The mass – charge ratio analysis of both copper and palladium have shown that both metals lose unoxidised mass from the surface of the electrode in the dissolution regime of the voltammetry. Hence, it is not possible to apply **(5.5b)** to determine the mole fractions of each metal. However, it should be noted that the value of the experimental mass – charge ratio is close to that of the theoretical mass – charge ratio of palladium. Hence it is expected that most of the metal undergoing dissolution is palladium.

The third stage of dissolution occurs between 0.422 and 0.616 V. Between these potentials, the oxidation Cu (I) → (II) starts and is under potential control. This means that the bulk of current passed will be due to the Cu (I) → (II) oxidation, this will affect the mass – charge ratio. The value of the mass – charge ratio is 1.55 x 10^{-4} g C^{-1}.

The final stage of dissolution, between 0.616 and 0.901 V, occurs when the Cu (I) → (II) oxidation has reached diffusion control. The mass – charge ratio is 3.23 x 10^{-4} g C^{-1}. This mass charge ratio is higher than the third stage of dissolution, because the concentration of Cu (I) in the double layer is lower. Hence, the amount of charge passed for the Cu (I) → (II) oxidation is less. This means that more of the current passed is due to the dissolution process.

5.4 Platinum (II) Chloride in Ethaline 200

Previous work has been carried out on the speciation of $PtCl_2$ in Ethaline 200 by Hartley *et. al.*[2] Where the speciation of the platinum centre was shown to be $[PtCl_4]^{2-}$. The expected geometry is square planar, as the $[PtCl_4]^{2-}$ complex contains a Pt (II) centre, which has 16 electrons and a d^8 configuration.

The UV-Vis spectra of $PtCl_2$ dissolved in Ethaline 200 is displayed in *Figure 5.20*. The spectrum displays a λ_{max} at 315 nm (ε = 325 dm^3 mol^{-1} cm^{-1}). There are two shoulders on the λ_{max} peak at 247 nm (ε = 229 dm^3 mol^{-1} cm^{-1}) and 344 nm (ε = 240 dm^3 mol^{-1} cm^{-1}). There is one peak in the visible region of the spectrum at 478 nm (ε = 106 dm^3 mol^{-1} cm^{-1}), the absorbed light is in the blue region of the visible spectrum and gives the solution an orange colour. The molar extinction coefficient for the light absorbed in the visible region of the spectrum, is of a similar magnitude to that of the $[PdCl_4]^{2-}$. This is not unexpected as both metal centres are expected to be in a square planar configuration, due to the d^n configuration being d^8. The spectrum also agrees well with published literature.[13,14,15]

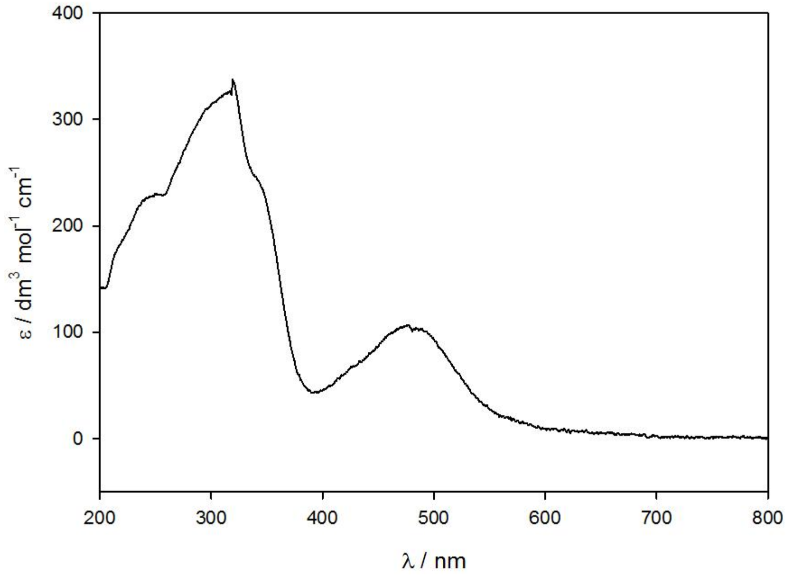

Figure 5.20: The electronic spectra of 1 mM $PtCl_2$ dissolved in Ethaline 200.

As with the palladium solution, the platinum complex formed is the tetrachloro species in solution, $[PtCl_4]^{2-}$. Hence it is expected that there will be very little variation in speciation when the solution is heated. The only observation made upon heating was formation of platinum particles in solution. It is proposed that $[PtCl_4]^{2-}$ has undergone disproportionation to form Pt (IV) and Pt (0) which aggregates and forms particles.

The electrochemistry of $PtCl_2$ dissolved in Ethaline 200, was investigated using CV. The CV, at 30 ^{o}C, does not display any well defined redox behaviour, with only the negative end of the electrochemical window giving a large response due to the breakdown of Ethaline. However there is a small reduction wave, with an onset potential of 0.388 V, which could be attributed to the reduction of platinum. It is expected that platinum will follow the same trend as displayed by nickel and palladium above and would display a large hysteresis in redox peaks due to the electrochemically irreversible nature of the redox couple. Hence, it is expected that the oxidation wave will be outside the electrochemical window of Ethaline 200. This means it is not possible to do analysis of the onset potentials and hence calculate the electrode potential at 30 °C. As the CV at 30 °C does not show useful data, it has been omitted.

When heated to 130 °C, the electrochemistry, only undergo a small change, where the reduction wave is shifted negatively to an onset potential of 0.061 V *Figure 5.21*.

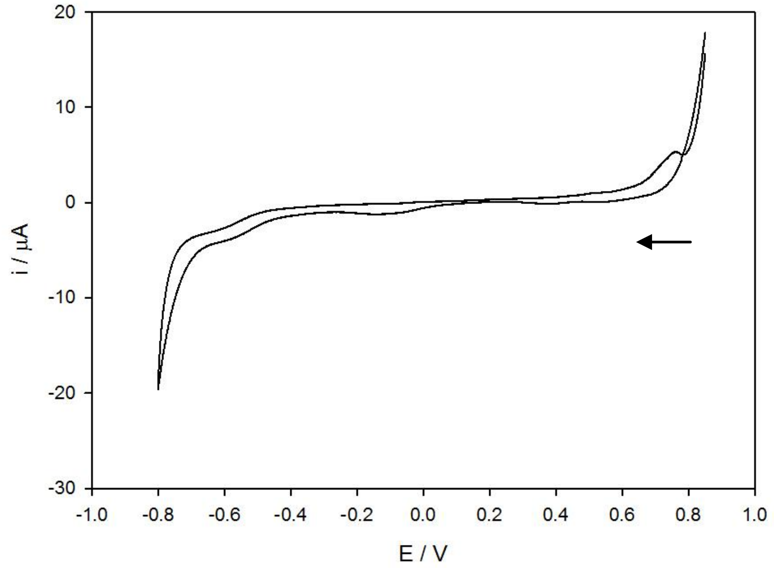

Figure 5.21: CV of 10 mM $PtCl_2$ dissolved in Ethaline 200 at 130 °C. Pt working electrode, 3.14 x 10^{-2} cm^2. Pt flag counter electrode. Ag wire reference electrode. Scan rate 10 mV s^{-1}

It is important to note that in *Figure 5.22*, the figure has only been produced up to a positive potential of 0.85 V. This is because a large positive current is observed above 0.85 V, which makes the scaling of the figure so that it is difficult to observe the reduction waves. The large positive current, is assigned to the oxidation of Pt and can be used to calculate the electrode potential. The electrode potential at 130 °C has been calculated to be 0.352 V. Using the Nernst equation it is possible to correct the value of the electrode potential, to calculate the formal electrode potential for $[PtCl_4]^{2-}$. The electrode potential is 0.432 V *versus* an Ag wire *pseudo* reference electrode. Or in context of existing literature,[5] 0.357 V with respect to a $[Fe(CN)_6]^{3-/4-}$ internal reference.

To further investigate the electrochemistry of $PtCl_2$ dissolved in Ethaline 200, CV was performed using the EQCM, *Figure 5.22*. The window of the CV was extended positively to 0.9 V so the positive current can be investigated.

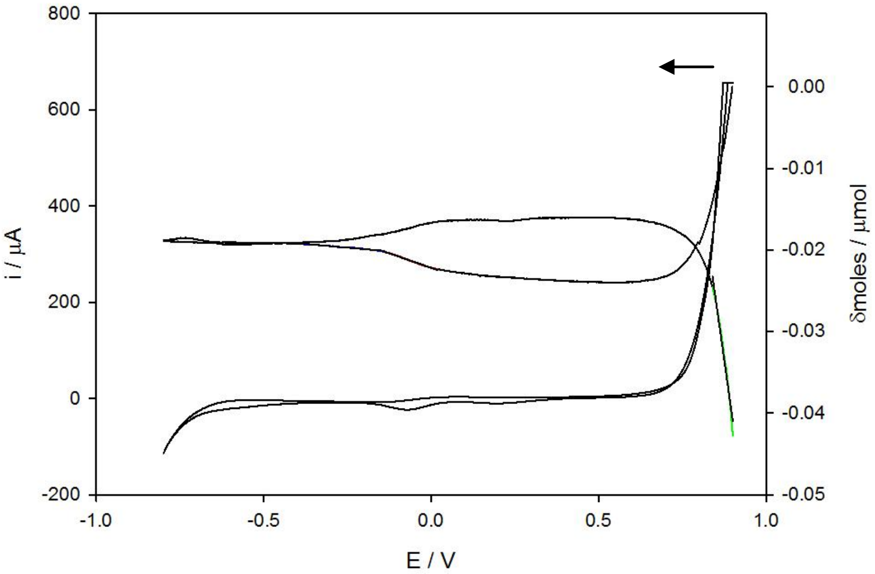

Figure 5.22: Using an EQCM to produce CV data of 10 mM $PtCl_2$ dissolved in Ethaline 200. Red: deposition of platinum, gradient: – 1.43 x 10^{-8} mol V^{-1}. Blue: deposition of platinum, gradient: – 3.61 x 10^{-9} mol V^{-1}. Green: stripping of platinum, gradient: – 2.92 x 10^{-7} mol V^{-1}. Pt working electrode, 0.205 cm^2. Pt gauze counter electrode. Ag wire reference electrode. Scan rate 10 mV s^{-1}

In *Figure 5.22* the change in mass plot is displayed with the CV to allow for comparison between the two. In the cathodic sweep, from 0.9 V sweeping negative down to – 0.8 V, the change in mass plot starts at 0 g. At 0.9 V, the sweep starts at a potential where dissolution of Pt is occurring. The dissolution of Pt occurs from *ca*. 0.9 – 0.68 V. From *ca*. 0.68 to 0.02 V there is little change in the mass of the electrode. Between *ca*. 0.02 to – 0.14 V there appears to be an increase in mass on to the surface of the electrode, this is attributed to the deposition of Pt under potential control. The rate of deposition appears to be 6.98 x 10^{-10} mol s^{-1} cm^{-2}. Diffusion takes control of the deposition between *ca*. – 0.14 to – 0.38 V. The rate of deposition decreases to 1.54 x 10^{-10} mol s^{-1} cm^{-2}. After *ca*. – 0.38 to – 0.8 V, there appears to be a passivation effect, where no more mass is being added to the surface of the electrode, it is unclear what is causing this.

The deposition of platinum is slower than any of the other elements under investigation. This is not an unexpected result, as the $[PtCl_4]^{2-}$ species is larger than any other species under investigation and hence the diffusion will be slower. Hence the deposition of Pt is expected to be under mass transport control. Also, for the deposition of platinum, four chloride ligands need to be dissociated from the platinum centre.

For the anodic sweep, positive from – 0.8V up to 0.9 V. The sweep starts in the region of the voltammogram where platinum does not appear to be being deposited, from *ca*. – 0.8 to – 0.37 V the mass of the crystal remains constant. This is the same range of potential where the mass remains constant in the cathodic sweep. Between *ca* – 0.37 to 0.02 V there is an increase in mass akin to that in the cathodic sweep. After the increase in mass, the CV enters a regime, from *ca*. 0.02 to 0.62 V, where nether an oxidative or reductive process is occurring, represented by no change in mass on the surface of the electrode. Finally, stripping of Pt occurs between *ca*. 0.62 – 0.9 V, the rate of dissolution is 1.42 x 10^{-8} mol s^{-1} cm^{-2}.

To gain more insight to the deposition and dissolution process, the mass – charge ratio has been analysed. For the mass – charge ratio it is possible to calculate the current efficiency. The theoretical mass – charge ratio is calculated by **(5.5)**.

$$\frac{\delta \mathrm{m}}{\delta \mathrm{Q}} = \frac{195.08}{2\mathrm{F}} = 1.01 \times 10^{-3}\,\mathrm{g\,C^{-1}} \quad (\mathbf{5.5})$$

The mass *versus* charge plot, *Figure 5.23*, shows a linear response for the deposition of Pt, between 0.125 and – 0.156 V. The experimentally determined mass – charge ratio has a value of 7.60 x 10^{-4} g C^{-1}. From which the current efficiency can be calculated to be 75 %, for the deposition of Pt. The stripping of Pt, which is occurring at both the beginning and end of the cycle, also displays a linear response. Unlike the other group 10 metals, but similarly to silver and gold in **Chapter 3**, the mass – charge ratio does not exceed the theoretical maximum. Hence it is possible to calculate the current efficiency for the dissolution, which was found to be 52 %.

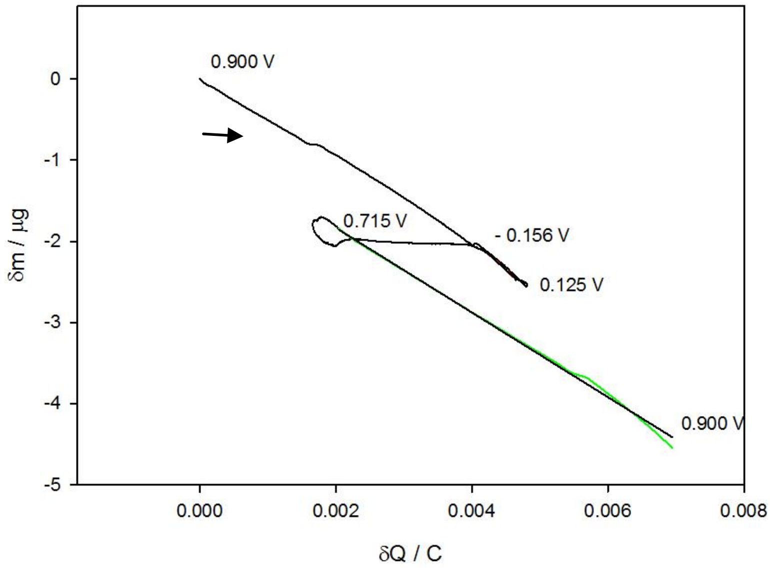

Figure 5.23: Plot of mass versus charge for CV of 10 mM $PtCl_2$ dissolved in Ethaline 200. Red; deposition of platinum, gradient – 7.61 x 10^{-4} g C^{-1}. Green; stripping of platinum, gradient – 5.21 x 10^{-4} g C^{-1}. Pt working electrode, 0.205 cm^2.

To investigate what effect copper will have on the electrochemistry, the CV of a $CuCl_2$ and $PtCl_2$ solution was performed. *Figure 5.24* displays the CV of the mixed solution.

The CV contains complex redox behaviour, some of which is recognisable from previous voltamagrams. There is what appears to be the electrochemically irreversible redox behaviour of the Pt (II)/(0) redox couple, with an electrode potential of 0.366 V. As well as the reversible redox behaviour of the Cu (II)/(I) redox couple, with an electrode potential of 0.511 V. Further to this, what appears to be the Cu (I)/(0) redox couple, with an electrode potential of – 0.434 V, peak at *ca*. – 0.4 V.However the oxidation peak, as seen before with the mixed gold and copper system, appears to be inhibited. The retardation of the copper oxidation is assigned to a deposition of a platinum layer on top of the copper, preventing dissolution of the copper. It is also possible that the copper and platinum has formed an alloy, preventing dissolution of copper.

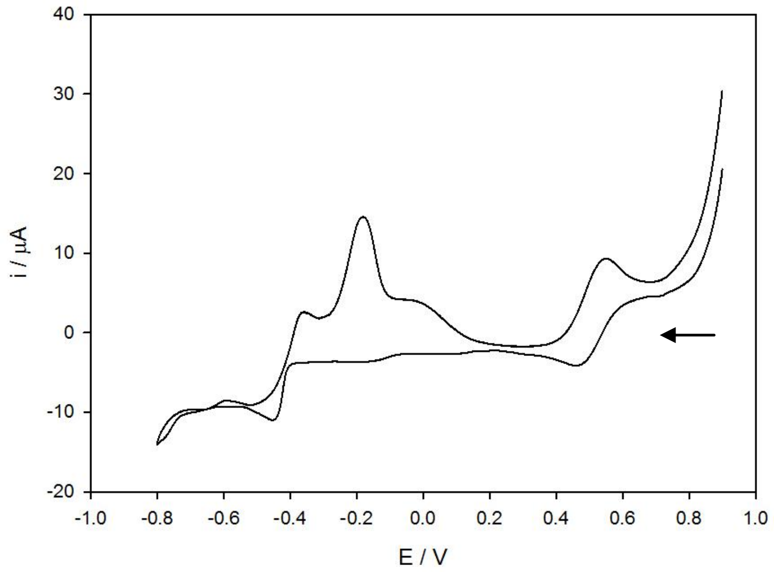

Figure 5.24: CV of 10 mM $PtCl_2$ & $CuCl_2$ dissolved in Ethaline 200. Pt working electrode, 3.14 x 10^{-2} cm^2. Pt flag counter electrode. Ag wire reference electrode. Scan rate 10 mV s^{-1}

There is an oxidation peak with onset potential – 0.273 V, peak *ca*. – 0.2 V, again could represent the oxidation of copper. The change from *quasi* – reversible, to irreversible behaviour explained by copper de-alloying from the surface of the electrode. This would also account for the shoulder, positive of the peak.

To further investigate the platinum and copper mixed system, EQCM was used to perform CV, *Figure 5.25*. This allows a plot to be produced where the CV can be compared to the change in mass on the surface of the electrode.

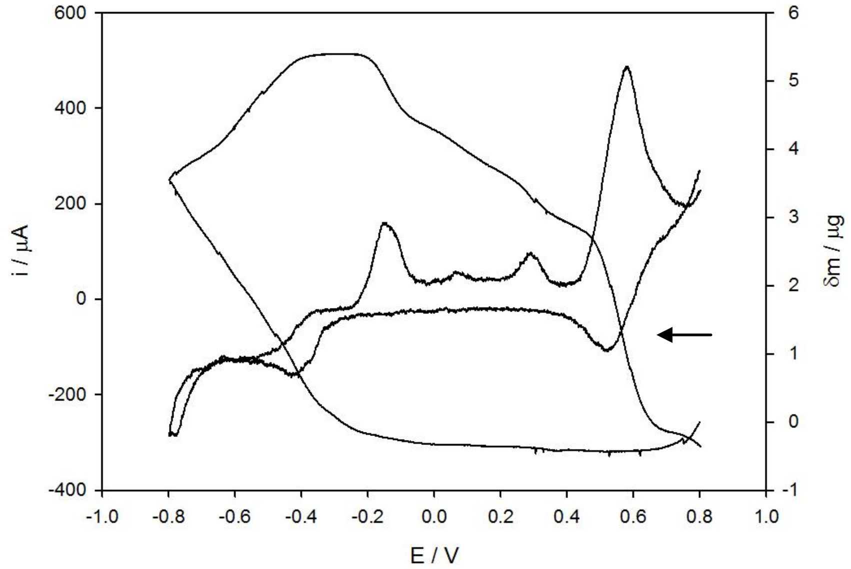

Figure 5.25: Using an EQCM to produce CV data of 10 mM $PtCl_2$ *&* $CuCl_2$ *dissolved in Ethaline 200. Pt working electrode, 0.205* cm^2*. Pt gauze counter electrode. Ag wire reference electrode. Scan rate 10 mV* s^{-1}*.*

It is important to note, that at the start of the CV in *Figure 5.25* that the sweep starts at 0.8 V, where oxidation of Pt is occurring. Hence there is a small loss of mass at the beginning of the cathodic sweep. As the experiment is performed with a Pt coating QCM crystal and the nature of the Pt electrochemistry, it is not possible to start a scan in a passive area As seen in previous EQCM experiments with copper, between *ca*. 0.65 to – 0.03 V, there is a small steady increase in mass. At *ca*. – 0.03 to – 0.25 V, there is a larger increase in mass that can be attributed to the deposition of Pt on the surface of the crystal. From *ca*. – 0.25 V the gradient of the slope changes, this is where Cu has started to be deposited and at *ca*. – 0.35 V there is a steady increase in on the surface of the electrode which continues to – 0.8 V.

At the start of the anodic sweep, deposition is occurring. The deposition between *ca*. – 0.8 to – 0.64 V, is of a slower rate than the deposition prior to the vertex potential. However, for the deposition between *ca*. – 0.64 to – 0.38 V, the rate of deposition has returned to a similar value to that before the vertex potential. This effect is attributed to the breakdown of Ethaline 200 at the end of the electrochemical window, the breakdown preventing deposition.

At *ca*. – 0.38 to – 0.22 V there is no change in mass, this is accounted for by the deposit inhibiting the dissolution of Cu. The inhibition is due to either Pt deposited on top of the Cu preventing it from leaving the surface, or alloying of the Cu with Pt, which would make the oxidation potential of the Cu more anodic.

Between *ca*. – 0.22 to – 0.09 V there is a rapid loss in mass that is attributed to loss of Cu from the surface of the electrode and represented in the CV by a positive current peak, with an onset potential of – 0.227 V.

After *ca*. – 0.09 V, between *ca*. – 0.9 to 0.48 V, the rate of mass loss slows, represented by a positive current in the CV. This is attributed to Cu being lost form the surface of the electrode. But in this incidence, the Cu is inhibited from leaving the surface, possibly due to alloying with Pt. It is proposed the slow mass lost, is due to de-alloying and dissolution of Cu. In the CV there is two peaks in the positive current between *ca*. – 0.9 to 0.48 V, at 0.023 and 0.230 V. These are attributed to higher concentrations of Cu being removed from the surface than for the base oxidation current. The fluctuation of change in mass plot is also attributed to this process.

Finally, between *ca*. 0.48 to 0.66 V there is a rapid loss of mass and the mass on the surface of the crystal returns to a similar value as at the start of the sweep. The oxidation peak current for the dissolution of the alloy form the surface is obscured by the Cu (II)/(I) redox couple. It should be noted however, that the shape of the oxidation current differs from the expected revisable behaviour of the Cu (II)/(I) peak and the peak current is much larger for the anodic sweep, than in the cathodic sweep.

To further analyse the results for the EQCM experiment, the mass – charge ratio has been analysed, *Figure 5.26*. For the deposition between – 0.350 to – 0.797 V, the mass – charge ratio displays a linear response with a value of 5.15 x 10^{-4} g C^{-1}. Using the value of the mass – charge ratio and **(5.68)** it is possible to calculate the mole fractions of the deposited metals. The atomic percentage of Cu in the deposit is 72 % and the atomic percentage of Pt is 28 %.

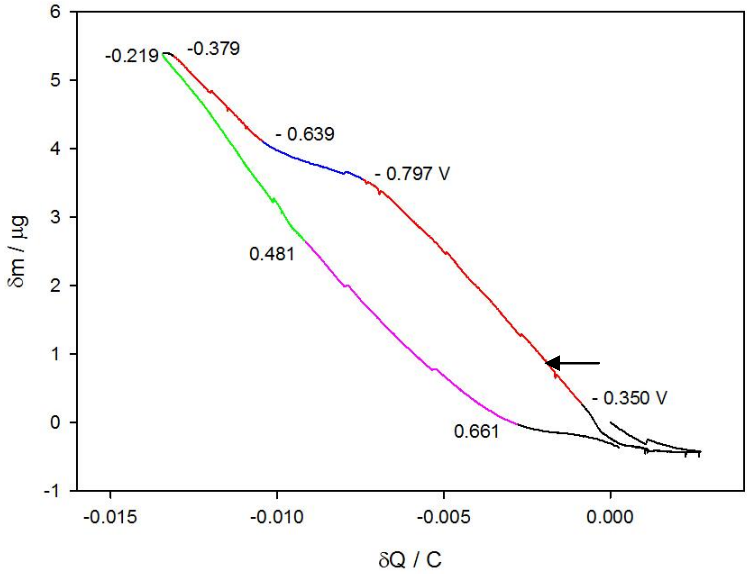

Figure 5.26: Plot of mass versus charge for CV of 10 mM $PtCl_2$ & $CuCl_2$ dissolved in Ethaline 200.

$$\chi_{Cu} = \frac{(\mathrm{RMM_{Pt}} - \frac{\delta m}{\delta Q}2Fb)}{(\frac{\delta m}{\delta Q}2Fa - \frac{\delta m}{\delta Q}2Fb - \mathrm{RMM_{Cu}} + \mathrm{RMM_{Pt}})} = 0.72 \quad \mathbf{(5.6)}$$

For the deposit between - 0.797 to – 0.639 V, the value of the mass – charge ratio decreases to 1.71 g C^{-1}. It is proposed that a reductive current is being passed due to the breakdown of Ethaline at the end of the electrochemical window, hence it is not possible to calculate the composition of the deposit at this stage.

For the final stage of deposition, the mass – charge ratio has a value of 4.71 x 10^{-4} gC^{-1}. The atomic percentages of Cu and Pt being deposited 68 % and 32 % respectively.

The dissolution process appears to occur in two stages. The first displays a linear mass – charge ratio of – 6.53 x 10^{-4} g C^{-1}, which is a similar value to the mass- charge ratio for the dissolution of Cu as shown in **Chapter 3**. As discussed previously, copper can disintegrate from the surface of the electrode, it is not possible to calculate the molar fractions for the dissolution process. But as the mass charge ratio is close to the theoretical value for Cu, it is suggested that it is mostly Cu being removed from the surface, between – 0.219 to 0.481 V.

For the second dissolution process, between 0.481 to 0.661 V the mass – charge ratio is 4.32 x 10^{-4} g C^{-1}. This is actually a lower value than both the Cu and Pt mass charge ratios. Suggesting that the current efficiency for both processes has been reduced by the deposition both metals on the surface of the electrode. However, the value of the mass – charge ratio is closer to that of Pt, suggesting that more Pt is undergoing dissolution than Cu.

5.5 Conclusions

In this chapter, the electrochemistry of the group 10 elements has been investigated.

By comparing EXAFS data to crystallographic data the speciation of the Ni (II) ion, when dissolved in Ethaline, has been postulated. UV-Vis spectroscopy, has been to support the conclusions drawn from the X – ray techniques. From the UV – Vis data it has been possible to characterise the change in speciation of the nickel systems with respect to temperature and hence suggest the species the electrochemically active metal species. Further the UV – Vis has also been used to determine the speciation of Pd (II) and Pt (II) ions when dissolved in Ethaline.

The previously undefined electrode potentials of $[NiCl_4]^{2-}$ and $[PtCl_4]^{2-}$ have been determined *versus* a Ag *psudo* reference electrode and put in to context of existing literature. It was found that the Ni (II)/(0) and Pt (II)/(0) was positive than the Cu (I)/(0) redox couple and hence it is expected that nickel and platinum can be galvanically deposited on to a copper substrate.

EQCM has been used to calculate the rate of electrochemical metal deposition, as well to perform mass – charge ratio analysis to determine the current efficiency.

Unlike the group 11 metals, which display *quasi* – reversible electrochemistry, the group 10 metals display irreversible electrochemistry. It is purposed that the irreversible nature of the redox couples is because group 10 metals have to undergo two electron processes.

Mixed metal solutions have been used to determine the effect that copper would have on the deposition of group 10 metals. The mass – charge ratio has been used to calculate the molar fractions of the metals in the deposit.

It is purposed that the deposits of palladium and platinum with copper form alloys. However, as with silver, it is difficult to determine what kind of deposit is formed with nickel, as the redox couples of nickel and copper have similar electrode potentials.

5.6 References

1. J. M. Hartley, C.-M. Ip, G. C. H. Forrest, K. Singh, S. J. Gurman, K. S. Ryder, A. P. Abbott, and G. Frisch, *Inorg. Chem.*, 2014, **53**, 6280 – 6288.
2. J. Hartley, Ph.D. Thesis, University of Leicester, 2013.

3. X. Wei, L. Yu, D. Wang, X. Jin, and G. Z. Chen, *Green Chem.*, 2008, **10**, 296 – 305.

4. C.-D. Gu and J.-P. Tu, *RSC Adv.*, 2011, **1**, 1220 – 1227.

5. A. P. Abbott, G. Frisch, S. J. Gurman, A. R. Hillman, J. Hartley, F. Holyoak, and K. S. Ryder, *Chem. Commun. (Camb).*, 2011, **47**, 10031 – 10033.

6. D. F. Shriver, P. W. Atkins, and C. H. Langford, in *Inorganic Chemistry*, Oxfrod University Press, Oxford, 2nd edn, 1994 , ch. 14, pp. 589 - 602.

7. D. M. Gruen and R. L. McBeth, *J. Phys. Chem.*, 1959, **63**, 393 – 398.

8. T. Rayment, presented in part at the University of Birmingham, Midland Electrochemistry Group Meeting, Birmingham, 2012.

9. G. H. Ayres, *Anal. Chem.*, 1953, **25**, 1622 – 1627.

10. J.-F. Boily and T. M. Seward, *Geochim. Cosmochim. Acta.*, 2005, **69**, 3773 – 3789.

11. C. M. Harris, S. E. Livingstone, and I. H. Reece, *J. Chem. Soc.*, 1959, 1505 – 1511.

12. A. K. Sundaram and E. B. Sandell, *J. Am. Chem. Soc.*, 1955, **77**, 855 – 857.

13. L. Gustafson and L. I. Elding, *Inorg. Chim. Acta*, 1976, **19**, 31 – 28.

14. P. Murray, K. R. Koch, and R. van Eldik, *Dalt. Trans.*, 2014, **43**, 6308 – 6314.

15. L. Trynda, D. Kwiatkowska, and W. Tyran, *Gen. Physiol. Biophys*, 1998, **17**, 25 – 36.

Chapter 6: Galvanic Deposition of Group 10 Elements from Ethaline 200

6.1 Introduction

6.2 Galvanic Deposition of Nickel on a Copper Substrate

6.3 Galvanic Deposition of Palladium on a Copper Substrate

6.4 Galvanic Deposition of Platinum on a Copper Substrate

6.5 Conclusions

6.6 References

6.1 Introduction

This chapter will discuss the galvanic deposition of the group 10 elements on to a copper substrate. The electrochemistry of the group 10 elements discussed in **Chapter 5** will be used to explain the thermodynamics of the galvanic reactions.

The literature precedent for the galvanic reaction of palladium[1] and platinum[2,3] with a copper substrate have been previously shown in aqueous solution, but not in Deep Eutectic Solvents. The galvanic deposition of nickel from a Deep Eutectic Solvent was published in 2014 by Ali *et. al.*,[4] however the characterisation of the deposition is not fully investigated.

The galvanic deposition of palladium is a well known application for the surface activation for the electroless deposition of nickel[1] and copper.[5] Where a seeding layer of palladium is used as a nucleation site for the catalysis of the electroless coatings, such as electroless nickel . The galvanic reaction has also been used to produce palladium microstructures on the surface of an electrode for the electrochemical hydrogen evolution reaction.[6]

The galvanic reaction of platinum with copper, has been used to produce platinum nanostructures. Such as, platinum coated copper nano wires[2] which have applications in the hydrogen oxidation reaction.

The change Gibbs free energy of the reactions between the group 10 elements and a copper substrate under standard conditions will be calculated from the formal electrode potentials determined in **Chapter 5**. The stoichiometry of the reactions will be predicted from the electrode potentials of the group 10 elements and a QCM experiment will be performed to support the theoretical productions. The rate of the reaction between the group 10 metals and a copper substrate will also be investigated using QCM.

The group 10 metals will be galvanically deposited on to a standard copper substrate and the morphology and compositing of the samples will be analysed. The morphology will be analysed by AFM and SEM, whist the composition of the samples will be characterised using EDX and XPS.

The aims of this work were:

- The calculation of the formal electrode potentials of the group 10 elements in Ethaline.
- Calculation of the change in Gibbs free energy for the galvanic reaction of group 10 metal ions with a copper substrate in Ethaline.
- Prediction of the reaction mechanism between the group 10 metal ions and a copper substrate and use of QCM methods to investigate the mechanism.
- Calculation of the rate of the galvanic reactions.
- Galvanically produce group 10 metal coating on a standardised copper substrate.
- Characterise the morphology and composition of the galvanically produced coatings.

6.2 Galvanic Deposition of Nickel on a Copper Substrate

The formal electrode potentials for Cu (I)/(0) and Ni (II)/(0) were calculated in **Chapter 4** and **Chapter 5** and have a value of – 0.205 ± 0.06 V and – 0.021 V respectively, against a silver wire *pseudo* reference electrode. Hence, a reaction between $[NiCl_4]^{2-}$ and a copper substrate is thermodynamically favourable. It should be noted that the value of the Ni (II)/(0) redox couple is more positive that the Cu (I)/(0) redox couple, but more negative than the Cu (II)/(I) redox couple. Hence, it is likely that the $[NiCl_4]^{2-}$ ion will not undergo a reaction with Cu (I) species in solution. The above discussion means it is possible to produce a theoretical equation for the reaction between $[NiCl_4]^{2-}$ and a copper substrate, equation **(6.1)**.

$$[\mathrm{NiCl_4}]^{2-}_{(\mathrm{DES})} + 2\mathrm{Cu}^0_{(\mathrm{s})} \rightarrow \mathrm{Ni}^0_{(\mathrm{s})} + 2[\mathrm{CuCl_2}]^-_{(\mathrm{DES})} \quad \mathbf{(6.1)}$$

Using the above formal electrode potentials and equation **(4.2)** it is possible to calculate the electromotive force for the reaction in equation **(6.1)**, which was found to be E = 0.184 ± 0.06 V. This means that the change in Gibbs free energy can be calculated for the reaction between $[\mathrm{NiCl_4}]^{2-}$ and a Cu (0) substrate under standard conditions, using equation **(4.1)**, where the number of electrons transferred is two, n = 2. The change in Gibbs free energy was found to be $\Delta G = -35.5 \pm 11.6 \times 10^3$ J mol^{-1}.

It should be noted that in **Chapter 5**, a solution of $\mathrm{NiCl_2}$ dissolved in Ethaline needed to be heated to 130 $^{\circ}$C before an electrochemical response was observed, due to the need to form the electrochemically active $[\mathrm{NiCl_4}]^{2-}$ species. When varying the temperature, but keeping all other conditions standard, the change in Gibbs free energy will not be altered because the concentrations of both $[\mathrm{NiCl_4}]^{2-}$ and $[\mathrm{CuCl_2}]^-$ ions will be 1 M and hence the value of the natural logarithm will be ln(1) = 0.

To test the hypothesis, that the reaction of $[\mathrm{NiCl_4}]^{2-}$ with a Cu substrate, proceeds via equation **(6.1)**, a QCM experiment was performed, where varying amounts of copper were electrodeposited on the surface of a QCM crystal, from a separate, aqueous acid copper solution. The copper coated crystal was then immersed in a solution of $\mathrm{NiCl_2}$ dissolved in Ethaline, until the reaction has reached completion. The end of the deposition was judged to be at a time where the mass on the surface of the crystal has stopped changing. Once completed, a comparison of the mass, and hence the moles of copper or nickel, on the surface of the crystal at all three stages of deposition were compared, so that the stoichiometry of the reaction can be ascertained. The results of this experiment are given in *Table 6.1*.

The results of the experiment displays that, in some cases, more nickel is deposited than is possible for the reaction stoichiometry suggested in equation **(6.1)**. This result is in contrast to what was expected when considering the thermodynamics of each possible reaction, where the thermodynamics show that the reactions with a copper substrate should proceed via the Cu (I)/(0) oxidation. It is proposed that in the cases of reactions where copper was deposited for 60 s and 120 s, that copper has been prevented from leaving the surface of the QCM and hence halting the reaction. As copper is heavier than nickel this will mean that the weight on the surface of the electrode is greater than expected. So when the calculation for the number of moles of nickel present on the surface of the electrode is performed, the copper present skews the result. Hence it is proposed that the reaction does occur via equation **(6.1)**, and not via a 1 : 1 stoichiometry where copper is oxidised to Cu (II).

Table 6.1: Comparison of the number of moles of copper and nickel deposited on the surface of a QCM crystal.

Cu deposition time / s	Moles of Cu deposited / x 10^{-7} mol	Moles of Ni deposited / x 10^{-7} mol	Yield / %
60	0.99	0.50	101
120	1.76	1.03	117
180	2.79	1.17	84

Further analysis of the QCM experiment can be performed by analysing the change in mass on the surface of the crystal with respect to time, *Figure 6.1*.

The profile of the change in mass *versus* time plot shows an initial large change in mass which proceeds in a linearly with respect to time for the first *ca*. 400 s, where the mass loss starts to level off. This shows that the rate of reaction is slowing, due to the amount of copper available to undergo dissolution and leave the surface being hindered by the nickel deposited on top of the copper. The rate of reaction keep slowing until the change in mass ceases to decrease, at *ca*. 900 s, which indicates that the end of the reaction has been reached.

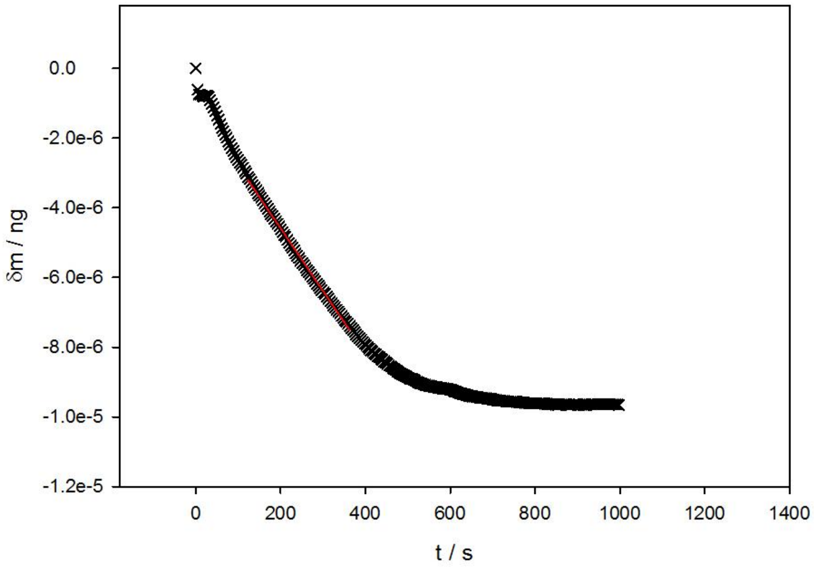

Figure 6.1: Change in mass versus time plot, for the galvanic deposition of nickel on a copper substrate. Gradient of change in mass plot – 1.10 x 10^{-8} *g* s^{-1}*. Au working electrode, 0.205* cm^2*.*

Using the gradient of the change in mass *versus* time plot it is possible to calculate the rate reaction by calculating the gradient in change in moles, followed by dividing by the surface area of the electrode. To calculate the change in mole per second, equation **(6.2)** is used.

$$\delta\mathrm{m} = \delta\mathrm{mol} \times (\mathrm{RMM_{Ni}} - 2\mathrm{RMM_{Cu}}) \quad \mathbf{(6.2)}$$

The rate of reaction was calculated to be 7.84 x 10^{-10} mol s^{-1} cm^{-2}. The rate of reaction is slower than both the electrolytic deposition of nickel and the electrolytic dissolution of copper. It is suggested that the relatively low concentration of electrochemically active $[NiCl_4]^{2-}$, compared to the other metal salts, is responsible for the slow reaction kinetics. It should be noted that once the $[NiCl_4]^{2-}$ in the electrochemical double layer undergoes reaction, the $[NiCl_4]^{2-}$ species needs to be regenerated. For the electrolytic deposition of nickel, there will be a high chloride environment in the double layer, where chloride ions associated with the $[NiCl_4]^{2-}$ are liberated from the metal complex. Whereas in the galvanic reaction system, oxidised copper produced at the surface of the electrode is competing for the chloride ions in the electrical double layer. Hence there is less chloride available to form the electrochemically active $[NiCl_4]^{2-}$ complex, meaning the kinetics of the formation of the $[NiCl_4]^{2-}$ will be slower and hence the rate of reaction will be slower.

It is also instructive to consider the rate of reaction, if the reaction did not proceed via equation **(6.1)** but proceeded via the oxidation of copper to Cu (II) in a 1 : 1 stoichiometry with the nickel. This would require alteration of equation **(6.2)**, for the 1 : 1 ratio of the reaction, meaning equation **(6.3)** would be used to calculate the rate of reaction.

$$\delta \mathrm{m} = \delta \mathrm{mol} \text{ x } (\mathrm{RMM_{Ni}} - \mathrm{RMM_{Cu}}) \quad (\mathbf{6.3})$$

If the reaction did proceed in a 1 : 1 stoichiometry, the rate of reaction would be $1.10 \text{ x } 10^{-8}$ mol s^{-1} cm^{-2}. This rate of reaction is faster than the rate of electrolytic deposition for nickel, considering this and the above discussion about chloride availability. It is proposed that the calculated kinetics for the reaction supports the reaction proceeding via equation **(6.1)**.

To characterise the composition and morphology of galvanically deposited nickel, on a electrolytically coated copper substrate was prepared. The standard substrate was then immersed in a 0.1 M solution of $NiCl_2$ dissolved in Ethaline. Once plating was completed, the morphology of the sample was analysed by AFM and SEM.

A 3D representation of the surface was produced using AFM, *Figure 6.2*. There are still small grains present on the surface of the sample. These grains have a size range of *ca*. 70 – 150 nm in diameter. But unlike the silver and gold systems, the grains do not appear to cover the entire surface.

The surface roughness of the sample can be obtained from AFM by comparing the surface area of the sample to the area of a completely flat sample, 25 μm^2 in this measurement. The surface roughness was calculated from five 25 μm^2 scans. The average surface area was found to be 26.1 ± 0.5 μm^2 which is a difference in surface area of 4 ± 2 %.

The surface roughness of the sample is actually smoother than the underlying copper substrate, 28.2 ± 0.8 μm^2, 12 ± 3%. It is proposed however, that the nickel does follow the trend of the deposition in **Chapter 4** and has a nodular, grain structure on the surface of the sample, which has the same bulk morphology as the underlying substrate. It is proposed that in this sample, the roughness of the copper deposit is less than that which was measured for the control sample.

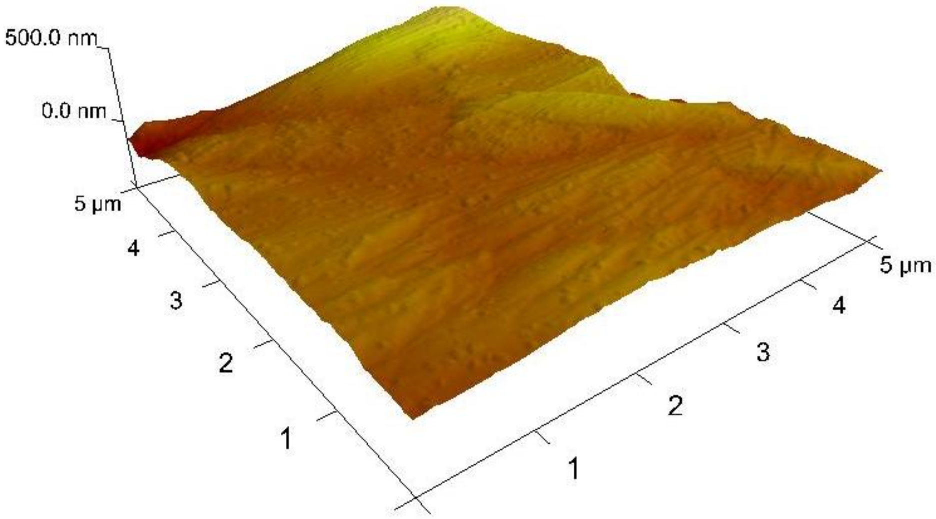

Figure 6.2: Atomic force micrograph of a galvanic nickel coating of a copper substrate.

The secondary electron SEM image, *Figure 6.3,* supports the results gathered from the AFM. The nickel coating does not appear to consist of a fully granular structure, but smooth, non – granular regions are present. As discussed above, the bulk morphology appears to be crystalline, similar to the underlying copper substrate.

The image displays that pores are present in the surface of the coating. These pores allow for the dissolution of the underlying copper substrate in to the solution, so that the redox reaction can continue to proceed and deposition of nickel can still occur.

It is suggested, that the slow rate of reaction of nickel ions with copper, promotes growth of the nickel film laterally, from already established nucleation sites. This is in contrast to the silver and gold system in **Chapter 4**, where the much faster rate of reaction promotes the formation of nucleation sites, instead of lateral growth from nucleation sites, as seen in the nickel system.

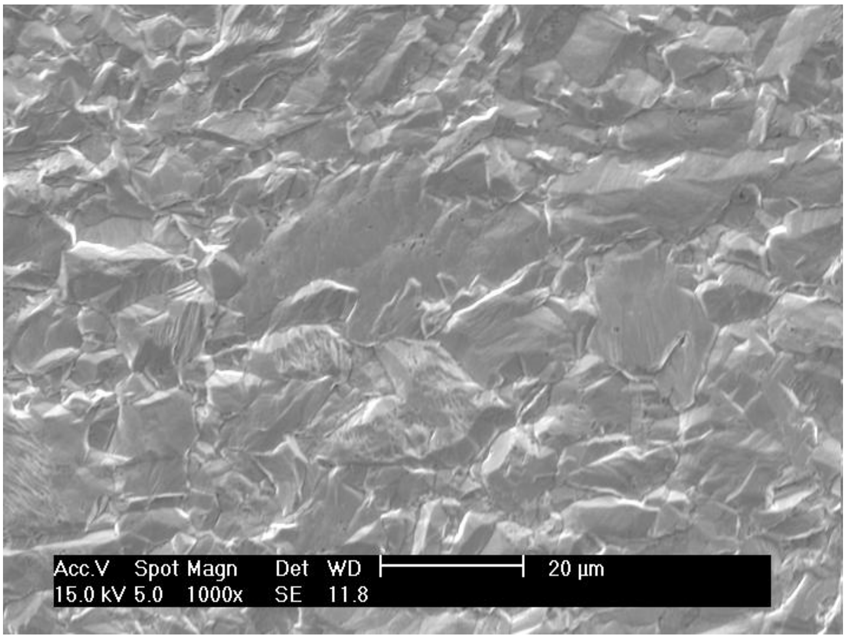

Figure 6.3: Secondary electron SEM image of a galvanic nickel coating of a copper substrate.

The pores on the surface of the coating are more evident in the back scattered electron SEM image, *Figure 6.4*. The pores appear to be on the sub micron scale and AFM analysis suggests that the pores are *ca*. 150 nm in diameter.

The back scattered image appears to be a constant shade, indicating that the surface is of a uniform composition. It should be noted however, that the difference in atomic mass between nickel and copper is only small, meaning, that identifying regions of copper or nickel would be difficult.

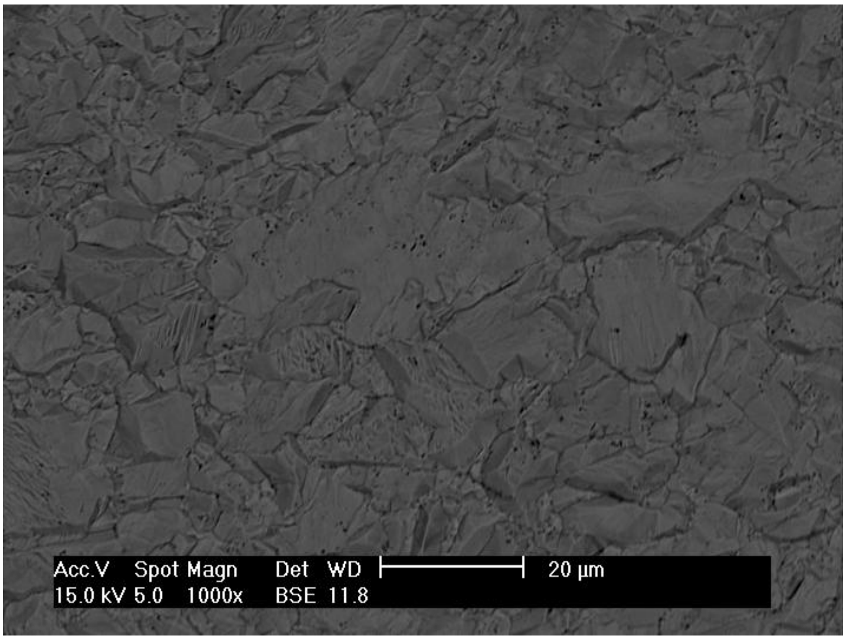

Figure 6.4: Back scattered electron SEM image of a galvanic nickel coating of a copper substrate.

To characterise the elements present in the sample the EDX spectrum was obtained, *Figure 6.5*. The results of the EDX analysis show only copper and nickel in the sample, with atomic percentages of 97% and 3% respectively. It is proposed that the deep interaction volume of the primary electron beam with the sample means that the majority of the X-rays are produced in the pure copper substrate. Hence the atomic concentration of nickel in the sample will be low.

It should be noted that there is apparently no residual contaminates, such as chlorine or nitrogen, from the preparation of the sample. It is expected that again the large copper signal is potentially masking the response from the surface contaminates.

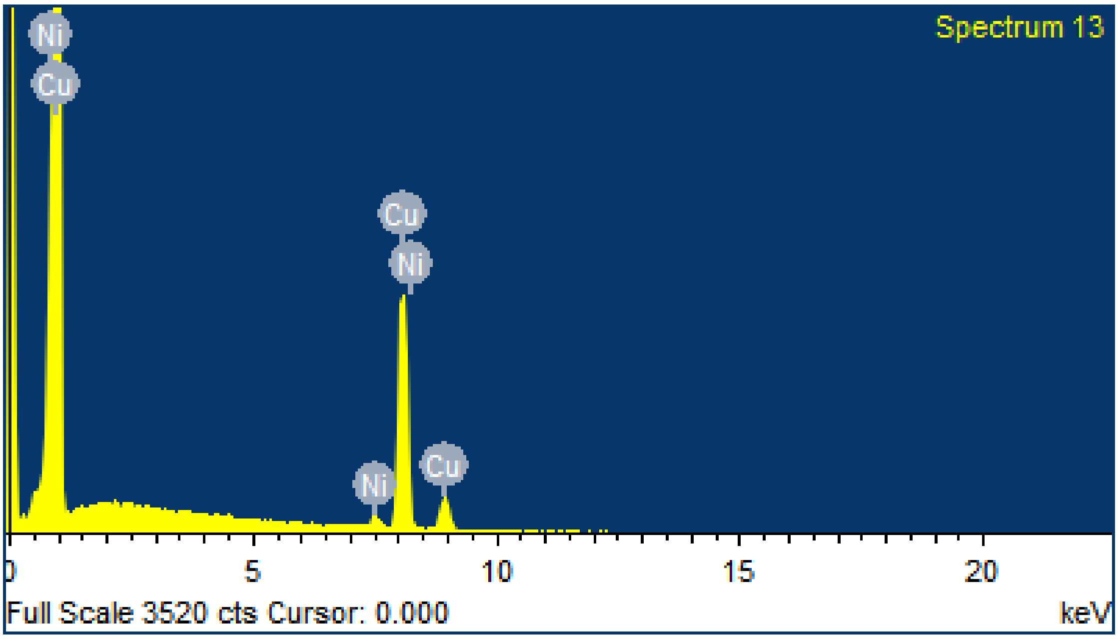

Figure 6.5: EDX spectrum of a galvanic nickel coating of a copper substrate.

To analyse the surface of the sample and avoid interference from the substrate, XPS has been used. *Figure 6.6* displays the XPS spectrum for the galvanic nickel plated, copper substrate sample.

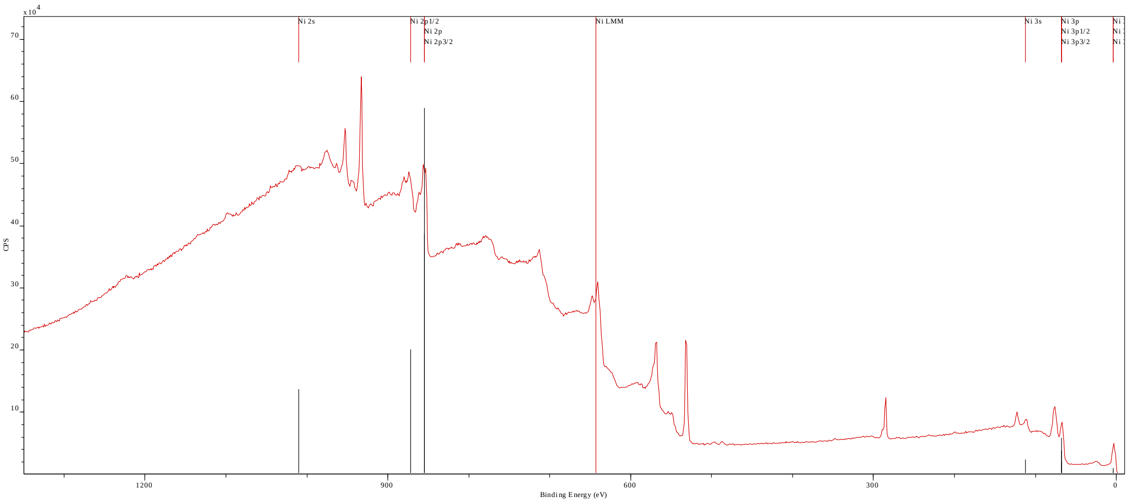

Figure 6.6: XPS spectrum of galvanic of a nickel coating of a copper substrate.

The spectrum displays the expected peaks for nickel, as well as a large contribution from copper. Other peaks present in the survey spectrum are oxygen and carbon, however expected peaks for chloride and nitrogen are absent. This suggests that the carbon and oxygen contamination comes from the atmosphere and choline chloride is not present on the surface.

To further characterise the surface, the high resolution XPS spectra were obtained for carbon, nitrogen, oxygen, chlorine, copper and nickel. The atomic concentrations of the elements are shown in *Table 6.2*.

Table 6.2: Elemental composition of a nickel coating of a copper substrate.

Element	Orbital Scanned	Atomic Percentage / %
Ni	2p	25
Cu	2p	12
C	1s	29
O	1s	33
N	1s	0
Cl	2p	1

The surface of the sample contains a significant amount of copper, 12%, this is however significantly less than was observed in the EDX spectrum, as the volume of the sample under analysis is only the first *ca*. 10 nm of the surface.

The high resolution spectra for copper and nickel, *Figure 6.7*, display the expected doublet peaks for copper spectrum and a complex nickel spectrum and complex nickel behaviour.

The copper spectrum has two sets of doublets, the main bulk copper electron transitions and smaller transitions for Cu (II) species,[7] which have been shifted to a higher binding energy. Both sets of peaks display the expected 1 : 2 ratio for 2p electron transitions, as well as the 20 eV peak separation associated with copper transitions.[8] Of the copper present at the surface of the sample, only 7% is in the form of copper oxide and 93% is copper.

The nickel spectrum displays three sets of doubles. The doublets display the expected 2 : 1 peak ratio, as well as a peak separation of *ca*. 17 eV. It is proposed that the double for peaks occurring at 853 eV and 890 eV represent the bulk, unoxidised nickel, which is beneath the surface oxide. The two other sets of doublets at 856 eV, 873 eV and 862 eV, 879 eV represent the oxidised nickel species, NiO.[9]

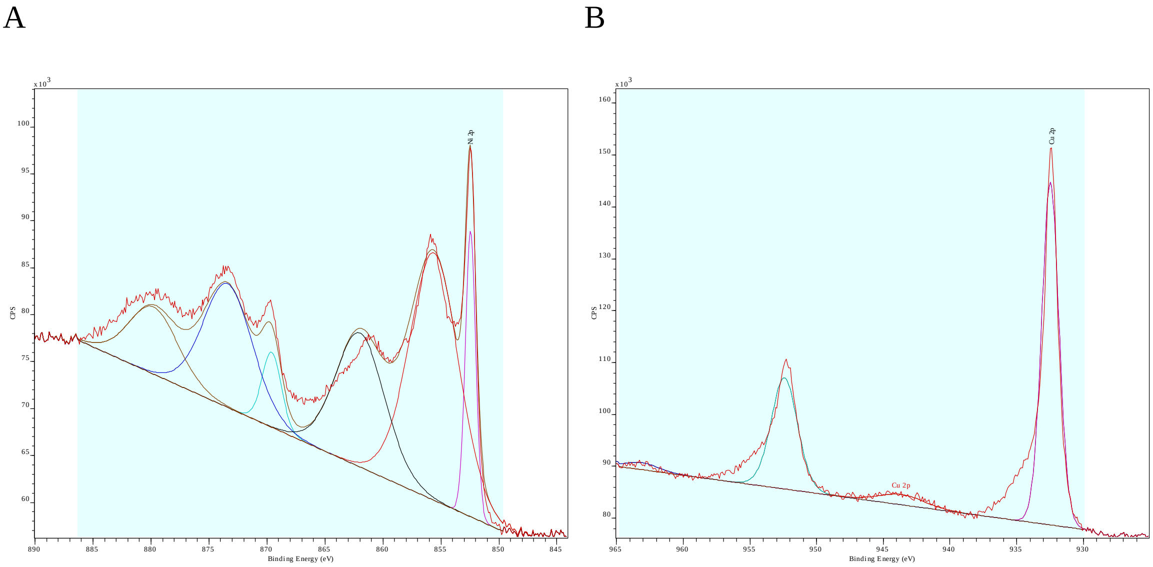

Figure 6.7: High resolution XPS spectra of A: Ni and B: Cu, of a galvanic nickel coating of a copper substrate.

It is proposed that nickel and copper could form an alloy on the surface of the sample, which could explain why copper appears of the surface of the sample, as shown by the electrochemistry in **Chapter 5** and copper – nickel binary phase diagram.[10] It is possible that copper has been left exposed to the air, due to an incomplete coating of nickel and hence has undergone oxidation. Or that some of the copper that has undergone dissolution has been re – deposited with the nickel in the coating.

6.3 Galvanic Deposition of Palladium on a Copper Substrate

The formal electrode of the palladium (II)/(0) redox couple, against a Ag wire *pseudo* reference electrode, can be calculated using the Nernst equation and was found to be $E^{o'} = 0.039$ V. This electrode potential is more positive than formal electrode potential of the Cu (I)/(0) redox couple and more negative than the Cu (II)/(I). Hence, it is expected that a spontaneous reaction between a solution of $PdCl_2$ dissolved in Ethaline and a copper substrate will occur, via equation **(6.4)**.

$$[\mathrm{PdCl_4}]^{2-}_{(\mathrm{DES})} + 2\mathrm{Cu}^0_{(\mathrm{s})} \rightarrow \mathrm{Pd}^0_{(\mathrm{s})} + 2[\mathrm{CuCl_2}]^-_{(\mathrm{DES})} \quad \mathbf{(6.4)}$$

Using the formal electrode potentials of both the Cu (I)/(0) and Pd (II)/(0) and equation **(4.2)** it is possible to calculate the electromotive force for the reaction between Pd (II) ions and a copper substrate. The electromotive force was found to be $E_{e.m.f.}$ = 0.364 ± 0.06 V. Once the electromotive force has been has been established, it is possible to calculate the change in Gibbs free energy for the reaction, using equation **(4.1)**. The Gibbs free energy for the reaction under standard conditions was found to be $\Delta G = -63.0 \pm 10 \times 10^3$ J mol^{-1}.

The stoichiometry of the reaction was investigated using a QCM experiment, where a QCM crystal was electrolytically plated with copper and then immersed in a solution of $PdCl_2$ dissolved in Ethaline, to prove that the reaction proceeded via equation **(6.4)**. *Table 6.3* displays the number of moles of copper and palladium deposited on the surface of the crystal.

The number of moles of palladium deposited supports the theory that the reaction between $[PdCl_4]^{2-}$ and a copper substrate proceeds via the Cu (I)/(0) redox couple posited in equation **(6.4)**. As was with the gold case in **Chapter 4**, the yield of the reaction is lower than expected. Loss of unoxidised copper without the deposition of palladium could be a contributing factor to the low yield. Also if the experiment has not proceeded to 100% completion, leaving copper on the surface of the crystal, the yield will be low yield, due to the atomic weight of copper being less than that of palladium.

Table 6.3: Comparison of the number of moles of copper and palladium deposited on the surface of a QCM crystal.

Cu deposition time / s	Moles of Cu deposited / x 10^{-7} mol	Moles of Pd deposited / x 10^{-7} mol	Yield / %
60	1.20	0.57	95
120	2.59	0.85	65
180	4.64	1.47	63

Interestingly, using the trace in change in mass *versus* time plot, *Figure 6.8*, for the reaction of Pd (II) ions with a copper substrate, it is easy to test whether the reaction proceeds via equation **(6.4)**. If the reaction does proceed as predicted in a 2 : 1 ratio of palladium to copper respectively. Then the change in mass is expected to be negative as the atomic mass of copper is more than half of that of palladium. *I.e.* 2 moles of copper weigh 127.09 g, whereas 1 mole of palladium weights 106.42 g. If the reaction did proceed via a 1 : 1 ratio, then there would be a net gain in mass on the surface of the crystal.

Figure 6.8 displays an initial drop in the mass on the surface of the crystal, followed by a small gain in mass and a large drop in mass again, until the end point of the reaction, where the change in mass ceases to occur.

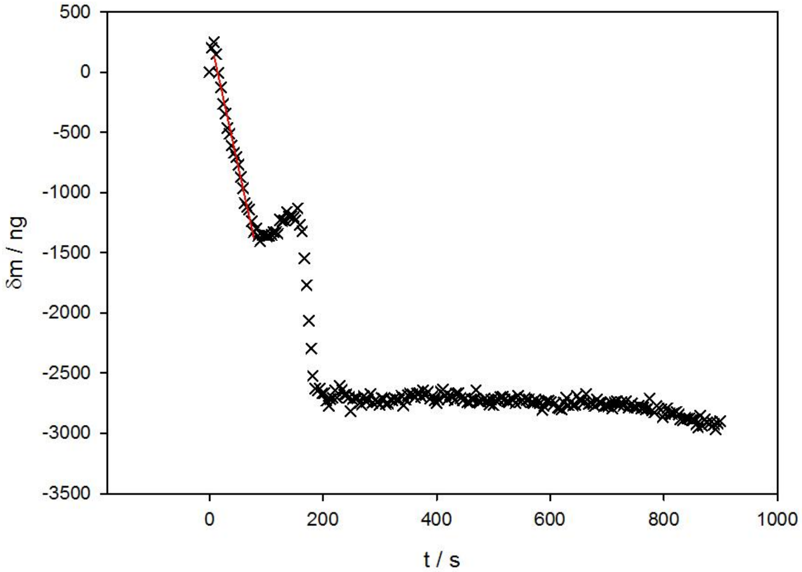

Figure 6.8: Change in mass versus time plot, for the galvanic deposition of palladium on a copper substrate. Gradient of change in mass plot – 2.16 x 10^{-8} g s^{-1}. Pt working electrode, 0.205 cm^2.

It is possible to calculate the rate of reaction from the change in mass *versus* time profile by converting the gradient using equation **(6.5)** and the surface area of the electrode. The rate of reaction has been calculated to be 5.09 x 10^{-9} mol s^{-1} cm^{-2}. The rate of reaction calculated is faster than the electrolytic rate of reaction calculated in **Chapter 5**. It is proposed that copper being delaminated from the surface of the electrode, leads to a faster loss of mass than is expected. Hence, the calculated rate of reaction is quicker than the expected value.

$$\delta\mathrm{m} = \delta\mathrm{mol\,x\,(RMM_{Pd} - \ 2RMM_{Cu})} \quad (\mathbf{6.5})$$

The small gain in mass, in the profile of the reaction, could be explained by a couple of options. First, that the electrical double layer of the solution has become saturated, leading to the precipitation of metal salts have deposited on the surface of the crystal, leading to an increase in mass. Or second, that the concentration of the $[PdCl_4]^{2-}$ ion in the electrical double layer has become very low and the concentration of $[CuCl_2]^-$ has become high enough so that the reverse reaction has occurred.

It is possible to calculate the concentration of Pd (II) and Cu (I) ions required for the reverse reaction by making the following assumptions and using the Nernst equation for the reverse reaction, **(6.6)**.

$$\mathrm{E_{cell} = E + \frac{RT}{nF}\ln(\frac{[Cu^{+}]^2}{[Pd^{2+}]})} \quad (\mathbf{6.6})$$

Then using Faraday's law, equation **(4.1)**, it is possible to calculate the change in Gibbs free energy for the cell, G_{cell}, by multiplying **(6.6)** by – nF, to give equation **(6.7)**.

$$\mathrm{\Delta G_{cell} = -nFE - RT\ln\left(\frac{[Cu^{+}]^2}{[Pd^{2+}]}\right)} \quad (\mathbf{6.7})$$

The assumption is made, that the concentration of Cu (I) and Pd (II) ions in the double layer is controlled by equation **(6.8)**.

$$\mathrm{[Pd^{2+}] + \frac{[Cu^{+}]}{2} = 0.1\ M} \quad (\mathbf{6.8})$$

It is then possible to create a theoretic plot of ΔG_{cell} *versus* $\ln\frac{[Cu^{+}]^{2}}{[Pd^{2+}]}$, *Figure 6.9*, for varying concentrations of Cu (I) and Pd (II). Where the gradient of the plot is m = – RT and the Y – intercept is C = – nFE.

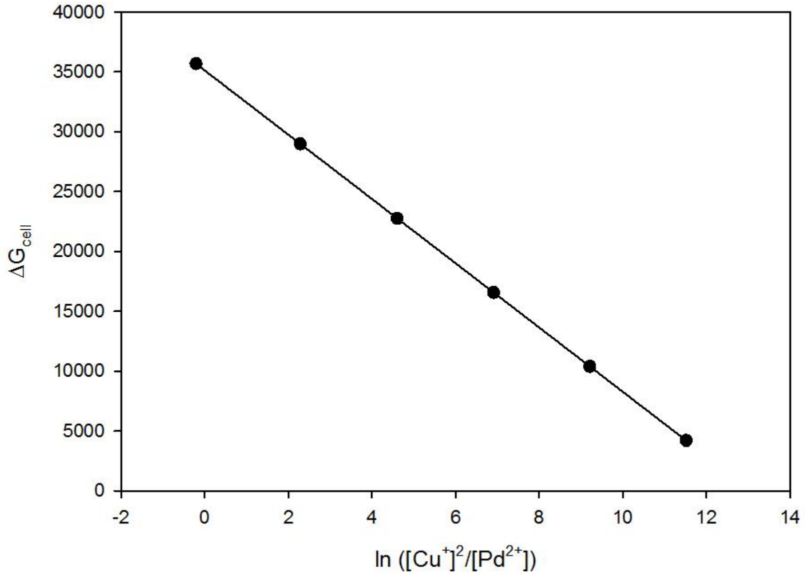

Figure 6.9: Straight line plot generated using theoretical concentrations of Cu(I) and Pd (II) in the electrical double layer.

The point at which the reverse reaction will occur, is where the Gibbs free energy for the cell is zero, $\Delta G_{cell} = 0$. Hence, it is possible to calculate the value of X which can then be equated to $\ln\frac{[Cu^{+}]^{2}}{[Pd^{2+}]}$, equation **(6.9)**.

$$\text{For } Y = 0, X = \frac{-C}{M} = \frac{-nFE}{-RT} = \ln\left(\frac{[Cu^{+}]^{2}}{[Pd^{2+}]}\right) \quad \mathbf{(6.9)}$$

Once a value for X has been established, it is possible to use equations **(6.8)** and **(6.9)**, as simultaneous equation to calculate the values for the concentration of Cu (I) and Pd (II) ions. The concentration of Cu (I) and Pd (II) ions required for the reverse reaction is, $[Cu^{+}] = 0.19$ M and $[Pd^{2+}] = 5.95 \times 10^{-6}$ M.

In the case of the palladium system, it is expected that the concentrations of Cu (I) and Pd (II) ions in solution, is of an order of magnitude that could be present in the double layer of the solution. Meaning that it is possible that the reverse reaction could occur, redepositing copper on the surface of the electrode, leading to an increase in mass on the surface of the electrode, as seen in *Figure 6.8*. This is in contrast with the results seen in **Chapter 4**, where the concentration of gold required in the electrical double layer was minute, due to the large electromotive force for the reverse reaction of equation **(4.5a)**. It should also be noticed that stoichiometry of the reaction represented in equation **(6.4)**, means that for every mole of palladium that is deposited twice the number of moles of Cu (I) ions are liberated in to the electrical double layer. This has been taken into account in the analysis.

To investigate the morphology and composition of the galvanic palladium deposit, a standard electrolyticly plated copper substrate was prepared according to the method given in **Chapter 2**. Once the copper substrate was prepared, it was then immersed in a 0.1 M solution of $PdCl_2$ dissolved in Ethaline. Once platting was complete, the morphology of the deposit was analysed using AFM and SEM.

A 3D image of the surface has been generated using an AFM, *Figure 6.10*. The micrograph shows that the bulk morphology of the sample, as shown in previous systems, is similar to the underlying copper substrate. Palladium has been deposited on the surface of the bulk copper with a grain like structure, similar to the deposits seen in **Chapter 4** and less like the structure of the nickel deposit above. The grain size in the deposit ranges from *ca*. 200 – 300 nm.

The roughness of the sample be calculated from the 3D image, by comparing the surface area of the micrograph to the area of the scanned. The surface area of the deposit was found to be 31.3 ± 2.1 μm^2, which is a surface area differance of 25 ± 8%. The deposit is rougher than the underlying copper substrate, but not as rough as the silver substrate seen in **Chapter 4**. It is proposed that the slower rate of deposition, for palladium compared to silver, allows for more lateral growth of the coating and less formation of nucleation sites. It should also be noted that the error associated with the roughness in the palladium system is less than in the silver case.

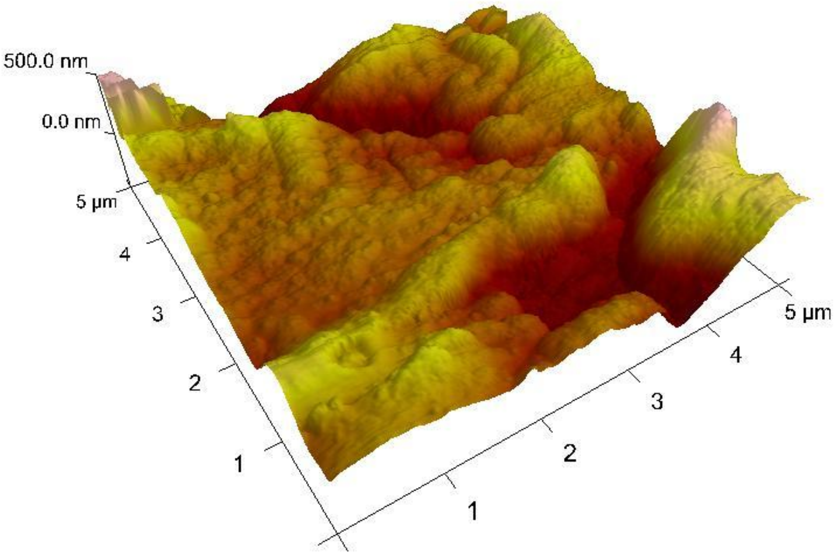

Figure 6.10: Atomic force micrograph of a galvanic palladium coating of a copper substrate.

The secondary electron image of the galvanic palladium deposit is displayed in *Figure 6.11*. The image shows a deposit where the granular structure observed in the AFM micrograph is not obvious, due to the finer structure of the deposit compared to those seen in **Chapter 4**. Instead the deposit appears more crystalline, akin to the deposit observed in the nickel system above.

The secondary electron image also shows that the surface of the sample is covered in both cracks and pores. The cracks and pores allow for copper to be oxidised and undergo dissolution, meaning that the reaction can continue and palladium can be reduced and deposited on the surface of the sample.

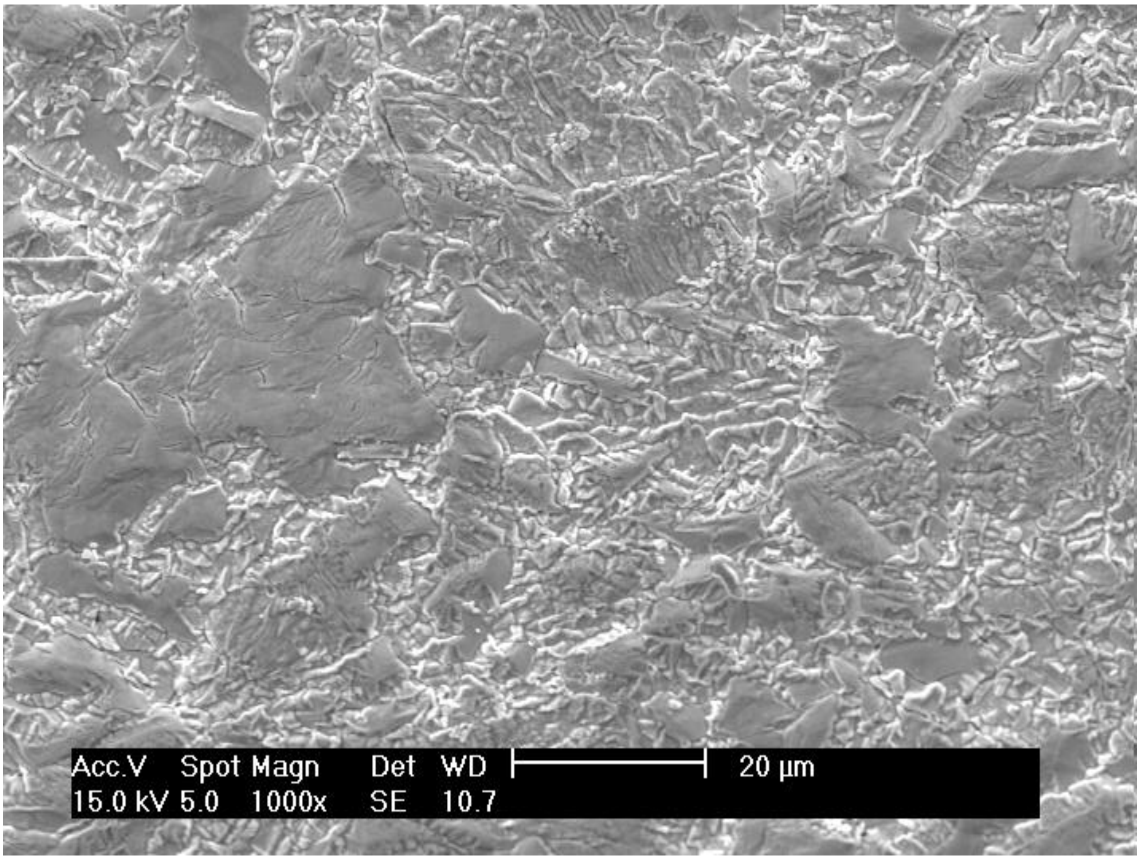

Figure 6.11: Secondary electron SEM image of a galvanic palladium coating of a copper substrate.

The cracks and pores, circled in red, on the surface of the sample are more clearly displayed in a back scattered electron image taken using SEM, *Figure 6.12*. The cracks appear to be up to *ca*. 10 μm in length. The pores appear on the sub micron level and using AFM have been measured to be up to *ca*. 100 nm in diameter.

The shading of the backscattered image implies that the elemental composition of the coating is uniform. Where the cracks and pores on the surface of the sample are shaded darker, due to the difficulty of the electrons leaving these areas and being reabsorbed by the surface.

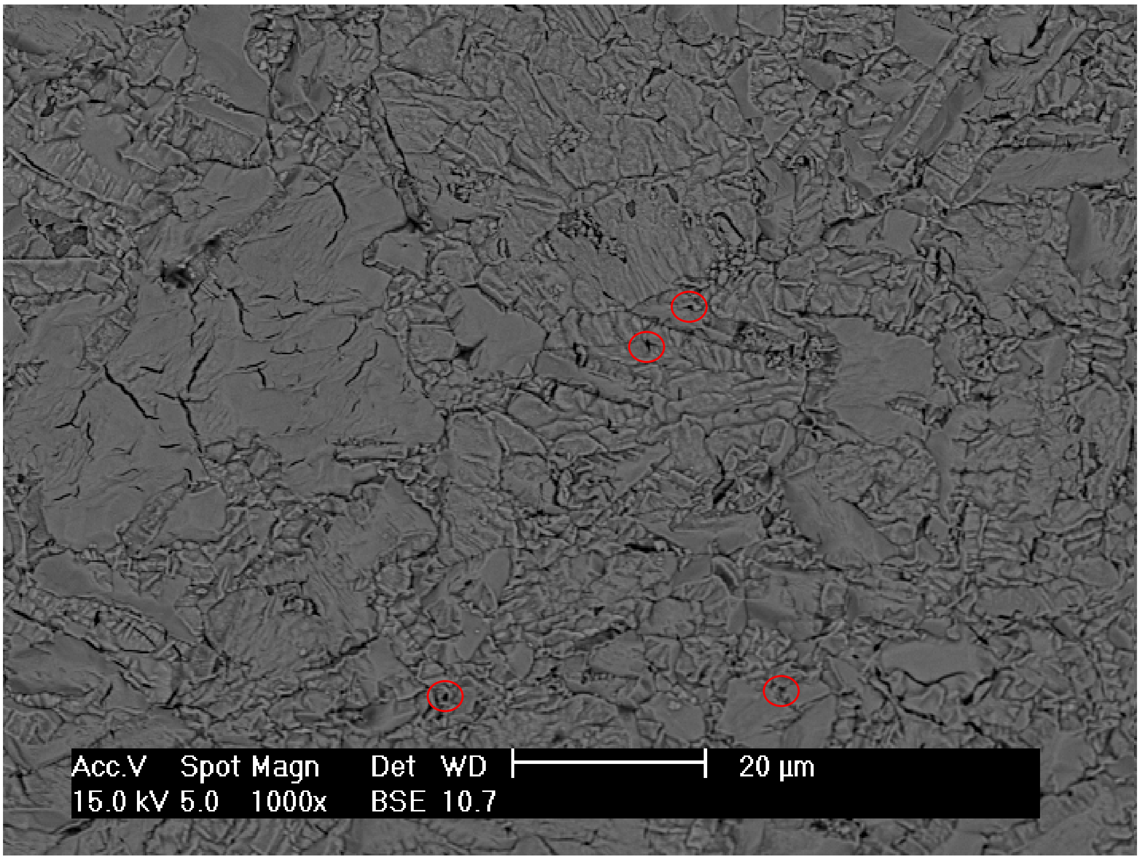

Figure 6.12: Back scattered electron SEM image of galvanic palladium coating of a copper substrate.

The EDX spectrum, *Figure 6.13*, was obtained to characterise the elements present in the bulk of the sample. The elements found in the sample were oxygen, chlorine, copper and palladium in atomic percentages of 6%, 6%, 64% and 24% respectively. It is proposed that the chlorine is a residue of the choline chloride, but the choline ion has been washed away. The oxygen present in the sample is most likely due to oxidation of the metal at the surface of the sample. It is suggested that the oxygen and chlorine present would be accompanied by nitrogen and carbon, if there was residual choline present.

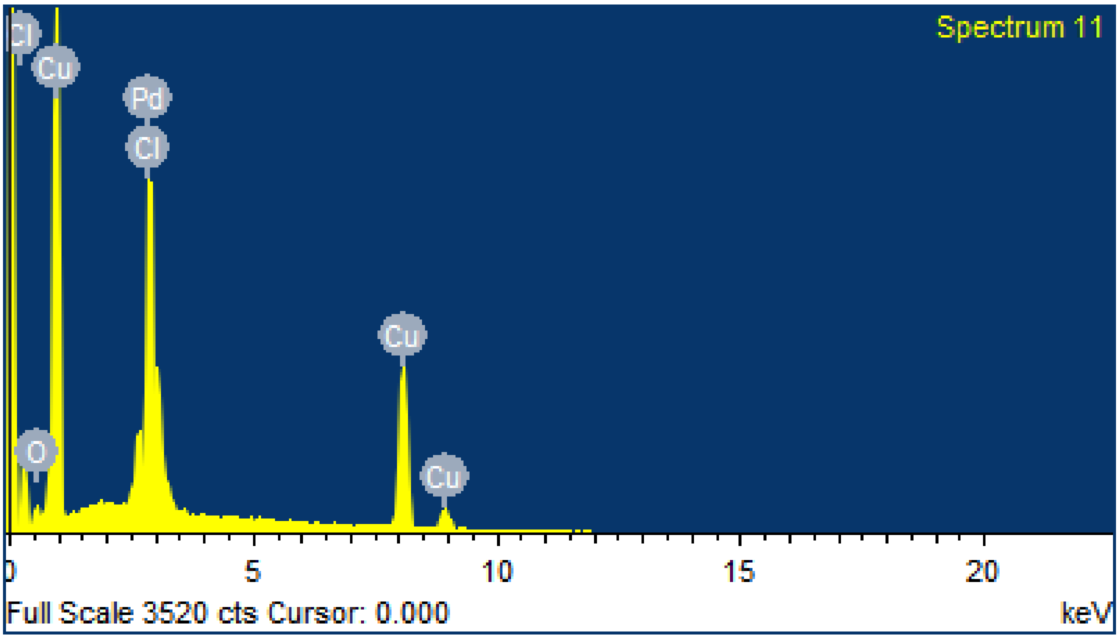

Figure 6.13: EDX spectrum of a galvanic gold coating of a copper substrate.

It should be noted that the atomic percentage of copper in the sample is higher than the percentage of palladium. It is proposed that the interaction volume of the primary electron beam penetrated the coating and is interacting with the underlying substrate. However, it is expected that some copper is present in the palladium coating. To find the elemental composition of just the coating, XPS has been used.

The XPS of the palladium coating is shown in *Figure 6.14*. The spectra displays the expected electronic transitions for palladium, as well as transition for carbon, oxygen and copper, at 284 eV, 532 eV, and 932 eV respectively. Interestingly the chlorine signal seen in the EDX spectra is not seen in the survey spectra of the XPS. It is proposed that chloride could be retained in pores in the surface of the surface, meaning chloride is retained deep in the sample. Hence, chlorine will be looked for using high resolution spectra.

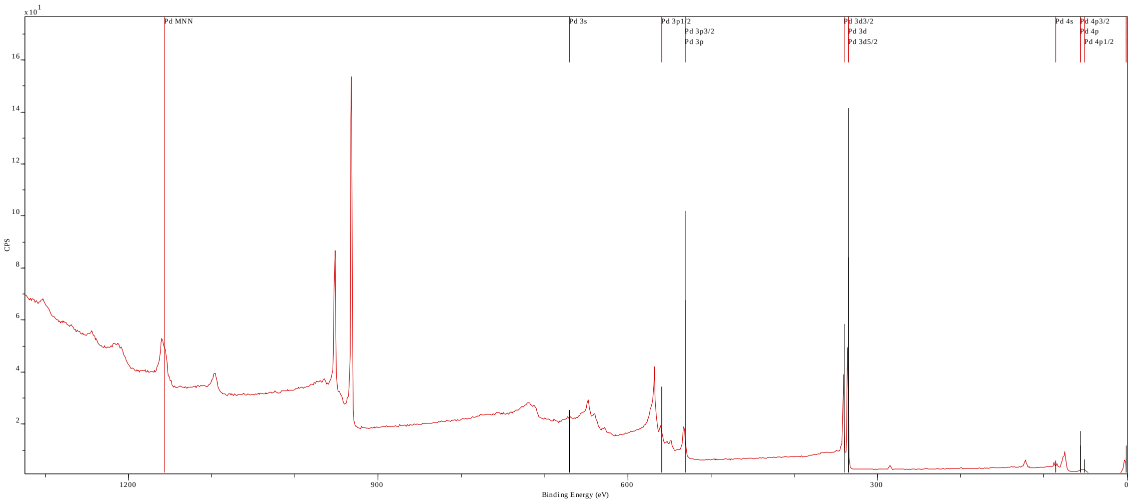

Figure 6.14: XPS spectrum of a galvanic palladium coating of a copper substrate.

The high resolution spectra for carbon, nitrogen oxygen, chlorine, copper and palladium were taken. From the high resolution spectra, it is possible to calculate the atomic percentages of elements on the surface of the sample, *Table 6.4*. It should be noted that the palladium 3p electron transitions overlap with the oxygen 1s transition. Meaning it is not possible to calculate the atomic percentage of oxygen on the surface of the sample, as there are no other suitable electron transitions for the analysis of the oxygen concentration.

Table 6.4: Elemental composition of a palladium coating of a copper substrate.

Element	Orbital Scanned	Atomic Percentage / %
Pd	3d	26
Cu	2p	60
C	1s	12
O	1s	N/A
N	1s	0
Cl	2p	2

There is a high atomic percentage of copper at the surface of the sample. It is suggested that there is at two possible reasons for the high copper concentration. The first reason is that copper atoms have moved through the palladium coating from the substrate to the surface of the sample. The second is that a large concentration of Cu (I) ions is built up in the electrical double layer and hence the reverse reaction, as discussed above, can occur.

The high resolution spectra of the copper 2p and the palladium 3d electron transitions are shown in *Figure 6.15*. The palladium spectrum shows the expected 2 : 3 doublet for the 3d 3/2 and 3d 5/2 electron transitions. As well as having a peak separation of 5 eV, this is indicative of the palladium 3d election transitions. It should be noted that there does not appear to be any sign of oxidised palladium species present in the spectrum of the palladium 3d region. The copper 2p spectrum shows the expected 1 : 2 doublet for the 2p 1/2 and 2p 3/2 region with a peak separation of 20 eV indication.

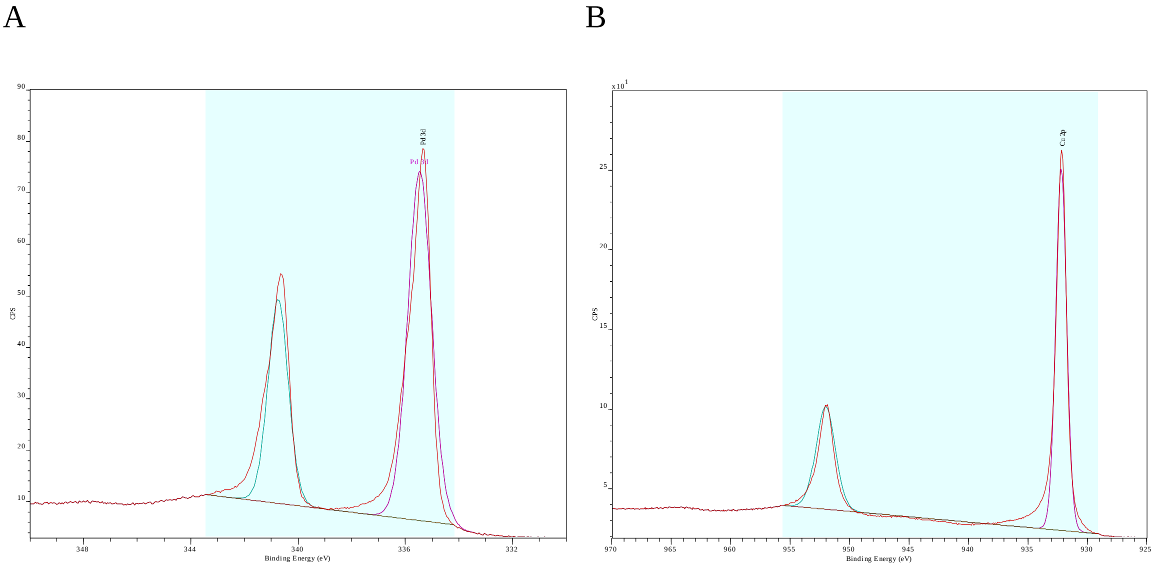

Figure 6.15: High resolution XPS spectra of A: Pd and B: Cu, of a galvanic silver coating of a copper substrate.

It is important to note that there is not any other doublets present representing copper oxides, as seen previously with silver and gold in **Chapter 4**. It is suggested that an alloy on copper and palladium has been formed on the surface of the sample, as shown by the electrochemistry in **Chapter 5** and copper – palladium binary phase diagram.[11] It is proposed that the alloying prevents oxidation of the copper and palladium present at the surface of the sample.

6.4 Galvanic Deposition of Platinum on a Copper Substrate

The formal electrode potential for the Pt (II)/(0) redox couple was calculated in **Chapter 5** and was found to be 0.432 V *versus* a Ag wire *pseudo* reference electrode. When compared to the copper redox couples, at – 0.325 ± 0.06 V and 0.595 V for the Cu (I)/(0) and Cu (II)/(I) redox couples respectively. It is likey that $[PtCl_4]^{2-}$ ions will undergo a reaction with a Cu (0) substrate, but will not react with $[CuCl_2]^-$ ions in solution. Hence, it is possible to write equation **(6.10)** for the theoretical reaction.

$$[\mathrm{PtCl_4}]^{2-}_{(\mathrm{DES})} + 2\mathrm{Cu}^0_{(\mathrm{s})} \rightarrow \mathrm{Pt}^0_{(\mathrm{s})} + 2[\mathrm{CuCl_2}]^-_{(\mathrm{DES})} \qquad (\mathbf{6.10})$$

Using the above formal electrode potentials, it is possible to calculate the electromotive force and hence the change in Gibbs free energy for the reaction in equitation **(6.10)**, under standard conditions. The electromotive force was calculated using equation **(4.2)** and was found to be E_{emf} = 0.757 ± 0.06 V. Then using equation **(4.1)** the change in Gibbs free energy can be calculated under standard conditions, $\Delta G = -14.6 \pm 11.6 \times 10^3$ J mol^{-1}.

It should be noted, that due to the slow kinetics of platinum electrochemistry, in **Chapter 5** heating was required so that an electrochemical response could be seen in the CV, and hence the galvanic deposition of platinum was performed at 130 ^{o}C. Under standard conditions, altering the temperature will not affect the change in Gibbs free energy for the reaction. As the electromotive force will not be altered because the equilibrium constant will be k = 1 and hence ln(k) = 0. It should be noted, that for a system where the concentration of copper is low, an increase in temperature will lead to an increase in electromotive force and hence an increase in the magnitude of the change in Gibbs free energy.

To investigate the stoichiometry of the reaction between $[PtCl_4]^{2-}$ ions and a Cu (0) substrate and test the hypothesis that the reaction proceeds via equation **(6.10)**, a QCM experiment was performed. Varying amounts of copper were electrolytically deposited on the surface of a QCM crystal. The crystals were then immersed in a 0.01 M solution of $PtCl_2$ dissolved in Ethaline at 130 ^{o}C, until the reaction was complete. *Table 6.5* shows the results of the stoichiometry experiment. The yield for all of the stoichiometry experiments was greater than expected if the reaction proceeds via equation **(6.10)**. The calculated number of moles of platinum are greater than expected, may be because there other species on the surface of the electrode adding to the mass.

Table 6.5: Comparison of the number of moles of copper and platinum deposited on the surface of a QCM crystal.

Cu deposition time / s	Moles of Cu deposited / x 10^{-7} mol	Moles of Pt deposited / x 10^{-7} mol	Yield / %
60	0.51	0.36	141
120	2.44	1.55	127
180	3.56	2.02	113

It was also observed that solutions of $PtCl_2$ dissolved in Ethaline are unstable and precipitate platinum metal particles, especially when heated. It is suggested that the precipitation of platinum particles is due to the disproportionation of the Pt (II) species via equation **(6.11)**. Precipitation of particles was observed during the stoichiometry experiments, it is proposed that disproportionation of the $[PtCl_4]^{2-}$ ion could lead to deposition more platinum on the surface of the QCM crystal that is possible via equation **(6.10)**.

Further analysis of the QCM experiment can be performed by plotting a graph of change in mass on the surface against time, *Figure 6.16*. A gain in mass on the surface of the electrode for the first *ca*. 280 s is observed. From *ca*. 280 s up until *ca*. 600 s there is a much slower increase in mass on the surface of the electrode, this is attributed to the deposition of platinum on the surface of the electrode via the disproportionation represented in equation **(6.11)**.

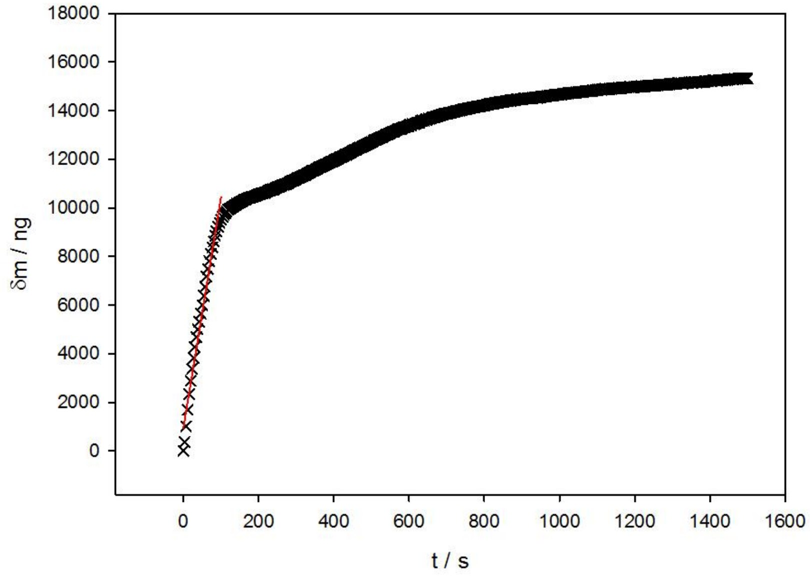

Figrue 6.16: Change in mass versus time plot, for the galvanic deposition of platinum on a copper substrate. Gradient of change in mass plot 9.49 x 10^{-8} *g* s^{-1}*. Pt working electrode, 0.205* cm^2*.*

$$2[\mathrm{PtCl_4}]^{2-}_{(\mathrm{DES})} \rightarrow \mathrm{Pt}^0_{(\mathrm{s})} + [\mathrm{PtCl_6}]^{2-}_{(\mathrm{DES})} + 2\mathrm{Cl}^- \quad \mathbf{(6.11)}$$

The rate of reaction can be calculated from the change in mass plot by converting the change in mass to the change in moles using equation **(6.12)**. Once the change in moles has been calculated, it is necessary to divide by the surface area of the electrode and hence calculate the rate of reaction.

$$\delta\mathrm{m} = \delta\mathrm{mol}\ \mathrm{x}\ (\mathrm{RMM_{Pt}} - 2\mathrm{RMM_{Cu}}) \quad \mathbf{(6.12)}$$

The rate of reaction was found to be 6.81 x 10^{-9} mol s^{-1} cm^{-2}. This is a faster rate of reaction than both the nickel and palladium above and those calculated in **Chapter 4**. Whilst it is unsurprising that the platinum deposits faster than nickel, it surprising that the platinum deposits faster than the other metals investigated, as the concentration of platinum used in the rate of reaction experiment is a factor of ten less than the other metals. The high rate of reaction can be attributed to the deposition of platinum via disproportionation, at the same time as the deposition of platinum via a galvanic reaction.

To characterise the composition and morphology of the galvanicly platinum deposit, a standard electrolyticly copper coated substrate was prepared. The standard substrate was then immersed in a 0.01 M solution of $PtCl_2$ dissolved in Ethaline, at 130 ^{o}C. The plated sample morphology was then analysed using AFM and SEM.

A 3D representation of the surface has been produced using AFM, *Figure 6.17*. The micrograph shown in *Figure 6.17* shows that the platinum has similar morphology as previous galvanic coatings. Where the bulk morphology is the same as that of the underlying electrolytic copper substrate and the platinum is deposited in a granular structure on the surface of the copper. The grains vary in size with diameters of *ca*. 130 – 250 nm.

The roughness of the sample has been calculated by comparing the surface area of the microgram, to the area of the sample scanned. The surface area of the sample was found to be 28.1 ± 1.3 μm^2, which is a change in surface area of 13 ± 5%. The surface roughness is very close to that of the copper substrate, surface area of 28.2 ± 0.8 μm^2 and difference in surface area of 12 ± 3 %. However, it should be noted that the variation in surface area associated with the platinum sample is greater than the copper substrate.

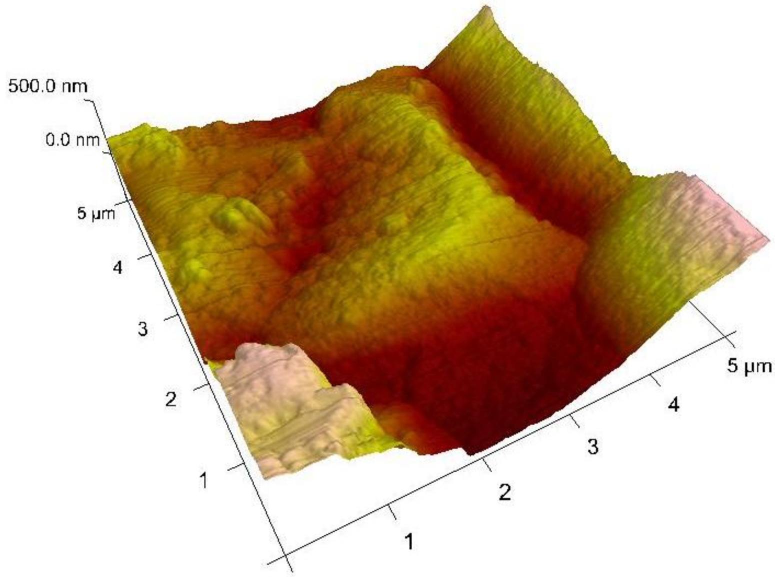

Figure 6.17: Atomic force micrograph of galvanic platinum coating of a copper substrate.

The secondary electron SEM image, *Figure 6.18* supports the above micrograph obtained from AFM, where bulk morphology of the sample is similar to the underlying copper substrate. The granular structure of the deposit is not obviously observed in the secondary electron image, this is similar to what was observed above with the palladium system. It is suggested that due to the finer grain structure of the platinum deposit, compared to those seen in **Chapter 4**, that the grain structure is not obvious when analysed using secondary electron imaging with SEM.

There appears to be particulate on the surface of the sample. It is suggested that these particles are produced during the washing stages of sample preparation, where unstable platinum species are formed and quickly undergo reduction. There are pores in the surface of the coating, as seen in the previous coatings, which allow for the oxidation and dissolution of copper into solution, meaning that the reduction and deposition of platinum can continue on the surface of the electrode.

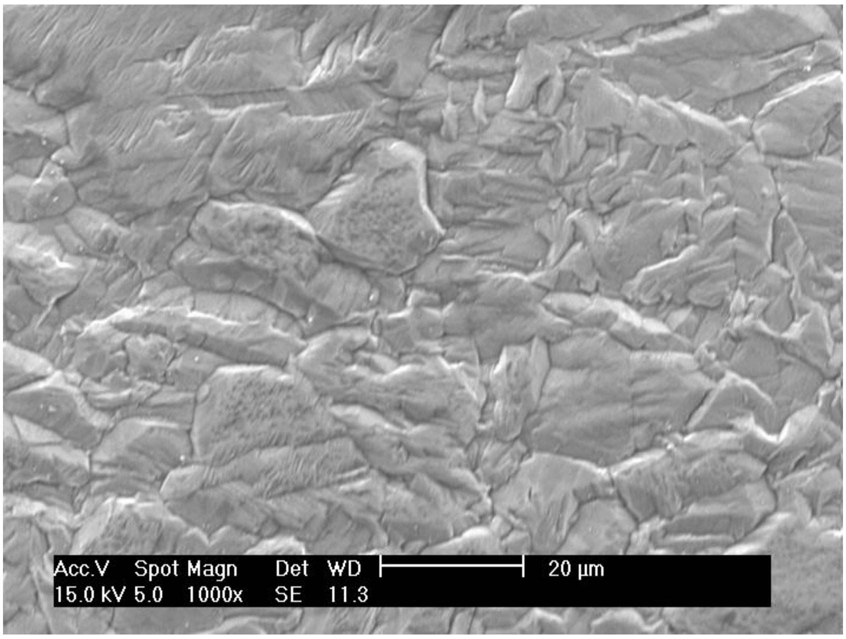

Figure 6.18: Secondary electron SEM image of a galvanic palladium coating of a copper substrate.

The pore in the surface of the coating are more obvious when observed via back scattered electron imaging from SEM, *Figure 6.19*..

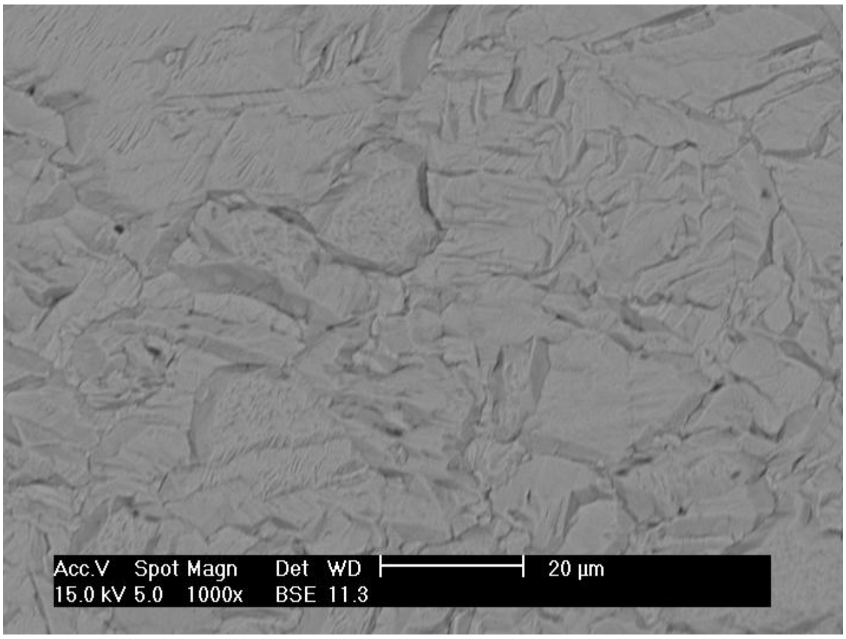

Figure 6.19: Back scattered electron SEM image of a galvanic platinum coating of a copper substrate.

The pores in the coating appear to be larger than previous deposit systems. Unfortunately however, there were no pores captured in the AFM micrograph, so the size of the pore has not been measured

The shading of the back scattered image is homogenous. Meaning that the surface composition, is uniform across the entire sample. The bulk elemental composition of the sample was analysed using EDX spectroscopy, *Figure 6.20*.

The EDX spectrum contains carbon, oxygen, chlorine, copper and platinum in atomic percentages of 74%, 4%, 1%, 14% and 7% respectively. It is proposed that there is contamination of the surface of the sample. Ethaline or a chemical involved in the rinsing process, has not been full removed from the surface of the sample, leading to contamination carbon oxygen and chlorine. The concentration of copper in the sample is higher than that of platinum. It is suggested that the high concentration of copper in the spectrum is due to the large interaction volume of the primary electrum beam in a SEM, with the sample. Hence, to find the composition of just the sample XPS has been used.

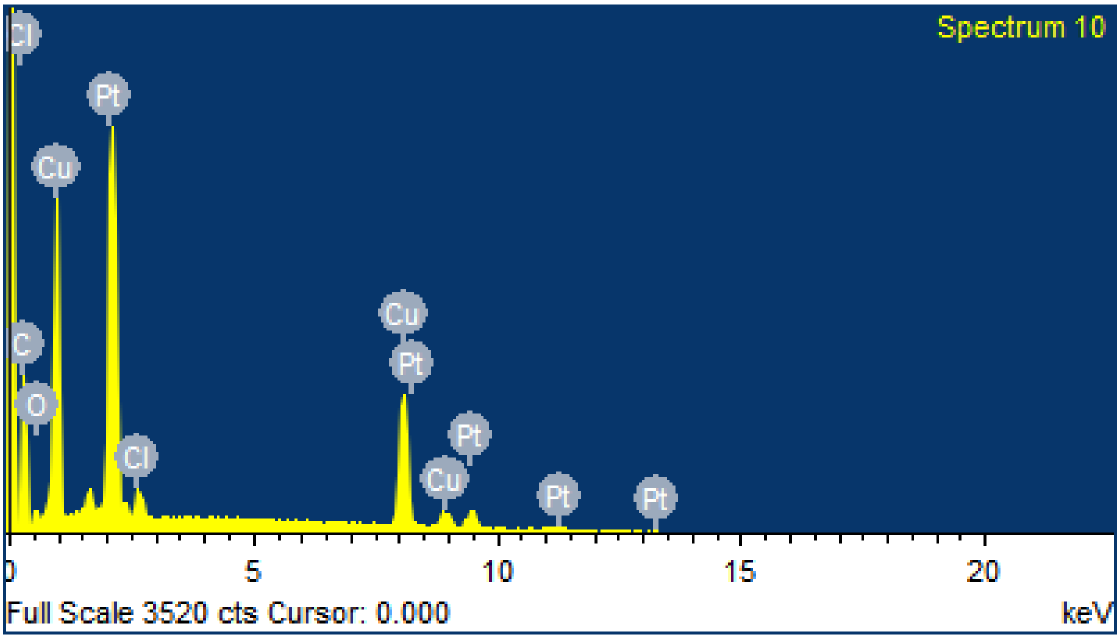

Figure 6.20: EDX spectrum of a galvanic platinum coating of a copper substrate.

The XPS of the platinum sample, *Figure 6.21*, shows the expected peaks representing platinum, as well as peaks representing carbon, oxygen, chlorine and copper at *ca*. 285 eV, 530 eV, 198 eV and 930 eV respectively. It is suggested that the contaminated on the surface of the sample come from residual Ethaline. To ascertain the atomic percentages of elements in the sample, high resolution XPS spectra were taken.

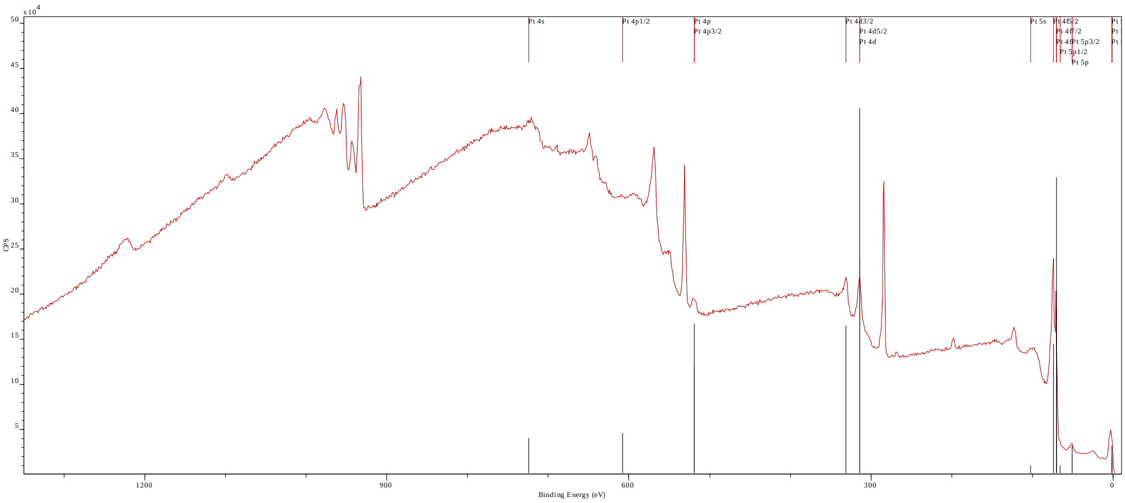

Figure 6.21: XPS spectrum of galvanic of a platinum coating of a copper substrate.

The high resolution spectra of carbon, nitrogen, oxygen, chlorine, copper and platinum were taken to further characterise the sample. The atomic percentages of elements present are given in Table 6.6.

Table 6.6: Elemental composition of a nickel coating of a copper substrate.

Element	Orbital Scanned	Atomic Percentage / %
Pt	4d	3
Cu	2p	13
C	1s	60
O	1s	22
N	1s	0
Cl	2p	2

The sample contains a large carbon contamination, it is proposed that Ethaline or a chemical used in the rinsing process is responsible for the contamination. It should be noted that the atomic concentration of platinum is approximately a quarter that of copper. This is similar to the palladium system above, where the concentration of copper in the film was also greater than that of palladium.

It should also be noticed that for the quantification of the concentration of platinum, the Pt 4d electron tranistion is used instead of the Pt 4f electron transition. This is due to overlap of the Pt 4f and the Cu 3p electron transitions, meaning that the concentration of platinum in the system would have been skewed.

The high resolution spectra for copper and platinum are shown in *Figure 6.22.* The Pt 3d 3/2 and Pt 3d 5/2 transitions show the expected 2 : 3 ratio, for the d orbital transition doublet, and the expected 17 eV peak separation for the Pt 3d doublet. It should be noted that there is no sign of oxidation in the Pt 3d spectrum or in the Pt 4f spectrum.

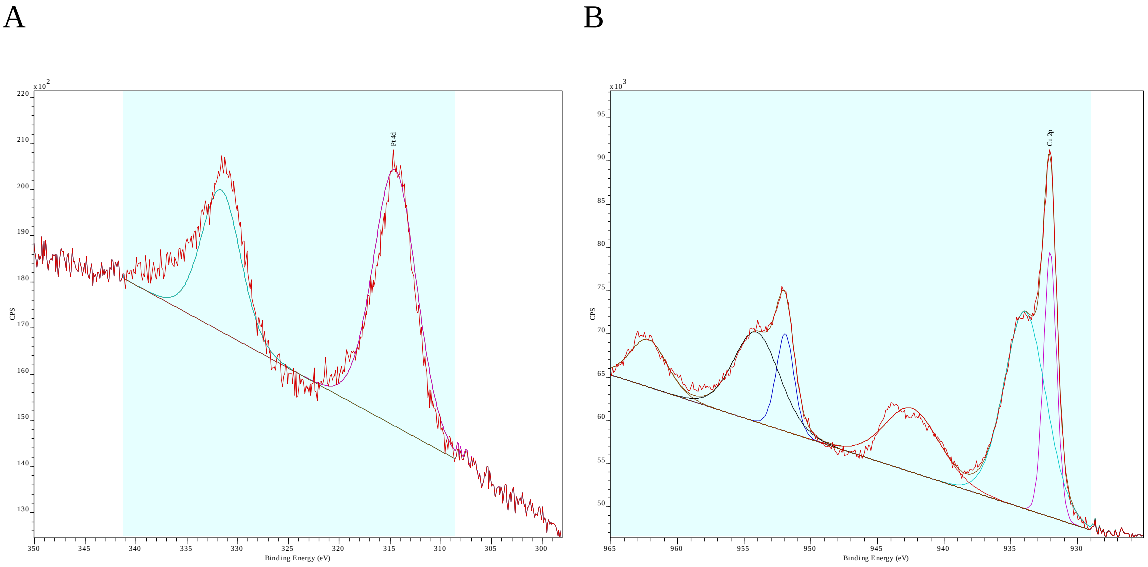

Figure 6.22: High resolution XPS spectra of A: Pt and B: Cu, of a galvanic platinum coating of a copper substrate.

The copper spectrum displays three sets of doublets, attributed to pure copper at 932 eV, copper oxides at 934 eV and a divalent Cu (II) species, at 944 eV.[7] All three sets of peak display the expected 1 : 2 ratio for p orbital electron transition. It should also be noted that all three doublets have a peak separation of 20 eV. Of the copper present at the surface, 23% of the copper is unoxidised Cu (0) and 77% of the copper has been oxidised. This suggests poor coverage of the platinum coating and oxidation of the underlying copper substrate.

6.5 Conclusions

In this chapter the galvanic deposition of the group 10 metals onto a standard copper substrate has been characterised.

The formal electrode potentials for nickel, palladium and platinum in Ethaline 200 and the Gibbs free energy for the reaction of a copper substrate and group 10 metal ions, under standard conditions have been calculated.

Using QCM methods, the stoichiometry of the galvanic reactions between copper substrate and group 10 ions has been established. It was found that all metals proceed in a 2 : 1 stoichiometry, where two copper atoms are oxidised, 2Cu (0) → (I), for every one atom of group 10 metal that is reduced. The rate of reaction between copper substrate and group 10 metal ions has also been characterised using a QCM experiment. By tracing the change in mass on the surface of a QCM crystal with respect to time and calculating the change in moles from the change in mass. It was also suggested from this experiment, that platinum undergoes disproportionation and hence is deposited on the surface, without the oxidation of copper.

Calculations have been made to find the concentration of Cu (I) and Pd (II) ions in the electrical double layer required to perform the reverse reaction of Cu (I) ions with a Pd (0) substrate. The result calculated could feasibly explain the profile of the change in mass plot, where a gain in the profile is attributed to the reverse reaction.

All group 10 metals have also been deposited on a standard copper substrate and the deposit morphology and composition have been characterised. The morphology has been characterised using AFM and SEM, whilst the composition was characterised using EDX and XPS. The amount of copper in the samples rules out the deposition of group 10 metal deposits as a method of surface protection for copper.

Further work could include XRF spectroscopy to determine the thickness of the group 10 metal deposits. The thickness of the coatings was attempted by AFM was attempted, however due to the rough morphology of the underlying copper structure, the thickness of the sample was not obtainable.

Depth profiling of the samples using XPS could reveal how the composition of sample changes through the depth of the coating. It is proposed that depending on the how the copper concentration varies thought the samples, it will be possible to tell how the copper has come to be incorporated in the coating. Where if the concentration of copper increases through the sample, it means that the copper present at the surface of the sample is due to diffusion of copper from the underlying substrate. Whereas if the concentration of copper decreases through the sample, it means that the copper has been re-deposited on the surface of the sample.

6.6 References

1 R. C. Agarwala and V. Agarwala, *Sadhana*, 2003, **28**, 475 – 493.

2 S. M. Alia, B. S. Pivovar, and Y. Yan, *J. Am. Chem. Soc.*, 2013, **135**, 13473 – 13478.

3 D.-Y. Park, H. S. Jung, Y. Rheem, C. M. Hangarter, Y.-I. Lee, J. M. Ko, Y.-H. Choa, and N. V. Myung, *Electrochim. Acta*, 2010, **55**, 4212 – 4216.

4 M. R. Ali, M. Z. Rahman, and S. S. Saha, *Indian J. Chem. Techn.*, 2014, **21**, 127 – 133.

5 S. W. Suh, J. J. Kim, S. H. Kim, and B. K. Park, *J. Ind. Eng. Chem.*, 2012, **18**, 290 – 294.

6 R. Ojani, J. B. Raoof, and E. Hasheminejad, *Int. J. Hydrog. Energ.*, 2013, **38**, 92 – 99.

7 I. Platzman, R. Brener, H. Haick, and R. Tannenbaum, *J. Phy. Chem. C*, 2008, **112**, 1101 – 1108.

8 *CasaXPS 2.3.15*, 2009, Casa Softwere Ltd.

9 A. P. Grosvenor, M. C. Biesinger, R. S. C. Smart, and N. S. McIntyre, *Surf. Sci.*, 2006, **600**, 1771 – 1779.

10 M. A. Turchanin, P. G. Agraval, and A. R. Abdulov, *Powder Met. Met. C+*, 2007, **46**, 467 – 477.

11 P. R. Subramanin and D. E. Laughlin, *J. Phase Equlib.*, 1991, **12**, 231 – 243.

Chapter 7: Conclusions and Future Work

7.1 Conclusions

In this work, the speciation and electrochemistry of the group 10 and 11 metals has been characterised, in Ethaline 200.

It was found that all of the metal centres, bar the Ni (II) centre, formed anionic chloro complexes when dissolved in a solution of Ethaline 200. The Ni (II) ion formed a cationic triethylene glycol complex, $[Ni(C_2H_6O_2)]^{2+}$, at room temperature. However when heated it was found that the $[Ni(C_2H_6O_2)]^{2+}$ would undergo an exchange with the chloride ions present in solution and the anionic nickel tetrachloride complex, $[NiCl_4]^{2-}$ would be formed.

The electrochemistry of the metal chloro complexes were characterised using a range of techniques. From cyclic voltammetry using macroelectrodes, the electrode potential of the group 10 and 11 metal redox couples were established, with reference to a silver wire *pseudo* reference electrode. The redox couples analysed were Cu (II)/(I), Cu (I)/(0), Ag (I)/(0), Au (I)/(0), Ni (II)/(0), Pd (II)/(0) and Pt (II)/(0). Using the Nernst equation to correct for temperature and concentration, the values of the formal electrode potentials were calculated for all of the redox couples including the previously uncharacterised Ni (II)/(0) and Pt (II)/(0) redox couples, which have been calculated and put in to the context of established literature.

Characterisation of the electrochemical deposition and dissolution of the group 10 and 11 elements was carried out using an electrochemical quartz crystal microbalance. The EQCM allowed, from the data obtained, the calculation of the rate of the electrochemical deposition and stripping metals, by following the change in mass on the surface of the crystal with respect to time. Further analysis of the EQCM data allowed for the calculating of the current efficiency of the electrochemical reactions. It was possible to calculate the current efficiency for the deposition of all the metals, from analysis of the mass – charge ratio. However, it was not possible to calculate the current efficiency for the dissolution of copper, as it was found that the copper disintegrated from the surface of the electrode. It was possible to calculate a current efficiency for the dissolution of the other metals examined, nickel and palladium both exhibited two stages of dissolution, where the second stage of dissolution represented the disintegration of the metal from the surface.

Analysis of mixed metal salt systems has been performed, where the effect of the addition of copper on the electrochemistry of the other group 10 and 11 metal salts has been investigated. The composition of the electrochemically deposited coatings, deposited from the mixed metal systems, was determined using EQCM. The composition was determined using the current efficiency for the individual metal salts and the mass – charge ratio of the mixed systems.

Galvanically deposited coatings of the group 10 and 11 metals were produced on a standardised copper substrate. The morphology of which was investigated using atomic force microscopy and scanning electron microscopy. The roughness of the coatings was established by AFM and compared to the copper substrate. AFM also reviled that the coatings were deposited with a fine granular structure. The secondary electron images obtained from SEM, showed bulk morphology of the deposits was dominated by the underlying morphology of the copper substrate, with the fine granular structure observed by AFM deposited on the surface. The secondary electron micrographs also displayed pores and cracks in the surface of the coatings, these allow for the dissolution and diffusion of the underlying copper substrate in to the solution, meaning the galvanic reaction can continue to occur. The back scattered electron images, obtained from SEM, revealed that the coatings appeared to be of a consistent elemental composition. Also in the back scattered image, the pores in the surface of the coatings are better visualised.

The composition of the group 10 and 11 metal coating of copper were characterised using energy dispersive and X – ray photoelectron spectroscopy. The EDX of the samples reviled the bulk composition of the samples, where the spectra were dominated by the copper of the substrate. The composition of solely the coatings was analysed using XPS. It was shown that all bar the silver system included a significant atomic percentage of copper at the surface of the coating.

Using the formal electrode potentials, it has been possible predict the galvanic reactions that will occur between a copper substrate and a solution of group 10 and 11 metal ions. It is also possible to calculate the change in Gibbs free energy for the galvanic reactions under standard conditions. Quartz crystal microbalance experiments were performed to support the predicted reaction for the galvanic displacement of copper. It was shown by the change in moles of the deposited element on the surface of the electrode, that all of the galvanic displacement reactions proceed via the oxidation of Cu (0) → Cu (I). By following the change in mass on the surface of a copper coated quartz crystal microbalance, the rate of the galvanic reactions was determined.

From the data collected in this thesis, the equation of the galvanic reactions has been predicted. The morphology and composition of the galvanically deposited coatings has been characterised

Of the goals set out in the introduction. The determination of metal species in Ethaline *via* UV – Vis has been achieved. The speciation of the Ni (II) ions has been investigated using a number of analytical methods, X – ray methods revealed that at room temperature the speciation of the metal centre is dominated by the ethylene glycol ligand. UV – Vis revealed that as temperature increased the nickel centre underwent conversion to the nickel tetrachloride species. It was suggested that for the electrolytic deposition of nickel, requires the nickel centre to be in the nickel (II) tetrachloride configuration.

The electrode potentials of the deposition of dissolution of metals were established. An EQCM was used to determine the rate of the electrochemical reactions. The current efficiency of the reactions was determined using analysis of the mass charge ratio. It was implied by the mass – charge ratio analysis, that for some of the dissolution processes, the coating does not undergo full dissolution, but small, unoxidised, metal flakes fall from the surface of the electrode. Hence it was not possible to calculate the current efficiency of some of the dissolution processes.

Galvanic coatings of all the group 10 and 11 metals where produce on a copper substrate. The equations of the reactions between the group 10 and 11 metals and a copper substrate were predicted from the determined metal speciation in Ethaline and the calculated formal electrode potentials of the deposition and dissolution process of the individual metals. The stoichiometry of the reactions was explored using a QCM experiment and the results were compared to the predicted equations of the galvanic reactions. Further the rate of the galvanic reactions was determined using a QCM experiment.

The morphology of the deposited coatings was characterised using AFM and SEM and the composition was characterised from EDX and XPS.

7.2 Future Work

Whilst the composition of electrolyticly deposited coatings from the mixed metal salt systems on the surface of a QCM has been determined via the mass – charge ratio, it would be instructive to analyse these coatings via XPS to determine to accuracy of the mass – charge ratio analysis. It would also be instructive to perform X – ray defraction on the coatings, to determine the crystallinity of the deposits and if an alloy or co – deposit is fromed on the surface of the crystal.

Depth profiling XPS could also be used to determine the nature of the galvanic deposits. Whether the copper content of the galvanically deposited samples is due to diffusion of copper from the substrate to the surface of the sample, or if copper has undergone dissolution and re – deposition on the surface of the sample, along with the other group 10 or 11 metal, could be determined.

The application of the galvanically deposited has been well established in the literature. The galvanically deposited coatings, from Deep Eutectic Solvent, could be tested in line with the applications presented in the literature.

Appendix 1: Derivation of Equation (2.8)

For the electrochemistry of a binary system, copper and silver.

$$\chi_{\mathrm{Cu}} + \chi_{\mathrm{Ag}} = 1$$

$$1 - \chi_{\mathrm{Cu}} = \chi_{\mathrm{Ag}} \quad (1)$$

$$\mathrm{Mass} = \chi_{\mathrm{Cu}}\mathrm{RMM}_{\mathrm{Cu}} + \chi_{\mathrm{Ag}}\mathrm{RMM}_{\mathrm{Ag}} \quad \text{Sub for 1}$$

$$\mathrm{M} = \chi_{\mathrm{Cu}}\mathrm{RMM}_{\mathrm{Cu}} + (1 - \chi_{\mathrm{Cu}})\mathrm{RMM}_{\mathrm{Ag}} \quad (2)$$

$$\mathrm{Charge} = \chi_{\mathrm{Cu}}2\mathrm{F} + \chi_{\mathrm{Ag}}\mathrm{F} \quad \text{Sub for 1}$$

$$\mathrm{Q} = \chi_{\mathrm{Cu}}2\mathrm{F} + (1 - \chi_{\mathrm{Cu}})\mathrm{F}$$

For current efficiency $\mathrm{a} = \frac{1}{\mathrm{c}}$ and $\mathrm{b} = \frac{1}{\mathrm{d}}$ where c and d are the current efficiency of copper and silver respectively.

$$\mathrm{Q} = \chi_{\mathrm{Cu}}2\mathrm{Fa} + (1 - \chi_{\mathrm{Cu}})\mathrm{F} \quad (3)$$

For mass – charge ratio $\frac{(2)}{(3)}$

$$\frac{\delta \mathrm{m}}{\delta \mathrm{Q}} = \frac{\chi_{\mathrm{Cu}}\mathrm{RMM}_{\mathrm{Cu}} + (1 - \chi_{\mathrm{Cu}})\mathrm{RMM}_{\mathrm{Ag}}}{\chi_{\mathrm{Cu}}2\mathrm{Fa} + (1 - \chi_{\mathrm{Cu}})\mathrm{Fb}}$$

$$\frac{\delta \mathrm{m}}{\delta \mathrm{Q}}(\chi_{\mathrm{Cu}}2\mathrm{Fa} + (1 - \chi_{\mathrm{Cu}})\mathrm{Fb}) = \chi_{\mathrm{Cu}}\mathrm{RMM}_{\mathrm{Cu}} + (1 - \chi_{\mathrm{Cu}})\mathrm{RMM}_{\mathrm{Ag}}$$

$$\frac{\delta \mathrm{m}}{\delta \mathrm{Q}}(\chi_{\mathrm{Cu}}2\mathrm{Fa} + \mathrm{Fb} - \chi_{\mathrm{Cu}}\mathrm{Fb}) = \chi_{\mathrm{Cu}}\mathrm{RMM}_{\mathrm{Cu}} - \chi_{\mathrm{Ag}}\mathrm{RMM}_{\mathrm{Ag}} + \mathrm{RMM}_{\mathrm{Ag}}$$

$$\frac{\delta \mathrm{m}}{\delta \mathrm{Q}}\chi_{\mathrm{Cu}}2\mathrm{Fa} + \frac{\delta \mathrm{m}}{\delta \mathrm{Q}}\mathrm{Fb} - \frac{\delta \mathrm{m}}{\delta \mathrm{Q}}\chi_{\mathrm{Cu}}\mathrm{Fb} = \chi_{\mathrm{Cu}}\mathrm{RMM}_{\mathrm{Cu}} - \chi_{\mathrm{Ag}}\mathrm{RMM}_{\mathrm{Ag}} + \mathrm{RMM}_{\mathrm{Ag}}$$

$$\frac{\delta \mathrm{m}}{\delta \mathrm{Q}}\chi_{\mathrm{Cu}}2\mathrm{Fa} - \frac{\delta \mathrm{m}}{\delta \mathrm{Q}}\chi_{\mathrm{Cu}}\mathrm{Fb} - \chi_{\mathrm{Cu}}\mathrm{RMM}_{\mathrm{Cu}} + \chi_{\mathrm{Ag}}\mathrm{RMM}_{\mathrm{Ag}} = \mathrm{RMM}_{\mathrm{Ag}} - \frac{\delta \mathrm{m}}{\delta \mathrm{Q}}\mathrm{Fb}$$

$$\chi_{\mathrm{Cu}}(\frac{\delta \mathrm{m}}{\delta \mathrm{Q}}2\mathrm{Fa} - \frac{\delta \mathrm{m}}{\delta \mathrm{Q}}\mathrm{Fb} - \mathrm{RMM}_{\mathrm{Cu}} + \mathrm{RMM}_{\mathrm{Ag}}) = \mathrm{RMM}_{\mathrm{Ag}} - \frac{\delta \mathrm{m}}{\delta \mathrm{Q}}\mathrm{Fb}$$

$$\chi_{\mathrm{Cu}}\left(\frac{\delta \mathrm{m}}{\delta \mathrm{Q}}2\mathrm{Fa}-\frac{\delta \mathrm{m}}{\delta \mathrm{Q}}\mathrm{Fb}-\mathrm{RMM}_{\mathrm{Cu}}+\mathrm{RMM}_{\mathrm{Ag}}\right)$$

$$=\frac{\mathrm{RMM}_{\mathrm{Ag}}-\frac{\delta \mathrm{m}}{\delta \mathrm{Q}}\mathrm{Fb}}{\left(\frac{\delta \mathrm{m}}{\delta \mathrm{Q}}2\mathrm{Fa}-\frac{\delta \mathrm{m}}{\delta \mathrm{Q}}\mathrm{Fb}-\mathrm{RMM}_{\mathrm{Cu}}+\mathrm{RMM}_{\mathrm{Ag}}\right)} \quad (\mathbf{2.8})$$

Appendix 2: Morphology of Standard Copper Substrate

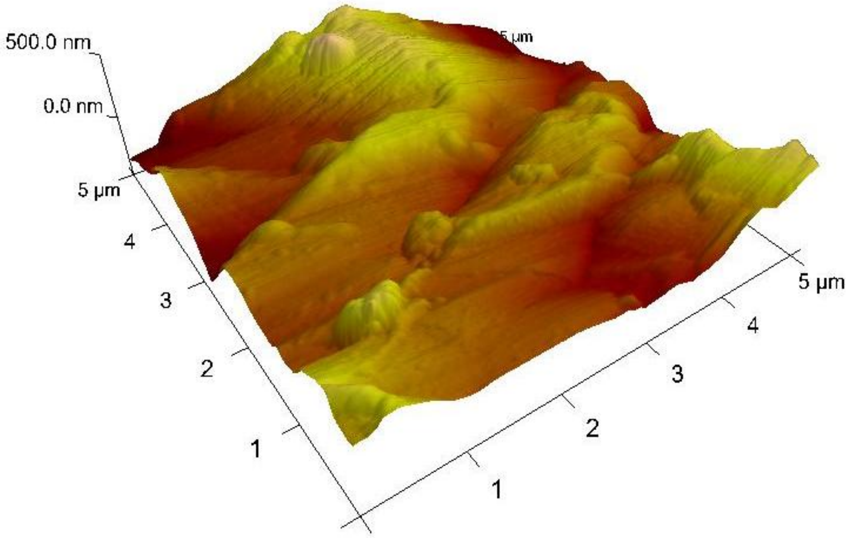

Figure A1.1: Atomic force micrograph of a standard copper substrate.

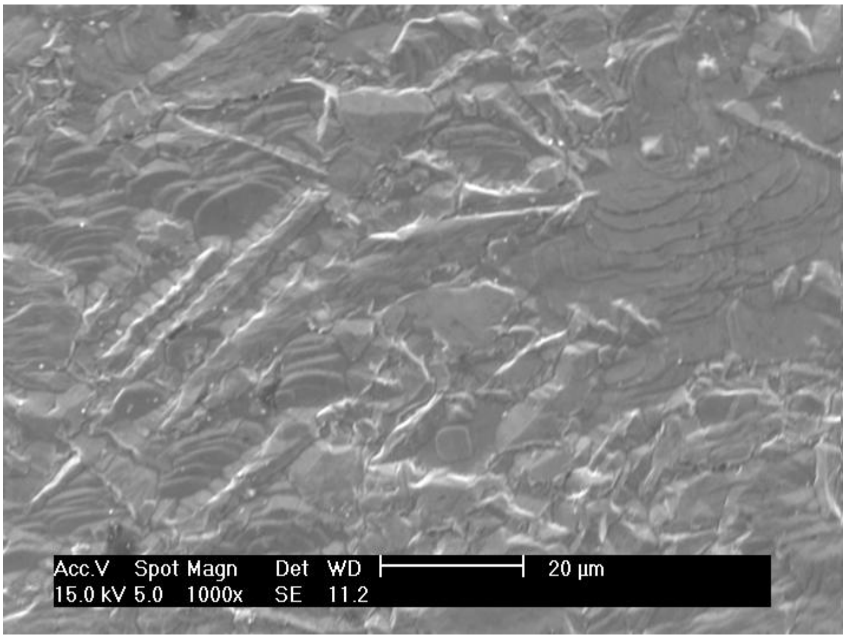

Figure A1.2: Secondary electron SEM image of a standard copper substrate.

Appendix 3: Industrial applications of the Galvanic Gold Deposition on an Electroless Nickel Substrate.

A3.1 Introduction

Presented in this chapter is industrial application of Ethaline as an alternative solvent for the galvanic deposition of gold, in the electroless nickel immersion gold (ENIG) process. The result presented here, represent research carried out as part of the ASPIS project and form basis of a paper to be published shortly.

ENIG is a surface coating that is used in the printed circuit board (PCB) industry.[1] It is important in the PCB industry to prevent oxidation of the copper tracks of a PCB. As copper oxides, such as Cu_2O, are very stable and can prevent the reflow of sold,[2,3] this leads the formation of brittle solder joints, which can cause failures of PCBs.

The ENIG process is involes the electroless deposition of nickel onto the copper tracks of a PCB, followed by the galvanic reaction of gold with the nickel to produce a gold finish. The gold acts as a tarnish resistant surface, due to its nobility and slow reactivity with air. If gold was deposited directly on the surface of the copper track, due to the solubility of gold and copper metals,[4] then copper would be able to defuse from to the surface of the samples and copper oxides could form. Hence, the electroless nickel is employed as a barrier layer between the copper and gold.

Current technology for the galvanic deposition of gold onto an electroless nickel surface uses acidic, cyanide based solutions. Obviously, the reduction in use of toxic chemicals is desirable. Also desirable is the deposition of gold from non acidic solution as this can lead to a problem called “black pad”.[5] It is theorised that black pad is caused by hyper corrosion of the electroless nickel barrier layer by the acidic solution used for the deposition of the galvanic gold.[5]

A3.2 Experimental

Preparation of copper hull cell test pieces was described in **Chapter 2**. The surface prepared copper hull cell test pieces were then activated by the galvanic deposition of a seed layer of palladium from an aqueous solution; $PdCl_2$ (50 ppm) and H_2SO_4 (2 ml L^{-1}) for 1 minute. The activated samples were then immersed in an acidic solution; H_2SO_4 (50 mL L^{-1}), to remove and residual palladium or copper ions from the surface of the sample. Nickel was the electrolessly deposited on the samples from an aqueous platting solution; $NiSO_4$ (0.1 M), $NaPH_2O_2$ (0.25 M), glycine (0.4 M), molonic acid (0.1 M), for 45 min at 80 ^{o}C, the platting solution was adjusted to pH 4.5 using conc. KOH.

The electroless nickel plated samples were then plated with gold, by immersing the samples in Ethaline solutions containing 5 mM gold salts for 45 min at 80 ^{o}C. The DES solutions were AuCl (11.6 mg), Au(CN) (11.1 mg) or $KAu(CN)_2$ (14.4 mg) dissolved in Ethaline (10 mL). The aqueous solution was $KAu(CN)_2$ (14.4 mg) and citric acid (193 mg, 0.1M) dissolved in water (10 mL), the solution was adjusted to pH 4.5 using conc. KOH.

The morphology of the substrates was examined *via* AFM and SEM as described in **Chapter 2**.

The above described method was used to produce a ENIG coating on a polished, gold, 10 MHz QCM with a piezoelectric active area of 0.23 cm^{-2}, i.e. copper was electrolytically platted on to the surface of the QCM, followed by activation, electroless nickel deposition and galvanic gold deposition from all gold solution.

Cyclic voltammetry was performed of the 5 mM gold solution using a three electrode cell at room temperature; 2 mm Pt disc working electrode, Pt flag counter electrode, Ag/AgCl wire pseudo reference electrode.

EXAFS experiments were performed on 0.1 M gold solution of AuCl, Au(CN) and $KAu(CN)_2$ dissolved in Ethaline at room temperature. The EXAFS was performed at the gold – L_{III} edge (11919 eV) using a double crystal Si (111) monochromator. A nine element detector (BM26A operation on seven elements) in total fluorescence yield mode was used for liquid samples. Solid references were measured with ion chamber detectors in transmission mode. EXAFS spectra were fitted using EXCURV[6], electron scattering parameters were calculated and used to determine the type and number of coordinating atomsm using the Hedin – Lundqvist potential.[7]

A3.3 Discussion

The speciation of the gold salts when dissolved in Ethaline was determined using EXAFS, *Figure A2.1*.

The Fourier transform of the EXAFS data produces a real space radial distribution diagram. These diagrams represent the distance of the coordinating atoms in the coordination sphere from the metal centre.

The real space radial distribution diagram calculated from EXAFS data collected form a solution of 0.1 M AuCl dissolved in Ethaline, *Figure A2.1 A)*, displays one peak at 2.26 Å representing the coordination of chloride to the metal centre. It was determined that two chloride ions are coordinated to the gold metal centre, hence the speciation of the gold centre when AuCl is dissolved in Ethaline is predicted to be the linear $[AuCl_2]^-$ complex.

The real space radial distribution diagram calculated from EXAFS data collected form a solution of 0.1 M Au(CN) dissolved in Ethaline, *Figure A2.1 B)*, displays three peaks indicative of atoms in the coordination sphere. The peak at 2.28 Å represents a chloride bound to the gold centre. The peak at 1.94 Å represents a carbon atom bound to the gold centre. Finally the peak at 3.08 Å is represents the nitrogen bound to the carbon in the cyanide molecule, this represents a bond length of 1.14 Å for the cyanide C ≡ N bond. From these data, the speciation of the gold centre is predicted to be the linear complex $[Au(CN)Cl]^-$ when Au(CN) is dissolved in Ethaline.

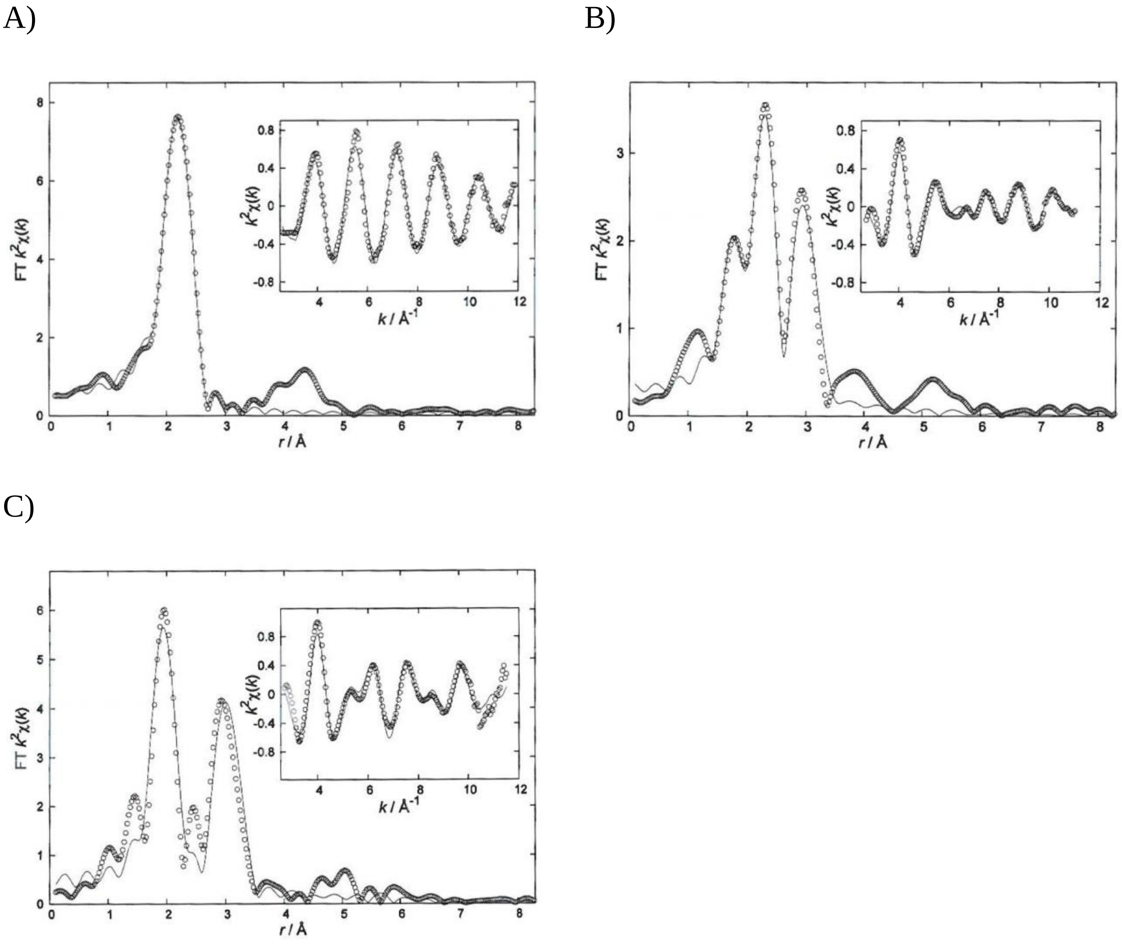
A)

B)

C)

Figure A2.1: Fourier transform of EXAFS data of 0.1 M gold salts dissolved in Ethaline. Inserts show EXAFS data. A) 0.1 M AuCl dissolved in Ethaline. B) 0.1 M Au(CN) dissolved in Ethaline. C) 0.1 M $KAu(CN)_2$ dissolved in Ethaline.

The real space radial distribution diagram calculated from EXAFS data collected form a solution of $KAu(CN)_2$ dissolved in Ethaline, *Figure A2.1 C),* displays two peaks representing atoms in the coordination sphere. The peak at 1.99 Å represents the carbon atoms bound gold centre, it was determined that there were two carbon atoms bond to each gold centre. The second peak at 3.13 Å, represents the nitrogen molecule in the cyanide group, making the bond length of the C ≡ N bond 1.14 Å.

The affect that this change in speciation has on the electrochemistry of the gold centre is demonstrated in *Figure A2.2*.

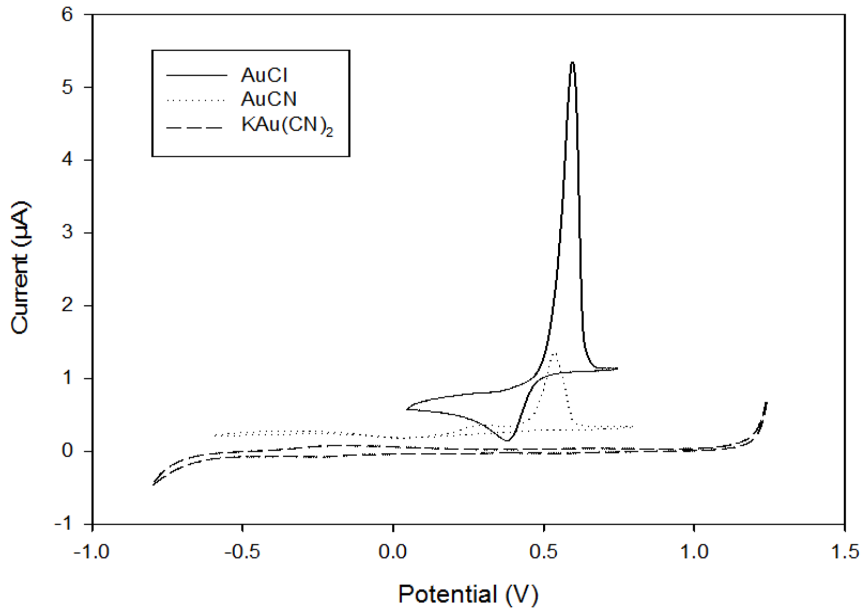

Figure A2.2: The cyclic voltammetry of 5 mM AuCl, Au(CN) and KAu(CN)$_2$ when dissolved in Ethaline. 2 mm Pt disc working electrode. Pt Flag counter electrode. Ag wire pseudo reference electrode. Scan rate 5 mV s^{-1}. The voltammagrams have been offset for clarity.

Discussion of the cyclic voltammogram of AuCl dissolved in Ethaline has been covered in **Chapter 4**.

The CV of Au(CN) dissolved in Ethaline shows a considerably smaller electrochemical response. The current passed for the dissolution of gold from the surface of the electrode was determined to be *ca*. 1 µA. When compared to the AuCl solution, which has an oxidation current of *ca*. 5 µA, it is clear that the electrochemical rate of deposition is much slower for the [Au(CN)Cl]$^-$ molecule than the [AuCl$_2$] molecule. This is probably due to the strong binding nature of the cyanide ligand.

The effect of the addition of a second strongly binding cyanide ligand, shows the same effect. Where the electrochemical deposition from the $[Au(CN)_2]$ species is further retarded when compared to the Au(CN) and AuCl systems.

The difference in the rate of electrochemical deposition of gold from various gold metal species is demonstrated by the galvanic deposition of gold on to an electroless nickel coating, *Figure A2.3*.

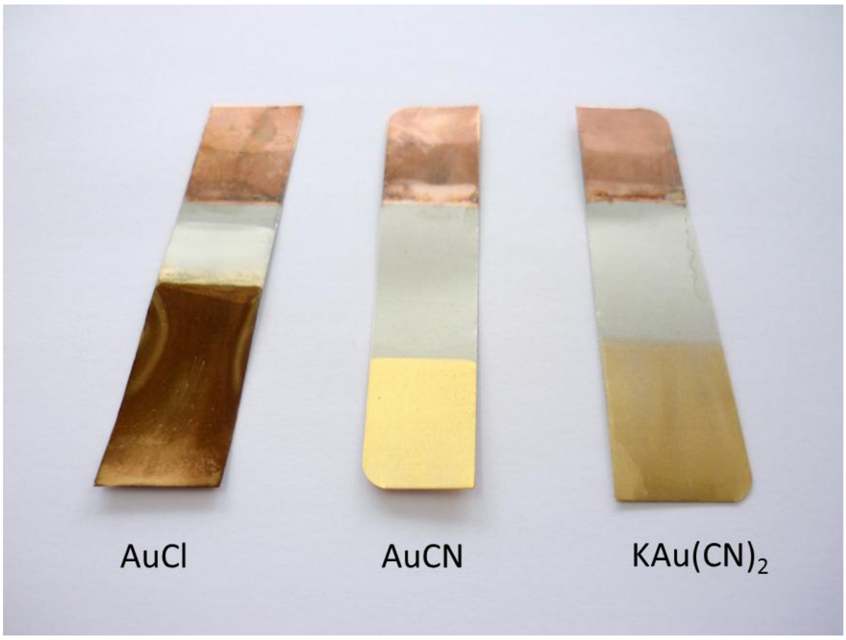

Figure A2.3: Galvanically deposited gold on to an electroless nickel substrate, from various gold salts dissolved in Ethaline.

It is clear from the gold coatings displayed in *Figure A2.3*, that the change in the gold centre speciation makes a significant difference in the deposit. It is proposed that the fast rate of gold deposition from the $[AuCl_2]^-$ salt produces lots of nucleation site, which leads to a dull granular coating with poor adhesion to the surface. Alternatively, the coating produced from the solution containing the $[Au(CN)_2]^-$ ion, has such a low rate of galvanic reaction, that the coating produced is very thin and incomplete. Finally the coating produced from the $[Au(CN)Cl]^-$ ion solution produces a bright complete coating, which is akin to the coating produced from the aqueous system. It is proposed that the rate of electrochemical reaction is fast enough to produce a complete coating, but not too fast that a granular coating is produced.

To investigate the rate of the galvanic reactions, QCM techniques have been employed. QCMs were electrolytically coated with copper, followed by the electroless deposition of nickel on to the surface. The coated QCMs were then immersed in one of the gold ion solutions, the change in mass was followed with respect to time and hence a comparison of the rate of reactions can be made, *Figure A2.4*.

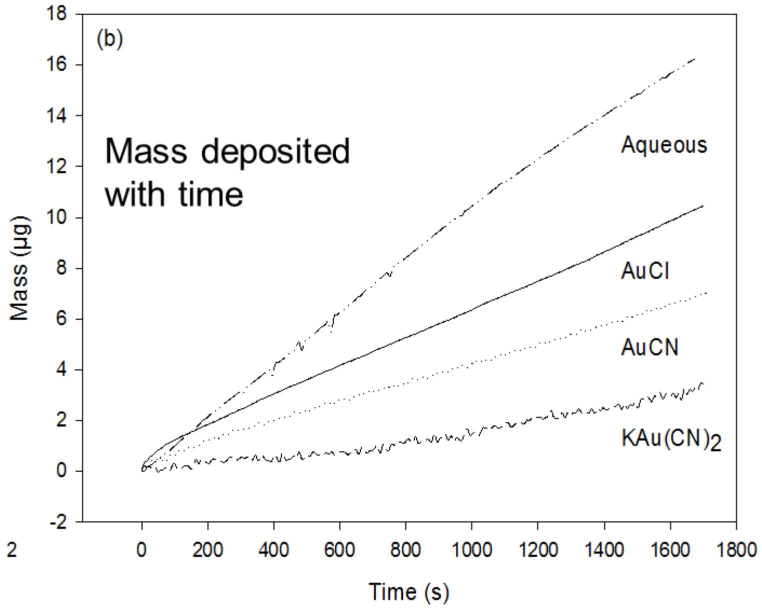

Figure A2.4: Change in mass with respect to time for the galvanic deposition of Au from various Au species dissolved in Ethaline and an aqueous solution.

As discussed above, it is expected that the rate of the galvanic reaction will be slowed with the addition of the strongly binding cyanide ligand. The results presented from the QCM experiment in *Figure A2.4*, are consistent with the discussion for the deposition of gold onto the bulk electroless nickel samples in *Figure A2.3*.

It was also postulated that the rate of the electrochemical reaction will have a direct affect on the morphology of the galvanic deposit, as shown by SEM analysis, *Figure A2.5*.

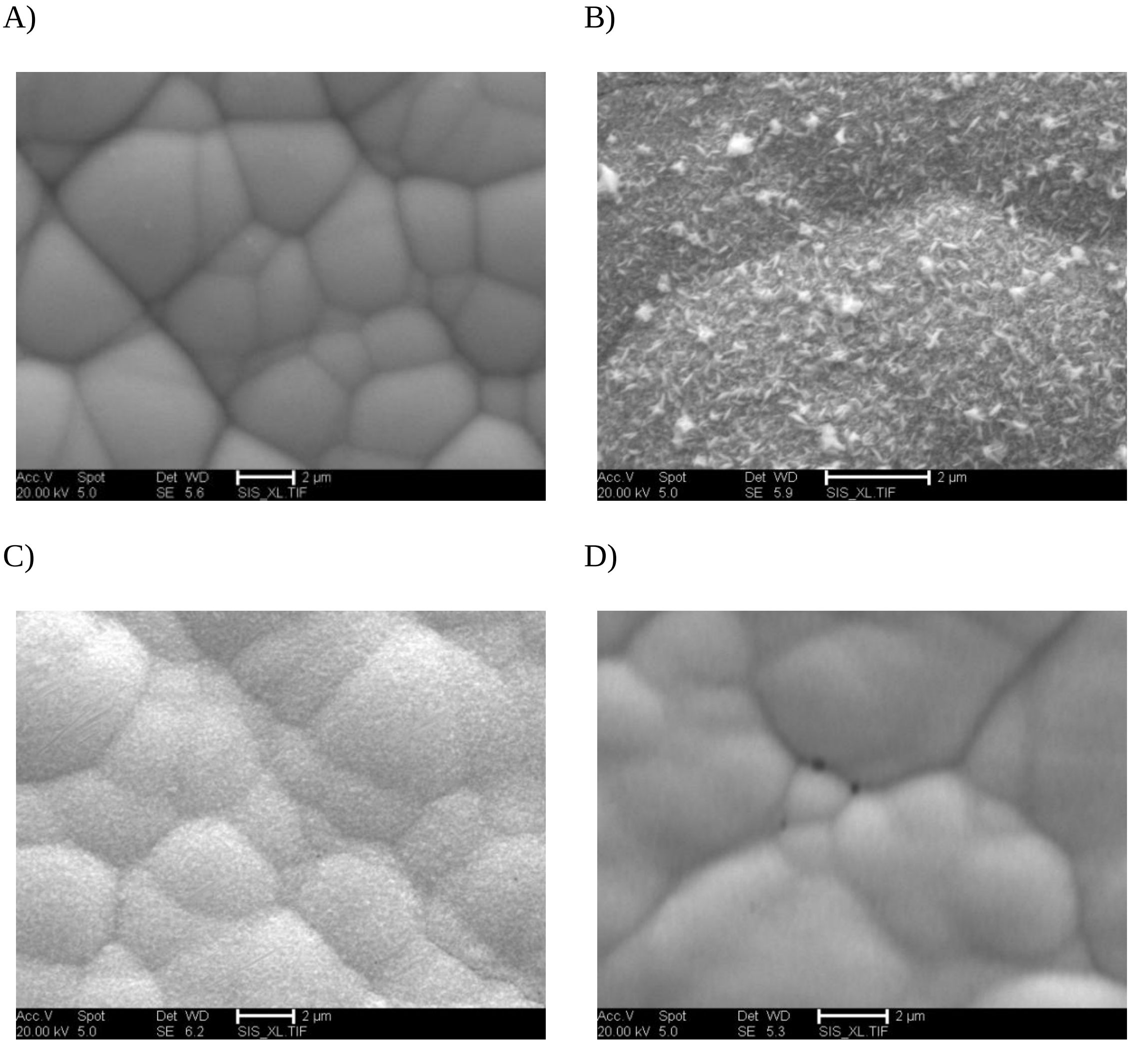

Figure A2.5: SEM images of galvanically deposited Au coatings from Ethaline. A) Electroless Ni substrate. B) Galvanic Au deposit from $[AuCl_2]^-$ ions. C) Galvanic Au deposit form $[Au(CN)Cl]^-$ ions. D) Galvanic Au deposit from $[Au(CN)_2]^-$ ions.

It is clear from the SEM images of the various galvanic gold deposits, that the rate of reaction makes a significant impact on the morphology of the deposit. The rapid rate of reaction of the $[AuCl_2]^-$ ions, produces coatings consisting of fine needle like structures. There are also larger particles that have been deposited on the surface of the structure. The image of the galvanic deposit produced by the ration of $[Au(CN)Cl]^{-1}$ ions shows a uniform deposit of gold with a very fine nodular structure, which appears be less rough than the coating deposited from $[AuCl_2]^-$ ions. Finally the coating deposited from $[Au(CN)_2]^-$ ions appears to have less features on the surface of the electroless nickel and appears smother than both previous deposits. It is proposed that the slowing of the rate of reaction, by the substitution of chloride with cyanide ligands, produces a much smoother deposit.

The roughness of the samples are better quantified using AFM, *Figure A2.6*, shows a smoothing of the samples when gold cyanide salts are used as the gold ion source for the reaction, *Table A2.1*.

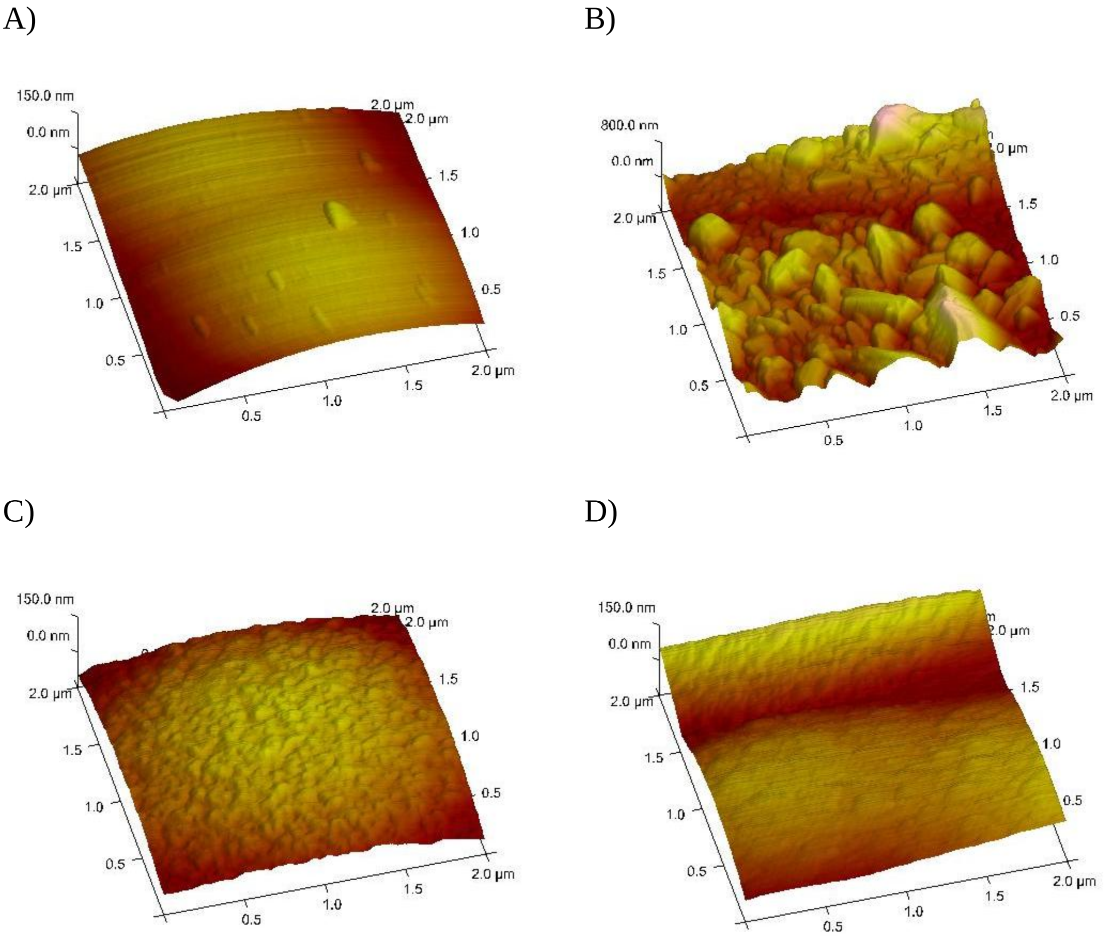

Figure A2.6: AFM images of galvanic Au deposits. A) Electroless Ni substrate. B) Galvanic Au deposit from [AuCl$_2$]$^-$ ions. C) Galvanic Au deposit form [Au(CN)Cl]$^-$ ions. D) Galvanic Au deposit from [Au(CN)$_2$]$^-$ ions.

Table A2.1: Roughness of galvanic Au deposits	
Au ion as source Au	% surface area difference
$[AuCl_2]^-$	180.0
$[Au(CN)Cl]^-$	4.0
$[Au(CN)_2]^-$	3.8

The comparison of the % surface area difference clearly shows that the coatings deposited from the gold cyanide salts have a much smoother surface compared to the deposit from the gold chloride salt.

A3.4 Conclusions

The use of Deep Eutectic Solvents has been shown to be an alternative media in which the galvanic deposition of gold can be performed. The use of DES has avoided the need for the use of acidic solution which can lead to issues in the printed circuit board industry, i.e. “black pad”.

The speciation of three gold salts, when dissolved in Ethaline, has been determined *via* EXAFS. The affect the difference in speciation has of the Au (I)/(0) redox couple has been shown *via* cyclic voltammetry and comment has been made on the kinetics of the electrochemical reaction. The $[AuCl_2]^-$ species with weakly bound Cl^- ligands reacting the fastest. Followed by the $[Au(CN)Cl]^-$ species with one strongly binding cyanide ligand and finally the $[Au(CN)_2]^-$ reacting slowest with two strongly binding cyanide ligands.

The various gold salts have been used in a galvanic reaction of gold ions with an electroless nickel substrate. It was shown that the addition of cyanide ligands, to the gold ion source, slowed that rate of the galvanic reactions. It was also shown that the speciation of the gold salt had a marked affect on the morphology produced. It was postulated that a slower rate of reaction, caused by the addition of cyanide ligands, produces a smoother, more uniform deposit.

A3.5 References

1. R. C. Agarwala and V. Agarwala, *Sadhana*, 2003, **28**, 475 – 493.
2. A. Abbott, J. Griffith, S. Nandhra, C. Oconnor, S. Postlethwaite, K. Ryder, and E. Smith, *Surf. Coat. Tech.*, 2008, **202**, 2033 – 2039.
3. J. Mittal, Y. W. Lin, and K. L. Lin, *Appl. Surf. Sci.*, 2010, **256**, 3531 – 3540.
4. H. Okamoto, D. J. Chakrabari, D. E. Laughlin, and T. B. Massalskl, *J. Phase Equlib.*, 1987, **8**, 454 – 474.
5. Y. S. Won, S. S. Park, J. Lee, J.-Y. Kim, and S.-J. Lee, *Appl. Surf. Sci.*, 2010, **257**, 56 – 61.
6. S. Tomic, B. G. Searle, A. Wander, N. M. Harrison, A. J. Dent, M. J. F. W., and J. E. Inglesfield, *CCLRC Tech. Rep. DL-TR-2005-001*, 2005.
7. S. J. Gurman, N. Binsted, and I. J. Ross, *J. Phy. Chem. C Solid State Phys.*, 1986, **19**, 1845 – 1861.

Appendix 4: Crystallographic data for the $[Ni(phen)_2(C_2H_6O_2)]2Cl \cdot 4(C_2H_6O_2)$ Complex

Identification code	12092	
Empirical formula	C30 H34 Cl2 N4 Ni O6	
Formula weight	676.22	
Temperature	150(2) K	
Wavelength	0.71073 Å	
Crystal system	Triclinic	
Space group	P-1	
Unit cell dimensions	a = 12.133(3) Å	□= 63.674(4)°.
	b = 12.283(3) Å	□= 63.441(4)°.
	c = 13.281(3) Å	□ = 60.698(5)°.
Volume	1478.5(6) $Å^3$	
Z	2	
Density (calculated)	1.519 Mg/m^3	
Absorption coefficient	0.888 mm^{-1}	
F(000)	704	
Crystal size	0.17 x 0.08 x 0.05 mm^3	
Theta range for data collection	1.79 to 25.00°.	
Index ranges	-14<=h<=14, -14<=k<=14, -15<=l<=15	
Reflections collected	10837	
Independent reflections	5170 [R(int) = 0.1073]	
Completeness to theta = 25.00°	99.3 %	
Absorption correction	Empirical	
Max. and min. transmission	0.862 and 0.472	
Refinement method	Full-matrix least-squares on F^2	
Data / restraints / parameters	5170 / 0 / 391	
Goodness-of-fit on F^2	0.887	
Final R indices [I>2sigma(I)]	R1 = 0.0725, wR2 = 0.1295	
R indices (all data)	R1 = 0.1242, wR2 = 0.1458	
Largest diff. peak and hole	0.870 and -0.571 $e.Å^{-3}$	